

Technische Universität Dortmund

Characterization of natural and consolidated stones from Jordan with non-destructive ultrasonic technique and physico-mechanical methods

Von der Fakultät Architektur und Bauingenieurwesen der Technischen Universität
Dortmund genehmigte Dissertation zur Erlangung des akademischen Grades

Doktor-Ingenieur

eingereicht von Abdelraheem Ahmad

Vorsitzender der Prüfungskommission: Prof. Dr.-Ing. W. Willems

1. Gutachter: Prof. Dr. rer.nat. B. Middendorf

2. Gutachter: Prof. Dr. rer. nat. R. Snethlage

Weitere Gutachter: Prof. Dr. rer. nat. St. Simon

(XJTU, China; Rathgen-Forschungslabor, Berlin)

Tag der Einreichung: 05.10.2011

Tag der mündlichen Prüfung: 08.12.2011

Acknowledgements

It is a great pleasure to thank the many people who made this dissertation possible. First of all, I am deeply indebted and thankful to my supervisors Prof. Dr. Stefan Simon (Rathgen-Forschungslabor) and Prof. Dr. Bernhard Middendorf (Technische Universität Dortmund) for their constant support and patient guidance throughout this work. The dissertation could only be completed smoothly with their constructive advice and valuable assistance.

I am also very thankful to Prof. Dr. Rolf Snethlage for the reading and evaluation of the dissertation. It is a great honor for me to have such a well-known professor with great knowledge and long experience in the examination and evaluation committee of my dissertation.

I would like to express my sincere gratitude to all my colleagues and staff members at Rathgen Research Laboratory (Rathgen-Forschungslabor) for their support and friendliness as well as for the warm family atmosphere we share in the lab. I am especially grateful to Dr. Marisa Pamplona for the fruitful discussions and critical reading of the dissertation.

I would like to appreciate and thank Prof. Dr. Gottfried Hauff and Dr. Peter Kozub (Fachhochschule Potsdam) for helping by the preparation of the stone specimens used in this work.

I would also like to express my thanks to Dr. André Glaubitt (Technische Universität Dortmund) for his help by mercury intrusion porosimetry analysis.

I am very grateful to Mr. Martin Mach and all the staff members of the Central Laboratory at the Bavarian State Conservation Office (Bayerisches Landesamt für Denkmalpflege, Zentrallabor) for hosting me and allowing me access to their instruments of biaxial flexural strength, drilling resistance and ultrasonic velocity measurements. Special thanks go to Dr. Mathias Kocher for the helpful discussions and suggestions.

For the valuable assistance by understanding and describing the microstructure of the studied stone samples, I am heartily thankful to Mr. Mahmoud Hassouneh and Prof. Dr. Abdulkader Abed (Department of Geology, University of Jordan), Prof. Dr. Gerhard Franz (Fachgebiet Mineralogie-Petrologie, Technische Universität Berlin), Dr. Ralf Milke (Institut für

Acknowledgements

Geologische Wissenschaften, Freie Universität Berlin), and Prof. Dr. Walid Saqqa (Department of Earth and Environmental Sciences, Yarmouk University).

I would also like to acknowledge Dr. George Hilbert (Remmers Fachplanung) for providing the consolidation products used in this study.

Special thanks go to Dr. May Shaer, former head of international cooperation at the Department of Antiquities in Jordan, for the assistance by getting the permission to study and obtain stone samples from different archaeological sites in Jordan.

I would also like to thank my professors and colleagues and all the member of staff at the Faculty of Archaeology and Anthropology in Yarmouk University in Jordan. In particular, I would like to thank Prof. Dr. Ziad al-Saad for his support and encouragement and Dr. Mustafa al-Naddaf for helping, among other things, with drilling resistance measurements.

Above all, I wish to thank my family, especially my mother and my father, for their love, patience and encouragement. Without their endless support and motivation it would have not been possible to complete this dissertation. I would like to thank them very much for all they are, and all they have done for me. To them I dedicate this dissertation.

Thanks are also extended to all those who contributed to this work with advice, suggestions or any other form of help.

Abstract

The purpose of this dissertation was to investigate different stone samples (limestone, basalt and marble) from five important archaeological sites in north and northeast Jordan for the purpose of their conservation. This research focused on the use of non-destructive ultrasonic technique as validated by traditional physico-mechanical methods for the study of the weathering of the selected stones and their durability and the evaluation of the effectiveness of consolidation treatments. The selected stones were characterized and the changes in their properties after artificial weathering and consolidation were studied.

It was found that the susceptibility of the studied stone samples to salt damage is determined by their petrophysical rather than mechanical properties. In terms of loss of stone material, the damage induced by the crystallization of salt in the stones seems to be dependent on their proportion of micropores and free porosity. Durability estimators for the evaluation of the weathering resistance of stone were consequently developed.

The study provided additional evidence that ultrasonic technique is an effective method for estimating the degree of cracking and evaluating the effectiveness of stone consolidation treatments. Ultrasonic velocity seemed to correlate well with the degree of cracking in the stones. This implies that weathering classification schemes, such as those already existed for marble, based on correlation between ultrasonic velocity and increasing porosity can be developed for the studied stones. However, it is necessary to study these correlations for the particular stones in fresh and different weathering conditions. This dissertation recommends the in situ application of ultrasonic technique for the assessment of the weathering condition of Jordanian archaeological stones and for the evaluation and control of consolidation treatments.

Kurzfassung

Ziel dieser Dissertation war es zunächst, verschiedene Steinproben (Kalkstein, Basalt und Marmor) von fünf bedeutenden archäologischen Orten des Nordens und Nordosten Jordaniens zu untersuchen und zu charakterisieren. Die Arbeit legt den Fokus auf die Anwendung von zerstörungsfreier Ultraschall-Technik, die mit den traditionellen physikalisch-mechanischen Methoden ergänzt und verglichen wurde, um die Verwitterung der ausgewählten Steine und ihre Dauerhaftigkeit zu studieren und die Wirksamkeit der Steinfestigungsverfahren zu evaluieren. Nach der Charakterisierung der ausgewählten Steinproben wurden die Veränderungen ihrer Eigenschaften nach künstlicher Verwitterung beziehungsweise Festigung studiert.

Im Ergebnis stellte sich heraus, dass die Anfälligkeit der untersuchten Steinproben gegen Salzverwitterung eher von ihren petro-physikalischen als von ihren mechanischen Eigenschaften abhängig ist. Hinsichtlich des Verlustes von Steinmaterial scheint der entstehende Schaden durch Salzkristallisierung in den Steinen von ihrem Anteil an Mikroporen und ihrer freien Porosität abzuhängen. So werden basierend auf diesen Ergebnissen Dauerhaftigkeitsparameter für die Evaluierung der Verwitterungsresistenz der Steine entwickelt. Die Arbeit ergab einen zusätzlichen Beleg dafür, dass die Ultraschall-Technik eine wirksame Methode zur Einschätzung des Grades von Rissen und der Evaluierung der Wirksamkeit von Steinfestigungsverfahren ist. Die Ultraschallgeschwindigkeit scheint gut zu korrelieren mit der Rissdichte in den Steinen. Daraus ergibt sich, dass Skalen zur Klassifizierung von Verwitterung, wie sie bereits für Marmor vorhanden sind, basierend auf der Korrelation zwischen Ultraschallgeschwindigkeit und ansteigender Porosität, für die hier untersuchten Steine entwickelt werden können. Jedoch ist es notwendig, diese Korrelationen an bestimmten Steinen in frischem und in unterschiedlichen verwitterten Zuständen zu studieren. Diese Dissertation empfiehlt die Vor-Ort-Anwendung von Ultraschall-Technik für die Bewertung des Verwitterungszustandes archäologischer Steine Jordaniens und für die Evaluierung und Kontrolle ihrer Festigungsverfahren.

Table of contents

Acknowledgments	iii
Abstract	v
List of figures	x
List of tables	xiii
List of abbreviations	xv
1 Introduction	1
1.1 General	1
1.2 Aim of the study	2
2 Weathering of stone	5
2.1 Weathering types	5
2.1.1 Physical weathering	6
2.1.1.1 Wetting	6
2.1.1.2 Salt weathering	6
2.1.1.3 Frost damage	9
2.1.1.4 Thermal weathering	11
2.1.2 Chemical weathering	12
2.1.2.1 Dissolution	12
2.1.2.2 Hydrolysis	13
2.1.2.3 Oxidation reactions	14
2.2 Weathering forms	14
3 Pore structure and water transport	16
3.1 Pore structure	16
3.1.1 Porosity	16
3.1.2 Pore size and pore size distribution	17
3.2 Water transport in porous materials	19
3.2.1 Water transport mechanisms	19
3.2.1.1 Diffusion of water vapor	20
3.2.1.2 Transport of liquid water	21
3.2.2 Water content and moisture storage	24
3.2.3 Evaporation	26
4 Evaluation of weathering and consolidation treatments	29
4.1 Stone durability and weathering assessment	29
4.1.1 Stone properties and durability	30
4.1.2 Accelerated weathering test	34
4.1.2.1 Crystallization damage by sodium sulfate	34
4.1.2.2 Crystallization pressure and stress on pore walls	37
4.2 Evaluation of consolidation treatments	40

Table of contents

4.2.1 Stone consolidation and evaluation of treatments	40
4.2.2 Consolidation materials for building stone	42
5 Non-destructive ultrasonic technique	45
5.1 Basic principles	45
5.2 Measuring techniques	47
5.3 Ultrasonic applications in stone conservation field	49
5.3.1 Characterization of stone	49
5.3.2 Assessment of the degree of stone weathering	50
5.3.3 Evaluation of the effectiveness and durability of conservation treatments	52
5.4 Important aspects and considerations	53
6 Materials and methods	55
6.1 Materials of the study	55
6.1.1 Classification of stone	55
6.1.2 Studied stone samples	59
6.1.2.1 Sound stone samples	61
6.1.2.2 Naturally weathered samples	68
6.2 Investigations	72
6.2.1 Physico-mechanical testing methods	72
6.2.1.1 Porosity and density by water absorption	72
6.2.1.2 Mercury intrusion porosimetry (MIP)	73
6.2.1.3 Capillary water uptake coefficient (w-value)	74
6.2.1.4 Drying curve	75
6.2.1.5 Water vapor diffusion resistance (μ -value)	76
6.2.1.6 Adsorption isotherm curve	77
6.2.1.7 Water micro-drop absorption	77
6.2.1.8 Color Measurement	78
6.2.1.9 Thermal expansion coefficient	78
6.2.1.10 Biaxial flexural strength and static modulus of elasticity	79
6.2.1.11 Drilling resistance	80
6.2.1.12 Fracture density	80
6.2.2 Petrographic and chemical analyses	81
6.2.2.1 X-ray diffraction	81
6.2.2.2 X-ray florescence	81
6.2.2.3 Microscopic analysis	81
6.2.3 Non-destructive ultrasonic methods	82
6.2.3.1 Velocity of longitudinal ultrasonic waves (pulse velocity V_p)	82
6.2.3.2 Calculation of dynamic modulus of elasticity (E_{dyn})	83
6.2.4 Artificial weathering	84
6.2.4.1 Salt crystallization test	84
6.2.4.2 Thermal weathering	85
6.2.5 Consolidation treatments	85
7 Results and discussion	86
7.1 Properties before and after weathering	87
7.1.1 Salt crystallization test	86
7.1.1.1 Visual examination	86
7.1.1.2 Porosity and density	88
7.1.1.3 Mercury intrusion porosimetry (MIP)	89

Table of contents

7.1.1.4 Capillary water uptake coefficient	92
7.1.1.5 Drying curve	93
7.1.1.6 Thermal expansion	96
7.1.1.7 Fracture density	97
7.1.1.8 Biaxial flexural strength and moduli of elasticity	97
7.1.1.9 Change of sample mass and total loss of stone material	99
7.1.1.10 Non-destructive ultrasonic pulse velocity (V_p)	102
7.1.1.11 Estimation of stone susceptibility to salt damage	106
7.1.2 Thermal weathering of marble	114
7.1.2.1 Porosity and pore size distribution	114
7.1.2.2 Capillary water absorption	116
7.1.2.3 Drying curve	117
7.1.2.4 Thermal expansion	119
7.1.2.5 Mechanical properties	119
7.1.2.6 Ultrasonic velocity	119
7.2 Properties before and after consolidation	121
7.2.1 Uptake of consolidation products	121
7.2.2 Porosity properties and density	122
7.2.3 Pore size distribution	124
7.2.4 Capillary water uptake coefficient (w-value)	126
7.2.5 Water vapor diffusion resistance (μ -value)	128
7.2.6 Drying curve	129
7.2.7 Color changes	131
7.2.8 Thermal expansion	131
7.2.9 Penetration depth as determined by water micro-drop absorption time	132
7.2.10 Drilling resistance measurement	134
7.2.11 Biaxial flexural strength and moduli of elasticity	136
7.2.12 Ultrasonic velocity (V_p)	141
8 Summary and conclusions	149
9 References	152
10 Curriculum Vitae	172

List of figures

Figure 2.1: Linear thermal expansion coefficients of calcite crystal along the different crystallographic axes.	11
Figure 2.2: Granular disintegration and scaling (or rather flaking) of stone induced by salt crystallization.	15
Figure 2.3: Delamination of a sandstone gravestone possibly resulting from frost action.	15
Figure 3.1: Porosity types.	17
Figure 3.2: Pore types.	17
Figure 3.3: Characterization methods of pore size and their measuring ranges.	19
Figure 3.4: Moisture transport mechanisms.	19
Figure 3.5: The mean free path of water molecule and water vapor diffusion and effusion.	21
Figure 3.6: Impact of surface tension (capillary ascension and capillary depression).	22
Figure 3.7: Water content of a porous material by increasing moistening as described by Rose (1965).	25
Figure 3.8: Water content of a porous hygroscopic building material.	26
Figure 3.9: Water occupation and distribution within the pore space of a stone.	28
Figure 4.1: Phase diagram of sodium sulfate.	35
Figure 5.1: Types of elastic waves in solids and their velocities.	46
Figure 5.2: Transmission ultrasonic technique.	48
Figure 6.1: Folk's classification system of carbonate rocks.	56
Figure 6.2: Textural classification of carbonate rocks.	56
Figure 6.3: Dunham's classification system of carbonate rocks.	57
Figure 6.4: The basalt tetrahedron.	58
Figure 6.5: Geological map of Jordan showing the locations of the studied stone samples.	59
Figure 6.6: Photomicrograph of the blue-dyed thin section of sample LA (PPL).	62
Figure 6.7: Photomicrograph of the thin section of sample LJ1 (PPL).	62
Figure 6.8: Photomicrograph of the thin section of sample LUQ1 (PPL).	63
Figure 6.9: Photomicrograph of the thin section of sample MUQ (PPL).	64
Figure 6.10: Photomicrograph of the thin section of sample MUQ (CPL).	65
Figure 6.11: Photomicrograph of the thin section of sample BUQ (PPL).	65
Figure 6.12: Photomicrograph of the thin section of sample BUQ (CPL).	66
Figure 6.13: Photomicrograph of the thin section of sample BUE (PPL).	66
Figure 6.14: Photomicrograph of the thin section of sample BUE (CPL).	66
Figure 6.15: Nomenclature of the common volcanic rocks.	67
Figure 6.16: Photomicrograph showing the microstructure of sample LH (PPL).	69
Figure 6.17: Photomicrograph showing the microstructure of sample LJ2 (PPL).	69

List of figures

Figure 6.18: Scanning electron microscope image showing the microstructure of sample LJ3.	70
Figure 6.19: Scanning electron microscope image showing the microstructure of sample LUQ2.	71
Figure 6.20: Drying curve of a porous material.	76
Figure 6.21: The used experimental set-up for measuring the thermal dilatation of stone.	78
Figure 7.1: Limestone samples before and after weathering.	87
Figure 7.2: Pore size distribution of the stones before and after salt weathering test	89
Figure 7.3: Capillary water absorption curves before and after salt weathering.	93
Figure 7.4: The drying curves of the stones before and after weathering.	95
Figure 7.5: Thermal expansion coefficient before and after salt weathering.	96
Figure 7.6: Mass evolution during salt weathering test - Cubic specimens.	99
Figure 7.7: Mass evolution during salt weathering test – Prismatic specimens.	100
Figure 7.8: Percentage decrease in ultrasonic pulse velocity with increasing number of weathering cycles – Cubic specimens.	104
Figure 7.9: Diagram of the extracted principal components.	112
Figure 7.10: Graphical representation of marble porosity before and after weathering.	115
Figure 7.11: The pore size distributions of the marble sample before and after weathering.	115
Figure 7.12: The capillary water absorption curves of the marble sample before and after weathering.	117
Figure 7.13: Drying curves of the marble sample before and after thermal weathering.	118
Figure 7.14: Accessible and free porosities before and after consolidation treatments.	123
Figure 7.15: The MIP spectra of the untreated and treated samples.	124
Figure 7.16: Average w-value of the stone samples before and after consolidation treatments.	127
Figure 7.17: Capillary water absorption curves of the untreated and treated samples.	127
Figure 7.18: Drying curves of the weathered stones before and after consolidation with KSE 300 and KSE 300HV.	130
Figure 7.19: Thermal expansion coefficient of the weathered and treated samples.	132
Figure 7.20: Micro-drop water absorption time of the treated sample as a measure of penetration depth.	133
Figure 7.21: Drilling resistance profiles of the weathered and consolidated samples in the directions parallel and perpendicular to bedding.	135
Figure 7.22: Biaxial flexural strength in depth profile of the treated and untreated samples.	137
Figure 7.23: Static modulus of elasticity in depth profile of the treated and untreated samples.	139
Figure 7.24: Dynamic modulus of elasticity before and after consolidation treatments.	140
Figure 7.25: Average ultrasonic velocity of treated and untreated limestone samples measured in cubic specimens along three orthogonal directions (46 kHz).	142
Figure 7.26: Ultrasonic pulse velocity in depth profile of the weathered and treated samples measured in two directions (parallel and perpendicular to beddings) with ultrasonic	

List of figures

frequency of 46 kHz.	145
Figure 7.27: Ultrasonic pulse velocity in depth profile of the weathered and treated samples measured in two directions (parallel and perpendicular to beddings) with ultrasonic frequency of 350 kHz.	147

List of tables

Table 3.1: Classification of pore size diameter in different fields.	18
Table 4.1: Requirements for assessing the effectiveness of consolidation treatments.	42
Table 5.1: Classification of marble damage after Köhler (1991).	51
Table 5.2: Suitable ultrasonic frequency and specimen dimension for an ultrasonic propagation velocity of $\sim 3 \text{ km.s}^{-1}$.	54
Table 6.1: Mineralogical composition of the stone samples.	60
Table 6.2: Chemical composition of the stone samples	61
Table 6.3: The petrographic description of the sound limestone samples.	64
Table 6.4: The textural properties of the studied marble sample.	65
Table 6.5: CIPW-Norms of the basalt samples.	67
Table 6.6: The petrographic description of the basalt samples.	68
Table 6.7: The petrographic description of the naturally-weathered samples.	71
Table 7.1: Porosity and density before and after various numbers of weathering cycles.	88
Table 7.2: Mercury intrusion porosimetry data of the stones before and after salt weathering.	92
Table 7.3: Capillary water absorption before and after 25 cycles of salt weathering.	92
Table 7.4: Drying rate and critical moisture content before and after weathering.	96
Table 7.5: Fracture density of the stones with increasing weathering and percentage of total change.	97
Table 7.6: Biaxial flexural strength and moduli of elasticity before and after salt weathering.	98
Table 7.7: Total dry weight loss (DWL) after 25 cycles of salt weathering.	101
Table 7.8: Ultrasonic pulse velocity in dry and water saturated cubes before and after salt weathering. Measurements were carried out using an ultrasonic frequency of 46 kHz.	102
Table 7.9: Ultrasonic velocity V_p and its percentage of variation with increasing number of salt weathering cycles – Cubic specimens measured with an ultrasonic frequency of 46 kHz.	104
Table 7.10: Ultrasonic velocity V_p before and after salt weathering test (25 cycles) – Prismatic specimens measured with an ultrasonic frequency of 46 kHz.	105
Table 7.11: Ultrasonic V_p before and after salt weathering test (25 cycles) – Prismatic specimens measured with an ultrasonic frequency of 250 kHz.	106
Table 7.12: The physico-mechanical properties of the studied stone samples before weathering.	107
Table (7.13): Pearson correlation coefficients between stone damage and physico-mechanical properties.	108
Table 7.14: Correlations found between DWL and the durability estimator ($DE = W_{\text{abs}} * P_{\text{micro}}$).	110
Table 7.15: Properties of marble before and after thermal weathering.	114
Table 7.16: Mercury intrusion porosimetry data of marble before and after thermal weathering.	116
Table 7.17: Uptake of consolidation product and the amount of dry deposited material in the cubic	

List of tables

and prismatic specimens treated by total immersion and the drill cores treated by capillary rise.	121
Table 7.18: Porosity properties and density before and after consolidation.	122
Table 7.19: MIP results before and after consolidation treatments.	126
Table 7.20: Water vapor diffusion resistance of treated and untreated samples and the percentage increase after treatment.	129
Table 7.21: Drying rate and critical moisture content before and after consolidation.	129
Table 7.22: The variations in chromatic parameters of the treated limestone samples.	131
Table 7.23: The calculated anisotropy in ultrasonic velocity before and after treatment.	143
Table 7.24: Ultrasonic pulse velocity in untreated and treated prismatic specimens measured using ultrasonic frequency of 46 kHz and 250 kHz along one direction (perpendicular to bedding planes).	144

List of abbreviations

N_t	Accessible porosity [%]
N_{48}	Free porosity [%]
W-value	Capillary water absorption coefficient [$\text{kg}/(\text{m}^2 \cdot \text{h}^{1/2})$]
$W_{\text{abs}48}$	Water absorption after 48 h immersion in water [%]
ρ_{real}	Real density [g/cm^3]
ρ_{bulk}	Bulk density [g/cm^3]
S	Saturation coefficient [-]
g	Drying rate [$\text{g}/(\text{m}^2 \cdot \text{h})$]
μ -value	Water vapor diffusion resistance coefficient [-]
V_p	Velocity of the longitudinal ultrasonic wave (ultrasonic pulse velocity) [m/s]
V_s	Velocity of the transverse ultrasonic wave [m/s]
$V_{P\text{-dry}}$	Ultrasonic pulse velocity in dry specimens [m/s]
$V_{P\text{-sat}}$	Ultrasonic pulse velocity in water-saturated specimens [m/s]
A	Anisotropy [%]
DR	Drilling resistance [N]
F_D	Fracture density [mm^2/mm^3]
α_T	Linear thermal expansion coefficient [$10^{-6}/\text{K}$]
β_{BFS}	Biaxial flexural strength [N/mm^2]
E_{stat}	Static modulus of elasticity [kN/mm^2]
E_{dyn}	Dynamic modulus of elasticity [kN/mm^2]
DWL	Total dry weight loss [%]
MIP	Mercury intrusion porosimetry
$P_{m0.1}$	Percentage of porosity with pore radius $r < 0.1 \mu\text{m}$ (microporosity) [%]
P_{m5}	Percentage of porosity with pore radius $r < 5 \mu\text{m}$ [%]
$P_{s\text{Cap}}$	Percentage of porosity of small capillary pores ($0.1 < r < 5 \mu\text{m}$) ($P_{m0.1-5}$) [%]
P_{LCap}	Percentage of porosity of large capillary pores ($r > 5 \mu\text{m}$) [%]
P_{Cap}	Percentage of porosity of capillary pores ($0.1 \mu\text{m} < r < 1 \text{mm}$) [%]
P_c	Total connected porosity calculated by MIP [%]
SSA	Specific surface area [m^2/g]
PCA	Principal component analysis

1 Introduction

1.1 General

Natural stone has been an important building material for thousands of years. A significant part of the world's cultural heritage is built of stone, and it is slowly but inexorably disappearing (Doehne and Price, 2010). Conservation measures need, therefore, to be taken in order to protect irreplaceable stone monuments and to maintain their cultural value and integrity as long as possible.

In Jordan, a land with a diverse cultural heritage mainly built of natural stone, the field of conservation is almost a new subject. There has been a number of studies about the investigation and conservation of Jordanian archaeological stone (e.g. Fitzner and Heinrichs, 1994; Heinrichs and Fitzner, 2000; Al-Naddaf, 2002; Paradise, 2002; Fitzner and Heinrichs 2005; Heinrichs, 2008). Nonetheless, the research on stone conservation there is still very limited and almost restricted to the very famous archaeological sites, particularly the Nabataean city of Petra in the south of Jordan which was carved into sandstone.

The archaeological sites in the north and northeast of Jordan are mainly built of local limestone and basalt. Imported marble was also used in some archaeological sites for decorative and architectural elements. In terms of scientific conservation, these stones are less studied compared to the sandstone of Petra. This work is, therefore, dedicated to investigate stone samples from north and northeast Jordan for the purpose of their conservation.

The conservation of stone is a comprehensive process that entails the characterization of the stone material and its chemical-mineralogical as well as physico-mechanical properties, the description and quantification of its weathering, the understanding of the causes and mechanisms of deterioration, and the application and follow-up of suitable conservation treatments (Fitzner, 2002; Doehne and Price, 2010). The determination of stone provenance and the research in the preservation of historic quarries are also important for the conservation of archaeological stone (Doehne and Price, 2010).

In order to get the required knowledge for the preservation and conservation of stone, various investigation methods are applied. The traditional techniques already in use for the

investigation of natural stone are generally destructive and mostly restricted in use to the laboratory. Owing to the significant importance of archaeological stone monuments and their integrity, new techniques that are primarily non-destructive in nature have been researched and introduced in the conservation field. Ultrasonic technique is one of the most promising non-destructive methods that are increasingly applied for the investigation of archaeological stone monuments and structures. Ultrasonic technique is characterized as well by ease of application, fast acquisition of data and capability for in situ applications (Mamillan, 1958; Simon et al., 1994).

Because of these advantages, the present study aims at the use of ultrasonic technique, validated by traditional methods, for the study of different stone samples (limestone, basalt and marble) from Jordanian archaeological sites. The work consists of studying the structure of the stones and the parameters that govern their deterioration and conservation. This will help to understand the weathering behavior of the stones and their durability and will guide decisions concerning control of deterioration and the necessary conservation treatments.

This work contributes to the research efforts dedicated to characterize Jordanian archaeological stones, including the determination of their microstructure and petrographic characteristics, which could correspondingly be used to determine the possible quarry sources. There have been only a few studies on this topic in Jordan; examples are Bashayrih (2003) and Abu-Jaber et al. (2007; 2009). A main aspect of this study is the contribution to the validation of non-destructive methods for the investigation of archaeological stone. Furthermore, the study aims at developing durability estimators for assessing the resistance of stone to weathering, which can be used to evaluate the level of deterioration and to select suitable materials for restoration works or for new architectural construction. This research tests also the effectiveness of two products of consolidation on the studied limestones.

1.2 Aim of the study

In order to contribute to the preservation and conservation of archaeological stone in Jordan, stone samples from five important and representative archaeological sites (Umm Qeis, Jarash, Ajlun, Umm El-Jimal, and Hallabat) in the north and northeast of Jordan are investigated. The main aim is to study the weathering of the stone samples and their durability and to evaluate

the effectiveness of consolidation treatments focusing on the use of non-destructive ultrasonic methods. For the achievement of this aim, the following research topics are considered:

- What are the microstructural characteristics of the selected stone samples?
- How to describe and quantify their deterioration, and what are the most important parameters affecting their durability?
- How to evaluate and select suitable consolidation product?

In order to address these issues, the following methodology is followed:

- Natural stone samples are selected from five important archaeological sites in north and northeast Jordan. The stones are categorized into two groups of samples (sound and naturally weathered stones) based on preliminary characterization by physical tests and ultrasonic velocity measurements.
- The selected samples are petrographically studied in order to determine their microstructure as well as geological formation. This information can be further used to determine the possible quarry source of the stones, which is important for replacement of stone and research purposes.
- The sound stones are artificially weathered (by salt crystallization test for limestone and basalt and by thermal weathering treatment for marble) and their various properties before and after weathering are studied in order to assess their weathering characteristics and durability.
- The naturally weathered samples are treated by consolidation products and the changes in their properties are studied in order to evaluate the effectiveness of consolidation treatment.

This thesis starts with a brief description of the weathering processes of stone. As the weathering of stone is almost related to the presence of water and is highly determined by pore spaces characteristics, the pore structure of stone and the water transport properties are

also described. The state of the art for weathering assessment and evaluation of consolidation treatments is then discussed. The work proceeds by presenting an overview of the use of non-destructive ultrasonic technique for the investigation of stone. The practical part of the study starts hereafter by describing the characteristics of the studied stone samples and the methods of their investigation. Finally, the results of investigations of the studied stones are discussed and the conclusions of the study are presented.

2 Weathering of stone

In the widest sense of the term, weathering is defined as the whole sequence of reactions of the lithosphere (rocks) with the atmosphere, the hydrosphere (water), and the biosphere (organisms). The changes produced by weathering in rocks are governed by thermodynamics laws (Amoroso and Fassina, 1983). The heterogeneous system composed of the rock and its surrounding environment undergoes irreversible changes in form of material-energy exchange until the entropy approaches its maximum value and the available energy is the least; that is, in theory, until equilibrium is reached (Knöfel, 1980; Neisel, 1995).

From a geological point of view, weathering can be defined as the alteration of rocks under the direct influence of water and atmosphere at or near the earth's surface (Dearman, 1974). When rocks are cut and used in buildings, the chance of deterioration generally increases because other factors get involved (Siegesmund et al., 2002). These factors might include the type of use and the location of the stone in the building, its micro-environment (micro-climate), and the interaction with other building materials. In addition to natural weathering, stone and building materials are also subject to deterioration from anthropogenic factors such as air pollution (Charola, 2004).

The term weathering is usually used to refer to the natural process of rocks decay (Charola, 2004; Siegesmund et al., 2002). However, throughout this work, it is interchangeably used with the term deterioration to indicate all processes that unfavorably alter stone and the corresponding changes in its structure and properties.

2.1 Weathering types

According to the nature of weathering process, three different types of weathering can be distinguished; physical, chemical and biological weathering. However, the biological weathering resulting from the activity of organisms (from bacteria to plants to animals) can be either physical or chemical in character (Pidwirny, 2006). A short description of the physical and chemical weathering is presented in the following subchapters.

2.1.1 Physical weathering

Physical weathering describes mainly the mechanical breakdown and structural disintegration of stone without changing its chemical and mineralogical composition. It is mostly related to the action of water and its connection with other agents such as soluble salts. Water penetrates into the stone and brings it to suffer wetting-drying and freezing-thawing cycles. Furthermore, water acts to transport soluble salts into the stone which then undergo several crystallization cycles, subjecting the stone to destructive pressures (Charola 2004). Physical weathering includes the following factors:

2.1.1.1 Wetting

Wetting is the adsorption of water on pore walls. The adsorbed water reduces the mechanical strength of the stone as it may expand when adsorbing water and contract in drying. Cyclic wetting and drying tend to induce mechanical stresses that rupture the stone (Gauri and Bandyopadhyay, 1999). The presence of clay minerals, salts, and some conservation products such as consolidants enhances the expansion-contraction process and induces therefore further mechanical stresses (Charola 2004). The adsorbed water acts as well to decrease the cohesiveness between the stone grains by disrupting the intermolecular forces causing a reduction in the strength of the stone (Gauri and Bandyopadhyay 1999).

2.1.1.2 Salt weathering

Salt weathering is one of the most damaging processes of historical monuments and architectural structures. The damage of porous building materials due to soluble salts has long been known and regularly studied. An increasing scientific interest in this subject in the recent years is clearly evident, particularly as a comprehensive understanding of the mechanism of salt weathering and the key parameters controlling it is still lacking (Rodriguez-Navarro and Doehne, 1999; Doehne, 2002; Charola, 2004). Salts in building stone may originate from different sources such as soil, atmospheric pollutants, salt spray, inappropriate treatments, inherent salt content or interactions with other building materials (Neisel, 1995; Charola, 2000; Doehne and Price, 2010). When dissolved in water, salts can penetrate into the porous network of stone and may then crystallize there causing damage. Different mechanisms have been proposed to explain the extensive damage of salts in porous materials. These include,

among others, *the hydrostatic crystallization pressure, the hydration pressure and the linear crystal growth pressure.*

Hydrostatic crystallization pressure: This pressure develops when the total volume of the precipitated salt crystals and the saturated solution is larger than that of the supersaturated solution before crystallization (Duttlinger and Knöfel, 1993). Correns and Steinborn (1939) calculated this pressure using the following equation:

$$p = \frac{1}{V_1} \cdot \frac{V_1 - V}{\beta_t} + p_1 \quad (2.1)$$

p = hydrostatic crystallization pressure [atm]; p_1 = atmospheric pressure [atm]; V_1 = the volume of the saturated solution and crystals under p_1 [L]; V = volume of the supersaturated solution under p [L]; β_t = compressibility coefficient of the solution at temperature t [atm⁻¹].

However, the magnitude of this pressure is likely small and can be simply released as the pore system is partially filled with water in practice (Tsui et al., 2003; Espinosa et al., 2008)

Hydration pressure: Salts can usually exist in a number of hydration states. The transition from a lower hydration state to a higher one is accompanied by volume expansion in the salt crystal. This can result in a significant pressure on the pore walls of the material. According to Charola (2000), the hydration pressure was postulated by Mortensen (1933), who proposed an equation for its calculation.

$$P = \frac{nRT}{(V_h - V_a)} \ln\left(\frac{p_w}{p'_w}\right) \quad (2.2)$$

P = hydration pressure [atm]; n = No. of moles of water gained upon hydration; R = ideal gas constant [L·atm/(mol·K)]; T = temperature [K]; V_h = molar volume of the hydrate [L/mol]; V_a = molar volume of the anhydrous salt [L/mol]; p_w = water vapor pressure at temperature T [atm]; p'_w = water vapor pressure of the hydrated salt [atm].

The hydration mechanism has been most of the time examined to try to explain the highly deteriorating effect of sodium sulfate on stone (Charola, 2000). However, experimental studies with environmental scanning electron microscope (ESEM) show that the hydration transition of the sodium sulfate anhydrous phase (thenardite) to the decahydrate phase (mirabilite) is a dissolution-precipitation process and not a continuous expansion of thenardite with moisture absorption (Doehne, 1994; Rodriguez-Navarro and Doehne, 1999). This rules

out the hydration pressure as a credible cause of the observed deterioration by sodium sulfate (Tsui et al., 2003).

Linear crystal growth pressure (usually referred to as **crystallization pressure**): This is the pressure resulted from the growing crystal in the direction of confining pore wall and is widely expressed by the equation of Correns (1949) and Correns and Steinborn (1939):

$$P = \frac{RT}{v} \ln\left(\frac{C}{C_s}\right) \quad (2.3)$$

P = linear growth pressure of crystal (crystallization pressure) [atm]; R = ideal gas constant [L·atm/(mol·K)]; T = temperature [K]; v = molar volume of the solid salt [L/mol]; C/C_s = supersaturation ratio.

According to Steiger (2005a), different expressions for this equation have been proposed (e.g. Neugebauer (1973); Xie and Beaudoin (1992); Benavente et al. (1999)). However, all these equations are relating the crystallization pressure to the degree of supersaturation. According to Charola (2000), Willman and Wilson (1965; 1968) developed another approach for calculating crystallization pressure from a thermodynamic model by analogy with the thermodynamic description of damage caused by frost (see equation 2.4), which was established by Everett (1961). This is based on the properties of curved interfaces between the crystal and the solution (Steiger, 2005a).

Both approaches were used to theoretically calculate crystallization pressures and were often seen as representing two different mechanisms (Steiger, 2005a). Winkler and Singer (1972) and Winkler (1975) calculated the potential salt crystallization pressures in pores based on Corren's equation. However, Corren's equation was subject to criticism because of the unrealistic high supersaturation ratios assumed. It is applicable only for low supersaturation ratios (Duttlinger and Knöfel, 1993). According to Sawdy et al. (2008), this model was shown by Rijniers et al. (2005) to only account for high pressures in very small pores (< 10 nm). However, Houck and Scherer (2006) point out that this conclusion is valid when the crystal is in equilibrium with a solution that bathes its entire surface. High pressures can also develop in large pores if the solution is only present as a film between the crystal and pore wall.

Many authors, such as Fitzner and Snethlage (1982), Zehnder and Arnold (1989), and Rossi-Manaresi and Tucci (1991), preferred to use the second approach specially as it is apparently more realistic to calculate crystallization pressure on the basis of a measurable quantity such

as pore size distribution (Steiger, 2005a). Rodriguez-Navarro and Doehne (1999), among others, point out that this approach does not take into account the Washburn equation (eq. 3.2) which implies that upon evaporation, the saturated solution is suctioned from the larger pores towards the smaller ones where it concentrates. Thus, once a critical saturation is reached, crystallization will take place in the smaller pores, not in the large ones (Rodriguez-Navarro and Doehne, 1999). However, some authors point out recently that these two approaches are actually equivalent in that the driving force for crystallization and stress development in Everett's model is also supersaturation (Scherer, 1999; Flatt, 2002; Steiger, 2005a; b).

Other mechanisms can also contribute to salt damage in porous building materials. These include differential thermal expansion (certain salts have higher coefficients of linear expansion than do the minerals of the rocks in whose pores they occur), osmotic pressure, enhanced wet/dry cycling (caused by deliquescent salts), as well as chemical mechanisms (Goudie, 1998; Doehne, 2002). Although there is still controversy as to the actual mechanism of salt damage in porous building materials, many authors seem to have a common consensus on crystallization pressure as the most plausible deterioration mechanism.

Literature reviews on salt weathering can be found in Duttlinger and Knöfel (1993), Goudie and Viles (1997), Charola (2000), and Doehne, (2002). For problems of salts in masonry see Simon and Drdácký (2006).

2.1.1.3 Frost damage

Frost action plays an important role in stone damage in cold climates. Three main theories for frost damage are described in literature; *the volumetric expansion*, *the hydraulic pressure*, and *the crystallization theory* (or *Ice lens theory*) (Hirschwald, 1912; Ross et al., 1991; Miglio et al., 2000; Setzer, 2002).

The **volume expansion** theory is related to the characteristic property of water, which expands by cooling below +4 °C and by freezing to ice. The density of ice is lower than that of water, which results in a volume expansion of around 9% when pure water transforms to ice under atmospheric pressure (Hirschwald, 1912). The volume expansion resulting from the freezing of water in the pores of a stone will generate pressure on the pore wall. When the generated

shattering force exceeds the tensile strength of the stone, failure occurs. The stone may also rupture due to the fatigue caused by cyclic freezing and thawing (Lienhart, 1993).

The *hydraulic pressure* theory relies also on the volume expansion associated with the freezing of water, but ice is not the damaging phase in this case. Owing to the resulting volume expansion, a growing ice crystal will push away the unfrozen water from the pore. If this water is expelled into fine pores at a high rate, there will be a considerable resistance to flow leading to the development of hydraulic pressure (Powers, 1945; Ross et al., 1991). Chatterji and Christensen (1979) described a second mechanism whereby hydrostatic pressure can develop in a water-saturated stone when the water in the pores can not escape (Ross et al., 1991).

The *crystallization theory* was proposed as a mechanism for frost damage by Taber (1929; 1930), who suggested that frost damage may be due to a crystallization process in which an ice crystal continues to grow in a pore and builds up pressure on its wall (Ross et al., 1991). The freezing point of water in small pores is depressed because of the higher specific interfacial energies (Snethlage, 1984). By decreasing temperature, ice tends, therefore, to form and grow in large pores, whereas the water in very fine capillaries remains unfrozen even at very low subfreezing temperatures (due to high vapor pressure) (Gauri and Bandyopadhyay, 1999). Everett (1961) pointed out that frost damage could occur when the ice crystal formed in large pores continues to grow by withdrawing water from the adjacent micropores. The suction force causing this water migration is determined by the pressure difference at the curved meniscus of the ice-water interface, and it is regarded to be equivalent with the shattering force (Matsuoka, 1990). When the ice crystal fills the large pore, it will either grow into the surrounding smaller pores or exert pressure on the pore wall causing damage (Miglio et al., 2000). The generated pressure can be expressed by the following equation (Snethlage, 1984):

$$\Delta p = 2\sigma_{iw} \left(\frac{1}{r} - \frac{1}{R} \right) \quad (2.4)$$

Δp = the difference between ice pressure and pore water pressure [N/m²] (convenient unit: N/mm²);
 σ_{iw} = the free energy of the ice-water interface [N/m]; r = the radius of the capillary pore [m] (convenient unit: μm); R = the radius of the large pore [m] (convenient unit: μm).

According to Ross et al. (1991), it is unlikely that any single mechanism of frost action will completely explain the damage observed in stone. In practice, all these mechanisms can

contribute to the induced damage, but one mechanism might be dominant depending on the prevailing freezing conditions. Frost damage is controlled both by environmental factors such as the intensity (critical temperature for crack propagation), rate and duration of freezing and by the mechanical and physical properties of stone such as tensile strength, critical saturation and degree of pore filling with water, porosity and pore size distribution (Lienhart, 1993).

2.1.1.4 Thermal weathering

The thermal weathering of stone is related to the thermal characteristics of its mineral constituents. The minerals forming a stone expand and contract as a result of temperature changes. The resulting relative change in length is proportional to the magnitude of temperature change by the linear thermal expansion coefficient as given in the following equation (Kleber et al., 1998):

$$\frac{\Delta l}{l_0} = \frac{(l - l_0)}{l_0} = \alpha \cdot \Delta T \quad (2.5)$$

l_0 = initial length [mm]; l = final length [mm]; α = linear thermal expansion coefficient [$10^{-6}/\text{K}$]; ΔT = temperature change (final temperature – initial temperature) [K].

Different minerals have different thermal expansion coefficients and correspondingly different expansions and contractions by temperature changes. Furthermore, the thermal expansion coefficient of a crystal is often directionally dependent; it differs along the different crystallographic axes. This is particularly significant for calcite crystals, which have a distinctive thermal anisotropy. When heated, a calcite crystal (Figure 2.1) expands in the direction parallel to the c-axis and contracts in the normal directions (Lewin, 1990; Kleber et al., 1998).

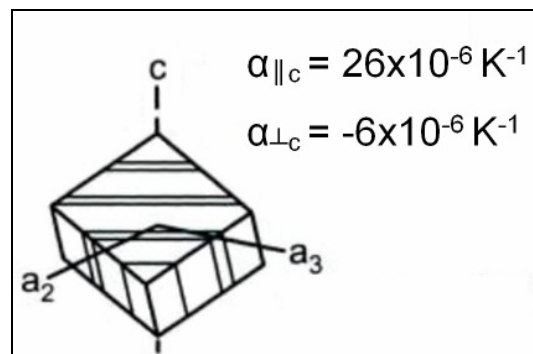


Figure 2.1: Linear thermal expansion coefficients of calcite crystal along the different crystallographic axes in an average temperature range from around 0–100 °C (from Ruedrich et al., 2002).

Because of the anisotropy and differences in thermal expansion coefficients of the constituent mineral grains, temperature variations will produce thermal stresses in the stone that may eventually lead to structural disintegration. This is especially significant in stones with large crystals such as marble and granite (Charola, 2004). Many authors have studied thermal weathering of stone, especially marble (Kessler, 1919; Sage, 1988; Siegesmund et al., 2000; Simon, 2001; Zeisig et al., 2002; Ruedrich et al., 2002; Malaga-Starzec et al., 2002; Rodríguez-Gordillo and Sáez-Pérez, 2005). The studies emphasize that thermal stresses resulting from changes in temperature can be sufficiently large to produce microfractures and microcracks in and between the mineral grains of the stone (Robertson, 1982). Kessler (1919) found that thermally treated marbles show a remarkable non-reversible change in length especially during the first heating cycle (Sage, 1988; Siegesmund et al. 2000; Simon, 2001). Even small, but continuous temperature variations may cause damage (Winkler 1997; Zeisig et al., 2002; Ruedrich et al., 2002). Kocher (2004) showed that the thermal stress resulting from temperature increase can be equal to or even greater than the resulting stress from the swelling of clay minerals in sandstone. He points out that the influence of the changes in diurnal ($\Delta T_{\max} = 40\text{ }^{\circ}\text{C}$) and seasonal ($\Delta T_{\max} = 80\text{ }^{\circ}\text{C}$) temperatures in moderate climatic zones on the weathering of stone is comparable to, if not even more significant than, that of the variation of moisture.

2.1.2 Chemical weathering

Chemical weathering is the alteration of the chemical and mineralogical composition of stone by a number of different processes such as dissolution, oxidation, hydration and hydrolysis (Pidwirny, 2006). Water, with its different gaseous constituents such as CO_2 , and SO_2 , is the most important agent in these chemical reactions; it acts as a solvent and also as a chemical reactant (Neisel, 1995).

2.1.2.1 Dissolution

Dissolution is the process whereby some minerals or part of their chemical composition dissolve in water. The elements of alkali (K, Na) and alkaline earth (Ca, Mg) belong to the readily soluble mineral constituents, because of their low ion potentials (quotient of ion

charge over ion radius) (Villwock, 1966; Neisel, 1995). The simplest solution reactions are primarily related to salts (Winkler, 1975). Chloride and magnesium sulfate are among the most soluble substances in water. Gypsum dissolves less readily in water and carbonates solubility is even lower (Ollier, 1984; Neisel, 1995).

With increasing ion potential, the pH-value of water plays an important role in the solubility of a substance (Ollier, 1984; Neisel, 1995). The solubility of rock forming minerals increases generally with the decrease in pH of the water, i.e. in acidic solutions (Steiger et al., 2011). Therefore, the dissolution of atmospheric gases (either naturally occurring or products of pollution) in rain water increases its corrosive effects.

In natural environment, the carbonate minerals react with carbon dioxide dissolved in rain water and the resulting dissolved ions are drained away from the stone, causing surface erosion over time. In polluted environment, the deposition of gaseous pollutants and aerosols on the surface of carbonate stones is responsible for the accelerated rate of their deterioration. Carbonate stone reacts with the adsorbed sulfur and nitrogen oxides and undergoes mineral alteration, which results in the dissolution of the emerging products in areas exposed to rain or washout and the development of crusts, largely made of gypsum, in sheltered places (Gauri and Bandyopadhyay 1999).

2.1.2.2 Hydrolysis

Hydrolysis is the dissolution and alteration of minerals by the reaction of their ions with the ions of water (OH^- and H^+). It results in the decomposition of the rock surface by forming new compounds and by increasing the pH-value of the solution involved through the release of the hydroxyl ions. Hydrolysis is especially effective in the weathering of common silicate and aluminosilicate minerals because of their electrically charged crystal surfaces (Pidwirny, 2006). The weathering of silicate minerals (such as feldspar) follows by leaching out the soluble elements (alkali and earth alkaline metal ions) from the silicate network and replacing them with the dissociated hydrogen ions. As the process proceeds, the alumina-silicate network will loosen and aluminum and silica are dissolved and drained away as well. This may result in the formation of clay minerals (hydrated alumina silicate), which settle in place or can be transported and deposited elsewhere (Neisel, 1995; Gauri and Bandyopadhyay 1999).

2.1.2.3 Oxidation reactions

Oxidation is the reaction of a compound with oxygen that results in the increase of the oxidation state of the compound by the removal of one or more electrons (Pidwirny, 2006). The oxidation of divalent metal cations to a higher valence (oxidation) state occurs mainly by the chemical reaction with the oxygen dissolved in water, which induces red-brown color changes in stone (Neisel, 1995). Oxidation is an important process in the alteration of iron and magnesium rich minerals. The oxidation of Iron II to Iron III results in color changes and weakens the structure of the mineral. Oxidation reactions can be especially harmful for stones (limestone or marble) containing sulfide minerals such as pyrite, which oxidized and hydrated to form iron sulfate and sulfuric acid. Thus, not only red iron rust spots will be produced, but also the released sulfuric acid will accelerate the chemical weathering of the other mineral constituents of the stone (Villwock, 1966; Neisel, 1995).

2.2 Weathering forms

The action of the complex weathering processes on building stones results in different changes in their properties and nature. Weathering changes the original structure, mineralogy, and chemistry of the stone material leading eventually to total disintegration. These changes manifest themselves in the form of a broad spectrum of deterioration patterns. The categorization and classification of weathering forms is important for the characterization, quantification and rating of stone weathering (Fitzner et al., 1995). Geometrical and phenomenological descriptions and classification schemes for macroscopic weathering forms on building stone have been established and developed (Fitzner and Kowantzki, 1990; 1991; Fitzner et al., 1992; Fitzner et al., 1995; Fitzner and Heinrichs, 2002). One of the problems relating to the description and classification of weathering is finding a common language (Doehne and Price, 2010). To overcome terminological confusions and to simplify the recognition and comparison of different degradation forms, an illustrated glossary on stone deterioration patterns has been recently prepared by ICOMOS Stone Committee (ICOMOS-ISCS, 2008). Figure (2.2) shows weathering patterns of flaking and powdering that are most commonly found on stone due to salt crystallization (Charola, 2000). Figure (2.3) shows the detachment of laminated stone, possibly due to frost damage.



Figure 2.2: Granular disintegration and flaking of stone induced by salt crystallization (from ICOMOS-ISCS, 2008).



Figure 2.3: Delamination of a sandstone gravestone possibly resulting from frost action (from ICOMOS-ISCS, 2008).

It is clearly evident that water is the driving force behind almost all weathering processes. The transport and storage of water within the porous material is controlled by its pore structure. Therefore, the study of the porous system of the material and water transport and storage properties constitutes the basis for understanding weathering processes and their influence on the material (Snethlage, 1984). The next chapter presents a description of pore structure and the mechanisms of water transport and storage in porous building materials.

3 Pore structure and water transport

3.1 Pore structure

Stones, or rocks in general, are characterized by a complex pore structure. This structure influences the different properties of the stone and controls its weathering processes (Fitzner and Basten, 1994). The description of pore space characteristics is, therefore, an indispensable step.

3.1.1 Porosity

Porosity is a fundamental property of rocks. It refers to the ratio of the volume of voids to the total volume of the rock, expressed as a percentage. In general, porosity can be classified based on different geometric, morphologic and diagenetic aspects or criteria. On the basis of petrogenesis, the porosity of a rock can be divided into primary porosity which refers to the porosity at the time of deposition or formation and secondary porosity that develops long after the rock's formation (Tucker and Wright 1990; Fitzner and Basten, 1994). These two porosity types can be further classified based on their shape and position in the fabric of the rock. Pores and cracks that exist between the grains or crystals of the rock are referred to as interparticle (or intergranular) porosity, whereas intraparticle porosity describes the pore space within the grains or crystals (Fitzner and Basten, 1994). Choquette and Pray (1970) divided the porosity in sedimentary carbonate rocks into different types as shown in Figure (3.1).

Based on the permeability or typology, the pore space can be classified into open pores and closed pores. Closed porosity refers to all those pores that are totally isolated from the external surface of the material, allowing no access of water either in liquid or vapor phase. Open porosity, on the other hand, comprises the connected pores which are accessible to fluids and external atmosphere. These pores can be further classified based on their interconnectedness as shown in Figure (3.2). For weathering processes, only open pores are of significant importance (Meng, 1993).

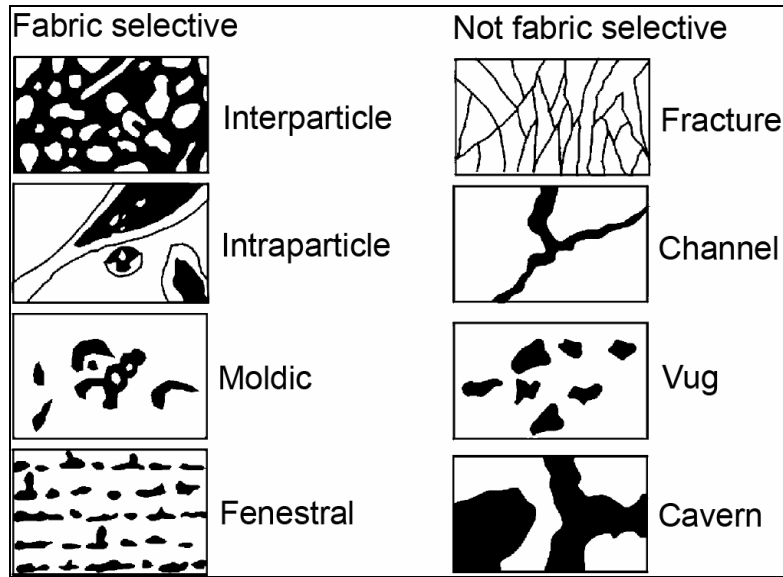


Figure 3.1: Porosity types (from Tuğrul, 2004, after Choquette and Pray, 1970).

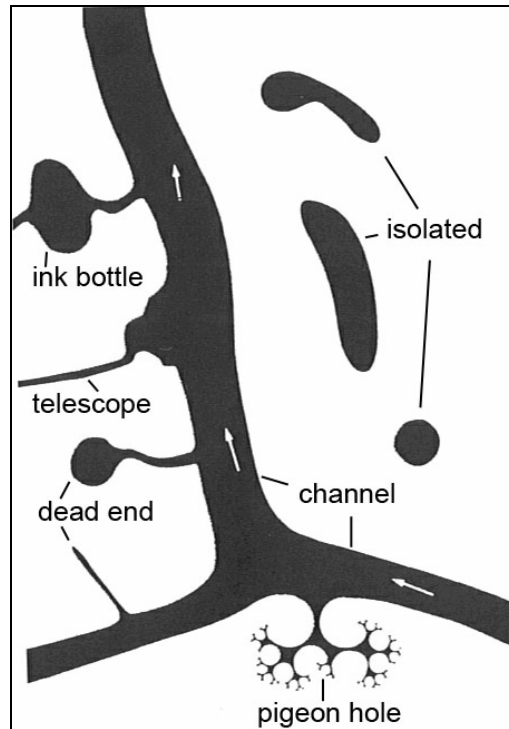


Figure 3.2: Pore types (Fitzner and Basten, 1994).

3.1.2 Pore size and pore size distribution

The pore structure of a material is also characterized by the size of pores. This parameter is particularly significant because it controls the water absorption and transport properties in the material (Vos, 1976; Yu and Oguchi, 2009a). Pores in stones vary in size from a few nanometers to several millimeters. Voids of larger size are referred to as cavities rather than

pores, whereas pores in the Angstrom (\AA) range are not considered permeable (Fitzner and Basten, 1994; Borrelli, 1999).

The classification of pores according to their size is important to help understand the influences of pores of various sizes on the properties of porous materials. However, people in different fields use different classification schemes for pore sizes (Table 3.1).

Table 3.1: Classification of pore size diameter in different fields.

Building physics classification (Klopfer, 1985) (water transport mechanism)	Micropores < 0.1 μm	Capillary pores 0.1 μm – 1 mm	Macropores > 1 mm
IUPAC-classification (Gregg and Sing, 1982) (adsorption mechanism)	Micropores < 2 nm	Mesopores 2 nm – 50 nm	Macropores > 50 nm
Concrete science (Romberg, 1978; Stark and Wicht, 2001)	Gel pores < 10 nm	Capillary pores 10 nm – 100 μm	Air pores 1 μm - 1 mm

In building physics and conservation field, three main groups of pore sizes are distinguished: micropores, capillary pores and macropores. The division limits between these pore types is not that sharp, particularly for micropores. Different studies usually report different dividing pore radii for micropores; the upper limit often ranges between 0.05 μm and 5 μm (Yu and Oguchi, 2009a). In this study, the following classification of pore radius size is used:

- Micropores: $r < 0.1 \mu\text{m}$
- Capillary pores: $0.1 \mu\text{m} < r < 1 \text{ mm}$
(Small capillaries: $0.1 \mu\text{m} < r < 5 \mu\text{m}$; large capillaries: $5 \mu\text{m} < r < 1 \text{ mm}$)
- Macropores: $r > 1 \text{ mm}$; where r is the pore radius.

Because of the complexity of pore structure and the wide range of pore sizes, different methods and measurement procedures are usually used and combined to characterize the pore space and to determine the size of pores. Direct characterization of pore space can be achieved by light and electron microscopes. Indirect measurements of pore parameters are carried out by a number of methods that are mainly based on the intrusion and extrusion of liquid phases in pores or the adsorption of gases on their surfaces (Fitzner and Basten, 1994). Figure (3.3) shows the different methods usually used to characterize and measure the pores of stone and their measuring ranges.

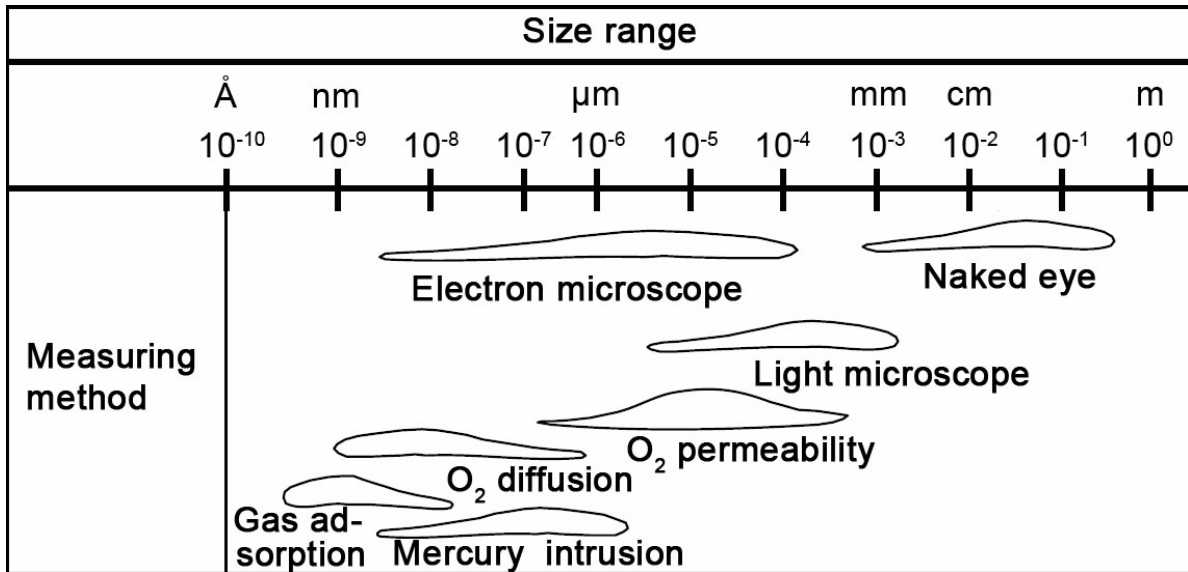


Figure 3.3: Characterization methods of pore size and their measuring ranges (after Setzer, 1975).

3.2 Water transport in porous materials

3.2.1 Water transport mechanisms

Water can enter a porous material either in liquid or vapor phase (Charola, 2000). The transport characteristics of water within the porous material depend on the pore size. Figure (3.4) shows the various mechanisms of water transport in pores of different sizes. An explanation of these mechanisms is presented in the following sections.

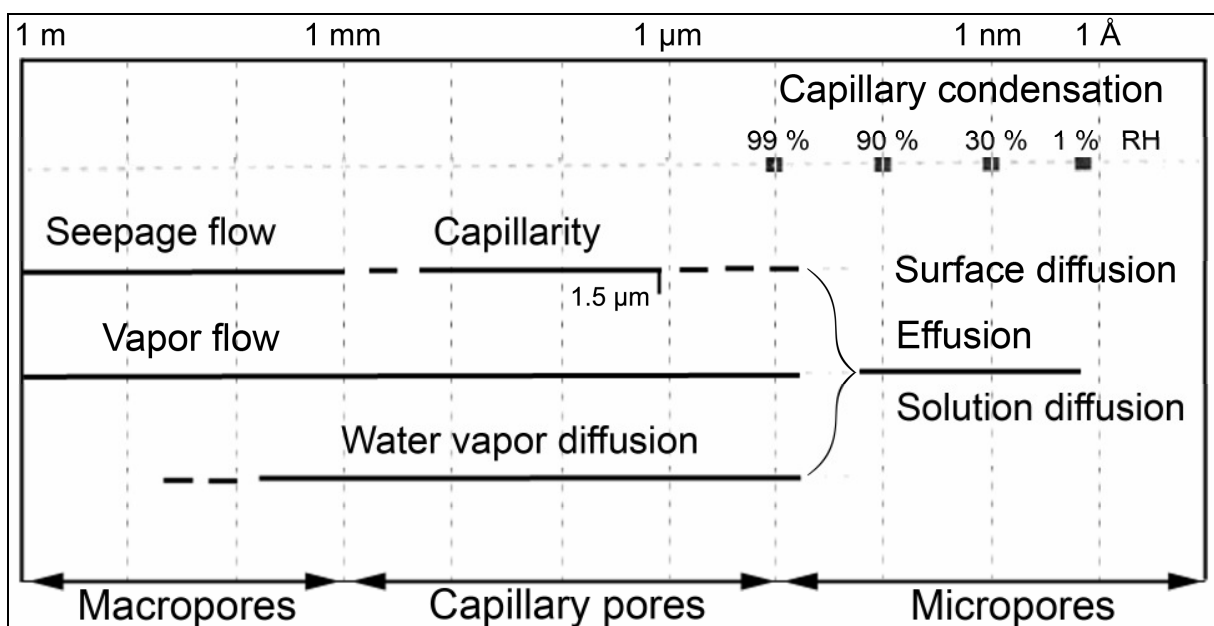


Figure 3.4: Moisture transport mechanisms (from Snehlage, 1984 and Neisel, 1995; after Klopfer, 1979; 1980).

3.2.1.1 Diffusion of water vapor

The diffusion of water vapor into and within a porous material is based on the thermal intrinsic movement of the water molecules (Brownian molecular motion) (Klopfer and Homman, 2008). In contact with moist air, a hygroscopic porous building material (such as building stone) adsorbs moisture by adsorption of water molecules on the surfaces of their pores until the equilibrium moisture is reached. The equilibrium hygroscopic moisture content of the porous material at constant temperature depends on the relative humidity of the surrounding air. If the porous material contains hygroscopic salts, its equilibrium moisture increases depending on the type and amount of salt (Künzel, 2007). In the same way, a moist material will release water (desorb) with decreasing relative humidity until the water vapor pressure in its pores is in equilibrium with that in the ambient air. At a constant temperature, the moisture content of a porous material is a function of the relative humidity. The change in the moisture content of the porous material with increasing and decreasing relative humidity is thus given by the adsorption and desorption isotherms (Amoroso and Fassina, 1983; Snethlage, 1984; Künzel, 1995).

The diffusion of moisture takes place in the direction of partial pressure gradient of water vapor. The adsorbed water film on the pore walls of a hygroscopic material is composed of one or more molecular layers (thickness of one molecular layer of water is approximately 0.3 nm) (Neisel, 1995).

The diffused water molecules in the pores of a stone undergo a set of collisions between each other and with the walls of pores. The traveled way of these molecules will, therefore, be in form of a zigzag line. The mean free path between two successive collisions for a water molecule in air at normal conditions of 20 °C temperature and a total pressure of 1 bar is around 40 nm. The pore diameter needs, therefore, to be at least 100 nm in order to allow for more collisions between the water molecules than with the pore walls, and correspondingly to allow for *water vapor diffusion* (Klopfer and Homman, 2008). The upper pore limit for water vapor diffusion lies, however, in the centimeter range where masses movement owing to *convection diffusion* takes place (Neisel, 1995). In fine pores smaller than 10 nm, that is smaller than the mean free path of water molecules, the traveled way of water molecules is

determined more by their collisions with pore walls than with each other, giving rise to *water vapor effusion* (Knudsen molecular transport) (Figure 3.5) (Klopfer and Homman, 2008).

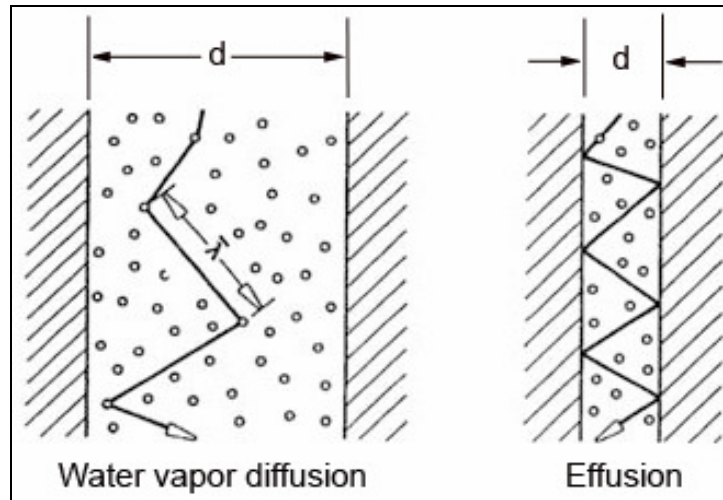


Figure 3.5: The mean free path of water molecule and water vapor diffusion and effusion (Klopfer and Homman, 2008).

When the temperature of a stone surface is lower than the dew point temperature of the ambient air, condensation occurs on the surface. Condensation could also interstitially occur inside the pores of the material even when the temperature of the surface is above the dew-point temperature (Torraca, 1982; Amoroso and Fassina, 1983). Capillary condensation is a result of the decreased vapor pressure above the liquid meniscus in small pores which has strong curvature (Meng, 1993). For average relative humidity, the capillary condensation is possible in pores smaller than $0.1 \mu\text{m}$ (micropores). The pores moistened by capillary condensation are filled with water although the outer conditions allow no condensation in macroscopic pores. This condensed water is not easily released from the pores of the material (Snethlage, 1984).

3.2.1.2 Transport of liquid water

Building stones absorb and transport liquid water into their capillary pore structure by the action of capillarity. This is particularly important in pores of small radius (capillary pores). The capillary action is a result of the attraction of water and pore wall (adhesion-wetting) and the surface tension of water (cohesion) (Charola, 2000).

The molecules of a water film are attracted to each other by intermolecular forces. The water molecules at the surface do not have other like molecules on all sides of them as the internal

molecules. Consequently, they cohere more strongly to those directly associated with them on the surface. This enhancement of the intermolecular attractive forces at the surface is responsible for the surface tension of water, which is 0.0728 N/m at 20 °C.

Because of the attractive intermolecular forces, liquids tend to achieve the smallest possible surface area. Therefore, liquids tend to form spherical drops when freely suspended as the spherical configuration represents the smallest surface-to-volume ratio. On contact with solids, a liquid drop forms an angle with the surface of the solid. The contact angle is determined by the resultant force of the cohesive liquid-liquid molecular forces and the adhesive solid-liquid forces and depends on the characteristics of the solid and liquid involved (Gauri and Bandyopadhyay 1999). For a contact angle between 0° and 90° ($0^\circ < \theta < 90^\circ$), we speak of a wetting liquid that rises in capillary pores of the material, resulting in capillary ascension. A non-wetting liquid, on the other hand, forms a contact angle between 90° and 180° with the pore wall, and is correspondingly pulled down in the pore resulting in capillary depression (Figure 3.6).

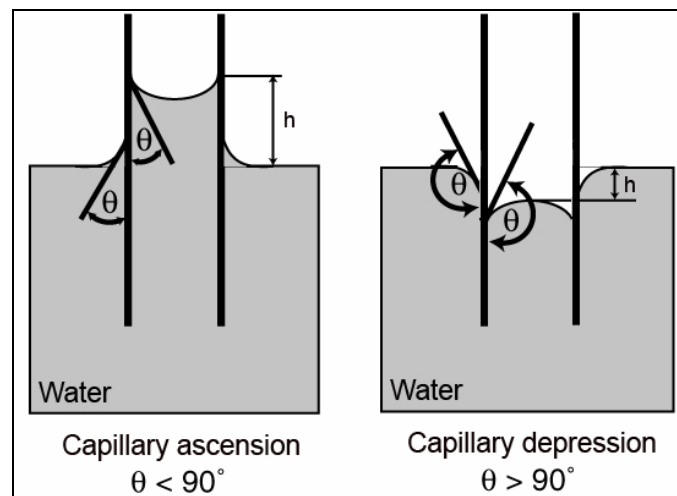


Figure 3.6: Impact of surface tension of water (capillary ascension and capillary depression) (from Snethlage, 1984).

Building stones are composed of carbonates, silicates, aluminates or oxides. These compounds contain oxygen atoms which are electronegative or hydroxyl groups which are polar because of the higher electronegativity of the oxygen atom. Pore surfaces with polar atoms (oxygen) or groups (hydroxyl) show strong attraction for polar molecules, such as water. Therefore, such surfaces attract water molecules and are called hydrophilic (Torraca, 1982; Amoroso and Fassina, 1983). Correspondingly, liquid water can be absorbed and

transported (either horizontally or vertically) within the capillary pores of building stones by **capillary action** (capillarity). The driving force here is the negative capillary pressure given by the simple form of Young and Laplace equation (Karkare and Fort, 1993).

$$p_c = p_w - p_a = \frac{2\sigma}{r_\kappa} \quad (3.1)$$

p_c = negative capillary pressure [Pa= N/m²]; p_w = pressure inside water [Pa]; p_a = ambient air pressure [N/m²]; σ = surface tension of water [N/m]; r_κ = mean curvature radius [m].

For cylindrical capillary pores, the mean curvature radius depends on the radius of the capillary pore ($r_\kappa = r/\cos\theta$) and the capillary pressure is, thus, given by Washburn equation (Meng, 1993).

$$p_c = \frac{2\sigma}{r} \cos\theta \quad (3.2)$$

p_c = negative capillary pressure [Pa]; σ = surface tension of water [N/m]; r = capillary pore radius [m] (convenient unit: μm); θ = contact angle (water-pore wall) [°].

Capillary water transport is generally effective in the pore radius size range from 0.1 μm to 1 mm. However, at a negative pressure of 1 bar (10⁵ N/m²), the continuity of the water column is interrupted because the apparent tensile strength of water is exceeded. The negative capillary pressure reaches 1 bar at the pore radius of 1.5 μm . This pore radius determines, therefore, the lower limit for capillary water transport. In smaller pores, the capillary liquid transport is probably replaced by **surface diffusion** (Klopper, 1979; 1980; Snethlage, 1984). **Surface diffusion** describes the molecular motion within the adsorbed water film (thickness up to 20 molecular layers) on the mineral surfaces of the pores (Neisel, 1995).

The water front inside the pore of a stone exhibits a typical concave meniscus, because the centre of the water surface is drawn inwards by the attraction of water molecules while close to the pore surface the attraction towards the pore walls prevails (Torraca, 1982; Amoroso and Fassina, 1983). The capillary action is determined by the combined effect of four forces, namely capillary force, force of gravity, viscosity, and external pressure force (Snethlage, 1984). The capillary force is usually large enough to offset the force of gravity and make water rises inside pores of sufficiently small size, resulting in capillary rise. If water suction is not counterbalanced by other mechanism such as evaporation, the capillary rise against gravity might theoretically reach a height of many meters (Torraca, 1982).

In pores larger than 1 mm, the effect of gravity on the liquid columns inside the pores is greater than the capillary force. Therefore, liquid water infiltrates and moves freely within the pore space following the laws of hydrostatic pressure; water will run down large openings and cracks. The *seepage flow* due to gravitation depends on the permeability of the material and it falls within the validity limits of Darcy's law¹ for laminar water flow (Neisel, 1995; Klopfer and Homann, 2008).

Other mechanisms of water transport in the liquid phase include hydraulic flow, electrokinesis, and osmosis (Künzel, 1995). More details about the mechanisms of water transport and storage in porous building materials can be found in Klopfer and Homann (2008).

3.2.2 Water content and moisture storage

The distribution and transport of water within the pores of a stone is actually determined by various mechanisms that act in parallel. These mechanisms depend on the *water content* of the pores and on their *size*. The widely varied pore radii of stone give rise to the simultaneous action of different transport and storage mechanisms. Pores smaller than 10 nm constitute the molecular water transport region where effusion takes place. In pores larger than 1 μm (continuous transport region), the water transport takes place by capillary forces and water flow, or rather by diffusion when the pores are not filled with water. In the transition region with pore size between 10 nm and 1 μm , various mechanisms of moisture transport are operative (Leimer, 2004).

The *water content* of the stone is determined by the temperature and relative humidity of the ambient air. Figure (3.7) shows the different phases of the water content of a porous material by increasing moistening as described by Rose (1965). In a very dry stone, all the diffused water vapor into the stone will be first adsorbed on the pore walls (phase A). This adsorbed water remains immovable because of high adhesive forces and one can not yet speak of an actual transport (Klopfer and Homann, 2008). When the pore walls are overlaid with one or more molecular layers of water (phase B), water vapor begins to diffuse into the adjacent

¹ an empirical relationship between the instantaneous liquid flow through a porous medium; the cross-sectional area perpendicular to the flow, the viscosity of the liquid and the pressure drop over a given distance.

pores. With increasing water vapor content, the capillary pores will be filled with liquid water because of the incipient capillary condensation (phase C). In this phase, the water transport takes place by vapor diffusion in large pores and by capillary forces in small capillaries. As the total moisture rises, the adsorbed water film becomes sufficiently thick to allow for surface diffusion, and the water transport increases appreciably because a continuous water transport in the liquid phase is now possible (phase D). In phase (E), the pores contain enough water to allow for an effective non-saturated flow and capillary conduction. The pores in the last phase (phase F) are saturated with water and transport takes place by capillarity and by saturated flow according to Darcy's law (Klopfer and Homann, 2008).

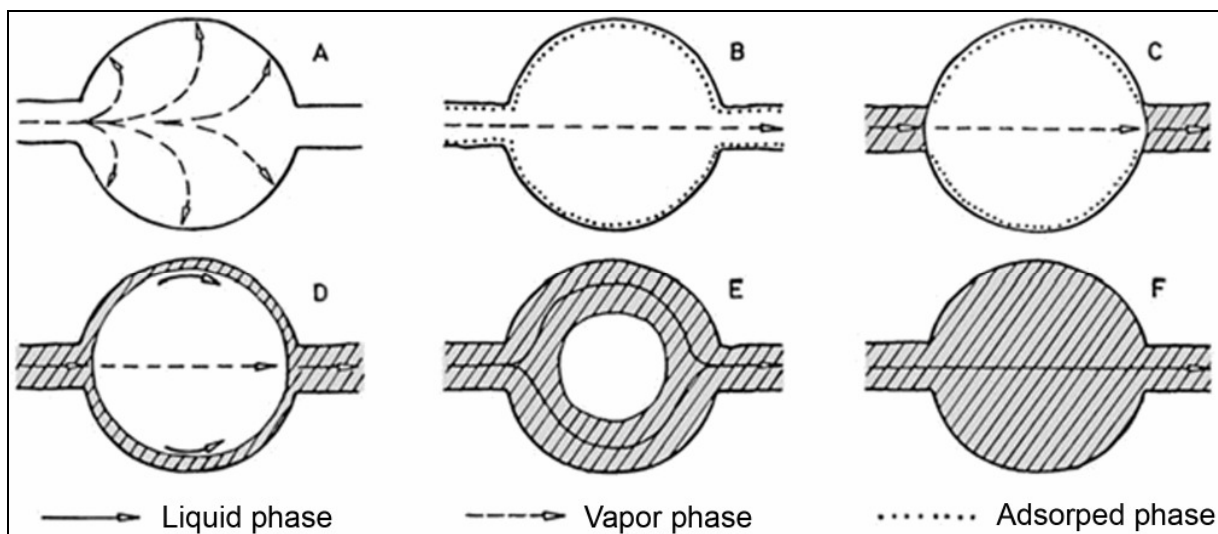


Figure 3.7: Water content of a porous material by increasing moistening as described by Rose (1965) (from Klopfer and Homann, 2008).

It is clear from this diagram that moisture transport in a relatively dry stone takes place by water vapor diffusion, which is then increasingly replaced by capillary condensation. At high moisture content, more efficient transport mechanisms such as capillary conduction and water flow come into play (Leimer, 2004).

The moisture content of a building material can be expressed as a fraction or ratio of the volume of water to the total volume of the material (ψ) or as fraction or ratio of the mass of water to the total mass of the material (u). The possible water content of a hygroscopic capillary-active building material from dry to water saturated conditions is shown in Figure (3.8) (Klopfer and Homann, 2008). Three regions of moisture content can be distinguished: the sorption moisture region (hygroscopic region), the capillary water region (super-hygroscopic region), and the supersaturated region. The hygroscopic region characterizes the

sorption moisture region from the dry state up to equilibrium hygroscopic moisture of 95% pore relative humidity (ψ_{95} or u_{95}); this characterizes the situation in which all micropores are filled with water. In this region the water transport takes place by water vapor diffusion, and the moisture storage is determined by the adsorption process. The capillary water region follows the hygroscopic region and characterizes the water filling of larger pores up to free water saturation (capillary saturation) (ψ_f or u_f). The water transport here is determined by non-saturated water flow and capillarity. In the supersaturated region, the relative humidity in the pores is 100% (regardless of the water content) and no more equilibrium states do exist. This region can not be reached by normal suction or only after a very long time by dissolution of the encapsulated pore air in water. It occurs in practice through diffusion in the temperature gradient, and in laboratory through suction under pressure. The maximum water content (ψ_{\max} or u_{\max}) corresponds to the complete filling of all accessible pores (Künzel, 1995; Klopfer and Homann, 2008).

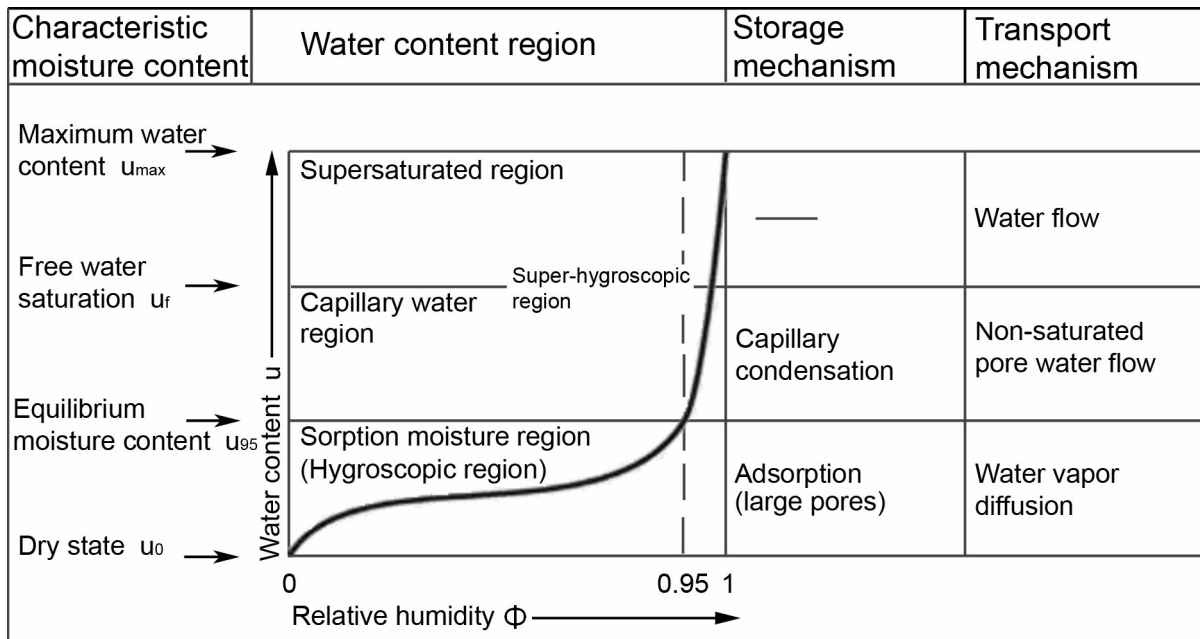


Figure 3.8: Water content of a porous hygroscopic building material (from Klopfer and Hofmann, 2008).

3.2.3 Evaporation

Most of the damage in buildings occurs during the drying process. Evaporation from the surface of a porous body is governed by the environmental conditions (temperature, relative humidity, air velocity) and the pore structure of the material. “When a water-saturated stone dries, evaporation takes place initially from the surface at a rate that depends on the

environmental conditions. In the absence of ventilation and at high relative humidity, the evaporation rate is very low and the surface remains wetted. If ventilation occurs, the evaporation rate increases and the surface will remain wetted, allowing evaporation to continue at a constant rate, as long as the movement of water to the surface is quickly enough to compensate for the loss by evaporation'' (Amoroso and Fassina, 1983).

Inside the pores, the lack of air circulation causes rapid saturation (RH ~ 100%) so that an efficient evaporation occurs only on the external surface (Torraca, 1982). However, this equilibrium can not remain for long time because of the widely varied pores size distribution of stone. Water molecules in larger pores will pass into the vapor phase more rapidly than those in smaller ones. When the amount of water brought to the surface becomes too small to keep the surface wetted, the evaporation rate falls off. Therefore, in materials in which water can move easily, most of the drying takes place at the surface. In dense materials, however, the initially constant evaporation rate persists for only a small proportion of the drying period; the surface may dry long before all the pores have emptied, and at some point below the surface, the material may still be saturated. The water front retreats into the stone and the drying velocity decreases rapidly. The moisture content corresponding to this discontinuity is called the critical moisture content (Amoroso and Fassina, 1983). Below this critical water content, the transport of the liquid water to the surface is no longer possible and the less efficient water vapor diffusion is operative. The drying rate drops at this stage, when considerable amount of water may still be present. The complete drying of the material is quite difficult (Torraca, 1982; Amoroso and Fassina, 1983).

Figure (3.9) summarizes the sequence of water occupation and distribution within the pore space of a stone (hydrophilic material) as passing through four levels of increasing water content (Torraca, 1982). The first level (level 1) represents the completely dry material with all pores empty. The second level (level 2) corresponds to the adsorption of water on the surfaces of capillary pores until they are filled. The surfaces of large pores at this stage are still dry. At the third level (level 3), the surface of large pore adsorbs water from capillaries. Finally, both capillary and large pores are filled with water (level 4). This sequence is reversed when the material dries. However, level 3 occurs mainly upon wetting, while level 2 upon drying. Any water content above that corresponding to level 3 should allow for water transport in the liquid phase. This level might thus be equivalent to the critical moisture content (Torraca, 1982).

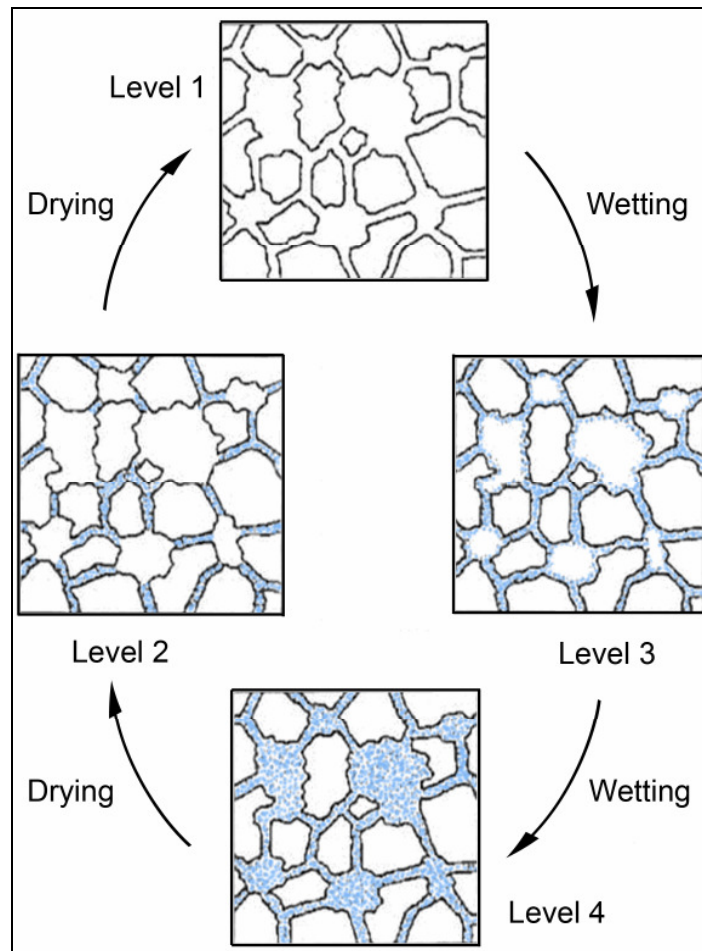


Figure 3.9: Water occupation and distribution within the pore space of a stone (modified from Gauri and Bandyopadhyay, 1999 after Torraca, 1982).

4 Evaluation of weathering and consolidation treatments

Having explained the different weathering types of stone and the pore structure and water transport properties which control weathering, the state of the art for the study and evaluation of stone deterioration and consolidation treatments is presented in this chapter.

In the first section, an overview of the assessment of stone durability and weathering is given and the most important properties that affect stone durability are discussed. Accelerated weathering tests as an approach for studying stone deterioration and assessing its durability are considered and the nature of the induced stress on the pore walls is further explained.

In the second section of this chapter, the consolidation of stone and the evaluation of the effectiveness of consolidation treatments are presented. Alkoxysilane (ethyl silicates) consolidants and their particular application on carbonate stones are briefly discussed.

4.1 Stone durability and weathering assessment

The assessment of the intensity of stone deterioration is an essential aim for preservation and conservation purposes (Siegesmund et al., 2002). For the quantification of deterioration, a fundamental understanding of stone weathering mechanisms and their influence on stone structure is necessary. Weathering processes affect the physical and mechanical properties of stone and induce various changes in its structure (Nicholson, 2001; Benavente et al., 2004). Changes in stone due to weathering might include modification of porosity and pore structure, development of cracks and loss of stone cohesion (Tuğrul, 2004).

The study of these changes and the correlation of stone properties in different weathering conditions with easily measurable quantities help to develop classification schemes whereby the deterioration level of stone can be assessed. For example, Köhler (1991) used the correlation between ultrasonic pulse velocity and porosity of marble with increasing weathering to develop a classification scheme for evaluating the deterioration of marble.

However, stone deterioration processes are controlled by multiple factors; intrinsic factors inherent to the stone and its natural heterogeneity and extrinsic factors related to the surrounding environment (Siegesmund et al., 2002). The interactions between the various properties of stone and the weathering processes affecting them do create a complex system.

In such a complex system there is no single controlling parameter, but rather a multiplicity of factors is actually involved (Nicholson, 2001).

A simple and good approach for assessing the weathering and durability of stone is, therefore, to consider a certain type of weathering processes and try to determine the most important parameters controlling this weathering (Bourgès, 2006). Such an approach has been widely used for testing building stone in the field of civil engineering and architecture (Nicholson, 2001; Benavente et al., 2004; Angeli et al., 2007; Yu and Oguchi, 2009a; 2009b). However, the focus in these studies is mostly on the test of stone durability for the selection of suitable building materials rather than on the assessment of stone weathering state for conservation purposes.

The approach of studying the changes in stone properties upon artificial weathering is used here to provide the necessary information for assessing the deterioration of the selected stones and their durability. The different parameters that influence the durability of stone and its weathering are discussed below.

4.1.1 Stone properties and durability

The durability of building stones can be defined as a measure of their ability to endure and maintain their essential and distinctive characteristics of strength, resistance to decay and appearance in relation to specific manner, purpose and environment of use (Benavente et al., 2004). It follows from this definition that durability is determined based not only on the properties of stone and its natural characteristics (i.e. its intrinsic quality), but also on the environmental conditions to which it is subjected.

Durability tests are primarily used to help determining the suitability of stones for various applications in new construction works (Ross et al., 1991). However, these tests are also useful in conservation field for understanding the particular weathering behaviors of stone, assessing its weathering degree, and selecting the appropriate materials for restoration works.

The durability of a stone can be assessed by direct experiments such as salt crystallization and freeze-thaw tests that are intended to subject the stone to similar conditions to those encountered in the field, but in a more aggressive form (Building Research Establishment, 1989; Ross et al., 1991). However, such tests are generally time consuming and costly. Many

studies have been, therefore, dedicated to develop durability estimators based on correlations between stone damage, induced by artificial weathering, and the properties of stone upon which durability is dependent (Ross et al. 1991).

In general, pore structure and rock fabric characteristics are the main properties that control weathering (Ross et al., 1991; Ordonez et al., 1997; Nicholson, 2001; Pérez-Bernel and Bello, 2002; Tuğrul, 2004). *Porosity* is one of the most fundamental properties of stone. It impacts all its physical and mechanical properties. The stone mechanical strength and modulus of elasticity, for example, decrease with increasing porosity (Wittmann, 1992; Winkler, 1997). Weathering agents can penetrate into the stone through its porous system. Therefore, porosity affects the weathering process of the stone and can be considered as the simplest estimator for stone durability (Benavente et al., 2004). Although it provides useful information about the flow of weathering agents, porosity alone can not be sufficient to assess durability because it gives no indication of the way in which the pores are distributed within the stone (Building Research Establishment, 1989).

As shown in Chapter three, *pore size distribution* is one of the most important parameters controlling the absorption and transport of liquid within stone. Gauri and Bandyopadhyay (1999) emphasize the importance of determining pore properties for the quantification of weathering. Weathering processes, particularly salt and frost damage, are largely dependent on pore size (Everett, 1961; Fitzner and Snethlage, 1982; Punuru et al., 1990; Pérez-Bernel and Bello, 2002). Stones with the same total porosity can differ markedly in their weathering resistance if their pore size distribution, especially the proportion of micropores and small capillaries, is different (Cardell et al., 2003; Bourgès et al., 2008a; Yu and Oguchi, 2009a).

The weathering of stone is found to be enhanced by decrease in pore size (Hudec, 1978; Robertson, 1982). According to Angeli et al. (2008), Russell (1927) was the first to introduce the idea that susceptibility to salt deterioration is higher for stones with higher proportions of micropores. Honeyborne and Harris (1958) gave an empirical criterion of durability based on the proportion of pores larger than 5 μm in diameter. This pore diameter has been found to be a useful dividing value between fine and coarse pores for pore distributions determined by the water suction method (suction plate technique) (Building Research Establishment, 1989). The precise measurement of porosity with mercury intrusion porosimetry (MIP) in an indefinite range of pore sizes has enabled the development of reasonably accurate classifications of

pores (Punuru et al., 1990). Recent studies have also confirmed the role of micropores in salt crystallization damage (Scherer, 1999; Flatt, 2002; Steiger, 2005a,b; Yu and Oguchi, 2009a). However, different studies reported often different sizes and ranges of micropores in respect to damage by salt crystallization (Yu and Oguchi, 2009a).

Rossi-Manaresi and Tucci (1991) and Theoulakis and Moropoulou (1997) showed that salt damage can be significant only for stones with a particular pore size distribution, namely when a substantial amount of small pores coexists with a considerable proportion of larger ones. They emphasized, therefore, the importance of examining the pore size distribution of stone before drawing any conclusion about salt damage.

Pore geometry and connectivity have also important implications on the weathering process of stone. Scherer (2004) points out that damage due to salt crystallization is greater in points where micropores are connected to macropores. Channel cylindrical pores limit the number of such points and correspondingly stones with cylindrical pore are expected to be more durable than those containing a network of spherical micro-and macropores (Angeli et al., 2008). Buj and Gisbert (2010) point out recently that stones with high percentage of micropores are less susceptible to salt damage if their pore network is characterized by high tortuosity (twistedness or crookedness) and low connectivity.

Saturation coefficient (Hirschwald coefficient), calculated as the ratio of free porosity to accessible porosity, constitutes also an important property of stone. It depends on the configuration of pores (Leary, 1981). This coefficient was first developed to assess durability of stone to frost damage. In practice, saturation coefficients higher than 0.8 indicate susceptibility to frost whereas those below 0.6 indicate resistance, but one cannot say with absolute certainty in either case (Ross et al., 1991). Benavente et al. (2004) point out that this coefficient affects durability because stones which absorb a large amount of water are more susceptible to deterioration. However, many stones have saturation coefficients in a gray middle area around 0.7, and in this region the saturation coefficient on its own cannot be a reliable indicator of durability (Sperling and Cooke, 1985; Building Research Establishment, 1989). The correlation between saturation coefficient and porosity yields a better measure for stone durability. This correlation is still insufficient and further knowledge on pore structure is needed (Leary, 1981).

Capillary water absorption coefficient (w-value) represents the rate of water uptake through a certain area of stone. This property is closely related to the pore structure and can therefore be correlated to the durability of the stone (Benavente et al., 2004).

In addition to these petrophysical properties, the *mechanical characteristics* of stone have considerable influences on its weathering and durability. The strength of a material represents generally its ability to withstand mechanical stresses. Mechanical stresses on building stone are mainly of two types: compressive and tensile stresses. A description of the different mechanical tests and their measurement configurations can be found in Kocher (2004). *The stone mechanical strength* decreases with increasing weathering. Tensile strength is particularly useful for studying the microfracturing of building stone due to thermal and mechanical stresses (Robertson, 1982).

The relationship between the applied stress and the resulted deformation (strain) describes the mechanical behavior of materials. The static *modulus of elasticity*, calculated from the linear elastic part of the stress-strain curve, expresses the materials resistance to deformation. Microcracks change the elasticity of stone. Therefore, the modulus of elasticity can be used to detect increased porosity, fracturing, and susceptibility to deterioration (Robertson, 1982). Gauri and Bandyopadhyay (1999) point out that static modulus of elasticity is commonly used for the selection of materials in new construction and restoration works. These authors used the change in this modulus in increasing cycles of salt crystallization as a measure of stone deterioration.

It follows from the above discussion that there is no single parameter of stone that can fully determine its weathering susceptibility. Therefore, various properties of stone are usually combined to obtain an improved indication of durability. Porosity is usually correlated with other stone properties such as pore size distribution, saturation coefficient and capillarity (Leary, 1981; Building Research Establishment, 1989; Ross et al., 1991; Nicholson, 2001; Mohammad, 2003; Yu and Oguchi, 2009a). The combined use of microporosity and saturation has been usefully used to asses the durability of stone (Building Research Establishment, 1989; Niesel, 1981). Moreover, the correlation between the mechanical properties and the petrophysical and hydric properties of stone enhances further the estimation of stone durability and weathering (Benavente et al, 2004). Theoulakis and Moropoulou (1997) point out that the susceptibility of stone to salt damage is a function of mechanical and structural properties. These properties are associated with durability and with one another

(Niesel, 1981). For example, the textural and fabric characteristics, particularly pore and fracture geometry, are the main features controlling the strength of stone (Tuğrul, 2004). The comparison of theoretical crystallization pressures calculated from mercury porosimetry data with mechanical strength allows the assessment of stone susceptibility to salt damage (Rossi-Manaresi and Tucci, 1991; Theoulakis and Moropoulou, 1997). Some examples of durability estimators, based on correlations between stone properties, are given in Yu and Oguchi (2009a).

4.1.2 Accelerated weathering test

Different weathering tests can be carried out on stone to assess its durability and weathering susceptibility. These include salt crystallization tests, acid immersion tests, and freeze-thaw experiments, among others. Thermal weathering can also be used, particularly for marble. According to Ross et al. (1991), salt crystallization tests were proposed by Brard (de Thury et al. 1828) to assess frost resistance and are largely used today as a measure of the durability of porous building materials, mainly because of their extensive damaging potential.

Accelerated durability tests with salt crystallization are usually carried out either by repeated cycles of soaking in salt solution followed by drying or by partial immersion in salt solution to allow continuous capillary rise. Sodium sulfate is one of the most destructive salts and it is, therefore, widely used in accelerated weathering tests of building materials (Flatt, 2002; Tsui et al. 2003; Steiger and Asmussen, 2008).

In this study, salt crystallization test with cyclic impregnation in sodium sulfate solution is selected for studying the deterioration of limestone and basalt samples. For the study of marble deterioration, thermal weathering was applied. Thermal degradation of marble is already discussed in Section 2.1.1.4. More detailed description of the crystallization damage by sodium sulfate salt and the nature of the applied stress on pore walls are presented below.

4.1.2.1 Crystallization damage by sodium sulfate

Sodium sulfate has two stable phases; anhydrate called thenardite (Na_2SO_4) and a decahydrate called mirabilite ($\text{Na}_2\text{SO}_4 \cdot 10\text{H}_2\text{O}$). Figure (4.1) shows the phase diagram of sodium sulfate. At room temperature (20 °C), the equilibrium relative humidity of a saturated solution of

mirabilite is around 93%. As humidity decreases, mirabilite becomes less stable with respect to thenardite and a phase transition occurs at relative humidity of around 75% (Flatt, 2002). Mirabilite becomes unstable at temperatures above 32 °C. As temperature drops to lower values, the range of humidity at which it is stable increases (Flatt, 2002; Katzoff, 2006). If a solution of sodium sulfate dries at temperatures below 32 °C, mirabilite will likely precipitate and eventually transform to thenardite at low humidity (Scherer, 2004).

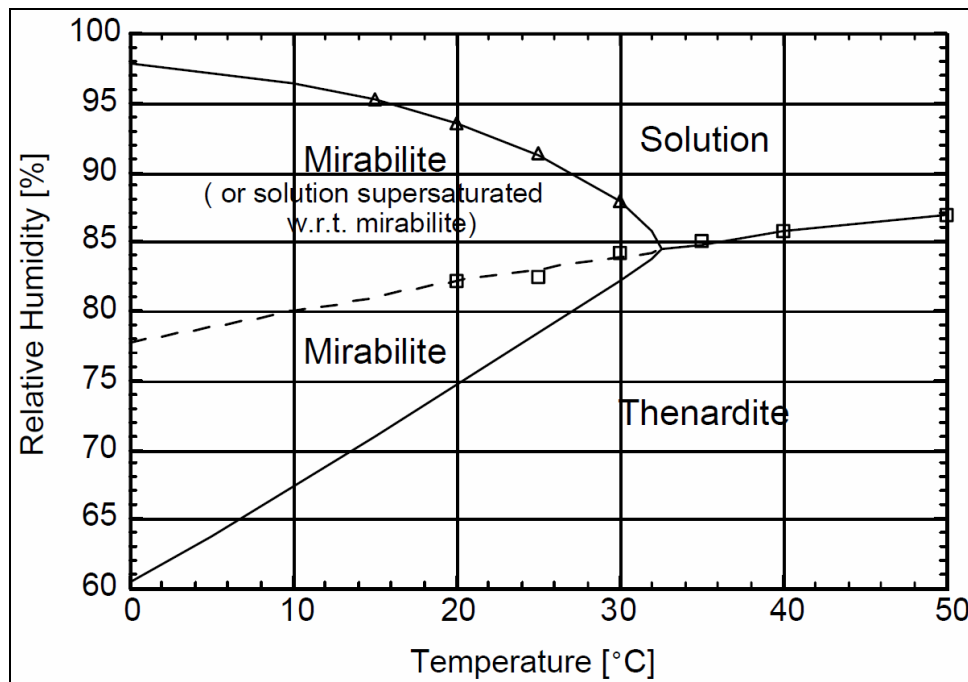


Figure 4.1: Phase diagram of sodium sulfate. The continuous lines indicate the boundaries of the stable phases. The dashed line corresponds to a solution in metastable equilibrium with respect to thenardite and supersaturated with respect to mirabilite (from Flatt, 2002; experimental data from Kracek, 1928).

In weathering experiments of stone with sodium sulfate salt by *cyclic total impregnation and drying (cyclic wetting and drying)*, the main damage is found to occur during the impregnation rather than the drying cycle (Scherer, 2004). This damage was previously attributed to the hydration pressure associated with increase in volume as thenardite transforms to mirabilite (Flatt, 2002; Scherer, 2004; Steiger and Asmussen, 2008). However, the hydration transition of thenardite to mirabilite by progressive absorption of water is unlikely because of the lattice mismatch between the two phases (Chatterji and Jensen, 1989; Flatt, 2002). This has been confirmed experimentally by Rodriguez-Navarro and Doehne (1999); they showed this transition to be a dissolution-precipitation process. The crystallization of mirabilite from a highly supersaturated solution seems to account for the extensive damage by sodium sulfate during impregnation cycles (Chatterji and Jensen, 1989;

Flatt, 2002; Tsui et al., 2003; Steiger and Asmussen, 2008). Chatterji and Jensen (1989) recognized that the solubility of thenardite becomes increasingly larger than that of mirabilite for temperatures below 32 °C (Tsui, 2003). The dissolution of thenardite at ambient temperature produces, therefore, a highly supersaturated solution with respect to mirabilite (Flatt, 2002; Tsui, 2003). In repeated cycles of wetting and drying, the thenardite precipitated in the sample during the drying cycle will dissolve as the stone is impregnated in the solution for the following cycle. The dissolution of thenardite will continue until it reaches its equilibrium concentration which is, at ambient condition, highly supersaturated with respect to mirabilite. The precipitation and growth of mirabilite from such a highly supersaturated solution will develop stresses that are substantially larger than the tensile strength of most stones and building materials and they can develop over a region of the porous network large enough to propagate strength limiting flaws (Flatt, 2002; Tsui, 2003; Scherer, 2004; Steiger and Asmussen, 2008). The contribution of crystallization during evaporation to the damage induced in wetting–drying experiments can not be unambiguously determined (Steiger and Asmussen, 2008). Steiger and Asmussen (2008) mentioned that the dissolution-crystallization mechanism during immersion induces high supersaturation in pores of any size. Therefore, large crystals in large pores that do not have small entries (as it is required for pressure development due to evaporation under equilibrium conditions) could also generate pressure (Steiger and Asmussen, 2008; Yu and Oguchi, 2009a).

In experiments with continuous partial immersion in salt solution that allows for *constant capillary rise*, the evaporation and diffusion kinetics are the most important parameters controlling damage. Rapid evaporation due to low RH conditions produces high supersaturation degrees that might induce damage by mirabilite precipitation. However, direct precipitation of thenardite is also observed at low RH (Rodriguez-Navarro and Doehne, 1999). Owing to its greater crystallization pressure, thenardite may produce larger damage than mirabilite (Sperling and Cooke, 1985; Rodriguez-Navarro and Doehne, 1999). Rodriguez-Navarro et al. (2000) found that both mirabilite and thenardite may precipitate under conditions of fast evaporation driven by low ambient relative humidity, and even with lower relative humidities only thenardite could be precipitated. The authors concluded therefore, that thenardite crystallization is probably responsible for the enhanced damage observed in evaporation experiments with constant capillary rise under low relative humidities (Tsui et al., 2003). Steiger and Asmussen (2008) point out, however, that although thenardite can generate greater crystallization pressure than mirabilite under such conditions, the

evaporation experiment carried out at different temperatures still indicate that mirabilite is the more damaging phase. This is probably attributed to the greater molar volume of mirabilite, which results in a larger degree of pore space filling and a larger contact area between the growing crystal and the pore wall, i.e. a more efficient propagation of stress. In summary, damage in evaporation experiments at moderate to high RH is caused by mirabilite (or eventually the metastable phase sodium sulfate heptahydrate at very low temperatures). At low RH, the anhydrous phases of sodium sulfate crystallize out as well and might thus generate a greater crystallization pressure (Steiger and Asmussen, 2008).

4.1.2.2 Crystallization pressure and stress on pore walls

As pointed out earlier in Chapter two, the crystallization pressure seems to be the most important mechanism of salt weathering in porous building materials. Many authors have discussed, in reference to relevant previous works such as Taber (1916) and Correns and Steinborn (1939), the necessary conditions for this pressure to develop (e.g. Amoroso and Fassina (1983), Scherer (1999; 2000), Flatt (2002), and Steiger (2005a)). Two important requirements are highlighted:

1. In order that a crystal continues to grow upon its loaded surface, a thin film (1-2 nm) of supersaturated solution must exist between the crystal and the confining pore wall. This film acts as a diffusion path furnishing the crystal with the material necessary for growth and transfer the resulting mechanical stress to the pore wall. The characteristics of this film have been already described by Taber (1916) and Weyl (1959). The differential surface energy (interfacial energy) plays an important role in the formation of this film. Scherer (1999; 2000; 2004) explains that the growing crystal will resist touching the pore wall and will exert pressure against it if the energy of the crystal-wall interface is greater than the sum of crystal-liquid and wall-liquid interface energy. Because of this disjoining pressure (the repulsive force between the salt and dry pore wall), the dry contact between crystal and pore wall will be prevented until the maximum crystallization pressure is reached. Below this pressure the crystal will retain a liquid film between itself and the pore wall and try to push it away with a force that depends on the driving force for growth. Without this disjoining pressure, the crystal will grow into contact with the pore wall and no crystallization pressure will be generated.

2. The loaded surfaces of the crystal must be in contact with a supersaturated solution in order to allow a continuous growth. If the growing crystal is composed of a substance whose solubility increases with pressure, then any increase in load has to be compensated by an increased concentration of the solution (Amoroso and Fassina, 1983; Steiger, 2005a).

The driving force for salt crystallization is thus supersaturation which can be produced by evaporation, drop in temperature, or addition of solution. High supersaturation could also be created by transition from one hydration state to another such as thenardite-mirabilite transition.

The crystallization of salt in pores results in mechanical stress that is transmitted to the pore walls by the thin supersaturated film. Salt crystals can grow in pore classes with radius larger than 1 nm (Espinosa et al., 2008). In stone with a wide range of pore sizes, salt crystals in the solution are subjected to unequal pressure and the system is under unstable equilibrium. The solution may become supersaturated with respect to crystals in large pores, while at the same time it tends to dissolve crystals growing in small pores as they are under greater pressure (Amoroso and Fassina, 1983).

According to Everett's model (or Willmann and Wilson, 1965; 1968), salt crystallization preferentially takes place in large pores ($r > 0.1$ or $10 \mu\text{m}$) because large crystals have a lower chemical potential and their formation is thus thermodynamically favorable (Rossi-Manaresi and Tucci, 1991). Therefore, salt solution will be withdrawn from the surrounding smaller pores and large crystals will grow at the expense of the smaller ones (Rossi-Manaresi and Tucci, 1991; Theoulakis and Moropoulou, 1997). Even when the crystals completely fill the large pores they will refuse to grow into the surrounding micropores because this involves a higher chemical potential. The large crystals instead keep growing against the confining pore wall and build up pressure (Everett, 1961; Theoulakis and Moropoulou, 1997; Scherer, 2004; Steiger, 2005; Yu and Oguchi, 2009). This suggests that stones with large capillaries connected by a network of micropores are highly susceptible to damage by salt crystallization (Rodriguez-Navarro and Doehne, 1999).

However, Steiger (2005b) points out that Everett's model is actually a particular case of crystallization under equilibrium condition, namely when a crystal grows in a large pore with small entries. Scherer (1999) describes in detail the origin of stress in equilibrium condition; that is when the crystal is entirely surrounded by the solution so that it remains in mechanical equilibrium. The author reviewed the thermodynamics of crystallization pressure and came to support the theory of Correns. However, he points out that the tensile stress on pore wall is estimated to be half that large. The maximum crystallization pressure is related to supersaturation ratio, but other factors such as interfacial energies (of wall-liquid and crystal-liquid boundaries), pore radius and pressure in solution are setting the lower limit of the generated stress. He gave the following equation for the maximum (when the contact angle $\theta = 180^\circ$) compressive radial stress on a crystal in a cylindrical pore:

$$\sigma_r = \frac{\gamma_{sl}}{r_p} - \frac{\gamma_{cl}}{(r_p - \delta)} - p_l, \theta = 180^\circ \quad (4.1)$$

σ_r = the total radial stress [N/m²] (convenient unit MPa = N/mm²); γ_{sl} = the solid-liquid interfacial energy [N/m]; γ_{cl} = the crystal-liquid interfacial energy [N/m]; r_p = the radius of the pore [m] (convenient unit μm); δ = the thickness of the solution film between the crystal and the pore wall [m] (convenient unit μm); p_l = the pressure in the liquid [N/m²] (convenient unit MPa); θ = the contact angle between the crystal and the pore wall [$^\circ$].

The compressive radial stress is counteracted by a tensile stress of approximately equal magnitude. This tensile stress is what causes damage to stone (Scherer, 1999; Flatt, 2002).

Under *equilibrium* condition, the generated stress is inversely proportional to pore radius; that is stress is higher in small pores. Scherer (2004) points out that sufficiently high stresses to damage stone (stresses in the MPa range) are only expected in nanometric pores (10–50 nm or smaller). While such small pores are present in concrete, they are relatively rare in natural stone (Houck and Scherer, 2006; Steiger 2005b). Furthermore, crystals grow simultaneously in pores of different sizes (Scherer, 1999). When supersaturation is consumed, crystals in small pores will tend to dissolve in favor of those in the large pores. This means that the high crystallization pressure developed in small pores will only be a transient pressure. However, the expected limitations in ions transport into large pores, especially when they are widely spread in the stone, may allow for a longer duration and a greater magnitude of transient stresses. The general expectation that small pores generate the largest crystallization pressure is, therefore, still valid (Flatt, 2002).

However, Scherer (2000; 2004; 2006) points out that high crystallization pressures can also develop in large pores, if the solution becomes discontinuous due to evaporation and subsists only as a trapped film between the crystal and pore wall. Further evaporation will thus produce high supersaturation and the growing crystal will exert an increasing pressure on the pore wall. In such a *non-equilibrium* situation the generated pressure is only limited by RH (kinetic factors) and the disjoining pressure, which can amount to tens of megapascals.

Crystallization of salt within the pores of a stone can thus result in the development of high stresses on pore walls. These stresses can exceed the tensile strength of stone which is usually around 3-9 MPa. (Flatt, 2002; Katzoff, 2006). However, Scherer (1999) shows that stress from crystallization in single pores is not likely to induce cracking and failure in stone structure because the affected volume is too small. For fracture to occur, crystallization must spread over a region of the material comparable in size to the strength controlling flaws (i.e. tens to hundreds of micron). This will require a sufficiently large driving force (high supersaturation) to allow for crack propagation through the porous network (Scherer, 1999).

4.2 Evaluation of consolidation treatments

4.2.1 Stone consolidation and evaluation of treatments

Weathering processes act to reduce and weaken the cohesion between the individual grains or grain aggregates of stone due to the effects of expansions and contractions which result for example from moisture changes, frost, salt crystallization, and temperature variations. This results in a reduction or loss of mechanical strength near the stone surface or at a certain depth inside the stone, leading thereby to granular disintegration or detachment of surface layers of stone. The mechanical strength of the weathered zone exhibits normally a gradual increase in depth profile from the outer surface towards its interior until it reaches that of the unweathered stone. The depth of weathering is dependent on the properties of the stone and its exposure conditions (Snethlage and Wendler, 1995). These changes are often accompanied by changes in porosity, moisture transport behavior and thermal characteristics (Sasse and Snethlage, 1997).

Consolidation treatments are needed to restore and strengthen the cohesion between the grains of the weathered stone. The aim is to restore the strength as well as other properties of the weathered zone to the level of the sound stone and to re-establish a homogeneous strength profile from the exterior treated surface to the sound interior stone. An over-strengthening of surface layer should be avoided (Snethlage and Wendler, 1995).

Stone consolidants should satisfy many performance requirements. These include penetrating at least through the weathered zone (typically a few centimeters) and into the sound stone, providing sufficient strengthening without blocking the pores (which could prevent escape of water vapor, and thereby raise the risk of frost damage), improving the properties of stone and its resistance to damage, and producing no or only minor changes in the color and appearance of the stone (ASTM E2167–01, 2001; Scherer and Wheeler, 2009). More details about the different performance requirements for stone consolidants and their evaluation methods can be found in Clifton (1980), Snethlage and Wendler (1995), Sasse and Snethlage (1997), and Laurenzi Tabasso and Simon (2006).

Beside mechanical strength, many parameters must be considered for the evaluation of the effectiveness of stone consolidation treatments. The modulus of elasticity, for example, is an essential parameter to evaluate the success of consolidation treatments and possible subsequent damage; there is a high risk of stone detachment and scaling when the modulus of elasticity of the treated surface layer is considerably higher than that of the sound stone (Snethlage and Wendler, 1995).

Table (4.1) lists some important parameters to evaluate the effectiveness of stone consolidation and the requirements they should fulfill for successful treatments.

Table 4.1: Requirements for assessing the effectiveness of consolidation treatments based on the changes in important stone properties after treatment as compared to untreated unweathered stone (Snethlage and Wendler, 1995, Sasse and Snethlage, 1997; Laurenzi Tabasso and Simon, 2006; Snethlage, 2008), (u: untreated; t: treated).

<i>Property</i>	<i>Symbol [Unit]</i>	<i>Requirement</i>
Color	–	No or minimum change ($\Delta E^* \leq 5$), no darkening or gloss.
Water uptake coefficient	w [kg/(m ² .h ^{0.5})]	$w_t \leq w_u$
Product penetration depth	s [cm] (measured through capillary rise after 5 minutes)	Deeper than the zone of maximum average moisture. Depending on the w-value of untreated stone: w = 0.1-0.5 → s = 1.0 cm w = 0.5-3.0 → s = 3.0 cm w > 3.0 → s = 6.0 cm
Water vapor permeability	μ [dimensionless]	Increase $\leq 20\%$ (i.e. $\mu_t \leq 1.2 \mu_u$)
Biaxial flexural strength	β_{BFS} [N/mm ²]	$\beta_{BFS,t} = \beta_{BFS,u}$ homogeneous strength profile, otherwise: $(\beta_{BFS,t} - \beta_{BFS,u})/\beta_{BFS,u} < 0.5$ (i.e. $\beta_{BFS,t} = 1.5 \beta_{BFS,u}$) and $\Delta\beta_{BFS,t}/\Delta x < 0.2$ N/mm ² .mm (x = depth)
Modulus of elasticity	E [kN/mm ²]	$E_t \leq 1.5 E_u$ and $E_t/\beta_{BFS,t} \leq E_u/\beta_{BFS,u}$ homogeneous profile as possible and $\Delta E/\Delta x \leq 1$ kN/mm ² .mm
Ultrasonic pulse velocity	V_p [km/s]	$V_{p,t} = V_{p,u}$ homogeneous profile
Drilling resistance	DR [N]	Homogeneous profile
Thermal dilatation	α_T [$10^{-6} \cdot K^{-1}$]	No increase against untreated stone (or increase $\leq 20\%$; i.e. $\alpha_t \leq 1.2 \alpha_u$)
Drying		No increase in drying duration

4.2.2 Consolidation materials for building stone

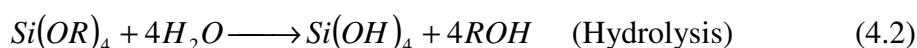
The scientific investigation into the conservation of building stones began in the nineteenth century and depended on the progress in chemical research (Snethlage and Wendler, 2000). Before this date, the well-known natural substances (such as linseed oil and bees wax) were being applied to protect natural stone. In the first half of the nineteenth century, synthetic

silicates, namely waterglass and fluorosilicates, were developed. These two products, in different varieties, dominated the whole market of stone conservation until the 2nd world war and even after. Only beginning from 1960s, after the reconstruction works in the cities destroyed by war and the growing awareness of the conservation of historic building fabric, new materials have been developed. These new materials originate predominantly from silicone-organic combinations and in part from synthetic resins (Herm et al., 1998). Nowadays, alkoxy silane compounds (tri- and tetraalkoxy silanes) are very famous as stone consolidants.

Alkoxy silanes

Alkoxy silanes, particularly ethyl silicates, were first suggested by Hoffman in 1861 for stone consolidation and they have been widely used as stone consolidants since the late 1960s (Grissom and Weiss, 1981; Snethlage and Wendler, 2000; Delgado Rodrigues, 2001; Wheeler, 2005).

Ethyl silicate consolidants are based on the hydrolysis reaction of monomeric or oligomeric tetraethoxy silane (TEOS) by water present in the pore space of stone and the subsequent condensation reaction of hydrolyzed silanol (Si-OH) groups by intermolecular release of water to form stable siloxane (Si-O-Si) bonds (see equations below). The resulted gel interacts with the mineral components of the stone, providing thereby a stable contact (Snethlage and Wendler, 2000).



Where: R = ethyl radical (C_2H_5)

The popular and well established use of ethyl silicates as stone consolidants is attributed to their basic properties (such as low viscosity and ability to form siloxane (Si-O-Si) bonds) and relatively good effectiveness, particularly with siliceous stones (Delgado Rodrigues, 2001; Wheeler, 2005). However, the consolidation effects of these consolidants are less satisfactory when applied to carbonate stones because of their inability to bond chemically with calcite crystals, which contain by itself few hydroxyl groups for alkoxy silanes to condense with (Goins et al., 1996; Wheeler, 2005; Scherer and Wheeler, 2009). Furthermore, Simon (2001) showed that there is an inhibiting effect of calcite surfaces on the hydrolysis reaction of alkoxy silanes.

Weiss et al. (2000a) approached the problem of insufficient bonding to carbonate surfaces by chemically altering the mineral's surface of the stone to create a hydroxyl-rich surface by reacting calcium ion (or calcite) with tartaric acid (ammonium hydrogen tartrate) to form calcium tartrate that potentially would condense with alkoxy silanes. Another approach to create linkages across the interface between calcite and alkoxy silane-derived gels is to employ alkoxy silane coupling agents, in which compatible alkyl groups (R) bond to calcite and the hydrolyzed alkoxy groups on the coupling agents form silanols to condense with the alkoxy silane consolidant (Wheeler et al., 2000; Wheeler, 2005). An overview of alkoxy silanes as stone consolidants can be found in Wheeler (2005).

In this study, two commercial alkoxy silane-based consolidation products (Funcosil KSE 300 and KSE 300HV) from Remmers were used for the consolidation of the studied limestone samples. The selection of alkoxy silane consolidants is based on their relatively satisfactory results and their frequent use (Maravelaki-Kalaitzaki et al., 2006). The two selected products have the same gel deposition rate (ca. 300 g/l) and almost the same characteristics, except that KSE 300HV contains an extra coupling agent for specific applications to limestone. Therefore, the effects of this added coupling agent on the effectiveness of the consolidant with limestone samples can be tested.

The changes in the properties of the tested stones before and after weathering and consolidation are going to be studied by physico-mechanical tests. A particular emphasis in this study is, however, given to the use of non-destructive ultrasonic velocity measurements. The next chapter is, therefore, assigned to explain the basic principles of this technique and its applications in the field of stone conservation.

5 Non-destructive ultrasonic technique

Ultrasonic technique has gained increasing importance in the field of stone conservation as an effective and non-destructive investigation method. The non-destructive nature of the technique allows the determination of the properties of stone materials without causing damage. This technique constitutes an effective alternative for destructive testing methods. In the field of civil engineering and architecture, for example, non-destructive ultrasonic measurements can substitute for the traditional mechanical tests, which are destructive and costly. This non-destructive characteristic, together with the possibility of in situ applications, is especially important for the study of significant archeological stone monuments and structures, where sampling that might detract their integrity is not allowed.

In this study, ultrasonic technique is used with other physico-mechanical methods to study the properties of stone before and after weathering and consolidation. The principles and possible applications of the technique for the investigation of building stone are discussed in this chapter. During this study, a review on this topic has been published by Ahmad et al. (2009).

5.1 Basic principles

Ultrasound refers to sound waves with frequencies above the upper limit of the range audible to human ear, which is about 20 kHz. Generally, a sound wave is a periodic mechanical disturbance that propagates through a gas, liquid or solid medium. In fluids (gases and liquids), sound waves are only of the longitudinal compression type, in which the particles of the medium are displaced in the direction of wave propagation. In solids, however, transverse shear waves with particle displacement perpendicular to the propagation direction of the wave do also occur. Pure longitudinal and transverse sound waves propagate in infinite solid mediums. Depending on the way of excitation and the form and dimensions of the solid material in relation to wavelength, other types of sound waves such as surface waves (Rayleigh wave), extensional (or quasi-longitudinal) waves, and bending (or flexural) waves can also occur (Sorge and Hauptmann, 1985). Figure (5.1) shows the various forms of sound waves in solid mediums and their velocities. The velocity of sound waves in a medium depends on its compressibility and density; i.e. it depends on the elastic and inertial properties of the medium (Jewett and Serway, 2008).

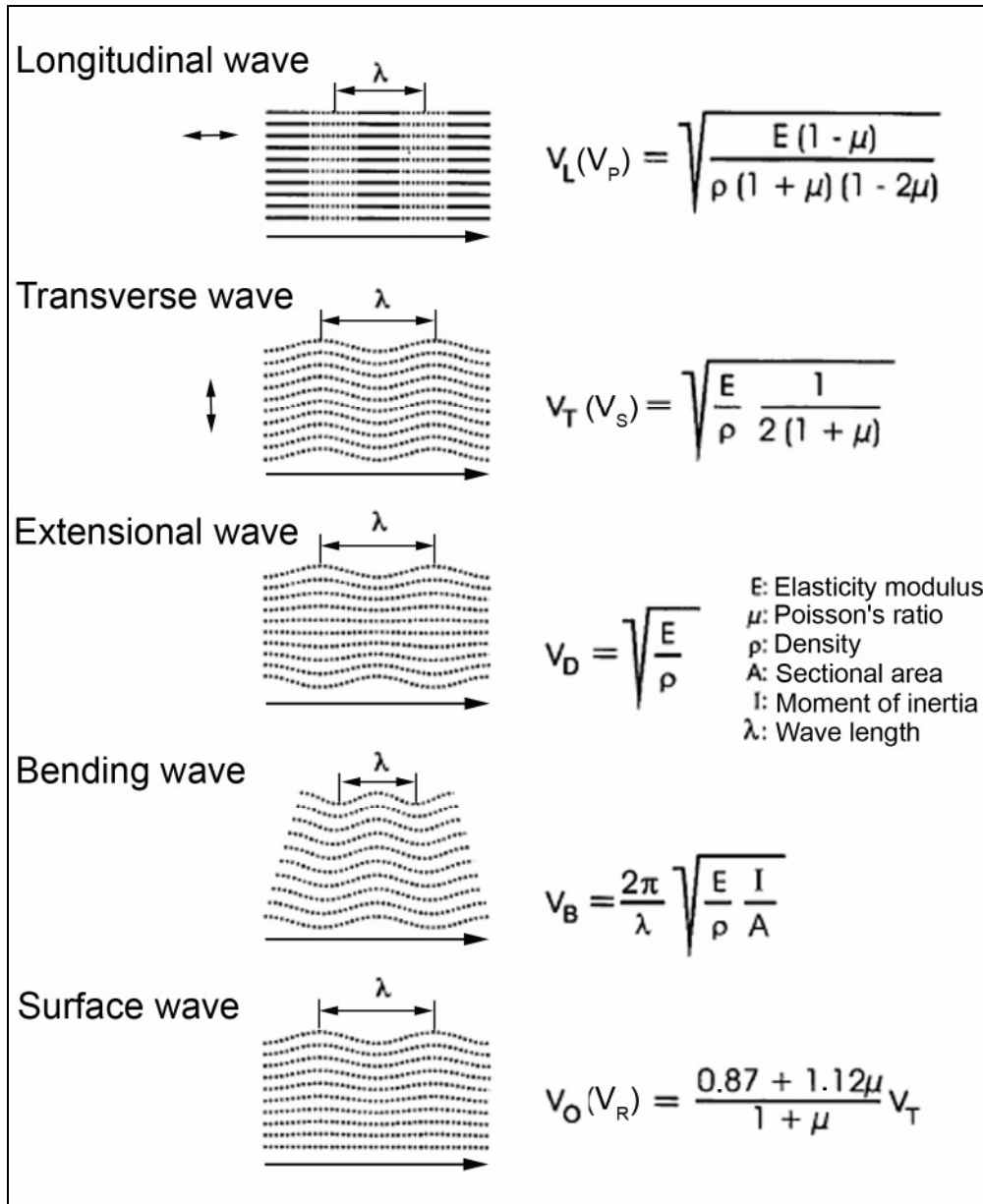


Figure 5.1: Types of elastic waves in solids and their velocities (DGZfP, 1999).

Sound waves, like all other waves, are characterized by their wavelength (λ) and frequency (f). The wavelength is the minimum distance between any two consecutive points with the same phase; that is between two points with the same position and direction of motion on the wave pattern such as two adjacent peaks. The wave frequency is the number of wavelengths that pass a reference point in one second (the number of oscillations per unit time). The wavelength of a wave is inversely proportional to its frequency as given in the following equation:

$$V = f \cdot \lambda \quad (5.1)$$

V = the velocity of the wave [m/s]; f = the frequency of the wave [Hz]; λ = the wavelength of the wave [m].

More details about the physics of ultrasound and sound waves in general can be found in Jewett and Serway (2008), Shutilov (translated by Alferrieff) (1988), Hull and John (1988), and Norton and Karczub (2003).

5.2 Measuring techniques

The real breakthrough in the generation and reception of ultrasound was achieved thanks to the work of the Curie brothers who discovered the piezoelectric effect¹ in quartz in 1880, and the mathematical deduction of the converse piezoelectric effect by Lippmann one year later (Woo, 2002).

Ultrasonic waves were first used to explore submarine objects, inspired by sonar systems, but there were also some attempts and proposals to apply ultrasound for flaw detection in metals (Deutsch, 2000). However, the industrial use of ultrasound as a non-destructive method for material testing started apparently in the 1940s.

Mamillan (1958) was the first to use ultrasound for the investigation and testing of building stone. Since then, ultrasonic methods have been widely used for the study and investigation of stone objects and structures in the fields of cultural heritage and civil engineering (stone masonry and concrete).

Ultrasonic testing consists effectively of propagating ultrasound waves through a material to measure either or both the travel time and any change of intensity of the wave for a given distance (Blitz and Simpson, 1996). Various ultrasonic techniques can be applied for the investigation of stone. In *transmission method*, the ultrasonic transmitter and receiver are placed opposite to each other on either side of the stone and the time needed for the wave to travel along the distance between them (*travel time*) is measured (Figure 5.2). This allows calculating the velocity of ultrasonic waves propagating through the stone, particularly the longitudinal waves. The velocity of ultrasonic waves depends on the physical and mechanical properties of the stone (such as density, porosity, and structure), its degree of water saturation and its level of deterioration (cracks, defects) (Ahmad et al., 2009).

¹ Piezoelectric effect: the generation of electric charges on the surface of certain crystals in response to applied mechanical stress.

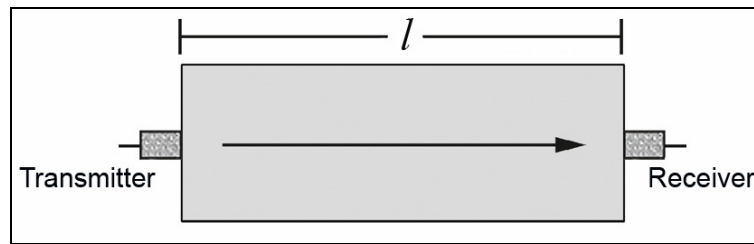


Figure 5.2: Transmission ultrasonic technique.

In addition to travel time, the *intensity* of the received ultrasonic wave, calculated from the first oscillation amplitude of the received signal, can be used to detect inhomogeneities and defects in stone structure. The intensity of ultrasonic waves decreases continuously along their whole travel path in the stone due to the absorption of energy and the scattering of the waves at microscopic interfaces and internal inhomogeneities. The measurement of intensity is very sensitive, and it requires a reproducible coupling of the transducer to the stone in order to allow the comparison between measurements. Such a coupling is, however, difficult to ensure, which restricts the practical use of this measuring procedure (Reinhardt et al., 2007; Glaubitt, 2008).

It is also possible to analyze and determine the individual frequencies of the ultrasonic impulse. The intensity of the individual frequencies can weaken variably according to the condition of the material. Changes in the *frequency spectrum* can therefore be used to characterize the condition of stone and to indicate changes due to weathering (Simon et al., 1994) or conservation (Meinhardt-Degen, 2005) and to check the setting and strength development in concrete (Jonas, 1996).

The transmission technique can be modified by changing the transmitter-receiver arrangement and the testing procedure in order to adapt it to different applications and specific problems and purposes (Bouineau, 1978; Zezza, 1990). The ultrasonic transducers can be moved in a stepwise manner on stone surface to allow for ***ultrasonic tomographic measurements***. In this technique, the travel times of transmitted waves between positions of known coordinates on a section of the stone are measured and used to calculate the ultrasonic velocity in each element of the investigated section, providing tomograms that show the velocity variations inside the stone. Ultrasonic tomography can be used to study and estimate the weathering degree of stone structures (Montoto et al., 1994; Simon, 2001) and to evaluate the effectiveness of consolidation treatments (Ettl and Sobott, 1999).

Surface methods depend on the pulse-echo technique, in which a transducer, coupled to the surface with a suitable elastic material, transmits ultrasound wave in stone and the reflected wave is received by another transducer placed on the same surface of the stone. Surface methods are more suitable for in situ applications where building structures are usually accessible from only one side. The travel time and the change in intensity or frequency spectrum of the reflected signal can also be measured here to provide information about the location and dimension of defects and changes in the structure of the material. These methods can be used to investigate weathering layers in building stones (Făcăoaru, 1990; Făcăoaru, and Lugnani, 1993; Simon and Lind, 1999; Christaras, 2003) and to estimate the depth of open cracks (Făcăoaru, and Lugnani, 1993; Christaras, 2003).

5.3 Ultrasonic applications in stone conservation field

The applications of ultrasonic technique for the investigation and conservation of building stone can be categorized in three groups; stone characterization and establishment of correlations with other stone parameters, assessment of the degree of deterioration, and evaluation of the effectiveness of conservation treatments (Chiesura et al., 1995; Ahmad et al., 2009).

5.3.1 Characterization of stone and establishment of correlations with stone parameters

Ultrasonic velocity measurements in transmission technique are usually used to characterize stone and determine its elastic and mechanical properties such as the dynamic modulus of elasticity and Poisson ratio. The elastic constants can be determined by measuring the velocity of two different ultrasonic waves of the stone, together with its density (Rentsch and Krompholz, 1961). The following equations show the calculation of dynamic modulus of elasticity and Poisson ratio using the velocities of longitudinal and transversal waves.

$$E_{dyn} = \rho V_p^2 (1 + \mu_{dyn}) \frac{1 - 2\mu_{dyn}}{1 - \mu_{dyn}} \quad (5.2)$$

$$\text{or: } E_{dyn} = 2\rho V_s^2 (1 + \mu_{dyn}) \quad (5.3)$$

$$\text{where: } \mu_{dyn} = \frac{V_p^2 - 2V_s^2}{2(V_p^2 - V_s^2)} \quad (5.4)$$

E_{dyn} = dynamic modulus of elasticity [Pa] (convenient unit GPa (or kN/mm²)); V_p = velocity of longitudinal ultrasonic wave [m/s]; V_s = velocity of transverse ultrasonic wave [m/s]; μ_{dyn} = dynamic Poisson ratio [-]; ρ = density [kg/m³].

On bar-shaped specimens with suitable dimension, the dynamic modulus of elasticity can be simply calculated only from the velocity of pure extensional waves. However, the generation and measurement of pure extensional waves is practically irrelevant. Erfurt and Krompholz (1996) described thoroughly the procedure for determining the elastic constants by measuring the travel time of longitudinal waves and the resonance oscillation frequency of extensional waves on bar-shaped laboratory samples. These must have suitable lateral dimension to allow the propagation of both longitudinal and extensional waves. The elastic constants can be used to detect changes in stone (Glaubitt, 2008).

The relationship between ultrasonic velocity and various stone properties, such as porosity, density and capillary water absorption for different stone types, particularly marble and limestone, has been widely studied. Ultrasonic velocity measurements have been also used to establish useful correlations with other stone parameters that can give information on properties that would otherwise have to be determined by destructive methods such as mechanical strength (Chiesura et al., 1995; Ahmad et al., 2009). Good linear correlations were also found between the dynamic modulus of elasticity, calculated from ultrasonic velocity measurements, and the static modulus measured by destructive mechanical tests (Christaras, 1996; Bourgès et al., 2008b). This correlation is affected by variations in pore space morphology in stone and it was found that the static modulus of elasticity is more affected by stone microcracks and deformations than the dynamic modulus (Bourgès et al., 2008b).

5.3.2 Assessment of the degree of stone weathering

The velocity of ultrasonic waves depends on the inertial and elastic properties of stone. The latter are greatly influenced by the effect of deterioration processes such as increase in porosity, development of cracks and general decrease in mechanical strength (Cardu et al., 1991). Therefore, correlating the changes in these properties with the measured ultrasonic

velocity helps to provide classification schemes for evaluating the degree of stone deterioration.

Köhler (1991) showed that the ultrasonic longitudinal velocity decreases markedly upon progressive structural damage of marble from around 5-6 km/s for fresh stone to values around 1 km/s for extremely weathered marble. He suggested an empirical classification system for marble that categorizes stone damage according to ultrasonic pulse velocity values (Table 5.1). Similar classification systems have been developed for limestone (Fitzner and Heinrichs, 1992; Simon and Lind, 1999). Köhler's classification system is based on a correlation between ultrasonic pulse velocity and porosity for marbles. However, many authors point out that an accurate interpretation of the relationship between ultrasonic pulse velocity and stone degradation demands comprehensive knowledge of the petrophysical properties of the stone and its fabric¹ (Durrast et al. 1999; Siegesmund et al., 1999; Weiss et al. 2000b). Based on various correlations between ultrasonic pulse velocity and important physico-mechanical properties as well as on personal observations and practical experience, Simon (2001) provided a slightly modified scheme of Köhler's classification system. Some examples for the use of ultrasonic technique for assessing the weathering conditions of stone sculptures can be found in Simon (2001) and Pamplona et al. (2010).

Table 5.1: Classification of marble damage after Köhler (1991).

<i>Ultrasonic pulse velocity (V_p) [km/s]</i>	<i>Description</i>	<i>Damage class</i>
>4.5	Fresh	I
3–4.5	Increasing porosity	II
2–3	Progressive granular disintegration	III
1–2	Danger of breakdown	IV
<1	Complete structural damage	V

Ultrasonic methods, particularly surface measurements, are also used in situ to determine the depth of open cracks and weathering layers (Bouineau, 1978; Simon and Lind, 1999; Christaras, 2003). Another application of ultrasonic velocity measurements on stone conservation is the evaluation and long-term monitoring of the condition of exterior stone objects and structures (Köhler, 1999; Recheis et al., 2000; Simon, 2001). This may provide useful information about the natural ageing process of the stone and its ability to withstand natural exposure conditions.

¹ The term 'fabric' as used here includes stone texture (crystallographic preferred orientation) and microstructure (geometry and morphology of grains and pores).

5.3.3 Evaluation of the effectiveness and durability of conservation treatments

Consolidation treatments are expected to influence stone properties favorably through imparting cohesion to the weathered parts and increasing their adhesion to the sound core. This should be directly reflected in form of an increase in the compactness of stone and its mechanical strength. Therefore, ultrasonic velocity measurements before and after conservation are used to control and assess the effectiveness of consolidation treatments and their long-term durability.

Since the late seventies, ultrasonic testing has been applied to study the effects of consolidation treatments on stone (Rossi-Manaresi and Ghezzi, 1978). Several examples of this type of application are found in the literature (Vergès-Belmin et al., 1991; Simon, 1996; Ettl and Sobott, 1999, Snethlage et al., 1999; Haake et al., 2004; Myrin and Malaga, 2006).

The velocity of ultrasonic waves in treated stone has been found to increase variably depending, among other things, on the nature and condition of stone and the type and application method of the consolidation product. Values up to around 150% increase in ultrasonic velocity after consolidation treatments of different stone types, particularly marble, have been reported (Chiesura et al., 1995). A maximum increase in ultrasonic velocity of highly weathered marble could be achieved by full impregnation with acrylic resin under pressure (Ibach method; Snethlage and Wihr (1979)). With this method, the ultrasonic velocity in the stone after treatment might considerably increase to values close to those of fresh marble (Snethlage et al., 1999; Lorenz and Ibach, 1999; Pamplona et al., 2011).

Ultrasonic velocity measurements can also be used to estimate the penetration depth of consolidants on drill core samples (Simon, 1996; Antonova et al., 1997). This can be correlated with stone properties measured in depth profile such as bi-axial flexural strength and drilling resistance measurements (Meinhardt-Degen, 2005).

A general review on the application of ultrasonic techniques for the investigation on natural building stone can be found in Ahmad et al. (2009) and Chiesura et al. (1995).

5.4 Important aspects and considerations

- Ultrasonic velocity is influenced by the degree of water saturation of pores. Water saturated stones exhibit generally higher ultrasonic longitudinal velocity because the velocity of ultrasound waves in water (1.48 km/s) is four and half times higher than in air (0.33 km/s). Esbert et al. (1991) reported an increase of ultrasonic velocity up to 35% in water-saturated limestone, dolomite and sandstone. The influence of water saturation degree on ultrasonic velocity is more significant for stones with porosity in form of fissures such as marble and granite. It seems that water can fill in a crack and bridge its sides more effectively, compared to pore walls, bringing about thereby a considerable increase in ultrasonic velocity for such stones (Delgado Rodrigues, 1982).

Ultrasonic velocity measurement in dry and water-saturated conditions may provide useful information about the pore space characteristics of stone. Such measurements have been used together with the theoretical velocity of unfissured rock, calculated using its mineral composition, to define quality indices for stone and evaluate crack density (Delgado Rodrigues, 1982; Bourguès, 2006).

- Research has proved the validity of ultrasonic testing for investigation of stone and other materials in general. However, some issues related to the accuracy and reproducibility of ultrasonic measurements need to be highlighted. Marini et al. (2004) point out that small changes in ultrasonic pulse velocity might reflect a large change in the condition of stone and it would be, therefore, better to measure pulse velocity within an accuracy of at least $\pm 2\%$. According to experience, the accuracy of in situ velocity measurement is, however, assumed to be $\pm 10\%$ (Simon, 2001). Parameters and issues that might influence the accuracy of ultrasonic measurements include suitable ultrasonic frequency, contact pressure, degree of water saturation and suitable coupling. To ensure accurate and reproducible results, the ultrasonic system needs to be calibrated and the measuring conditions should be established and kept constant during the test. Although it is often emphasized to select the suitable ultrasonic frequency, a thorough and comprehensive study about the influence of frequency on the accuracy of ultrasonic measurement is still lacking. For measuring the velocity of longitudinal ultrasonic waves, Rentsch and Krompholz (1961) provided a practical definition of the infinite medium, required to allow the propagation of pure undisturbed longitudinal waves, which implies that the measuring length or lateral dimension of the investigated

sample must be at least 1.5 of the wavelength. Using this criterion, the suitable frequency for investigating a sample of certain dimensions can be determined in reference to the relation between ultrasonic frequency and wavelength. In an unpublished document of the company Geotron-Elektronik, the influence of the ratio of measuring distance to ultrasonic wavelength (l/λ) on the accuracy of ultrasonic measurement for standard samples of Plexiglas was studied. Ratios below 2.5 ($l/\lambda < 2.5$) are considered unfavorable as they imply a measuring error of more than 3%. For ratios below 1 ($l/\lambda < 1.5$), a measuring error of more than 12% is to be expected (Krompholz, 2010). Suitable ultrasonic frequencies for an ultrasonic velocity of about 3 km/s in relation to the dimension of a specimen are shown in Table 5.2.

Table 5.2: Suitable ultrasonic frequency and specimen dimension for an ultrasonic propagation velocity of $\sim 3 \text{ km}\cdot\text{s}^{-1}$ (from McDUR-Acoutherm European Project, 2002).

<i>Transmitter frequency [kHz]</i>	<i>Wavelength [mm]</i>	<i>Specimen dimension [mm]</i>
33	~ 90	150–1500
45	~ 70	150–1000
54	~ 60	150–1000
150	~ 20	40–200
250	~ 12	30–150
350	~ 10	20–70
500	~ 6	15–50
1000	~ 3	10–50
2000	~ 1.5	5–50

6 Materials and methods

6.1 *Materials of the study*

The stone materials used in this study were selected from different archaeological sites in Jordan. Before describing the studied stone materials and their petrographic and mineralogical characteristics, the classification process of stone is briefly discussed.

6.1.1 Classification of stone

Limestone

Limestone is a sedimentary rock composed mainly of calcium carbonate, often in the form of minerals calcite and aragonite, and may contain varying amounts of magnesium carbonate in form of dolomite. It is developed from carbonate sediments as the parent carbonate rock.

The most commonly used classification systems of carbonate sediments and limestone are those of Folk (1959; 1962) and Dunham (1962). Both schemes classify carbonate rocks according to their textural properties.

Folk classification is based on the textural components of limestones; that is the grains (or allochems) and interstitial materials, the calcite cement (spar) and the microcrystalline matrix (micrite). The system first divides carbonate rocks into allochemical rocks that contain transported coarse ($> 10 \mu\text{m}$) carbonate grains and rocks lacking allochems and composed entirely of microcrystalline calcite. Allochems in carbonate rocks can be of four different types; fossils (or bio fragments), oolites (or ooids), pellets, and intraclasts. These allochems can be embedded in a matrix of dull microcrystalline calcite mud (micrite) or cemented by clear to translucent coarse crystalline calcite crystals (sparite). Accordingly, allochemical rocks can be further classified as shown in Figure (6.1).

Folk classification system has been going through levels of modification and refinement to provide further subdivisions of limestone and carbonate sediments. A modified scheme for further subdivision of carbonate sediments based on the ratio of allochems is shown in Figure (6.2).

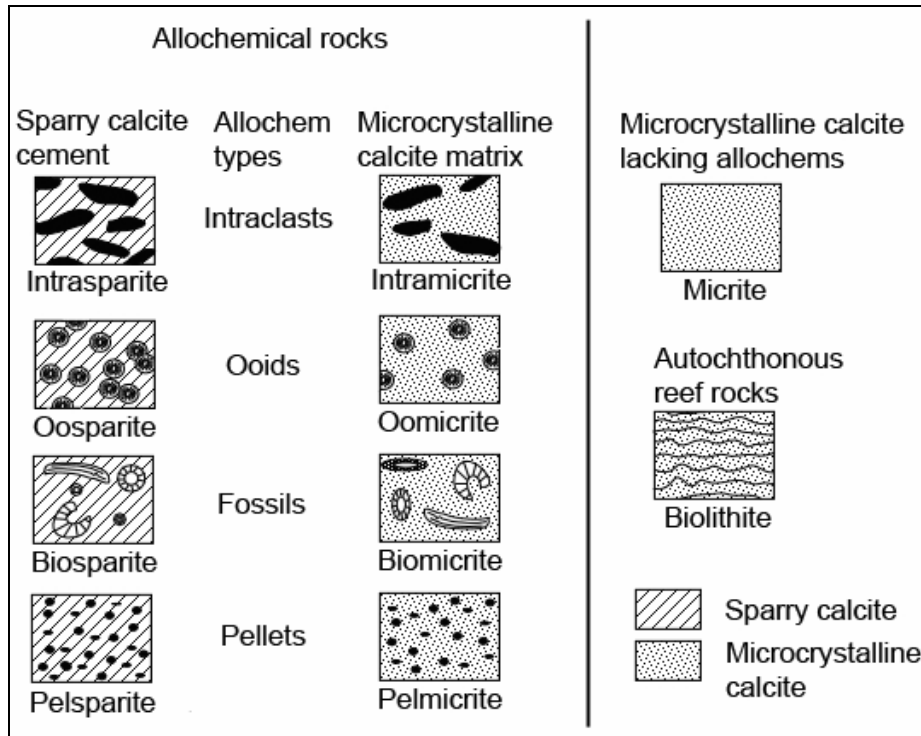


Figure 6.1: Folk's classification system of carbonate rocks (modified after Folk, 1959).

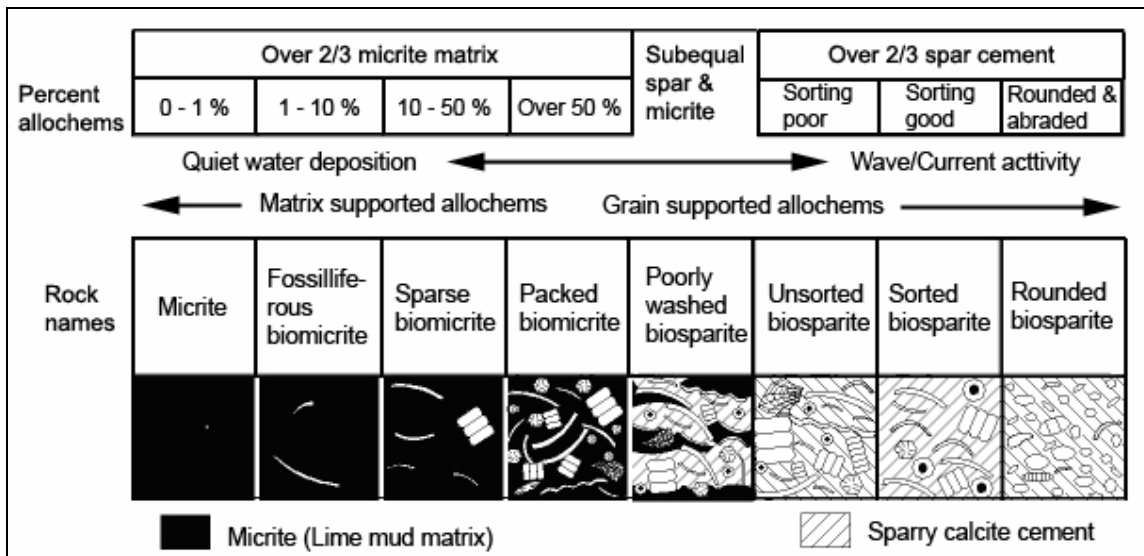


Figure 6.2: Textural classification of carbonate rocks (modified after Folk, 1962).

Alternatively, Dunham classification system deals with the depositional texture of carbonate rocks. Carbonate rocks are first divided as to whether their depositional texture is still recognizable or not. Carbonate rocks with recognizable depositional texture are further subdivided into rocks whose original components were not bound together during deposition and rocks with original components bound together as part of the deposition process

(boundstone). Based on the relative proportion of mud and the concept of mud/grain support, rocks originally not bound during deposition are further classified as shown in Figure (6.3).


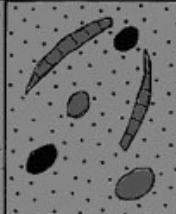
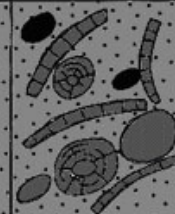
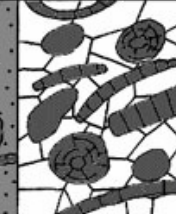
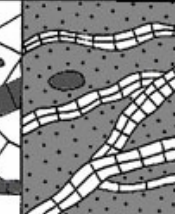
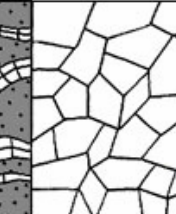
Depositional texture recognizable					Depositional texture not recognizable
Original components not bound together during deposition			Original components bound together during deposition		
Contains mud (Carbonate of clay and fine silt size)		Grain-supported	Lacks mud and is grain-supported	Boundstone	
Mud-supported	Less than 10% grains				
Mudstone	Wackstone	Packstone	Grainstone	Boundstone	Crystalline
					

Figure 6.3: Dunham's classification system of carbonate rocks (modified after Dunham, 1962).

Marble

Marble is a metamorphic rock consisting mainly of recrystallized calcite and/or dolomite. Different marbles can be distinguished and categorized based on their particular microstructure. For this purpose, many geometric and morphological characteristics of carbonate crystals such as relative grain size and grain boundary shape can be examined.

Marble is mainly composed of anhedral (xenoblastic) grains, mostly carbonates, and may contain euhedral (idioblastic) grains mostly of non-carbonate accessories. Marbles composed of equidimensional carbonate grains are said to have a *homeoblastic* texture (microstructure), as opposed to *heteroblastic* texture for marbles with inhomogeneous grain size. If the equigranular large carbonate grains have regular *straight to curve* boundaries, the marble is characterized by a *granoblastic* polygonal mosaic texture. On the other hand, highly interlocking and dentate grains result in a *sutured* grain boundary texture. Heteroblastic marble can have a mortar texture/fabric when the large crystals are surrounded by a fine-grained matrix (Capedri et al., 2004).

Basalt

Basalt is one of the most common igneous rocks. It is a dark colored, mafic¹ extrusive² volcanic rock composed particularly of the minerals plagioclase, pyroxene and olivine. On a chemical basis, basalts can be classified into three broad groups based on the degree of silica saturation. Using the CIPW-Norms³, the normative mineralogy of the rock can be calculated and plotted in the basalt tetrahedron (Figure 6.4), which is constructed using the normative components olivine, clinopyroxene, quartz and nepheline. The basalt tetrahedron is divided into three different volumes separated by two critical planes indicating the degree of silica saturation. Correspondingly, three types of basalt can be distinguished; quartz tholeiite (quartz-hypersthene normative Q+Hy), olivine tholeiite (olivine-hypersthene normative Ol+Hy), and alkali olivine basalt (Nepheline normative Ne) (Nelson, 2011).

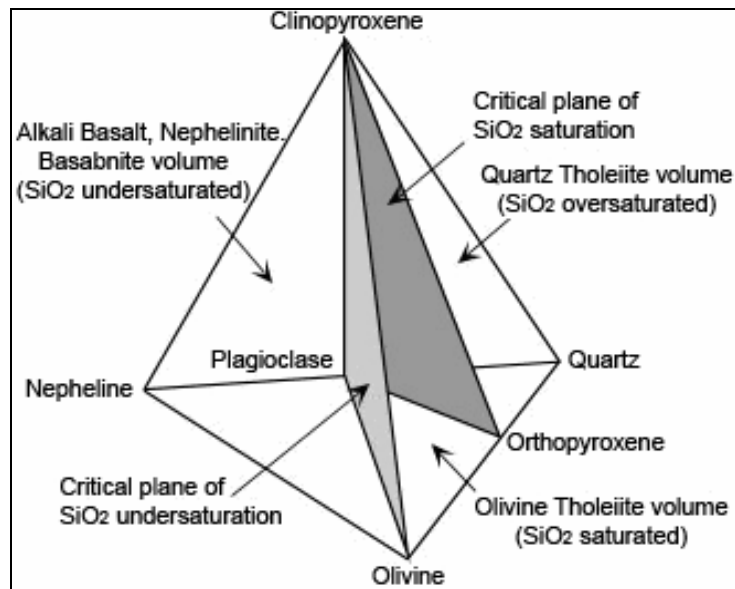


Figure 6.4: The basalt tetrahedron (after Yoder and Tilley, 1962)

Other chemical parameters such as the contents of silica and total alkalis can also be utilized for the classification of basalt and volcanic rocks in general. The total alkali ($\text{Na}_2\text{O} + \text{K}_2\text{O}$) versus silica (SiO_2) diagram (TAS diagram) can be used to classify volcanic rocks especially when their actual mineral composition can not be certainly determined. Rocks plotting in a specific field on the diagram can be further classified based on additional criteria such as their texture, normative mineralogy and chemical characteristics.

¹Rich in magnesium and iron and contain comparatively low content of silica and lighter elements (derived from New Latin *magnesium* + Latin *ferrum* iron + English *-ic*) in contrast to light-coloured *felsic* rocks composed mostly of silica and alkali feldspars.

² Formed on the Earth's surface by the cooling and solidification of extruded magma.

³ A norm developed by Cross, Iddings, Pirsson, and Washington to determine the hypothetical mineral assemblage (normative mineralogy) from whole-rock chemical analysis.

6.1.2 Studied stone samples

The studied stone samples were selected from five important archaeological sites in north and north-east Jordan (Figure 6.5). Limestone and basalt are the stones mainly outcrop in this part of Jordan, and the archeological sites there were almost built of them. From a conservation point of view, these stone types have been so far little studied, compared to the sandstone in the south of Jordan which has gained more interest, particularly because of the very famous Nabataean city of Petra which was carved into this rock (Fitzner and Heinrichs, 1994; Heinrichs and Fitzner, 2000; Al-Naddaf, 2002; Paradise, 2002; Simon et al., 2004; Fitzner and Heinrichs 2005; Heinrichs, 2008). Therefore, this study is dedicated to investigate some varieties of these stones from different aspects for conservation purposes.

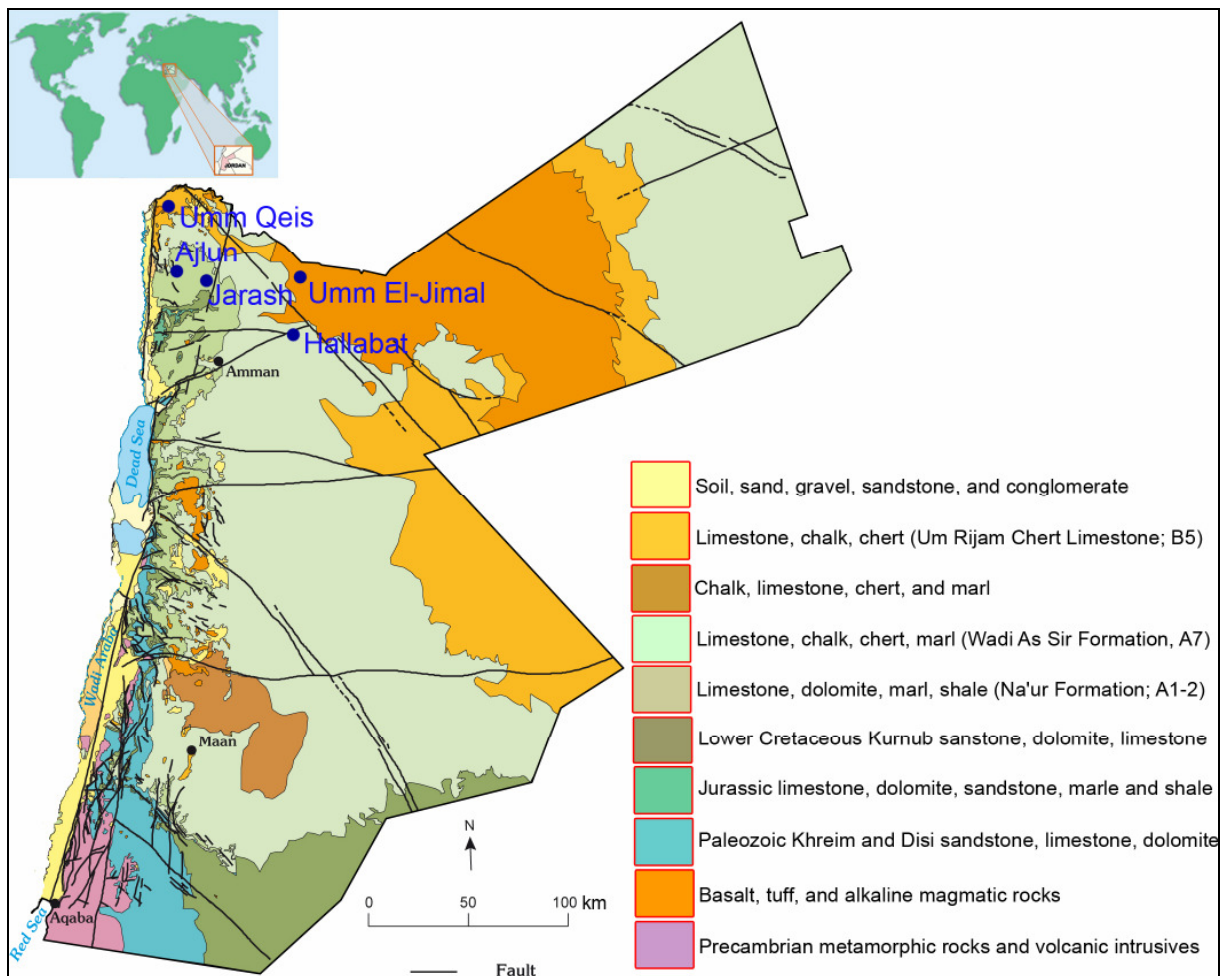


Figure 6.5: Geological map of Jordan showing the locations of the studied stone samples (modified from Water Data Banks Project, 1998).

According to the objectives of the study, two groups of samples were chosen. The first group is composed of sound materials of limestone, basalt and marble for the study of weathering behavior upon artificial ageing. The second group includes naturally weathered limestone samples for the investigation of their weathering state and the effects of conservation treatment with two products of consolidation. The categorization of the samples into sound and weathered stones was done based on visual examination and on the results of ultrasonic pulse velocity and physical properties measured in laboratory.

The composition of stone and its microstructure constitute an important intrinsic factor that governs its durability and resistance to weathering. Petrographic analysis yields important information about the mineralogical composition of the stone, the available alteration phases, the size, shape and contact of grains and other textural features and diagenetic properties. Therefore, it is an indispensable step to determine the composition and petrographic properties of stone. The petrographic analysis of the studied stone samples was performed using optical and polarizing microscope on thin sections, and was accomplished by X-ray diffraction and X-ray fluorescence measurements. The mineralogical and chemical compositions of the studied stone samples are summarized in Tables (6.1) and (6.2).

Table 6.1: Mineralogical composition of the stone samples.

	<i>Sample¹</i>	<i>Stone type</i>	<i>Site</i>	<i>Mineral composition</i>
<i>Sound samples</i>	LA	Limestone	Ajlun Castle	Calcite
	LJ1	Dolomitic Limestone	Jarash Arch. Site	Calcite, Ankerite, Dolomite, Quartz
	LUQ1	Limestone	Umm Qeis Arch. Site	Calcite, Quartz
	BUE	Basalt	Umm El-Jimal Arch. Site	Plagioclase (Labradorite), Clinopyroxene, Olivine
	BUQ	Basalt	Umm Qeis Arch. Site	Plagioclase (Labradorite), Clinopyroxene, Olivine
	MUQ	Marble	Umm Qeis Arch. Site	Calcite
<i>Naturally weathered samples</i>	LH	Limestone	Hallabat Palace	Calcite
	LJ2	Limestone	Jarash Arch. Site	Calcite
	LJ3	Limestone	Jarash Arch. Site	Calcite
	LUQ2	Limestone	Umm Qeis Arch. Site	Calcite, Quartz

¹ The first letter in the sample name refers to the type of the sample (L= Limestone, B= Basalt, M= Marble), the rest stands for the name of the site, from which the sample was taken. When two samples or more are taken from the same site, they are numbered.

Table 6.2: Chemical composition of the stone samples.

	<i>Sample</i>	<i>LA</i>	<i>LJ1</i>	<i>LUQ1</i>	<i>BUE</i>	<i>BUQ</i>	<i>MUQ</i>	<i>LH</i>	<i>LJ2</i>	<i>LJ3</i>	<i>LUQ2</i>
<i>%</i>	<i>SiO₂</i>	0.00	3.49	7.94	48.35	45.45	2.00	4.02	2.60	3.46	5.92
	<i>TiO₂</i>	0.06	0.01	0.05	2.30	1.61	0.04	0.03	0.04	0.01	0.03
	<i>Al₂O₃</i>	0.74	0.64	0.88	16.95	13.23	0.53	0.60	0.57	0.65	0.75
	<i>Fe₂O₃</i>	0.16	1.22	0.36	11.84	12.87	0.10	0.17	0.12	0.16	0.29
	<i>MnO</i>	0.00	0.01	0.00	0.16	0.17	0.00	0.00	0.00	0.00	0.00
	<i>MgO</i>	0.57	3.42	0.89	5.11	7.16	0.43	0.32	0.05	0.48	0.45
	<i>CaO</i>	46.30	42.81	47.34	10.25	14.99	47.02	47.22	46.20	46.72	46.20
	<i>Na₂O</i>	0.00	0.11	0.00	3.86	2.34	0.82	0.00	0.07	0.40	0.00
	<i>K₂O</i>	0.00	0.00	0.02	1.10	0.62	0.00	0.00	0.00	0.00	0.00
	<i>P₂O₅</i>	0.00	0.00	0.00	0.26	0.57	0.00	0.00	0.00	0.00	0.00
	<i>LOI¹</i>	43.35	43.89	42.67	0.36	1.01	43.84	43.27	43.64	44.03	43.12
<i>SUM</i>	91.18	95.60	100.15	100.54	100.02	94.78	95.63	93.29	95.91	96.76	
<i>ppm</i>	<i>Sr</i>	9	220	330	410	431	149	67	54	220	317
	<i>Ba</i>	-	-	31	96	440	32	171	341	90	261
	<i>Rb</i>	-	17	31	22	1	5	-	0	25	-
	<i>Y</i>	15	-	-	14	6	2	-	6	18	7
	<i>Zr</i>	2	17	23	151	124	11	13	10	27	31
	<i>Cr</i>	50	41	38	75	323	-	-	-	-	153
	<i>Cl</i>	-	17	-	151	156	-	-	-	-	-
	<i>S</i>	181	479	-	565	301	1707	1479	928	1522	1394
	<i>Cu</i>	3	13	5	29	41	-	19	3	7	3
	<i>Zn</i>	3002	221	548	70	138	-	280	405	394	31
<i>V</i>	-	-	-	293	211	-	-	-	-	-	

A detailed petrographic description of the studied stone samples (the sound and naturally weathered samples) is presented in the following sections.

6.1.2.1 Sound stone samples

For the first part of the work concerning the study of the effects of artificial weathering on the properties of stone, six samples of different stone types, namely limestone, basalt and marble, were selected. The petrographic properties of these stone samples are briefly described below.

The limestone samples

Sample LA (Figure 6.6): This sample was taken from Ajlun Castle and seems to be of the Upper Cretaceous limestone of the massive Wadi As-Sir Formation based on a comparison with relevant literature studies (e.g. Bender, 1974; Powell, 1989). In hand specimen, it is a yellowish grey massive limestone with very small cracks. In thin section, the sample is an unfossiliferous equi-granular recrystallized sparry limestone, composed of interlocking

¹ Loss On Ignition

anhedral to euhedral calcite crystals. The stone is characterized by intercrystalline (interparticle) porosity. Idiomorphic¹ (euhedral) crystal growth of sparry calcite, averaging around 0.15 mm across, is detected as well in fissures and pores.

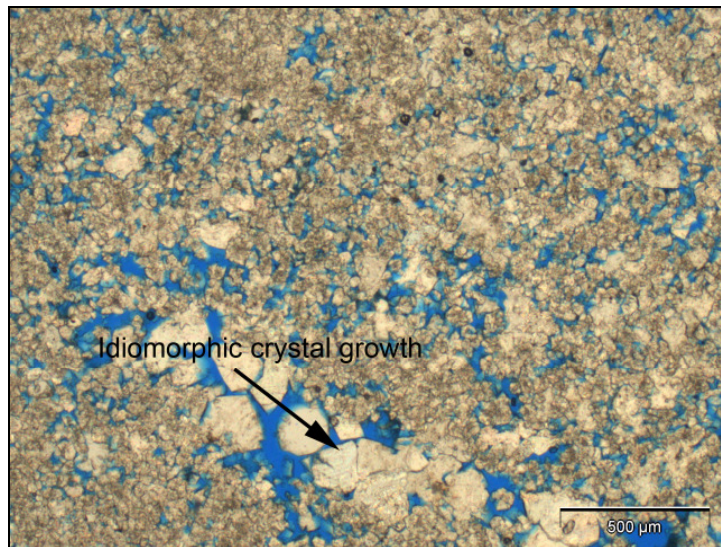


Figure 6.6: Photomicrograph of the blue-dyed thin section of sample LA (Plane-polarized light (PPL)); the blue areas indicate the pores in stone.

Sample LJ1 (Figure 6.7): Massive dolomitic Upper Cretaceous limestone, most likely of Na'ur Formation, from Jarash Archaeological Site. In hand specimen, it is a reddish yellow massive fine limestone with slight lamination.

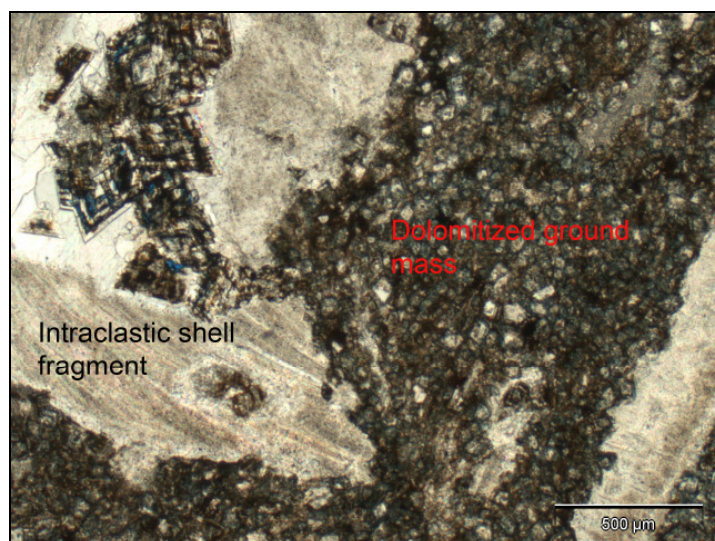


Figure 6.7: Photomicrograph of the thin section of sample LJ1 (PPL).

¹ Indicating or pertaining to a mineral constituent having its own characteristic outward crystalline form unaltered by other constituents of the rock.

In thin section, the stone is a dolomitic intraclastic biosparite (shell-fragment rudstone or rudist mudstone) with large-size bioclasts, mostly oyster (bivalves) shell fragment, imbedded in a fine-grained sparry ground mass. The matrix consists of dark brown dolomitized material with euhedral (rhombic) dolomite and ankerite (iron-rich dolomite) crystals, averaging 0.05-0.07 mm in size. The fossils and bioclasts vary in size and may reach 5 mm for elongated fragments. The pore space consists of intracrystalline (intraparticle) and minor intercrystalline (interparticle) porosity.

Sample LUQ1 (Figure 6.8): A massive limestone from Umm Qeis Archaeological Site, most probably of Umm Rijam Chert Limestone Formation (Eocene (Tertiary) in age). The stone is a whitish grey fossiliferous limestone with some small cavities or pores, which are sometimes filled with calcite. In thin section, it can be described as intrapelbiomicrite with abundant allochems (intraclasts, algae and bivalve fossil shells, pellets, and some pisolitic¹ grains). These allochemical components are embedded in a micritic matrix, which contain also patches of recrystallized sparry calcite. The stone is characterized by moldic porosity and intergranular microporosity.

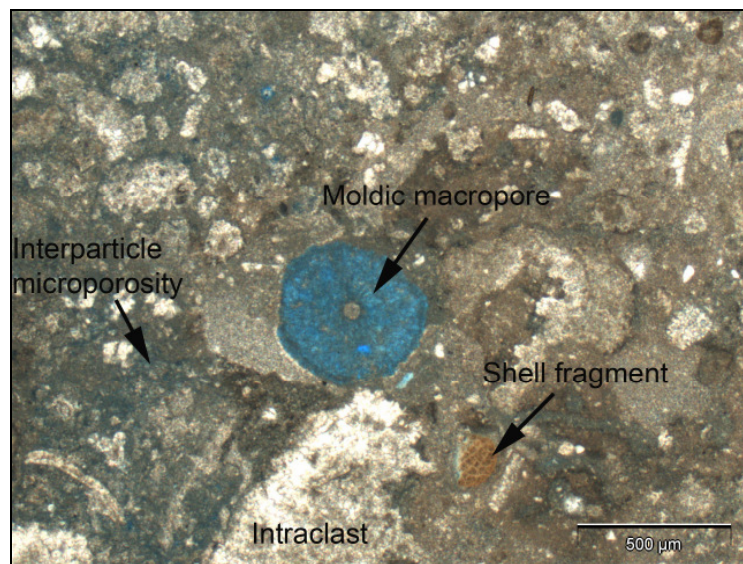


Figure 6.8: Photomicrograph of the thin section of sample LUQ1 (PPL).

The textural and petrographic properties of the sound limestones are summarized in Table (6.3).

¹ Pisolith: A small rounded accretionary mass, usually of calcium carbonate, larger and less regular than an oolite. Also called *pisolite*.

Table 6.3: The petrographic description of the sound limestone samples.

<i>Sample</i>	<i>Site</i>	<i>Geological formation</i>	<i>Microstructure</i>	<i>Porosity</i>	<i>Color</i>
<i>LA</i>	Ajlun	Wadi As-Sir Limestone Formation	Massive unfossiliferous recrystallized sparry limestone	Differential intercrystalline porosity	Yellowish grey
<i>LJI</i>	Jarash	Na'ur Limestone Formation	Dolomitic intraclastic biosparite	Minor intercrystalline and intracrystalline porosity	Reddish yellow
<i>LUQ1</i>	Umm Qeis	Umm Rijam Chert Limestone	Sparse intrapelbiomicrite	minor moldic porosity and intergranular micro-porosity	Whitish grey

The marble sample

The marble sample (**Sample MUQ** (Figures 6.9 and 6.10)) is a pure calcite grayish white marble. The study of the microstructure of the sample under polarizing microscope and the comparison with data from relevant literature indicate the Island of Proconnesus (modern Marmara, Turkey) as the most probable quarry source of the stone (Bashayrih, 2003; Capedri and Venturelli, 2004). The grain size varies between 0.2 mm and 2.5 mm, producing a medium-coarse grained metamorphic rock. The stone is characterized by a heteroblastic granular texture with irregular, embayed to sutured, grain boundaries. The recrystallization of calcite crystals during metamorphic thermal events resulted in large calcite crystals showing very nice rhombic cleavage and lamellar twinning. The randomly oriented crystals with irregular anhedral shape and interlocking mutual relations make the rock compact and massive with very low intercrystalline porosity.

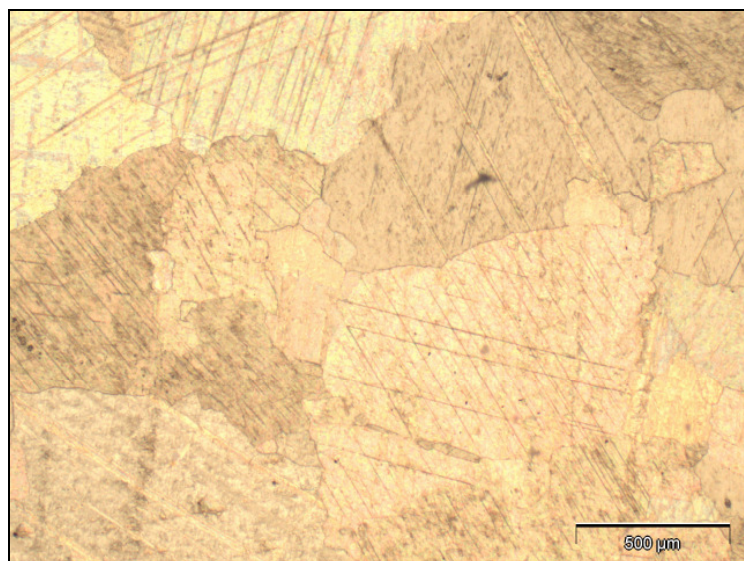


Figure 6.9: Photomicrograph of the thin section of sample MUQ (PPL).

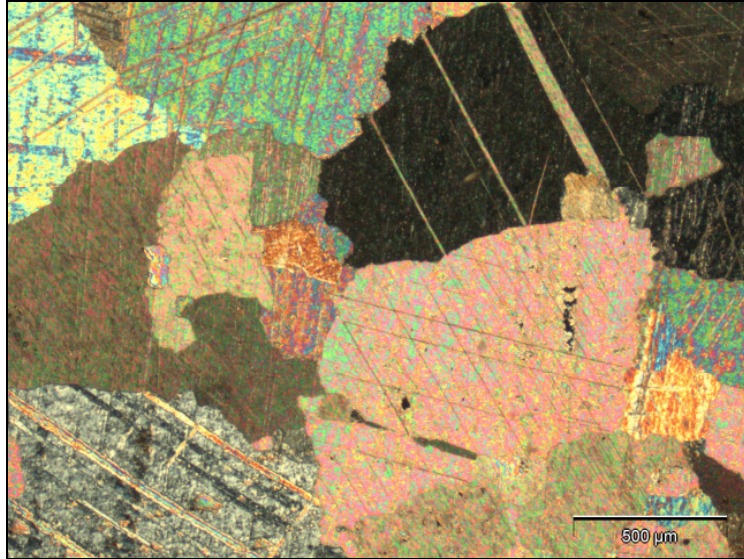


Figure 6.10: Photomicrograph of the thin section of sample MUQ in Cross-polarized light (CPL).

The textural properties of the stone are summarized in Table (6.4).

Table 6.4: The textural properties of the studied marble sample.

<i>Sample</i>	<i>Site</i>	<i>Stone type</i>	<i>Microstructure</i>	<i>Porosity</i>	<i>Color</i>
<i>MUQ</i>	Umm Qeis	Proconnesian marble	Interlocking heteroblastic, sutured, medium-coarse grained	Intergrain porosity	Grayish white

The basalt samples

Two basalt samples, **BUQ** (Figures 6.11 and 6.12) and **BUE** (Figures 6.13 and 6.14), were taken from two archaeological sites in Jordan, namely Umm Qeis (Plateau basalt of Early Pliocene age) and Umm El-Jimal (Late Tertiary (Neogene) basalt).

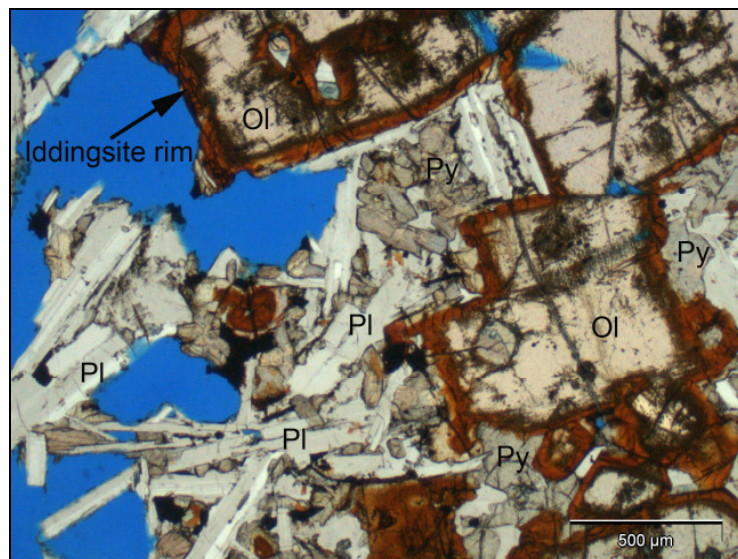


Figure 6.11: Photomicrograph of the thin section of sample BUQ (PPL). Ol= Olivine; Pl= Plagioclase; and Py= Pyroxene.

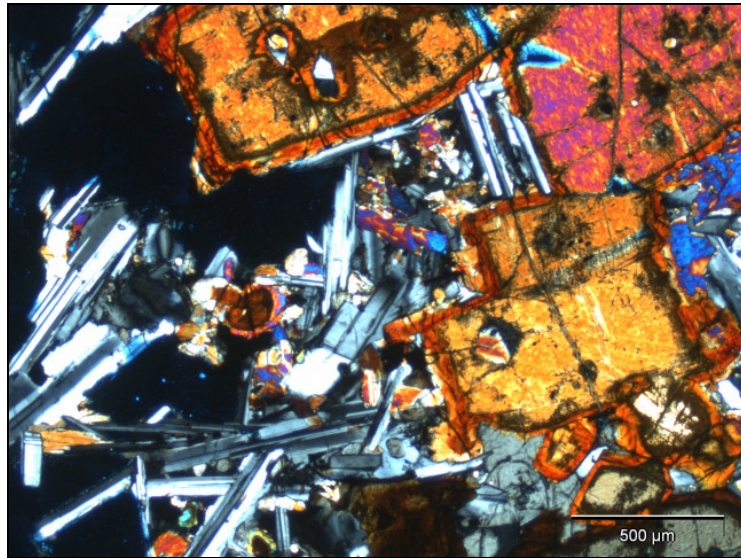


Figure 6.12: Photomicrograph of the thin section of sample BUQ above in cross-polarized light (CPL).

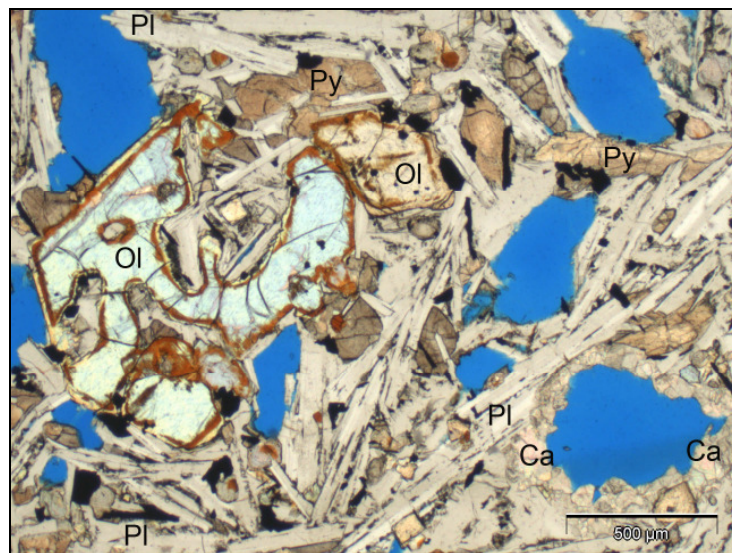


Figure 6.13: Photomicrograph of the thin section of sample BUE (PPL). Ol= Olivine; Pl= Plagioclase; Py= Pyroxene; and Ca= Calcite.

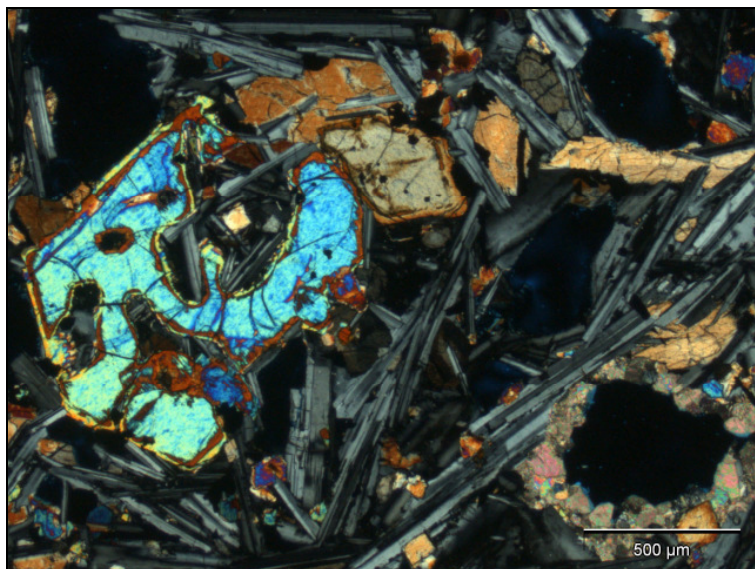


Figure 6.14: Photomicrograph of the thin section of sample BUE above in cross-polarized light (CPL).

The CIPW Norms (Table 6.5) of the basalt samples were calculated from the total chemical composition of the rock to determine the normative mineralogy. Nepheline and olivine are found to be among the normative minerals indicating a silica-undersaturated rock. Using the total alkali versus silica (TAS) diagram (Figure 6.15), the studied basalt samples are revealed to be of the alkali olivine basalt (AOB) type.

Table 6.5: CIPW-Norms of the basalt samples (calculated using KWare Magma Software (Wohletz, 1999)).

Normative minerals	BUE	BUQ
Albite (Ab)	23.39	8.08
Anorthite (An)	25.62	23.76
Orthoclase (Or)	6.48	3.66
Nepheline (Ne)	4.98	6.34
Diopside (Di)	19.52	38.84
Olivine (Ol)	13.35	12.12
Ilmenite (Il)	4.37	3.06
Magnetite (Mt)	1.73	1.89
Apatite (Ap)	0.57	1.24
Zircon	0.03	0.03
Chromite	0.01	0.07
Total	100.01	98.99

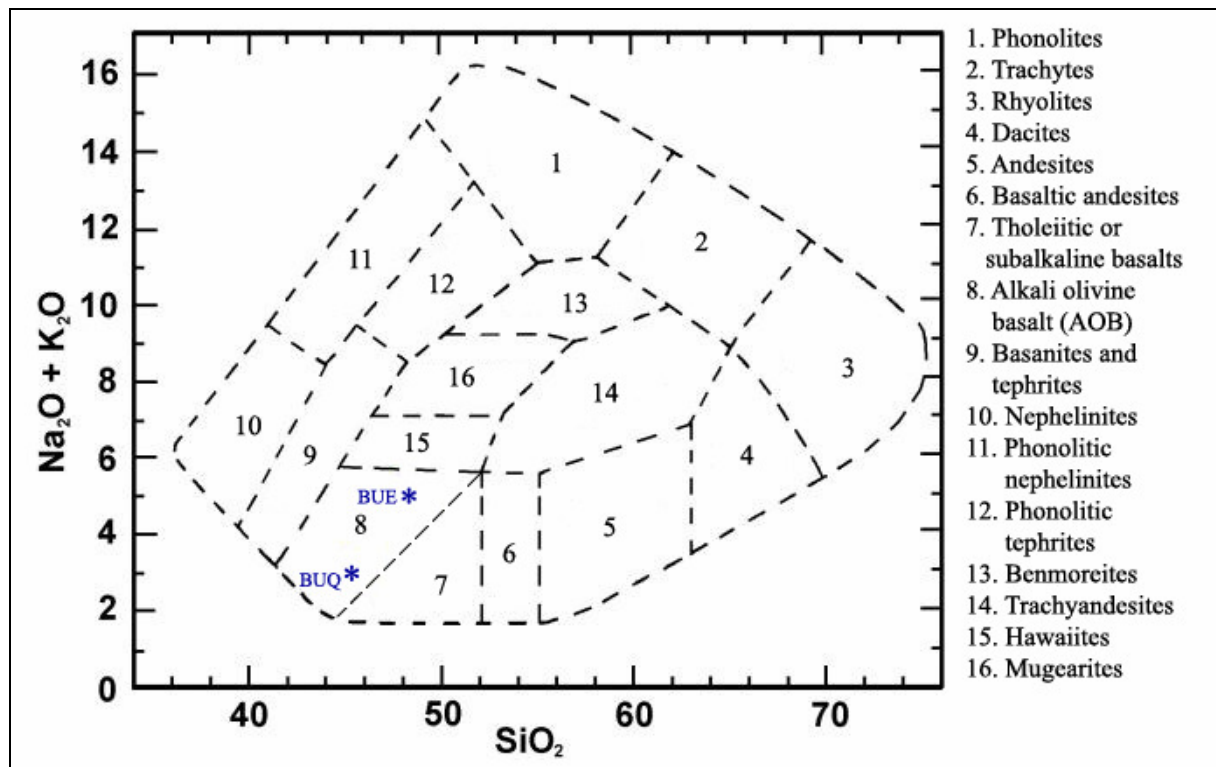


Figure 6.15: Nomenclature of the common volcanic rocks (from El-Akhal, 2004; after Cox et al., 1979).

The petrographic analysis showed that the studied basalt samples are nearly similar with a holocrystalline (completely crystalline) doleritic¹ medium-grained texture. They are generally porphyritic² with phenocrysts mainly of olivine and plagioclase in a finer matrix of pyroxene, plagioclase laths, some olivine and opaque minerals (Iron-Titan oxides). Carbonate and apatite occur sometimes in the matrix as well. The plagioclase laths are sometimes partially included within pyroxene giving rise to a sub-ophitic³ texture. Olivine phenocrysts are mostly weathered at their rims with iddingsite⁴ as an alteration product. This may eventually lead to complete dissolution of olivine grains and formation of interstitial secondary porosity. However, the other minerals, particularly plagioclase and pyroxene, are almost fresh and unweathered. The petrographic description of the studied basalt samples is summarized in Table (6.6).

Table 6.6: The petrographic description of the basalt samples.

<i>Sample</i>	<i>Site</i>	<i>Stone type</i>	<i>Texture</i>	<i>Phenocrysts</i>	<i>Groundmass</i>	<i>Porosity</i>
<i>BUQ</i>	Umm Qeis	Early Pliocene (Plateau basalt)	Doleritic medium-grained with sub-ophitic texture	Olivine, plagioclase and some carbonate	Plagioclase, pyroxene, some olivine, carbonate, opaque minerals and apatite	Secondary Some pores contain carbonates
<i>BUE</i>	Umm El-Jimal	Late Tertiary (Neogene) basalt	Ol-doleritic medium-grained	Olivine and plagioclase	Pyroxene, some olivine, carbonate and opaque minerals	Secondary Some pores contain carbonates

6.1.2.2 Naturally weathered samples

For the second part of the work concerning the study of the effects of consolidation treatments on the properties of stone, four different varieties of naturally weathered limestone samples were chosen. These stone samples are described below.

Sample LH (Figure 6.16): A pure calcitic Upper Cretaceous limestone, most probably of Wadi As-Sir Formation. The sample was taken from Hallabat Palace. In hand specimen, the sample is a light cream fine stone with small macropores and chalky patches. In thin section,

¹The typical texture of dolerite (or diabase in UK); which is a dark, mafic, and relatively coarse-grained igneous rock equivalent to volcanic (extrusive) basalt or plutonic (intrusive) gabbro.

² Composed of large-grained crystals (phenocrysts) dispersed in a fine-grained feldspathic matrix.

³ Ophitic: a texture in which lath-shaped plagioclase crystals are enclosed wholly or in part in later-formed augite, as commonly occurs in Dolerite (diabase).

⁴ A pseudomorph secondary mineral after olivine.

it can be classified as sparse fossiliferous (bioclasts and shell fragments composed chiefly of bivalve, algae and few gastropod) biomicrite (packstone) with sparry calcite growing in the fossil moulds. The porosity is characterized by diffused intergranular microporosity and moldic macroporosity.

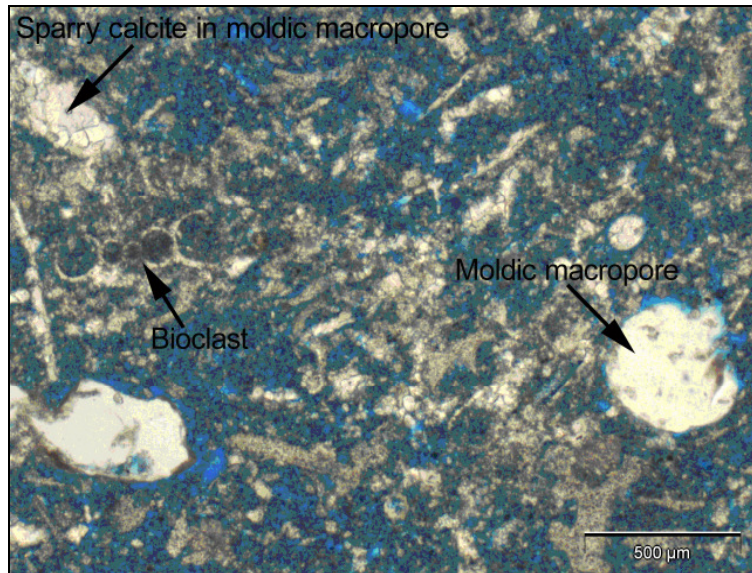


Figure 6.16: Photomicrograph showing the microstructure of sample LH (PPL).

Sample LJ2 (Figure 6.17): A pure calcitic limestone from Jarash Archaeological Site, which is mainly built of Upper Cretaceous limestone, most probably of Na'ur Limestone Formation. In hand specimen, the sample is a white chalky massive limestone showing stylolitic structure with irregular sub-horizontal thin brown cross-planes or veins. In thin section, the sample is classified as shell-fragment biosparite (shelly packstone).

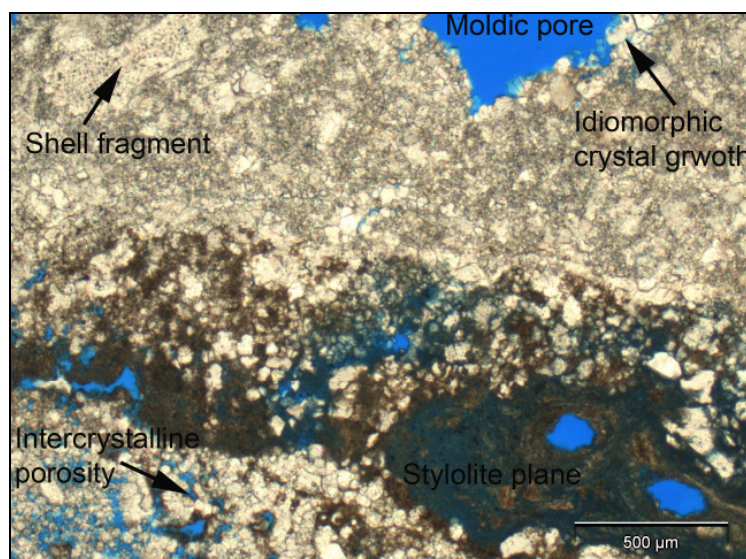


Figure 6.17: Photomicrograph showing the microstructure of sample LJ2 (PPL).

The groundmass is composed of sub-euhedral sparry calcite crystals with size ranging from about 0.03 mm to 0.3 mm. Idiomorphic crystal growth with recrystallized sparry calcite can be seen in shell cavities and along stylolitic planes. Small micritic veins penetrate the matrix in some parts. The sample is characterized by intercrystalline and moldic porosity.

Sample LJ3 (Figure 6.18): The stone is pure calcitic Upper Cretaceous limestone, possibly of Na'ur Limestone Formation, from Jarash Archaeological Site. In hand specimen, the stone is criss-crossed by numerous short irregular veins and patches of compact pale brown sparry calcite. It is a fossiliferous intraclastic limestone with vugs and cavities filled with coarse-grained calcite. It is characterized by inter-grain and fracture porosity.

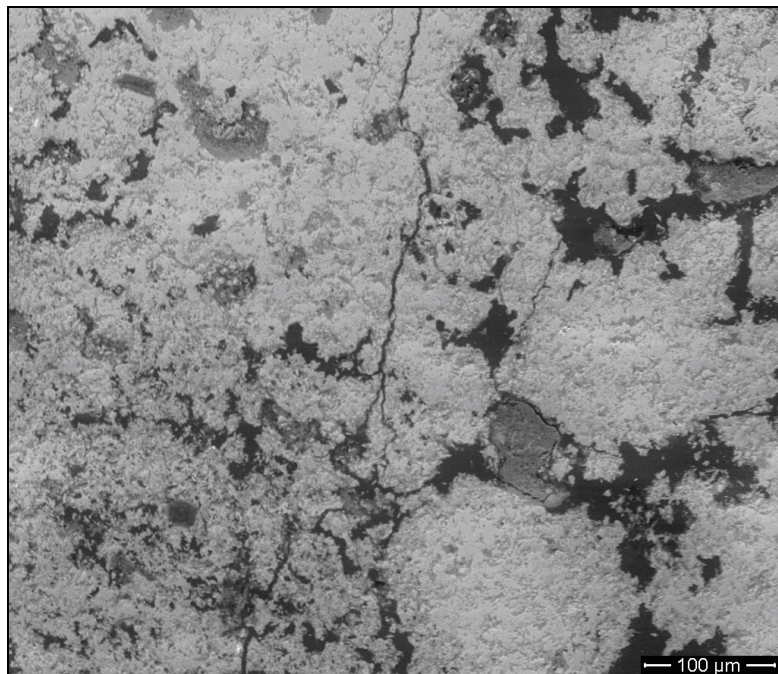


Figure 6.18: Scanning electron microscope image showing the microstructure of sample LJ3.

Sample LUQ2 (Figure 6.19): The sample was taken from Umm Qeis Archaeological Site, where Umm Rijam Chert Limestone Formation of the Tertiary age outcrops. It is a pure limestone with small amount of quartz. In hand specimen, the sample is a light beige chalky limestone with closely spaced bedding planes delineated by dark-brown thin veins. The stone can be classified as shell fragment biomicrite (wackstone). The sample is highly porous weathered limestone with diffused intergranular and fracture porosity.

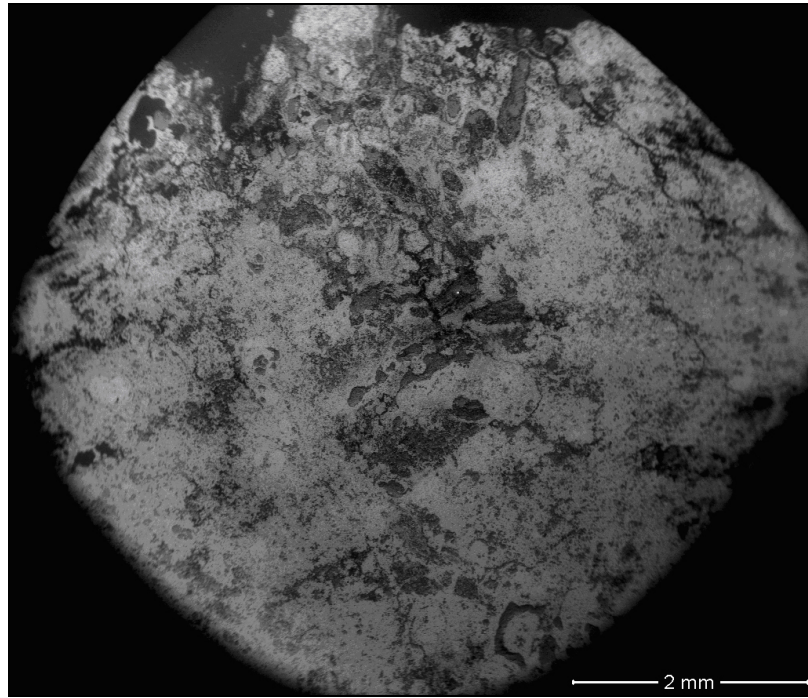


Figure 6.19: Scanning electron microscope image showing the microstructure of sample LUQ2.

The petrographic characteristics of the naturally-weathered limestone samples are shown in Table (6.7).

Table 6.7: The petrographic description of the naturally-weathered samples.

<i>Sample</i>	<i>Site</i>	<i>Geological formation</i>	<i>Microstructure</i>	<i>Porosity</i>	<i>Color</i>
<i>LH</i>	Hallabat	Wadi As-Sir Limestone Formation	Sparse fossiliferous biomicrite	Diffused intergranular micro-porosity and moldic macroporosity	Light cream
<i>LJ2</i>	Jarash	Na'ur Limestone Formation	Shell fragment biosparite	Intercrystalline and moldic porosity	White
<i>LJ3</i>	Jarash	Na'ur Limestone Formation	Fossiliferous intraclastic limestone	Intergranular and fracture porosity	Dark beige
<i>LUQ2</i>	Umm Qeis	Umm Rijam Chert Limestone Formation	Fossiliferous biomicrite	Diffused intergranular and fracture porosity	Light beige

6.2 Investigations

6.2.1 Physico-mechanical testing methods

6.2.1.1 Porosity and density by water absorption

Porosity accessible to water (N_t)

The porosity accessible to water corresponds to the ratio of the volume of pores accessible to water to the bulk volume of the sample, expressed in percent. It was measured by water absorption according to RILEM I.1. After drying at 60 °C to constant mass (M_1), the samples (5 cm cubes) were put into an evacuation vessel under vacuum (20 mm Hg pressure) for 24 hours to eliminate the air contained in the pores. Water was then slowly introduced into the vessel until the samples were completely immersed, and the vacuum was maintained for 24 hours afterwards. The samples were left under water for another 24 hours at atmospheric pressure. Finally, the samples were weighted separately under water (M_2) and directly after removing from water (M_3), and the accessible porosity was calculated as follows:

$$N_t = \frac{M_3 - M_1}{M_3 - M_2} \cdot 100 \quad (6.1)$$

N_t = porosity accessible to water [%]; M_1 = mass of the dried sample [g]; M_2 = mass of the saturated sample under water [g]; M_3 = mass of the saturated sample in air [g].

Bulk density (ρ_{bulk}) and real density (ρ_{real})

The bulk density (apparent density) is the ratio of the mass to the bulk volume of the stone sample. The real (grain/skeletal) density is the ratio of the mass to the impermeable volume of the sample (without pore space). These two densities can be determined from the above measured masses, in accordance with the norm RILEM I.2, as follows:

$$\rho_{bulk} = \frac{M_1}{M_1 - M_2} \quad (6.2)$$

$$\rho_{real} = \frac{M_1}{M_3 - M_2} \quad (6.2)$$

ρ_{bulk} = bulk density [g/cm³]; ρ_{real} = real density [g/cm³].

Free porosity (N_{48})

The free porosity represents the percent of open pores which can be filled with water under atmospheric pressure. It corresponds to the natural capacity of stone to absorb water. The free porosity was determined according to RILEM II.1. The dried samples were placed in a flat container and distilled water was added slowly to allow for capillary water absorption, before they were completely immersed in water. After 48 hours immersion in water, the samples were taken out, wiped lightly and weighted (M_{48}). The free porosity was calculated as follows:

$$N_{48} = \frac{M_{48} - M'_1}{V_{bulk}} = \frac{M_{48} - M'_1}{M_3 - M_2} \cdot 100 \quad (6.4)$$

N_{48} = free porosity after 48 hour immersion in water [%]; M_{48} = mass of the sample after 48 hour immersion in water [g]; M'_1 = the mass of the dried sample [g]; M_2 = mass of the saturated sample under water [g] as determined above for accessible porosity; M_3 = mass of the saturated sample in air [g] as determined above for accessible porosity.

Saturation coefficient (S)

The saturation coefficient (Hirschwald coefficient) denotes the percentage of pore volume which can be filled with water after complete immersion for a definite time at atmospheric pressure. It is calculated as the ratio of free porosity (N_{48}) to accessible porosity (N_i):

$$S = \frac{N_{48}}{N_i} \quad (6.5)$$

6.2.1.2 Mercury intrusion porosimetry (MIP)

Mercury porosimetry consists of injecting mercury into the porous structure of a solid material under controlled pressure. It is mainly based on the non-wetting behavior of mercury against solid surfaces. Mercury can, thus, be intruded into pores of different entry sizes by the application of increasing pressure (Gauri and Bandyopadhyay, 1999). The intruded pore size is inversely proportional to the applied pressure as given by Washburn equation:

$$r = -\frac{2 \cdot \sigma \cdot \cos \theta}{p} \quad (6.6)$$

r = pore radius [m] (convenient unit μm); σ = surface tension of mercury ($\sim 480 \cdot 10^{-3} \text{ N/m}$) [N/m]; θ = contact angle of mercury with the pore wall ($\sim 140^\circ$) [$^\circ$]; p = the applied pressure [N/m²] (convenient unit MPa (10^6 N/m^2)).

As the applied pressure increases, more and more smaller pores can be filled with mercury and consequently the total amount of intruded mercury increases. The volume of intruded mercury by gradual increase of pressure allows for the determination of the fractions of pores with different sizes, i.e. the pore size distribution of the stone. The calculation is based on the ideal model of cylindrical pores; the method does not estimate the real pore space geometry. What is actually measured by this method is the size of pore entry. If large pores are connected with smaller ones, they can be intruded with mercury only when the pressure necessary to allow intrusion into the smaller pores is reached. Consequently, the fraction of small pores in the stone is overestimated at the expense of large pores. This limiting effect is called the ink-bottle effect (see Figure 3.2).

In addition to pore size distribution, total connected porosity, specific pore surface area, and bulk and skeletal (grain) densities can also be determined from porosimetric data. The MIP method is used to characterize stone and to study its structure and behavior in response to weathering processes and consolidation treatments.

For the mercury intrusion porosimetry (MIP) in this study, a volume of around 20 ml of oven-dried small stone granules (2-4 mm in size) was used. The granules were prepared by snapping with pliers in order not to disturb the microstructure of the sample.

The mercury porosimetry measurements were carried out using the porosimeter combination PASCAL 140/240 (from Porotec) with a pressure in the range from 10 Pa to 200 MPa, whereby pore radii in the range of about 58 μm –3.7 nm can be measured.

6.2.1.3 Capillary water uptake coefficient (w-value)

The capillary water absorption coefficient (w-value) of a stone is the amount of water absorbed through a surface area of the stone per square root of time. It provides a measure for assessing the extent of stone damage and the success of conservation treatments.

The water uptake coefficient was measured on dry drill core specimens following the standard test DIN EN 1925. The specimens were placed in a water tank, so that the water level is around 2 mm above the bottom of the specimen and that was kept constant. The specimens were weighted in definite time intervals, which were selected depending on the type of the stone and its water absorption capacity. Highly absorbing stones (weathered stones) were weighted after 1, 3, 5, 10, 15, 30, 60, 480 and 1440 minutes. Stone with low water absorption capacities (sound stones) were weighted after 30, 60, 180, 480, 1440, 2880, and 4320 minutes.

The water absorption coefficient was then calculated as the slope of the linear part of the curve depicting the amount of water absorbed per area against the square root of time.

$$w = \frac{\Delta m}{A} \cdot \frac{1}{\sqrt{\Delta t}} \quad (6.7)$$

w = water absorption coefficient [$\text{kg}/(\text{m}^2 \cdot \text{h}^{1/2})$]; Δm = mass of absorbed water in time interval Δt [kg]; A = the area of the stone surface in contact with water [m^2]; Δt = time interval [h].

6.2.1.4 Drying curve

The evaporation curve of a material is obtained by plotting the density of vapor flow rate (g) evaporating from one surface of water-saturated sample of the material as a function of the remaining moisture content. The test was carried out under constant ambient conditions (20 °C and 45% RH) according to RILEM II.5. After immersion in water for 48 hours, the drill core samples (5 cm in diameter and around 8 cm long) were sealed to allow evaporation from only one surface. The mass of the sample was determined as function of time during the drying process and the results are graphically presented. The density of vapor flow rate can be calculated from the following equation:

$$g(t) = \frac{dM}{A dt} \quad (6.8)$$

g = density of vapor flow rate [$\text{g}/(\text{m}^2 \cdot \text{h})$]; M = mass of the sample [g]; A = area of the surface from which evaporation takes place [m^2]; t = time [h].

Two phases are distinguished in the one-dimensional evaporation process. The first phase persists as long as the moisture content of the material is greater than its critical moisture content. Water is transported to the surface by capillary conduction and the evaporation rate is fairly constant. During this phase, the moisture content of an initially wetted sample decreases linearly with time. In the evaporation curve (Figure 6.20), this is represented by the plateau (PL) (where g is calculated). The breaking point (P1) marks the second evaporation phase when the water front retreats into the material and the drying velocity decreases rapidly as evaporation takes place inside the material by vapor diffusion. The second breaking point (P2) represents the residual moisture stored in the smallest pores. It can sometimes be observed at low residual moisture below 10% and when two distinct pore radii maxima are characterized in the stone structure (Bourgès, 2006).

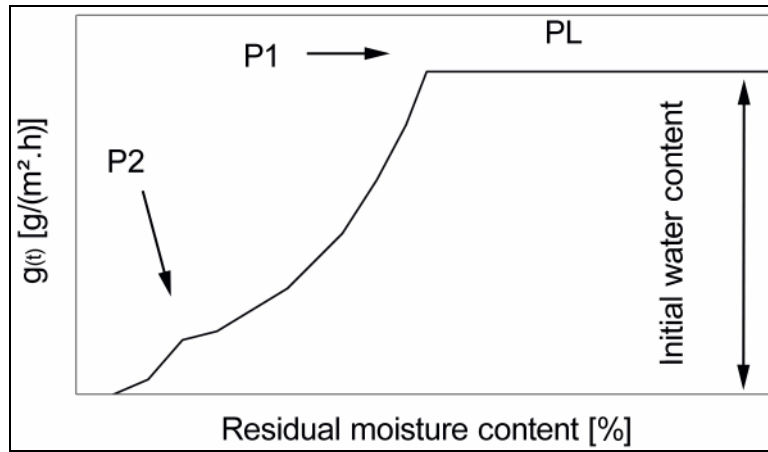


Figure 6.20: Drying curve of a porous material (from Bourgès, 2006).

This test is useful to obtain information about the changes occurred in the pore structure of the material due to weathering or consolidation processes and to assess the success of some conservation treatments such as water repellents.

6.2.1.5 Water vapor diffusion resistance coefficient (μ -value)

The water vapor diffusion resistance coefficient of a material (μ -value) is the ratio of water vapor permeability of air to that of the material. It is a dimensionless number that indicates how many times greater the resistance against water vapor diffusion of the material is than that of an equally thick layer of air ($\mu=1$) at the same temperature. The test was carried out in accordance with the norm DIN EN ISO 12572 using the wet-cup (45-100% RH) procedure. A dry 5 mm thick disc with a diameter of 5 cm was fixed on the top of a special beaker filled to one third with distilled water. The space between the disc and the beaker was sealed to allow water vapor transport only through the stone material. The beaker was weighted and placed in climatic chamber at 45% RH and 20 °C, and the decrease in its mass was measured every 24 hours. The water vapor diffusion resistance coefficient was then calculated as follows:

$$\mu = \frac{\delta_a}{\delta} = \frac{\delta_a \cdot \Delta p \cdot A}{G \cdot d} \quad (6.9)$$

μ = water vapor diffusion resistance coefficient [-]; δ_a = water vapor diffusion coefficient of air ($\sim 1.9 \cdot 10^{-10}$ kg/(m.s.Pa) [kg/(m.s.Pa)]; δ = water vapor permeability of the material [kg/(m.s.Pa)]; Δp = vapor pressure difference (gradient) on both sides of the specimen [Pa]; G = average amount of water vapor diffused through the material per unit time (water vapor diffusion flow) [kg/s]; A = area of the specimen [m²]; d = thickness of the specimen [m].

The μ -value of the material can be used to assess the influence of consolidation treatments on drying behavior.

6.2.1.6 Adsorption isotherm curve

The adsorption isotherm curve represents the relationship between the equilibrium hygroscopic moisture content of the material and the relative humidity of the ambient air at constant temperature. The adsorption isotherm curves for the weathered stones were determined according to DIN EN ISO 12571. After drying to constant mass at 60 °C, stone specimens (at least 2 g in mass) were placed in desiccators with saturated salt solutions of K_2CO_3 , NH_4NO_3 , NaCl, KCl, and K_2SO_4 at 20 °C, which correspond to specific relative humidities of 45%, 63%, 76%, 86% and 98% respectively. The specimens were repeatedly weighted until an equilibrium state is reached with the respective relative humidity. The equilibrium moisture contents for each sample at the different relative humidities were then calculated and graphically represented to obtain the adsorption isotherm curve.

The adsorption isotherm curve was determined to establish the necessary preconditions for consolidation treatments.

6.2.1.7 Water micro-drop absorption

The absorption rate of water micro-drop was used to determine the penetration depth of the consolidants into the treated stone samples. The rate of water absorption decreases in the treated stone due to the hydrophobing (water repellency) effect of the consolidant and, to a minor extent, because of the pore filling brought about by consolidation treatment (RILEM II.8a; Moreau et al., 2007). The water drop absorption test was performed based on RILEM II.8a. The treated core specimens were sectioned into 5 mm thick discs in depth profile, and the necessary time for the total absorption of a water droplet of 10 μ l put at the centre of each disc was recorded. The results obtained from treated and untreated stone allow for a rough estimation of the penetration depth of consolidation treatments.

6.2.1.8 Color measurement

Colorimetric measurement was used to determine the color differences due to consolidation treatments. The color changes were expressed in the CIE-Lab system recommended by the *Commission Internationale d'Eclairage* (CIE) in 1976. The $L^*a^*b^*$ color coordinates of the stones were measured before and after consolidation treatments exactly at the same positions. The recorded values are the average of five consecutive measurements. The total color differences are calculated using the following equation:

$$\Delta E = \sqrt{(\Delta L^*)^2 + (\Delta a^*)^2 + (\Delta b^*)^2} \quad (6.10)$$

ΔE = the change in color; ΔL^* = change in the brightness or lightness; Δa^* = change in the chromatic component a^* (red - green); Δb^* = change in the chromatic component b^* (yellow - blue).

Color measurements were performed using a portable colorimeter (Spectro-color from Dr. Lange) with a measuring geometry of diffus/8° (diffused polychromatic light and 8° viewing angle) and an illumination aperture of 10 mm in diameter.

6.2.1.9 Thermal expansion coefficient (α_T)

Measurements of the linear thermal expansion coefficient (α_T) of the stones were carried out using the displacement transducers (linear variable differential transformer (LVDT)) shown in Figure (6.21).

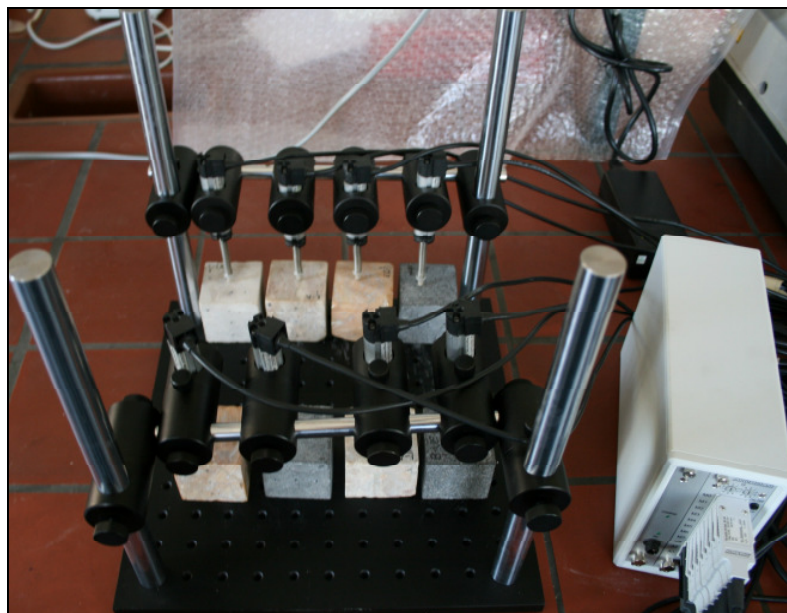


Figure 6.21: The used experimental set-up for measuring the thermal dilatation of stone.

The specimens were heated in oven at 60 °C for 48 hours and then placed outside in dilatometer to measure their deformation during cooling down to room temperature (~20 °C). The deformation of the specimen was recorded continuously by the data logger coupled to the dilatometer. The linear thermal expansion coefficient was calculated from the relative variation of length of specimens in the given temperature interval using the following equation (see Section 2.1.1.4).

$$\alpha_T = \Delta L / (l_o \cdot \Delta T) \quad (6.11)$$

α_T = linear thermal expansion coefficient [$10^{-6}/\text{K}$]; ΔL = variation in length due to the temperature change [mm]; l_o = length of the sample [mm]; ΔT = temperature range [K].

6.2.1.10 Biaxial flexural strength and static modulus of elasticity

The biaxial flexural strength (β_{BFS}) is measured by placing a stone core slice between two circular rings of different diameters and applying a concentric increasing load. The sample undergoes first an elastic deformation, where a static modulus of elasticity (E_{stat}) can be measured, before it eventually ruptures. The biaxial flexural strength and the static modulus of elasticity can be calculated using the following equations (Wittmann and Prim, 1983):

$$\beta_{BFS} = \frac{3 \cdot F_{max}}{4 \cdot \pi \cdot d^2} \cdot \left[2 \cdot (1 + \mu) \cdot \ln \frac{a}{b} + \frac{(1 - \mu) \cdot (a^2 - b^2)}{a^2} \cdot \frac{a^2}{r^2} \right] \quad (6.12)$$

$$E_{Stat} = \frac{1.5 \cdot F_{max}}{f_0 \cdot d^3} \cdot (1 - \mu^2) \cdot \left[b^2 \cdot \ln \frac{b}{a} + \frac{(a^2 - b^2) \cdot (3 + \mu)}{2 \cdot (1 + \mu)} \right] \quad (6.13)$$

β_{BFS} = biaxial flexural strength [N/mm^2]; E_{Stat} = static modulus of elasticity [N/mm^2]; F_{max} = maximum force [N]; d = thickness of the stone sample; μ = Poisson ratio (here $\mu=0.25$); a = radius of the lower ring [mm] ($a=19.5$ mm); b = radius of the upper ring [mm] ($b=6.5$ mm); r = radius of the stone sample [mm]; f_0 = deflection/bending of the slice at $1/3 F_{max}$ [mm].

The samples used for this test were 5 mm thick drill core slices with a diameter of 5 cm (thickness to diameter ratio = 1:10). Measurements were performed using a universal *Zwick Z010* apparatus with a preload of 5 N at a rate of 0.5 mm/min. The static modulus of elasticity was derived from the initial and linear part of the stress-strain curve; the slopes of stress strain curves were determined between 10-30% of the peak strength using linear fit. The static modulus calculated here does not necessarily agree with the one determined by compressive

strength test (Young's modulus). This test can be used to assess the depth of weathering and of penetration of consolidation products.

6.2.1.11 Drilling resistance

Drilling resistance is a micro-destructive technique that can be used, both in situ and in the laboratory, to evaluate the weathering extent of stone in depth profile and to assess the effectiveness and penetration depth of consolidation treatments. Two general groups of drilling machines are available in the market. The first group is based on the operating principle developed by Hirschwald (1908), where the time necessary to achieve a defined penetration depth at constant pressure and rotation speed is measured. The second group of drilling machines is represented by the Drilling Resistance Measurement System (DRMS), which was developed within the European EC Hardrock project (SMT4-CT96-2056) and is produced by SINT Technology (Italy). This machine is based on measuring the force that is necessary to drill a hole in the stone at constant rotational speed and penetration rate. An overview on drilling resistance can be found in Pamplona et al. (2007).

The DRMS machine produced by SINT Technology was used in this study with a diamond drill bit (*Diaber*) of 5 mm in diameter under the operative conditions of 600 rpm rotation speed and 10 mm/min penetration rate. Homogeneous artificial reference samples (ARS) were used for calibration. Holes of 1 cm in depth were drilled in dry specimens and the average value of at least three measurements was considered. The resulting profiles of drilling resistance provide information about the quality of the stone and the consolidation effect of the applied products.

6.2.1.12 Fracture density (F_D)

The fracture density is a measure of the total surface area of fractures per unit volume of stone (Nicholson, 2001). It affects the mechanical strength of the stone and its other properties, particularly the elastic properties. The fracture density can be estimated using the following stereological equation (Karcz and Dickman, 1979).

$$F_D = 2P_L \quad (6.14)$$

F_D = fracture density (fracture surface area per unit volume) [mm^2/mm^3]; P_L = number of point intersections of fractures per unit length of grid line [mm^{-1}].

This equation is statistical in nature; it describes only the average outcome of all possible encounters between the tested surfaces and superimposed grids. In this study, a 5x5 cm grid of 1 cm spacing lines was superimposed on the surfaces of each cubic specimen. The number of point intersections of all fractures visible to the naked eye was counted and used with the total grid length to calculate fracture density. This method is only used to determine the macrocracks; the more important microcracks are not visible to the naked eye and can not, therefore, be determined with this method. The fracture density was measured before and after weathering test.

6.2.2 Petrographic and chemical analyses

6.2.2.1 X-ray diffraction (XRD)

The qualitative analysis of the mineralogical composition of the studied stone samples was done using a Philips PW 1729 X-ray diffractometer with Cu-K α radiation (1.5418 Å), 30 kV and 30 mA. The measurements were carried out on powdered samples over measuring angles of 3° - 73° with a gradual increase of 0.02°/s and a measuring time of one second. The detection limits for mineral crystalline phases is around 3-5%.

6.2.2.2 X-ray fluorescence (XRF)

The studied stone samples were chemically analyzed using an Oxford ED2000 energy dispersive X-ray fluorescence spectrometer with Oxford XpertEase software. The instrument is equipped with 50-Watt silver tube and the detector has a resolution smaller than 150 eV (Mn). The samples (50 mg) were prepared by fine grinding and pressing as tablets (12 mm in diameter) after mixing with a binding agent (2% Plexigum solution in ethyl-acetate). Quantitative chemical analysis was performed by calibration with known standards.

6.2.2.3 Microscopic analysis

For the characterization of the microstructure of the studied stones and their mineral composition, petrographic analysis with Zeiss polarizing light microscope was carried out on

polished thin sections of the stones (~30 μm thick). This method provides useful information about the characteristics of the mineral grains forming the stone and its pore structure. It helps as well to identify the changes in the stone structure and its composition due to weathering processes.

6.2.3 Non-destructive ultrasonic methods

6.2.3.1 Velocity of longitudinal ultrasonic waves (pulse velocity V_p)

The longitudinal ultrasonic velocity was determined in direct transmission method as shown in Figure (5.2). The travel time of the wave between the transducers, arranged directly opposite to each other on both sides of the stone sample, was determined from the first-break arrival time of the received signal. The pulse velocity can thus be calculated as follows:

$$V_p = \frac{l}{t - t_0} \quad (6.15)$$

V_p = ultrasonic pulse velocity [m/s]; l = measuring distance [m]; t = measured time [μs]; t_0 = time correction value [μs].

The transducers were coupled to the surface with an elastic material (plastic-fermit) for better contact. The calibration of the system was done by bringing both transducers in contact with each other and measuring the specific time delay and by measuring a homogeneous reference material of Plexiglas with known ultrasonic velocity.

Measurements were carried out with portable ultrasonic device UKS 12 from Geotron-Elektronik. The system is composed of an ultrasonic generator USG 20 and 50 MHz Philips scopemeter. A point-shaped ultrasonic transmitter (UPG-T) vibrating at 46 kHz together with ultrasonic receiver (UPE-T) were used on cubic, prismatic and drill core samples to study the effects of weathering and consolidation products. A similar system with USG 30 ultrasonic generator and 100 MHz Fluke scopemeter (FLUKE 99B) was also used to measure ultrasonic velocity at other ultrasonic frequencies. A transducer combination of 250 kHz transmitter and the corresponding UPE-T receiver was used on the prismatic samples for comparison of results. For estimating the penetration depth of consolidants, a point-shaped 350 kHz UPG-T transmitter and UPE-T receiver were also used. Measurements with the second system were

performed at constant contact pressure of 3 bar (0.3 MPa) and evaluation was done with LightHouse software 2000-SM.

The accuracy of velocity measurement in transmission mode is assumed to be $\pm 10\%$ (or: ± 50 m/s).

The ultrasonic pulse velocity was measured along three perpendicular directions for the cubic samples and both parallel and perpendicular to bedding planes for the drill core samples. These measurements were also used to calculate the anisotropy indices of the stones according to the following equation:

$$A = \frac{V_{P_{\max}} - V_{P_{\min}}}{V_{P_{\max}}} \cdot 100\% \quad (6.16)$$

A = anisotropy [%]; $V_{P_{\max}}$ = maximum ultrasonic pulse velocity [m/s]; $V_{P_{\min}}$ = minimum ultrasonic pulse velocity [m/s].

6.2.3.2 Calculation of dynamic modulus of elasticity (E_{dyn})

The dynamic modulus of elasticity (E_{dyn}) was determined by the extensional wave measurement procedure (Erfurt and Krompholz, 1996), which involves measurements of the travel time of longitudinal wave and the resonance frequency of the base extensional wave. Extensional waves occur in bar-shaped prisms with lateral dimension sufficiently smaller than the wavelength. The used prismatic samples should have suitable dimension to allow for the propagation of both extensional and longitudinal waves.

Measurements were carried out using the portable ultrasonic system UKS 12 with USG 30 ultrasonic generator and 100 MHz Fluke 99B scopemeter. The transducer combination UPG-D/UPE-D vibrating at 20 kHz was used on the prismatic samples at contact pressure of 3 bar. Following the producer specifications, no coupling agent and amplifier were used and the width to length ratio of the specimen was 1:2.5 (ratio ranges between 1:2 and 1:4). The evaluation was performed with LightHouse software 2004-DW.

The measurements were performed before and after weathering and consolidation to indicate the changes in the elastic properties of the stones. Three specimens were tested for each stone and the average value of at least 3-5 measurements was calculated. The accuracy of measurement is assumed to be $\pm 10\%$.

6.2.4 Artificial weathering

Artificial weathering was carried out by salt crystallization test for the sound limestone and basalt samples and by thermal degradation for the marble sample. These artificial weathering tests are described below.

6.2.4.1 Salt crystallization test

The salt crystallization test was carried out by total immersion in a solution of sodium sulfate decahydrate ($\text{Na}_2\text{SO}_4 \cdot 10\text{H}_2\text{O}$) according to the standard test DIN EN 12370. The samples were first dried at 105 °C until constant mass is reached, and then they were allowed to cool down to room temperature and weighted. Every cycle of salt crystallization consisted of soaking the samples in a 14% solution of sodium sulfate decahydrate for two hours, and drying in an oven at 105 °C for 20 hours and then cooling down at room temperature for about two hours before weighting and re-soaking in fresh sodium sulfate solution for the next cycle. 25 salt weathering cycles were performed on the sound limestone and basalt samples. The ultrasonic pulse velocity in the samples was measured every five cycles. Porosity measurements were also performed on thoroughly rinsed specimens that were taken out after 10, 20 and 25 cycles. At the end of the test, the samples were submerged in distilled water that was changed daily before eventually rinsed thoroughly in water to remove all the salt from their pores. The temperature of the immersion water was above 32 °C to prevent damage during cleaning by crystallization of mirabilite (see Figure 4.1). The samples were finally dried in oven and the loss of stone material after the test is calculated from the change in the mass of specimen as a percentage of initial mass.

$$\Delta m = \frac{M_{d0} - M_{df}}{M_{d0}} \cdot 100\% \quad (6.17)$$

Δm = relative mass difference [%]; M_{d0} = dried mass before the test [g]; M_{df} = dried mass after the test [g].

The samples used in this test were 5 cm cubes, drill cores and 2x2x5 cm prisms.

6.2.4.2 Thermal weathering

The thermal degradation of the studied marble was performed by heating the specimens to 500 °C for one hour and cooling them down in the oven for two hours. The specimens were then immersed in water over night and conditioned at 60% RH and 20 °C for three weeks to allow the hydroxylation and carbonation of superficially calcinated pore walls (Haake et al., 2004). The altered marble obtained in this way is commonly comparable to so called *marmocotto* (cocked marble) (Moreau et al., 2007).

6.2.5 Consolidation treatments

The naturally weathered limestone samples showed generally an increasing strength profile towards the interior and they were treated with two silicic acid ester consolidants namely, Remmers KSE 300 and Remmers KSE 300HV. Based on the results of isotherm adsorption test, the samples were first preconditioned at suitable relative humidity. For the cubic and prismatic samples, the consolidants were applied by capillary uptake until saturation and then by total immersion for one hour. The drill core samples, on the other hand, were only treated by capillary suction for one hour in order to allow the determination of the penetration depth of the consolidants.

After consolidation treatment, the samples were conditioned at around 75% RH and 20 °C (in desiccator with a saturated salt solution of sodium chloride) for at least three weeks in order to achieve deposition of silica gel due to hydrolytic polycondensation of tetraethoxysilane. Afterwards the samples were examined again to evaluate their properties after treatment.

7 Results and discussion

7.1 Properties of stones before and after weathering

7.1.1 Salt crystallization test

The properties of the studied limestone and basalt samples before and after salt weathering test are described below.

7.1.1.1 Visual examination

The stone samples were visually inspected during and at the end of the weathering test. Signs of damage started to appear on the stones beginning from the 5th weathering cycle. Besides salt efflorescence which appeared on all stone samples and which could be removed by washing, some samples suffered other forms of weathering. For example, some macrocracks started to appear on the limestone samples LJ1 and LA after the 5th and 8th cycle respectively. Sample LUQ1 started to disintegrate gradually, indicating an ongoing loss of cohesion between grains.

At the end of salt crystallization test, the limestone samples exhibited two different weathering behaviors (Figure 7.1). The two samples LA and LJ1 were subject to fracturing without significant loss of stone material. On the contrary, the sample LUQ1 showed mainly granular disintegration and preferential weathering in form of pitting, and suffered relatively greater loss of stone material. Petrographically, this stone is described as intrapelbiomicrite with abundant allochems mainly fossil shell fragments (bivalves and algae). These components impart heterogeneity to the stone and constitute local weakness points and might be responsible for the observed differential weathering (Angeli et al, 2007). The basalt samples exhibited no considerable macroscopic signs of damage.

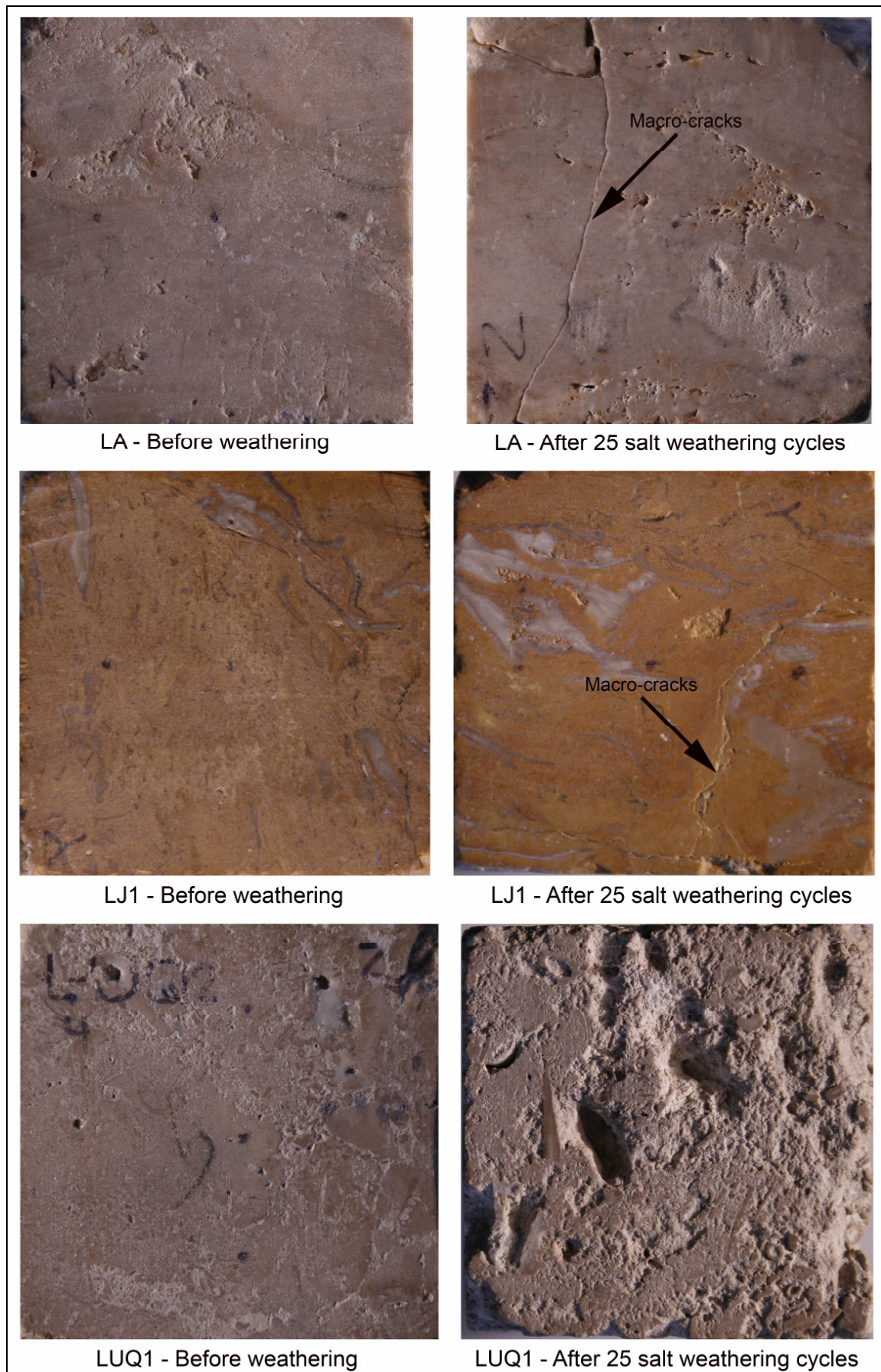


Figure 7.1: Limestone samples before and after weathering.

7.1.1.2 Porosity and density

The results of porosity and density measurements by water absorption before and after different numbers of salt weathering cycles are summarized in Table (7.1). These measurements were done after desalination of the samples by immersion in distilled water, which was changed daily, for one month and eventually by thorough rinsing with water. The limestone samples exhibited a slight continuous increase in total accessible porosity with increasing number of weathering cycles. The accessible porosity after 25 weathering cycles increased by 10%, 3% and 2% for samples LA, LJ1 and LUQ1 respectively. This indicates a continuous breaking up of grain contacts due to weathering, leading thereby to the development and enlargement of cracks and pores (Fitzner, 1988). On the other hand, the basalt samples showed a decrease in porosity, particularly at the beginning of the test. This might be attributed to pore-clogging by trapped salt crystals (Nicholson, 2001; Yu and Oguchi, 2009a).

Table 7.1: Porosity and density before and after various numbers of weathering cycles.

Sample	No. of weathering cycles	Accessible porosity (N_t) [%]	Free porosity (N_{48}) [%]	Real density (ρ_{real}) [g/cm ³]	Bulk density (ρ_{bulk}) [g/cm ³]	Saturation coefficient (S)
LA	0	6.95	3.60	2.71	2.52	0.52
	10	7.00	3.44	2.72	2.50	0.50
	20	7.04	3.51	2.71	2.49	0.49
	25	7.62	3.77	2.71	2.48	0.50
LJ1	0	6.44	4.42	2.74	2.56	0.68
	10	6.49	4.15	2.75	2.57	0.64
	20	6.51	4.43	2.72	2.57	0.68
	25	6.63	4.46	2.73	2.50	0.67
LUQ1	0	9.02	7.37	2.70	2.46	0.81
	10	9.03	7.38	2.71	2.47	0.82
	20	9.06	7.25	2.70	2.42	0.82
	25	9.15	7.65	2.71	2.46	0.83
BUE	0	11.54	3.21	3.02	2.67	0.28
	10	11.24	2.81	3.01	2.71	0.24
	20	11.51	2.40	3.00	2.71	0.23
	25	11.59	3.12	3.01	2.67	0.23
BUQ	0	9.78	2.97	2.96	2.67	0.30
	10	9.34	2.39	2.97	2.69	0.26
	20	9.75	2.82	2.97	2.68	0.28
	25	9.79	2.87	2.96	2.68	0.29

7.1.1.3 Mercury intrusion porosimetry (MIP)

The study of pore space characteristics and pore size distribution of stone is a very important requirement for the exact definition of weathering processes and the quantification of weathering degree (Fitzner, 1988). Mercury intrusion porosimetry (MIP) measurements were carried out on the stone samples before and after salt weathering test. Before measuring, the weathered specimens were thoroughly cleaned with distilled water to remove the salt contained in pores. The results are shown in Figure (7.2).

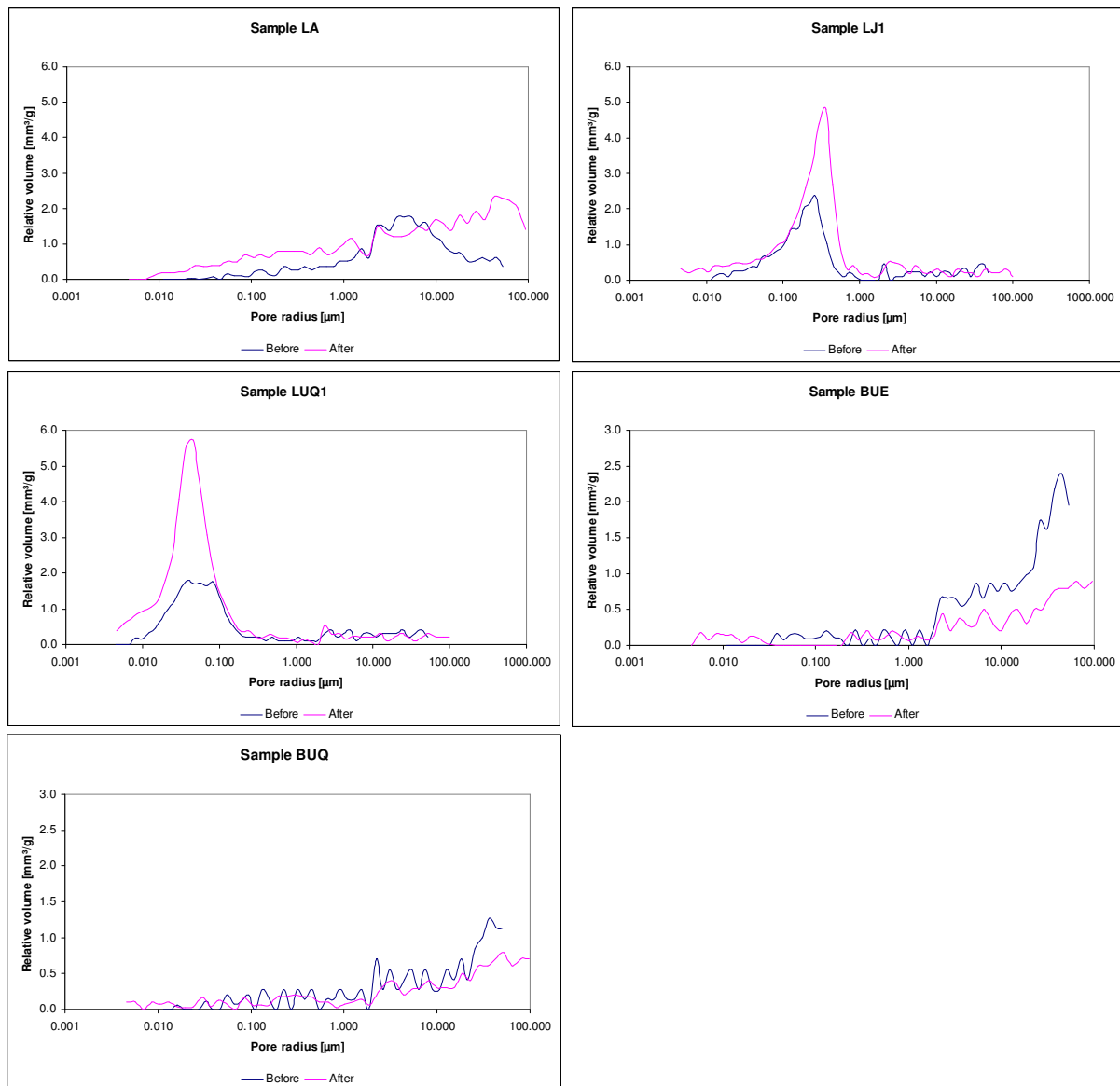


Figure 7.2: Pore size distribution of the stones before and after salt weathering test

MIP spectra before salt weathering

The pore size distribution of the sound limestone sample LA ranges from around 0.05 μm to 50 μm with an average pore radius of 4.89 μm . The main peaks lie in the pore size range from 1-10 μm . The stone is characterized by a relatively high proportion of capillary pores.

The other two limestone samples (LJ1 and LUQ1) have different MIP spectra with most of the pore entries around an average pore radius of 0.23 μm for LJ1 and 0.03 μm for LUQ1. The porosity of the sample LJ1 comprises small capillary pores and some micropores. The sample LUQ1, in contrast, is mainly characterized by microporosity with a small proportion of small capillaries.

The two basalt samples BUE and BUQ have nearly the same pore size distribution with average pore radii of 41.07 μm and 33.60 μm respectively. Several peaks in the pore range from about 1-50 μm occur and the samples are primarily characterized by large capillary pores.

MIP spectra after salt weathering

After weathering, the limestone samples exhibited higher connected porosity. This concurs with the results obtained by water absorption and may be partly attributed to the development and extension of cracks and the enlargement of small pores (Nicholson, 2001).

By comparing the MIP spectra of the sample LA before and after weathering, it can be seen that some microcracks¹ in the pore size range 0.007-1.5 μm were developed; new peaks appeared and the volume of pores in this range increased. The volume of pores in the size range 2.5-8 μm was decreased. The openings of many pores in this range seem to be enlarged as indicated by the peak shift towards larger macropores (Angeli et al., 2008). Due to this pore entry enlargement and crack development, the volume of pores with size range 8-53 μm was increased, and new pores and/or cracks appeared in the larger pore range 53-100 μm . In general, the weathered sample LA has a wider distribution of pores with an increased ratio of larger pores and an average pore radius of 41.09 μm .

For the sample LJ1, new microcracks were developed and the volume of pores in the size range 0.004-0.05 μm was slightly increased. The main change in the distribution of pores for this stone after weathering is the considerable peak increase in the main family of pores (~ 0.1-1 μm). A few macrocracks were also developed, particularly in the pore size range 53-100

¹ Microcracks ($r < 3 \mu\text{m}$) and macrocracks ($r \geq 3 \mu\text{m}$)

μm . The MIP spectra of the weathered sample LJ1 shows generally an increase in porosity of the main peaks with a slight shift towards larger pores and an average pore radius of $0.3 \mu\text{m}$.

The MIP spectra of the sample LUQ1 show the development of new microcracks and the significant increase of the main pore size volume in the range from around $0.01\text{-}0.1 \mu\text{m}$. Some macrocracks or pores appeared in the range of pores greater than $50 \mu\text{m}$, which might be a result of the enlargement of smaller pores. In general, the main family of pores in the sample LUQ1 was considerably increased after weathering and the average pore radius increased slightly to $0.04 \mu\text{m}$.

The basalt samples seem to have lower connected porosity after weathering. This is probably a result of the deposition of crystallized salt in pores due to the binding effect which sometimes occurs (Nicholson, 2001). Even after thorough cleaning with water, salt may still be trapped in the porous system of stone affecting thereby its pore size distribution.

The MIP spectra of sample BUE shows clearly the shift of pores in the size range $0.03\text{-}0.2 \mu\text{m}$ towards smaller micropores due to salt deposition on pore entries (Angeli et al., 2008). The volume of pores of the sound stone in the pore range of around $2\text{-}50 \mu\text{m}$ is noticeably greater than the corresponding one of the weathered stone. This might be mainly attributed to the partial filling of pore cavities with salt (Angeli et al., 2008). These observations confirm the pore infilling with salt as the reason behind the reduced connected porosity of the weathered stone. In general, the total pore volume of the sample decreased after weathering and peak shifts toward smaller pores occurred due to partial filling of pore with salt. Salt deposition took place mainly in the entries of micropores and inside the cavities of macropores. Few macrocracks were also developed particularly in the pore range greater than $50 \mu\text{m}$.

The sample BUQ exhibited nearly similar changes in its pore size distribution after weathering. The volume of larger pores was decreased after weathering owing to salt deposition in pore cavities and few micro- and macrocracks were developed.

Table (7.2) summarizes the MIP porosity values and the pore size distribution of the samples before and after salt weathering test.

Table 7.2: Mercury intrusion porosimetry data of the stones before (B) and after (A) salt weathering.

Sample		LA		LJI		LUQI		BUE		BUQ	
		B	A	B	A	B	A	B	A	B	A
Pore classes [%]	$r < 0.01 \mu\text{m}$	0.00	0.42	1.40	3.79	1.18	7.21	0.00	4.19	0.00	3.56
	$0.01 - 0.1 \mu\text{m}$	2.43	9.16	23.96	17.75	63.60	73.92	3.03	4.02	5.07	6.76
	$0.1 - 1 \mu\text{m}$	14.39	18.09	61.43	63.90	13.37	8.51	5.68	8.47	13.21	12.14
	$1 - 10 \mu\text{m}$	61.46	29.29	3.50	8.52	11.35	4.97	30.27	25.82	30.95	23.94
	$10 - 100 \mu\text{m}$	21.72	43.03	9.71	6.04	10.50	5.39	61.01	57.50	50.77	53.60
Avg. pore radius [μm]		4.89	41.09	0.23	0.30	0.03	0.04	41.07	61.87	33.60	41.08
Total porosity (P_c) [%]		7.45	12.23	5.87	9.63	6.24	11.48	6.87	3.93	4.47	3.77
Specific surface area [m^2/g]		0.06	0.39	0.50	1.07	1.02	3.14	0.05	0.22	0.05	0.24
Microporosity ($P_{m0.1}$) [%]		0.18	1.17	1.49	2.07	4.05	9.31	0.21	0.32	0.23	0.39
$P_{sCap.}(0.1 < r < 5 \mu\text{m})$ [%]		4.10	4.50	3.64	6.76	1.33	1.36	1.59	0.92	1.56	1.00
$P_{m5}(r < 5 \mu\text{m})$ [%]		4.28	5.67	5.13	8.83	5.38	10.68	1.80	1.25	1.78	1.39
$P_{L.Cap}(r > 5 \mu\text{m})$ [%]		3.17	6.56	0.74	0.79	0.87	0.80	5.07	2.68	2.69	2.38

In summary, salt crystallized in pores of varied sizes and modified them in different ways. Pore enlargement and crack developments can be seen in all weathered samples, albeit to varying extents. In the basalt samples, salt remained trapped in pores even after extensive rinsing with water. The remaining salt was either deposited in pore entries resulting in peak shifts towards smaller pores or inside pore cavities reducing thereby the total pore volume, particularly the volume of capillary pores.

However, it should be mentioned that some changes and differences in MIP spectra before and after weathering might actually be a result of heterogeneities in stone specimens and not really associated with weathering process.

7.1.1.4 Capillary water uptake coefficient

The capillary water uptake coefficients of the stone samples before and after weathering are shown in Table (7.3), and the capillary curves are represented in Figure (7.3). All the samples showed generally low capillary absorption capacity. This can be attributed to their relatively low porosity and percentage of capillary pores, which determine and control capillary water uptake.

Table 7.3: Capillary water absorption before and after 25 cycles of salt weathering.

Sample		LA	LJI	LUQI	BUE	BUQ
W-value [$\text{Kg}/(\text{m}^2 \cdot \text{h}^{1/2})$]	Before	0.79 ± 0.17	0.29 ± 0.09	0.25 ± 0.06	0.36 ± 0.03	0.28 ± 0.03
	After	0.92 ± 0.12	0.36 ± 0.01	0.36 ± 0.00	0.31 ± 0.02	0.26 ± 0.00

After weathering, the limestone samples exhibited a small increase in capillary water absorption coefficient. On the other hand, a slight decrease in capillary water uptake of the basalt samples can be seen. The differences in capillary water absorption before and after weathering are related to the corresponding changes in the proportion of capillary pores, particularly small capillaries (Bourgès, 2006). These results agree well with those of water uptake porosity and MIP.

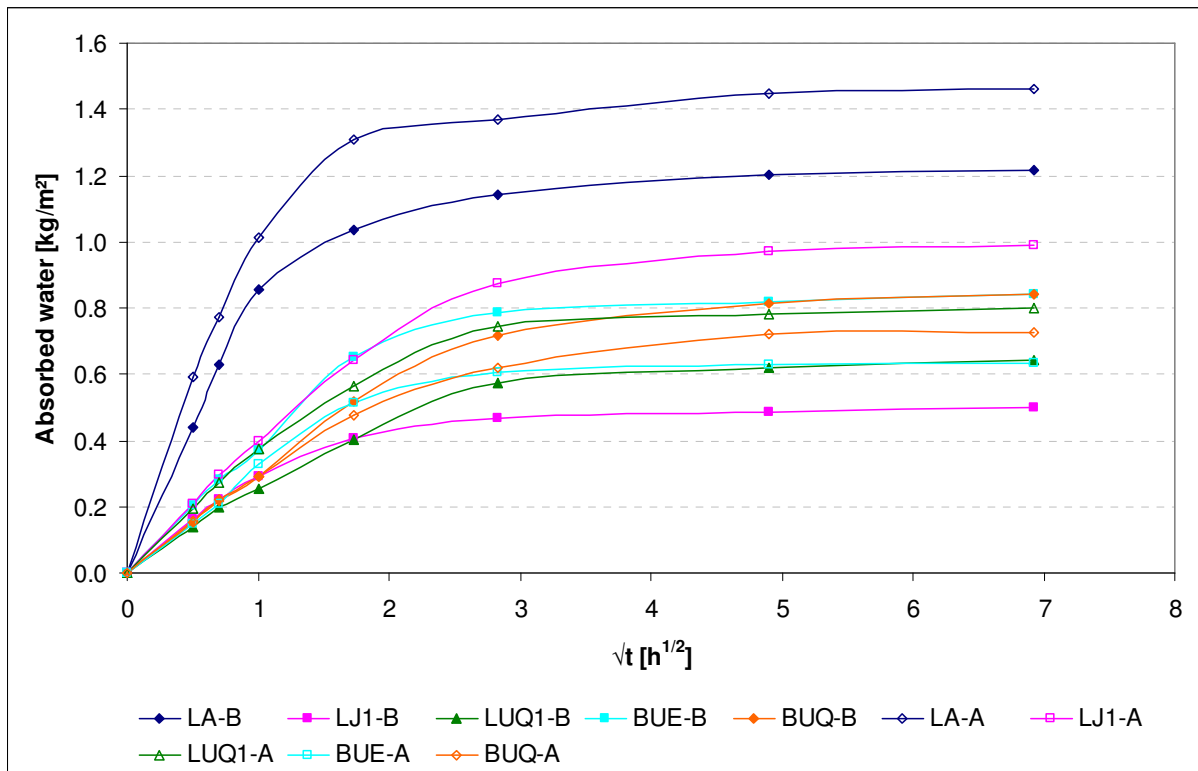


Figure 7.3: Capillary water absorption curves before and after salt weathering.

7.1.1.5 Drying curve

At constant climatic conditions (RH, temperature, and air velocity), the drying process of stone depends on its pore structure characteristics. The study of the changes in drying behavior of stone upon weathering helps therefore to characterize the variations and modifications in pore space. As explained in Sections (3.2.3) and (6.2.1.4), two main phases of drying process are distinguished; the capillary and diffusion phases. During the capillary phase, evaporation occurs at the surface of stone at high and constant rate. When the water content of the stone drops below the critical moisture content, the capillary forces are no longer sufficient to keep the surface wet and the water front retreats into the stone. At this

stage, evaporation takes place inside the material by water vapor diffusion. This results in a significant drop of the evaporation rate, which decreases continuously with decreasing water content.

The drying curves of the stone samples before and after weathering are shown in Figure (7.4). The general shape of the drying curves of all the stones is nearly the same with high fairly constant drying rate at the beginning, followed by a second stage in which the drying rate is continuously decreasing before it is relatively constant again when the loss of water is tiny. The initial water content of all the stones before and after weathering is almost the same due to the insignificant changes in free porosity.

After weathering, the limestone samples exhibited a larger drying rate and lower critical moisture content (longer plateau). Bourgès (2006) related the increase in drying rate more to macrocracks, which increase the surface roughness, than to real variations in pore structure. The studied limestone samples underwent macro-cracking that might have accelerated the rate of water flow, but it was generally found in this study that the drying rate is directly correlated to the proportion of capillary pores. The decrease in critical moisture content indicates an easier movement of water to the stone surface (i.e. an improved connectivity of pores). These changes result in a faster and more effective drying process of the weathered stones, particularly during the capillary phase.

On the contrary, the basalt samples showed a reduction in drying rate whereas the critical moisture content is almost the same before and after weathering. These stones exhibited a decrease of their proportions of capillary pores after weathering, which seems to be responsible for the reduction in drying rate. The presence of trapped salt in the pores of these stones might have also contributed to this reduction; salt changes the hygroscopic characteristics of stone such as the equilibrium moisture content (Künzel, 2007), and might thus affect the drying process.

All the stones exhibited also a more effective drying in the diffusion phase although their proportions of micropores were increased after weathering. This attests an increased permeability to water vapor (lower μ -value).

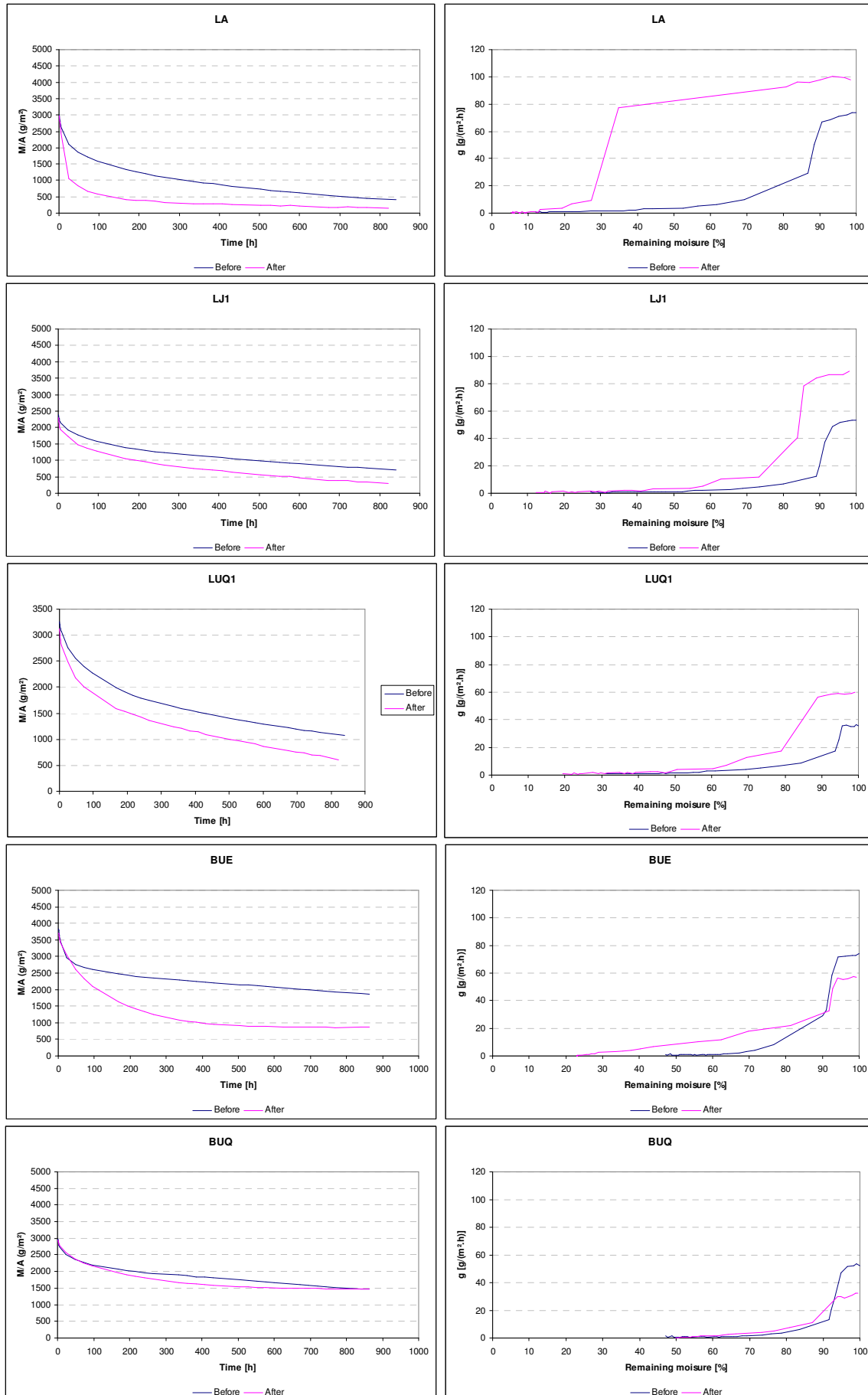


Figure 7.4: The drying curves of the stones before and after weathering.

Table (7.4) shows the changes in drying rate and critical moisture content of the stones after weathering.

Table 7.4: Drying rate and critical moisture content before and after weathering.

	<i>Sample</i>	<i>LA</i>	<i>LJ1</i>	<i>LUQ1</i>	<i>BUE</i>	<i>BUQ</i>
$g [g/(m^2.h)]$	Before	71 ± 3	52 ± 2	36 ± 0	73 ± 1	51 ± 2
	After	95 ± 7	85 ± 4	58 ± 1	55 ± 3	31 ± 1
$\mu_c (\Psi_c)$	Before	88	91	95	92	93
	After	35	86	89	93	94

7.1.1.6 Thermal expansion

The thermal expansion coefficients of the sound and artificially weathered samples (25 cycles of salt weathering) are shown in Figure (7.5).

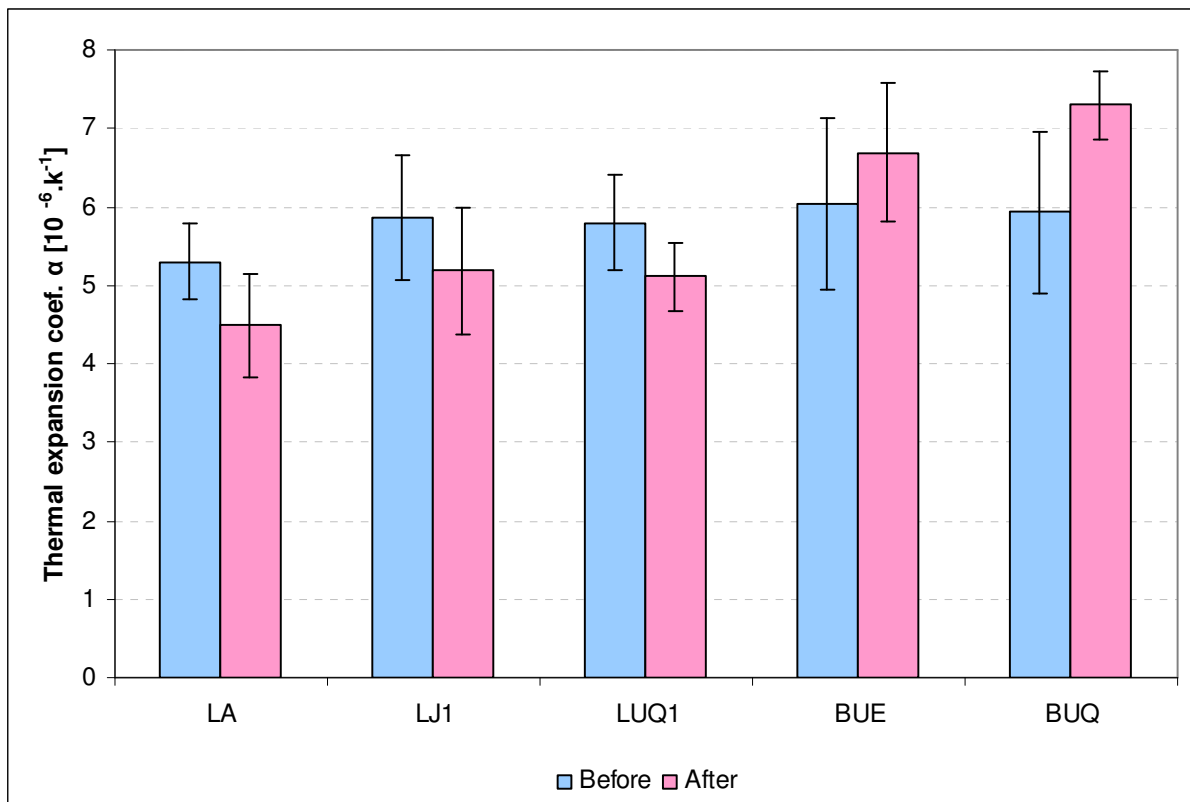


Figure 7.5: Thermal expansion coefficient before and after salt weathering.

The thermal expansion coefficient of the limestone samples was decreased after salt weathering test by 15%, 12%, and 12% for LA, LJ1, and LUQ1 respectively. The development and extension of cracks provide spaces where crystals can expand without

causing measurable dilatation, and hence the thermal expansion coefficient of the stone is reduced (Weiss et al., 2004).

On the contrary, the thermal expansion coefficient of the basalt samples was increased after salt weathering by 11% and 23% for BUE and BU1 respectively. This can be attributed to the salt crystals trapped in pores, which act to increase the thermal dilatation of stone (Al-Naddaf, 2009).

7.1.1.7 Fracture density

Table (7.5) shows the fracture density (F_D) of the stones with increasing weathering, as well as its final percentage of variation. The sound limestone samples showed varying degrees of cracking with the highest fracture density being $0.018 \text{ mm}^2/\text{mm}^3$ for LA.

The fracture density of the limestone samples increased continuously with increasing number of weathering cycles. The samples LJ1 and LA suffered substantial fracturing with percentage increase of 165% and 90% respectively. The sample LUQ1 exhibited a relatively lower percentage of increase in fracture density (35%). The basalt samples, however, showed no visible macrocracks within 25 cycles of salt weathering.

Table 7.5: Fracture density of the stones with increasing weathering and percentage of total change.

Sample	Fracture density F_D [mm^2/mm^3]				
	Sound	After 10 cycles	After 20 cycles	After 25 cycles	ΔF_D [%]
LA	0.018	0.025	0.028	0.033	90
LJ1	0.007	0.008	0.016	0.019	165
LUQ1	0.008	0.009	0.011	0.011	35
BUE	0.000	0.000	0.000	0.000	0
BUQ	0.000	0.000	0.000	0.000	0

7.1.1.8 Biaxial flexural strength (β_{BFS}) and moduli of elasticity (E_{stat} & E_{dyn})

The biaxial flexural strength (β_{BFS}) and static modulus of elasticity (E_{stat}) of the stones were measured on thin drill core slices according to Wittmann and Prim (1983). The dynamic modulus of elasticity (E_{dyn}) was measured using the velocity of ultrasonic waves on prismatic specimens. The results before and after weathering are summarized in Table (7.6). All the

samples showed a decrease of biaxial flexural strength after weathering. This is clearly evident for the limestone samples LA and LJ1, which underwent percent decrease of 40% and 30% respectively. A corresponding decrease in the static modulus of elasticity of all weathered samples is also evident, particularly for the samples LA and LJ1. The elastic and mechanical properties of a stone are highly influenced by microcracks and fracture density (Walsh, 1982). Therefore, the reduction in biaxial flexural strength and elasticity modulus was higher for the stone samples which were subject to greater fracturing and microcracking (LA and LJ1) as indicated by fracture density and MIP measurements. The basalt sample BUE showed also a considerable decrease of elastic modulus after weathering.

Table 7.6: Biaxial flexural strength and moduli of elasticity before and after salt weathering.

Sample		β_{BFS} [N/mm ²]	E_{Stat} [kN/mm ²]	E_{Dyn} [kN/mm ²]	$\Delta \beta_{BFS}$ [%]	ΔE_{Stat} [%]	ΔE_{Dyn} [%]
LA	Before	15.45±1.54	64.90±18.74	37.38±11.35	-40	-48	-9
	After	9.24±3.82	33.51±8.91	34.04±9.49			
LJ1	Before	18.53±3.64	96.38±14.83	68.72±3.18	-30	-55	-2
	After	12.91±3.48	42.95±16.15	67.27±5.12			
LUQ1	Before	17.36±1.91	67.54±13.20	49.54±4.94	-13	-10	-4
	After	15.06±3.98	60.52±4.78	47.57±4.75			
BUE	Before	20.01±1.06	115.89±20.85	64.66±4.60	-17	-35	-1
	After	16.69±3.01	75.27±21.89	63.80±4.97			
BUQ	Before	19.74±0.65	114.22±11.51	58.70±3.72	-13	-4	0
	After	17.10±3.23	109.54±17.67	58.70±3.24			

The dynamic modulus of elasticity of the stones was also reduced after weathering. However, the reduction in the static modulus of elasticity was much greater. The static modulus of elasticity of a rock is generally expected to be lower than dynamic modulus because of the influence of microcracks, which affect the deformation of the rock under static load more than the propagation of ultrasonic wave (microcracks can be easily closed or expanded during static measurement) (King, 1983; Guéguen and Palciauskas, 1994; Bourgès, 2006).

Contrary to this, the static modulus of elasticity for the studied stone samples is found to be greater than the dynamic one, except for the two weathered samples LA and LJ1. As mentioned earlier, these two samples exhibited higher degrees of microcracking and fracturing, and it seems that the increase in their density of microcracks after weathering, compared to their initial state of cracking before weathering, was significant so that a considerable reduction in E_{stat} has occurred.

On one side, this result confirms the statement that microcracks affects the static modulus of elasticity more than the dynamic one. On the other side, it is unclear then why at all E_{stat} is higher than E_{dyn} for most of the tested stone; one should expect E_{stat} to be almost equal to or smaller than E_{dyn} . A possible reason for this deviation might be that the static modulus obtained from biaxial flexural strength is not necessarily comparable to young modulus which is obtained by compressive strength and usually correlated to dynamic modulus.

7.1.1.9 Change of sample mass and total loss of stone material

The changes in mass of the samples with increasing weathering cycles for cubic and prismatic specimens are shown in Figures (7.6) and (7.7). The evolution of the sample mass with increasing salt weathering cycles can be usually described and divided into three stages (Angeli et al. 2007). The first stage corresponds to the increase of sample mass due to salt accumulation in pores. The second stage represents the variation of mass depending on a competition between salt uptake and stone damage in form of loss of material. Finally, the mass of the sample decreases continuously as salt uptake becomes negligible compared to damage. The second stage might sometimes be missing as the sample mass decreases continuously and passes directly to the third stage.

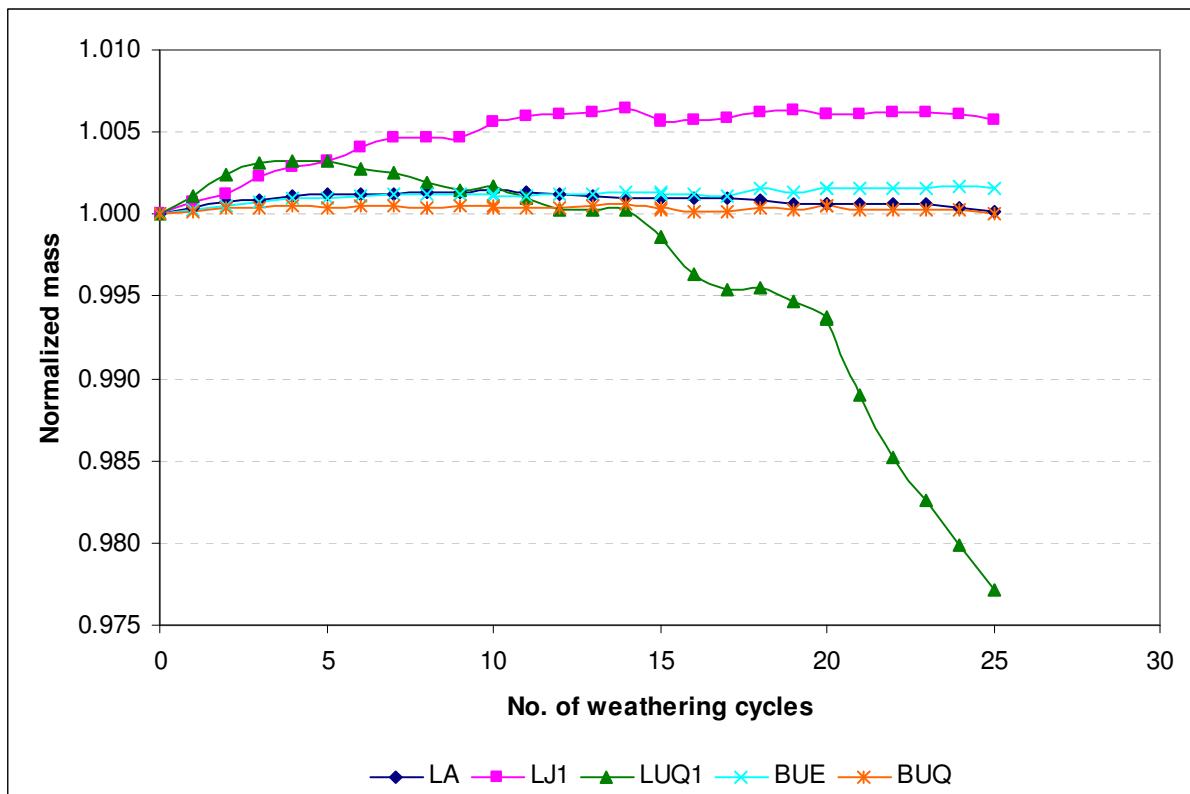


Figure 7.6: Mass evolution during salt weathering test - Cubic specimens.

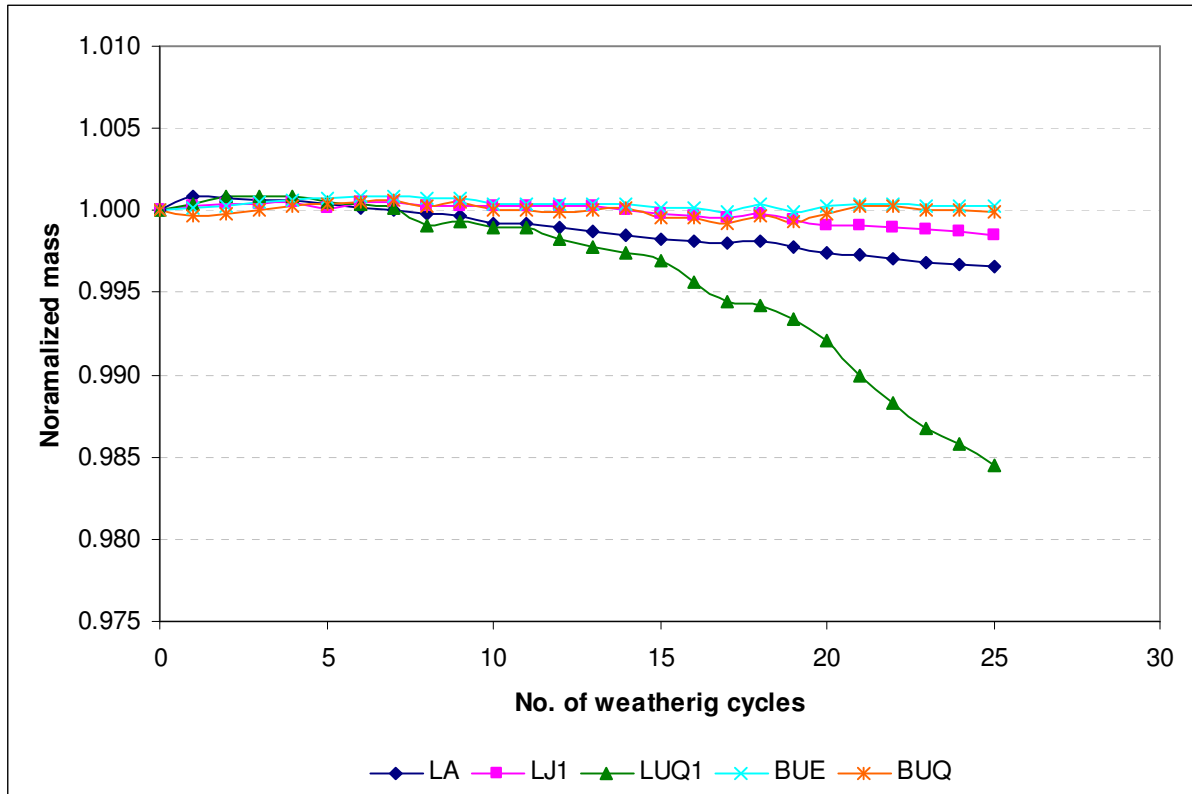


Figure 7.7: Mass evolution during salt weathering test – Prismatic specimens.

For the cubic specimens, only LUQ1 showed the 3-stage evolution described above. The sample mass was increasing continuously until the 5th cycle, when the first sign of damage appeared and a varying trend of mass decrease started. Beginning from the 14th cycle, the sample showed a clear continuous decrease in mass as the loss of material prevailed over salt uptake. All other samples had undergone a gradual increase in weight before a series of mass variations took place. However, a net increase in mass was kept till the end of the test, which indicates a negligible loss of stone material compared to salt uptake. Generally, all the studied stone samples, including LUQ2, showed good resistance to weathering and would require further salt contamination to achieve considerable weathering in form of mass loss.

For the prismatic specimens, the limestone samples showed a slightly different behavior of mass change. Samples LA and LJ1 exhibited again a two-stage evolution of mass. However, a more obvious trend towards mass reduction could be noticed. The mass evolution of the sample LUQ1 in prismatic and cubic specimens is similar.

The basalt samples showed nearly the same behavior for cubic and prismatic specimens; the two samples (BUE and BUQ) exhibited a continuous increase of mass until the 9th cycle,

followed by a variation of mass due to competition between salt uptake and loss of stone material.

The total loss of stone material (or dry weight loss DWL) is the parameter most frequently used to evaluate salt damage to building stone in durability tests (e.g. Benavente et al., 2001; Benavente et al., 2004; Yu and Oguchi, 2009a;b). The dry weight loss was calculated for cubic and prismatic specimens after extensive desalination with water and drying to constant mass by comparing the initial and final mass (see Section 6.2.4.1) (Table 7.7).

Table 7.7: Total dry weight loss (DWL) after 25 cycles of salt weathering.

<i>Sample</i>	<i>DWL [%]</i>	
	<i>Cubes</i>	<i>Prisms</i>
<i>LA</i>	0.241 ± 0.050	0.536 ± 0.056
<i>LJ1</i>	0.160 ± 0.022	0.344 ± 0.044
<i>LUQ1</i>	2.222 ± 0.608	2.065 ± 0.464
<i>BUE</i>	0.170 ± 0.009	0.248 ± 0.076
<i>BUQ</i>	0.098 ± 0.006	0.259 ± 0.040

Except for the heterogeneous allochems-rich sample LUQ1, the prismatic specimens were subject to slightly greater loss of material compared to the cubic ones. This might be attributed to the smaller dimensions of these specimens and their geometry, which facilitate the evaporation and crystallization of salt and make them thereby more prone to damage during the drying phase (Angeli et al., 2007).

However, the ranking of the stone samples with respect to weight loss is the same for cubic and prismatic specimens. Sample LUQ1 exhibited the greatest loss of stone material, followed by LA and LJ1 and finally the basalt samples.

In general, the differences in DWL between cubic and prismatic specimens are not that significant. The size and geometry of specimens seem thus to be less important for salt damage in total immersion experiments as compared to continuous partial immersion test, where evaporation, which depends on specimens' shape and size, is the driving force for supersaturation.

In terms of total dry weight loss, the studied stones showed generally quite good resistance to 25 cycles of salt weathering. This might be attributed to their relatively low porosity, pore space characteristics, and good mechanical resistance.

7.1.1.10 Non-destructive ultrasonic pulse velocity (V_p)

The velocity of longitudinal ultrasonic waves was measured on cubic specimens of each sample along three orthogonal directions before and after weathering. The anisotropy (A) of each specimen was calculated from the maximum and minimum velocity measured in the different directions. Measurements were carried out both in dry and water saturation conditions. The results are shown in Table (7.8).

Table 7.8: Ultrasonic pulse velocity in dry and water saturated cubes before and after salt weathering. Measurements were carried out using an ultrasonic frequency of 46 kHz.

Sample		V_{p-dry} [m/s]	Anisotropy [%]	$V_{p-saturated}$ [m/s]	$\Delta V_{p(sat-dry)}$ [%] $\left(\frac{V_{p,sat} - V_{p,dry}}{V_{p,dry}}\right) \cdot 100$
LA	before	4676 ± 200	3.93	5042 ± 194	7.84
	after 25c	3653	7.70	4806	31.55
LJ1	before	5185 ± 343	3.02	5258 ± 365	1.41
	after 25c	4699	4.42	5084	8.19
LUQ1	before	4598 ± 124	3.32	4661 ± 110	1.38
	after 25c	4257 ± 304	0.78	4470 ± 197	5.01
BUE	after	5098 ± 97	1.43	5196 ± 30	1.92
	after 25c	4913	1.10	4968	1.11
BUQ	before	5125 ± 112	1.57	5218 ± 116	1.82
	after 25c	4969	2.11	5023	1.10

The limestones, and to a lower extent the basalt samples, showed slight anisotropy (up to 5%). The anisotropy of the samples LA and LJ1 increased after weathering, which might indicate preferred fracturing and crack propagation along certain directions. The other samples showed generally a decrease in anisotropy after weathering.

For all stone samples, the velocity of longitudinal ultrasonic waves in water saturated specimens is higher than that in dry specimens. This has to do with the fact that the velocity of longitudinal waves in water is around four and half times higher than in air. The difference in

velocity between dry and water saturated conditions can be used to estimate the quality of stone and to obtain information about its pore structure. Fresh un-fissured stones have almost the same pulse velocity in dry and water saturation conditions. The increase in ultrasonic velocity in water saturated condition is particularly significant for stones with porosity in form of cracks. In contrast to pores, cracks can be easily bridged by water, which thus facilitates the propagation of longitudinal ultrasonic waves (Delgado Rodrigues, 1982). The increase of velocity in water saturated specimens before weathering was below 2% for all the stone samples, except sample LA which showed an increase of 7.84%. This sample exhibited already the highest fracture density.

After weathering, all the samples showed a reduction in ultrasonic velocity due to development and widening of cracks and fissures. The stones with the highest degree of cracking (LA and LJ1) suffered the highest reduction in ultrasonic velocity. These samples showed also a considerable increase of velocity in water-saturated specimens compared to dry ones. This confirms the mitigation of the influence of cracks on ultrasonic velocity in water saturated stones.

The basalt samples exhibited a lower reduction in ultrasonic velocity after weathering. No visible fracturing could be noticed in these samples and the damage in stone structure was limited; only small proportions of cracks that might affect ultrasonic velocity were developed after weathering as shown by MIP results. The increase in ultrasonic velocity in water-saturated condition for the basalt samples was lower after weathering, probably because of the reported reduction in porosity.

The weathering test was interrupted on several occasions (after 5, 10, 15, and 20 cycles) to allow repeated measurements of ultrasonic velocity. Table (7.9) shows the changes in ultrasonic longitudinal velocity of the cubic specimens with increasing number of weathering cycles. The relative changes in ultrasonic velocity are also represented in Figure (7.8).

Table 7.9: Ultrasonic velocity V_p and its percentage of variation with increasing number of salt weathering cycles – Cubic specimens measured with an ultrasonic frequency of 46 kHz.

Sample		Number of weathering cycles						$\Delta V_p (V_{p0} - V_{p25})$ [km/s]
		0	5	10	15	20	25	
LA	V_p [m/s]	4676	4269	4107	3749	3752	3653	1.022
	ΔV_p [%]	0	-9	-12	-20	-20	-22	
LJ1	V_p [m/s]	5185	5081	5056	4907	4871	4699	0.485
	ΔV_p [%]	0	-2	-2	-5	-6	-9	
LUQ1	V_p [m/s]	4598	4558	4599	4493	4473	4257	0.341
	ΔV_p [%]	0	-1	0	-2	-3	-7	
BUE	V_p [m/s]	5098	5080	5104	5087	4990	4913	0.185
	ΔV_p [%]	0	0	0	0	-2	-4	
BUQ	V_p [m/s]	5125	5113	5041	5078	5003	4969	0.156
	ΔV_p [%]	0	0	-2	-1	-2	-3	

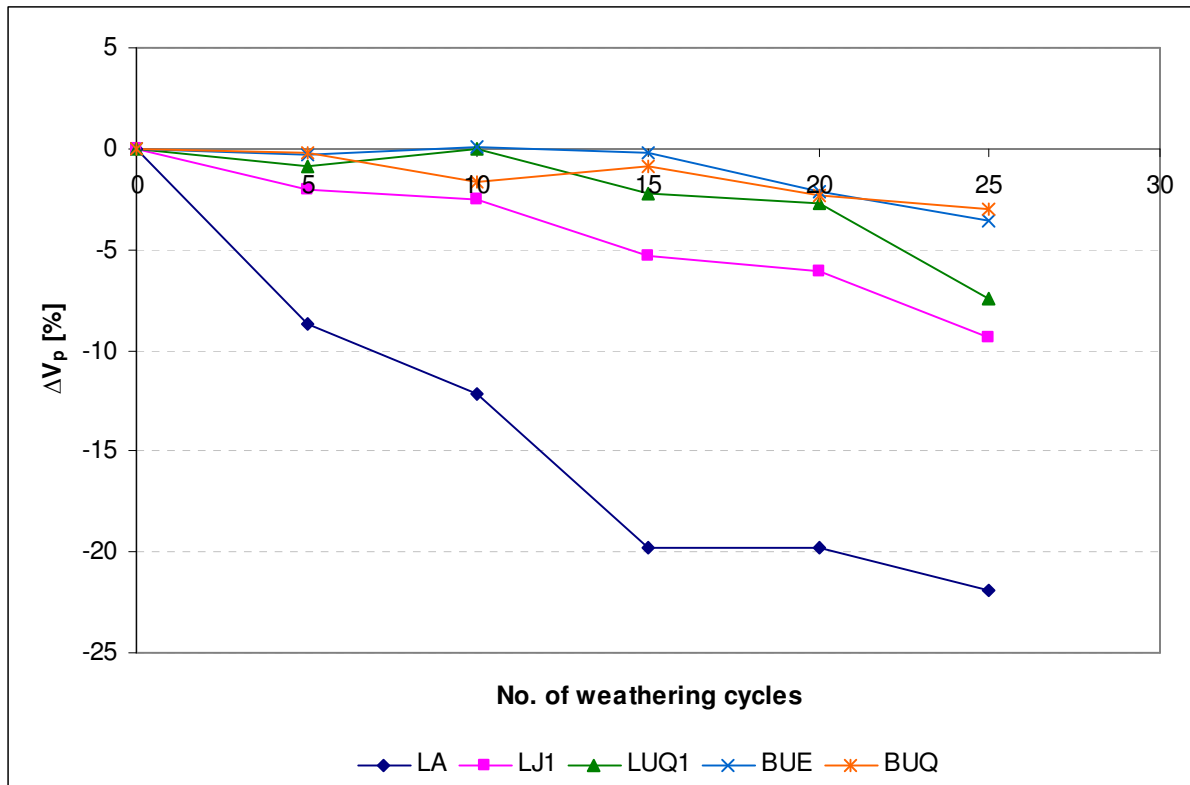


Figure 7.8: Percentage decrease in ultrasonic pulse velocity with increasing number of weathering cycles – Cubic specimens.

Sample LA suffered the largest decrease in ultrasonic velocity with a total reduction of 1.022 km/s, a percentage decrease of 22%. The velocity decreased markedly with increasing weathering particularly at the early stages; after the 15th weathering cycle, the reduction in velocity became less pronounced. Sample LJ1 underwent a steady decrease in ultrasonic

velocity with a total percentage reduction of 9%. The reduction in velocity became more significant with increasing number of weathering cycles. This is also the case for sample LUQ1, where a more obvious reduction in velocity at the end of the test can be seen. As mentioned earlier, all these limestone samples were subject to varying degrees of cracking as indicated by fracture density measurement and MIP spectra. These stones suffered also a remarkable loss of biaxial flexural strength. In light of these observations, the reduction in ultrasonic velocity for these samples is understandable.

The basalt samples exhibited slight (downward and upward) variations in ultrasonic velocity until the 15th cycle. After that, a more obvious downward trend in ultrasonic velocity can be seen.

Ultrasonic velocity was also measured on 2x2x5 cm prismatic specimens in the longest direction before and after salt weathering test. The results are summarized in Table (7.10). For LA and the basalt samples, small variations in ultrasonic velocity between cubic and prismatic specimens were registered. These might be a result of stone anisotropy, because the velocity in cubic specimens is the average value along three spatial directions whereas it is only measured along one direction in the prismatic specimens. The heterogeneity of specimens might also contribute to this deviation.

Table 7.10: Ultrasonic velocity V_p before and after salt weathering test (25 cycles) – Prismatic specimens measured with an ultrasonic frequency of 46 kHz.

Sample	Ultrasonic velocity V_p [m/s]		ΔV_p [%]
	before	after	
LA	4358 ± 95	3858 ± 30	11
LJ1	5174 ± 74	4825 ± 132	7
LUQ1	4527 ± 114	4367 ± 97	4
BUE	4912 ± 53	4755 ± 35	3
BUQ	4903 ± 25	4782 ± 49	2

The prismatic specimens showed slightly lower reduction of ultrasonic velocity than the cubic ones. However, the ranking of the samples is still the same with LA and LJ1 showing the highest reduction in ultrasonic velocity. Relatively speaking, the prismatic specimens suffered seemingly a lower degree of fracturing. However, the fact of measuring along only one direction might have implications on this result, particularly for samples LA and LJ1 which showed some anisotropy and appeared to suffer preferred fracturing along certain directions.

All previously mentioned measurements of ultrasonic velocity were performed using an ultrasonic frequency of 46 kHz. In order to determine the influence of the selected ultrasonic frequency on velocity results, ultrasonic velocity measurements with 250 kHz were also carried out on the same prismatic specimens before and after weathering. The results are shown in Table (7.11). Only small variations, generally within the accuracy limits of the used ultrasonic instrument, can be noticed.

However, it would be unjustified to jump to the conclusion that the selected ultrasonic frequency has no influence on the measured velocity. As discussed in Section 5.4, the selection of the suitable ultrasonic frequency in relation to the dimensions of investigated specimens (the ratio of the measuring distance to the wavelength) seems to have important implications on the accuracy of measurements. Therefore, this conclusion should only be kept if supported by a larger amount of experimental data.

Table 7.11: Ultrasonic V_p before and after salt weathering test (25 cycles) – Prismatic specimens measured with an ultrasonic frequency of 250 kHz.

<i>Sample</i>	<i>Ultrasonic velocity V_p [m/s]</i>		ΔV_p [%]
	<i>before</i>	<i>after</i>	
<i>LA</i>	4451 ± 93	3825 ± 89	14
<i>LJI</i>	5187 ± 44	4777 ± 83	8
<i>LUQI</i>	4469 ± 77	4240 ± 113	5
<i>BUE</i>	4948 ± 73	4820 ± 96	3
<i>BUQ</i>	4935 ± 17	4771 ± 51	3

7.1.1.11 Estimation of stone susceptibility to salt damage

In this section, the susceptibility of the studied stone samples to salt damage is going to be estimated based on their properties in the sound condition. The aim is to develop durability estimators from the physico-mechanical properties of the sound stone that can be used to predict and assess stone resistance to damage without the need for performing the time-consuming and costly accelerated weathering tests. This can be useful for durability tests that are intended to test the resistance of building stone to damage for a particular use under certain environmental conditions. It has also important applications in the field of conservation for replacing damaged stones and selecting suitable restoration materials.

For this purpose, the physico-mechanical properties of the stone samples before weathering are characterized and the induced damage after salt weathering test is to be evaluated using suitable parameters. Many studies have been dedicated to develop durability estimators from the different properties of stone and its pore structure characteristics (e.g. Benavente et al., 2001; Benavente et al., 2004; Yu and Oguchi, 2009a;b). In most of these studies, total dry weight loss (DWL) of stone is the only parameter used to indicate damage. A few authors have been considering the use of other additional parameters to provide a more reliable assessment of damage. For example, Nicholson (2001) used the change in fracture density besides DWL to evaluate damage. Angeli et al. (2007) proposed two parameters to quantify the alteration and weathering of stone.

In this study, the total dry weight loss (DWL) and the change in fracture density (ΔF_D) after weathering are used to indicate the damage induced in the tested stones in 25 cycles of salt weathering. These damage indicators are correlated with the petrophysical and mechanical properties of stone before weathering (Table 7.12) in order to understand the influence of the various properties on stone susceptibility to deterioration and to develop suitable durability estimators. Table (7.13) lists the Pearson correlation coefficients between total dry weight loss (DWL), percentage change of fracture density ($\% \Delta F_D$) and the physico-mechanical properties of stone.

Table 7.12: The physico-mechanical properties of the studied stone samples before weathering.

	DWL	$\% \Delta F_D$	N_{48}	S	ρ_{bulk}	$W_{abs,48}$	W	$P_{m0.1}$	P_{Cap}	P_{m5}	β_{BFS}	E_{stat}	E_{dyn}	V_{P-dry}	V_{P-sat}	ΔV_P
LA	0.241	90.48	3.60	0.52	2.52	1.43	0.79	0.18	7.27	4.28	15.45	64.90	37.38	4676	5042	7.84
LJI	0.160	164.71	4.42	0.68	2.56	1.73	0.29	1.49	4.38	5.13	18.53	96.38	68.72	5185	5258	1.41
LUQI	2.222	35.00	7.37	0.81	2.46	3.00	0.25	4.05	2.20	5.38	17.36	67.54	49.54	4598	4661	1.38
BUE	0.170	0.00	3.21	0.28	2.67	1.21	0.36	0.21	6.66	1.80	20.01	115.89	64.66	5098	5196	1.92
BUQ	0.098	0.00	2.97	0.30	2.67	1.11	0.28	0.23	4.24	1.78	19.74	114.22	58.70	5125	5218	1.82

Table (7.13): Pearson correlation coefficients between stone damage and physico-mechanical properties.

	DWL	% ΔF_D	N_{48}	S	ρ_{bulk}	$W_{abs.48}$	W	$P_{m0.1}$	P_{Cap}	P_{m5}	β_{BFS}	E_{stat}	E_{dyn}	V_{P-dry}	V_{P-sat}	ΔV_P
DWL	1.00															
% ΔF_D	-0.16	1.00														
N_{48}	0.96	0.12	1.00													
S	0.72	0.56	0.88	1.00												
ρ_{bulk}	-0.75	-0.43	-0.84	-0.92	1.00											
$W_{abs.48}$	0.96	0.12	1.00	0.88	-0.85	1.00										
W	-0.32	0.23	-0.34	-0.12	-0.19	-0.31	1.00									
$P_{m0.1}$	0.94	0.10	0.99	0.86	-0.76	0.99	-0.47	1.00								
P_{Cap}	-0.72	0.03	-0.75	-0.61	0.40	-0.74	0.76	-0.83	1.00							
P_{m5}	0.56	0.71	0.75	0.97	-0.92	0.76	0.08	0.71	-0.41	1.00						
β_{BFS}	-0.30	-0.44	-0.35	-0.55	0.79	-0.37	-0.74	-0.22	-0.15	-0.68	1.00					
E_{stat}	-0.59	-0.37	-0.63	-0.74	0.94	-0.65	-0.50	-0.52	0.14	-0.80	0.95	1.00				
E_{dyn}	-0.31	0.07	-0.20	-0.21	0.56	-0.23	-0.73	-0.08	-0.19	-0.28	0.86	0.80	1.00			
V_{P-dry}	-0.72	0.07	-0.63	-0.54	0.81	-0.65	-0.43	-0.52	0.15	-0.53	0.80	0.90	0.87	1.00		
V_{P-sat}	-0.96	0.18	-0.88	-0.67	0.80	-0.89	0.04	-0.82	0.53	-0.55	0.51	0.74	0.57	0.89	1.00	
% ΔV_P	-0.26	0.20	-0.29	-0.08	-0.24	-0.26	0.99	-0.42	0.68	0.11	-0.78	-0.55	-0.80	-0.49	-0.03	1.00

In terms of total dry weight loss (DWL), stones with high values of water absorption (or free porosity), saturation coefficient, and microporosity, as well as low values of ultrasonic velocity and bulk density showed generally higher degrees of damage. In its turn, fracture density influences mainly the mechanical and elastic properties of stone; higher fracture density implies lower strength, moduli of elasticity (particularly static modulus) and ultrasonic velocity. The increase in fracture density contributes also to higher connected porosity and capillary water uptake (w-value), and it is responsible for the increased difference between ultrasonic velocity in dry and water saturation conditions.

Based on the above mentioned correlations with stone properties, durability estimators for damage as indicated by DWL and change in fracture density are proposed. The dry weight loss in the tested stones (DWL) correlates very well with the product of microporosity (in this study $P_{m0.1}$ ($r < 0.1 \mu\text{m}$)) and water absorption ($W_{\text{abs}48}$), that is with ($W_{\text{abs}} * P_{\text{micro}}$); the Pearson correlation coefficient $r = 0.98$.

This durability estimator can be well interpreted by considering the nature of stress from salt crystallization on pore walls and the influence of pore structure characteristics. As discussed earlier in Chapter four, sufficiently high stresses to damage stone are mainly expected in very small pores. Micropores facilitate, therefore, the generation of high crystallization pressure and have to be considered for estimating the durability of stone. On the other hand, the capacity of stone to absorb water (or its free porosity) determines the uptake of salt and contributes correspondingly to stone damage.

This implies that stones which have both considerable amount of micropores and large free porosity are more susceptible to damage by salt crystallization. This agrees partly with the classical idea that stones with higher amounts of micropores are more susceptible to damage. However, this idea is valid as long as we are comparing stones with nearly the same porosity or when the proportion of pores is expressed as a fraction of total porosity. Cardell et al. (2003) and Buj and Gisbert (2010) found that stones with high porosity and low proportions of micropores are more susceptible to salt weathering than stones with low porosity and higher proportions of micropores. This estimator takes into account both the microporosity of stone (the proportion of micropores express as a percentage of total porosity) and its water absorption (or free porosity), and it seems to provide a reliable estimation of the resistance of stone to salt weathering and its durability.

To examine its validity, the proposed durability estimator ($W_{\text{abs}} * P_{\text{micro}}$) was applied and tested on various data from relevant literature studies. Good correlations between this estimator and DWL could be found (Table 7.14). The different types of stone used in these studies and the variations occurring in the number of weathering cycles performed, in the pore radius characterizing microporosity, and in the measuring method of water absorption may be responsible for the differences in the terms of the obtained empirical correlation equations.

Table 7.14: Correlations found between DWL and the durability estimator ($DE = W_{abs} * P_{micro}$).

	Stone types	Empirical correlation equation	Correlation coeff. (R^2)
<i>This study</i>	limestone and basalt	$DWL = 0.17DE + 0.04$	0.96
<i>Yu and Oguchi (2009 a,b)</i>	tuff, sandstone, rhyolite, travertine, dolomite and granite	$DWL = 0.19DE + 9.99$	0.89
<i>Mohammad (2003)</i>	Jordanian limestones	$DWL = 4.39DE - 2.32$	0.94
<i>Benavente et al. (2004)</i>	limestone and sandstone	$DWL = 0.14DE - 0.68$	0.79
<i>Nicholson (2001)</i>	limestone	$DWL = 0.08DE - 7.14$	0.70
<i>Buj and Gisbert (2010)</i>	limestone and sandstone	$DWL = 2.50DE - 3.13$	0.87

The fracturing behavior of stone depends on its mechanical and elastic properties. The percentage increase of fracture density ($\% \Delta F_D$) of the tested stones in this study correlates very well ($r = 0.99$; $R^2 = 0.98$) with the estimator that represents the multiplication product of the porosity of small capillaries (P_{sCap}), the ratio of micropores smaller than $5 \mu m$ to total porosity (P_{m5}), and the ratio of the dynamic modulus of elasticity to the static one (E_{dyn}/E_{stat}), that is [$P_{sCap} * (P_{m5}/N_t) * (E_{dyn}/E_{stat})$].

This could be interpreted as follows: P_{sCap} ($0.1 \mu m < r < 5 \mu m$) expresses the ratio of small capillary pores which control salt uptake. Small capillaries seem to be the most effective pores in salt absorption, and they work synergistically with micropores under equilibrium conditions to induce damage (Yu and Oguchi, 2009a). P_{m5} ($r < 5 \mu m$) indicates the proportion of micropores and small capillaries, where salt precipitation mainly occurs (Zehnder and Arnold, 1989; Yu and Oguchi, 2009a). These pores are subject to greater crystallization pressure, and they are particularly important for salt uptake by total immersion (Yu and Oguchi, 2009a). The fraction of these pores to total porosity (P_{m5}/N_t) may thus determine the extent of the stress field, i.e. the area of pore walls that is subject to stress. As pointed out by Scherer (1999), stress from salt crystallization must spread over a sufficiently large area of the porous network to allow for crack development and propagation; stress generated in single pores cannot induce fracturing. The ratio of the dynamic modulus of elasticity to the static one (E_{dyn}/E_{stat}) may reflect the degree of fracturing, because microcracks seem to influence E_{stat} more than E_{dyn} . The variation between the two moduli becomes larger with increasing

microcracking and may thus be used to indicate the amount of available microcracks in the stone.

The combination of the proposed estimators for loss of stone material and change in fracture density may provide an overall indication of stone damage by salt crystallization. The following estimator $[(W_{abs} * P_{m0.1} * P_{m5}) * \% \Delta V_P]$ is developed, which is almost the multiplication product of the two estimators mentioned above, with replacing E_{dyn}/E_{stat} by $\% \Delta V_P$. This simple estimator combines two aspects of stone damage (loss of stone material and fracturing) that seem to be important indicators for assessing stone durability. For the limestone samples, this indicator correlates very well ($r = 1.00$; $R^2 = 0.99$) with the product of dry weight loss and fracture density ($DWL * F_D$). When the basalt samples, which showed no cracking, are also considered, the correlation coefficient is slightly decreased ($r = 0.98$; $R^2 = 0.95$).

The physical meanings of the first three terms in this estimator are explained earlier in this section. As an alternative to the ratio (E_{dyn}/E_{stat}), the percentage difference in ultrasonic pulse velocity between dry and water-saturated conditions can be used to estimate the density of open cracks of stone in a non-destructive and simple way. In dry specimens, ultrasonic velocity depends on the intrinsic characteristics (the mineral composition and the spatial arrangement of the constituent crystals) of the stone and its pore space. In water saturated conditions, the effects of pore structure on the propagation of ultrasonic waves is mitigated and the measured velocity is more related to the intrinsic velocity of the stone (Strohmeier, 2003). The difference between these two velocities provides, therefore, information about the pore space of stone and can be used to estimate fracture density (Schild et al., 2001; Strohmeier, 2003).

As fractures propagate progressively, stone might be prone to greater loss of material due to the loosening of stone structure (splitting of larger pieces may then occur). At this stage, DWL may implicitly reflect the degree of cracking and could be solely used to indicate damage. Fracture density can be mainly seen as a separate indicator at the early stages of weathering. In this connection, Nicholson and Nicholson (2000) point out that pre-existing cracks are particularly important in the deterioration of stronger stones, whereas their direct influence diminishes in weaker ones as the influence of other properties and factors is more relevant.

Principal component analysis (PCA) was also performed in order to determine the most important controlling variables for stone damage due to salt and to identify the relationship between them. Based on PCA results, two principal components were extracted which explained 90.99% of the total variance (Figure 7.9). The first of which (PC1) accounts for 54.49% of the variance and is mainly associated with microporosity (specific surface area), water absorption, total dry weight loss, saturation coefficient, and water-saturated ultrasonic velocity. PC2 contributes to 36.50% of the total variance and is linked to mechanical strength (β_{BFS}), moduli of elasticity (E_{stat} and E_{dyn}), connected porosity, water uptake coefficient (w -value) and ultrasonic velocity (in dry specimens and the difference between dry and water-saturated conditions).

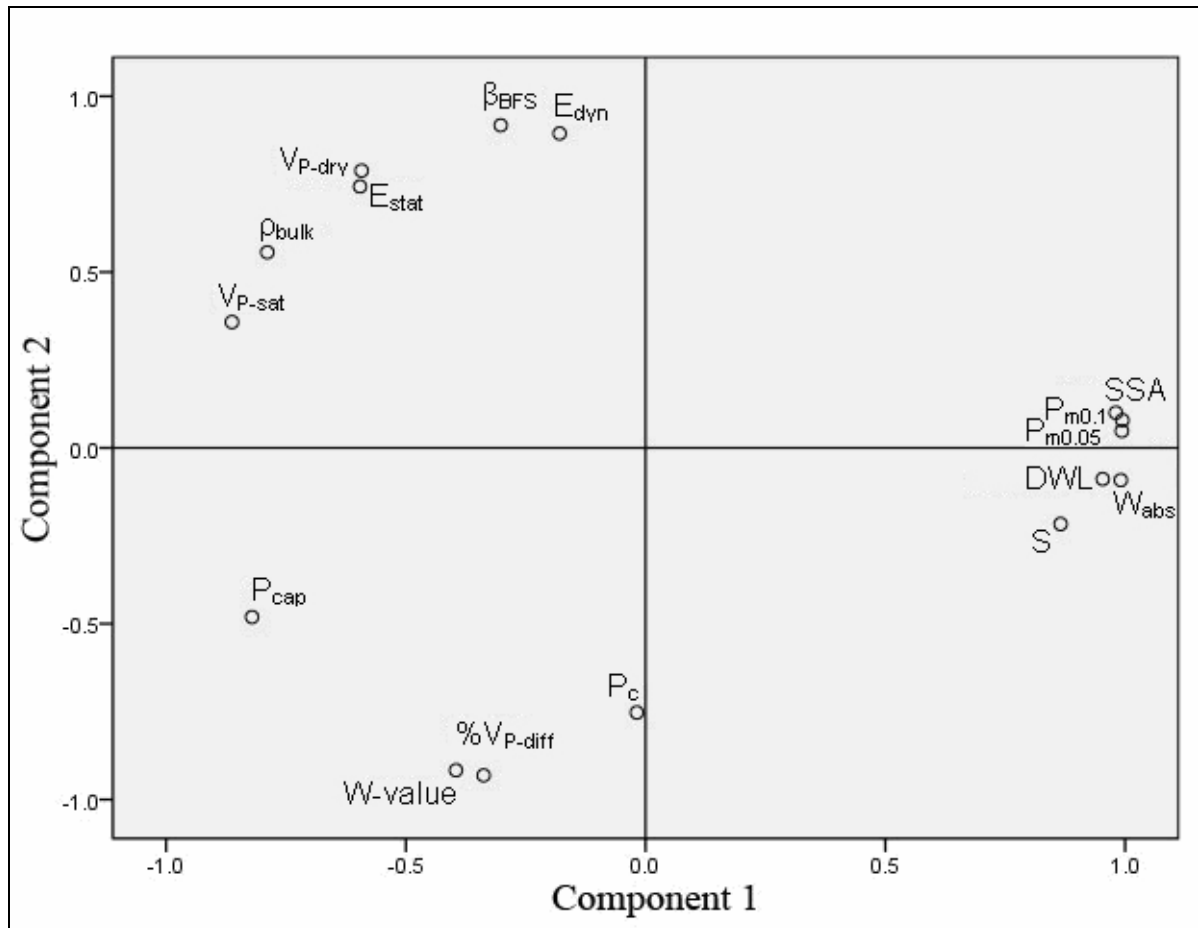


Figure 7.9: Diagram of the extracted principal components.

The loss of stone material shows strong (> 0.70) direct (positive) relationship with microporosity and water absorption and strong negative correlations with water-saturated ultrasonic velocity, proportion of large pores and bulk density. DWL is poorly related to the mechanical properties of stone. The mechanical and elastic properties have strong direct

loadings on dry ultrasonic velocity and strong inverse (negative) relationship with connected porosity, w -value and V_p difference in dry and water saturated conditions.

The first component (PC1) describes the variables which influence and determine stone damage in form of loss of stone material. It indicates that stones with high microporosity and water uptake and low intrinsic ultrasonic velocity are more susceptible to salt weathering. The second parameter (PC2) includes the mechanical and elastic properties and the variables that affect them. It indicates that stones with high porosity and fracture density, and correspondingly lower dry ultrasonic velocity and larger V_p difference between dry and water saturated conditions, are characterized by lower mechanical strength and moduli of elasticity.

Ultrasonic velocity in dry and water saturated condition correlates very well with both extracted components and could thus be effectively used to provide a rough estimation of stone durability and weathering resistance in a non-destructive way. It is particularly sensitive to the degree of fracturing of stone.

In summary, the results confirm the role of pore properties of stone in salt weathering, particularly pore size distribution which determines the extent of crystallization pressure and the capacity of water absorption. The mechanical and elastic properties seem not to be directly correlated with stone damage in form of DWL. This implies that a mechanically weak stone can be resistant to salt weathering, if it possesses a suitable pore size distribution. These results agree well with those of other authors such as Yu and Oguchi (2009a).

However, this is seemingly true only for strong stones and in the early stages of weathering. As explained earlier in this section, extensive fracturing will eventually lead to the splitting of larger pieces of stone material and consequently to a greater DWL. Furthermore, the mechanical and elastic properties are strongly correlated with the degree of fracturing, which can affect the mode of stone deterioration (Nicholson and Nicholson, 2000). Correspondingly, the mechanical and elastic properties have somehow significant impacts on stone durability.

Because of the small number of studied stone samples and the performed weathering cycles (the damage induced at the end of the 25 cycles was very small), no fully-reliable classification scheme for durability estimation can be developed. However, the results of this study might constitute a base for further comprehensive studies.

7.1.2 Thermal weathering of marble

The marble sample (MUQ) was subject to thermal weathering by heating to high temperature and its physico-mechanical properties were measured before and after weathering. The results are summarized in Table (7.15).

Table 7.15: Properties of marble before and after thermal weathering.

	<i>Before weathering</i>	<i>After weathering</i>	Δ [%]
N_t [%]	0.20 ± 0.03	1.71 ± 0.06	744
N_{48} [%]	0.17 ± 0.03	1.38 ± 0.06	719
ρ_{real} [g/cm ³]	2.72 ± 0.00	2.72 ± 0.00	0
ρ_{bulk} [g/cm ³]	2.71 ± 0.00	2.67 ± 0.00	-1
S	0.84 ± 0.10	0.81 ± 0.01	-3
w -value [Kg/(m ² .h ^{1/2})]	0.020 ± 0.006	0.652 ± 0.100	3197
g [g/(m ² .h)]	7.74 ± 1.68	117.16 ± 3.93	1414
α_T [10 ⁻⁶ .k ⁻¹]	$5,10 \pm 0,81$	2.75 ± 0.94	-46
β_{BFS} [N/mm ²]	17.97 ± 1.96	2.31 ± 0.26	-87
E_{stat} [kN/mm ²]	82.30 ± 23.96	2.40 ± 0.45	-97
E_{dyn} [kN/mm ²]	51.51 ± 2.38	24.18 ± 7.77	-53
V_{p-dry} (Cubes) [m/s]	4525 ± 277	1571 ± 58	-65
Anisotropy (A) [%]	6.82 ± 3.49	8.74 ± 2.75	28
V_{p-sat} (Cubes) [m/s]	5153 ± 41	2206 ± 69	-57
$((V_{P.sat} - V_{P.dry})/V_{P.dry}) \cdot 100$	13.89	40.44	191
V_p - 46 kHz (Prisms)	4126 ± 222	1649 ± 83	-60
V_p - 250 kHz (Prisms)	4233 ± 60	1698 ± 240	-60

7.1.2.1 Porosity and pore size distribution

The porosity of the marble sample increased markedly after weathering as can be seen in Table (7.15) and Figure (7.10) below. This increase of porosity is also confirmed by the MIP spectra of the stone (Figure 7.11). The thermally-induced cracks between calcite grains are responsible for this porosity increase. The average pore radius was slightly shifted downward (from 2.77 μ m to 2.19 μ m) indicating an increase in the proportion of microcracks.

It has to be mentioned that the porosity values measured with mercury intrusion porosimetry (Table 7.16) differ considerably from those measured with water absorption. This could be attributed to errors during the preparation of the granules used for mercury intrusion porosimetry measurements. The measurements with water absorption seem to be more reliable because they reported the expected porosity and density values of marble.

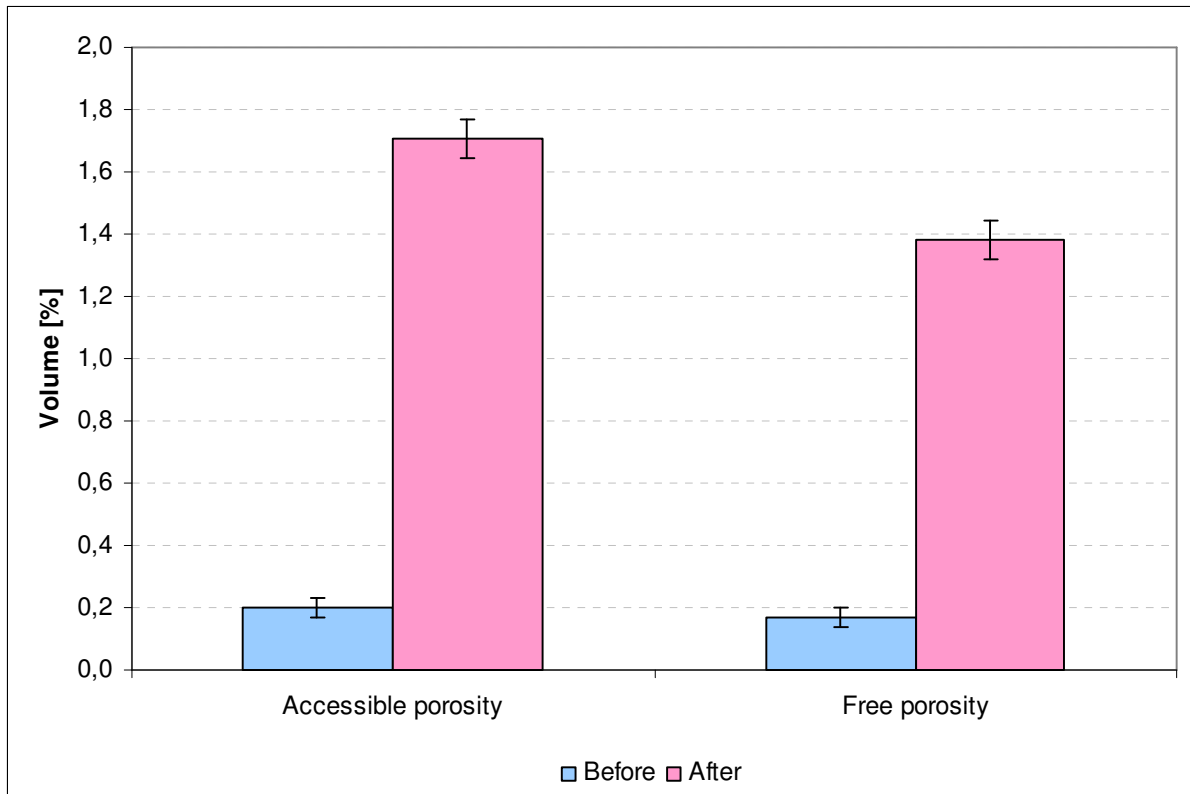


Figure 7.10: Graphical representation of marble porosity before and after weathering.

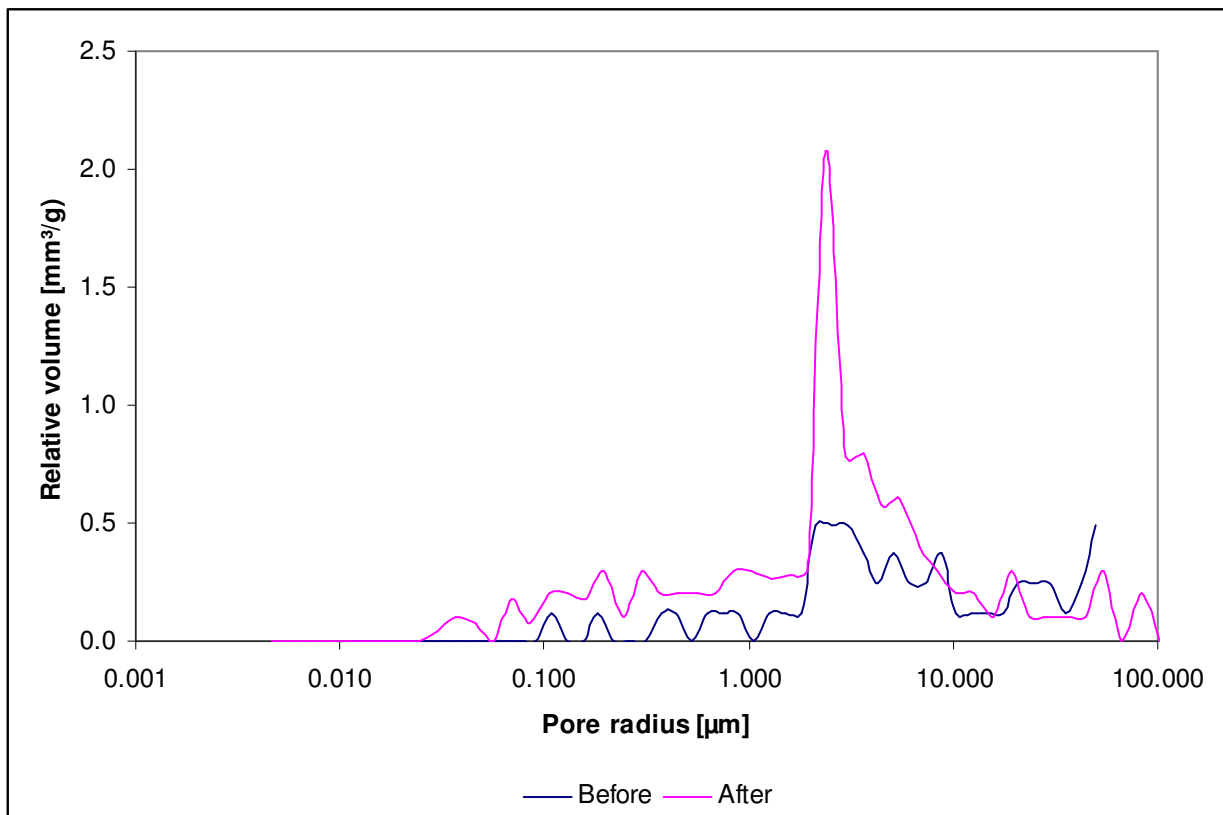


Figure 7.11: The pore size distributions of the marble sample before and after weathering.

The pore sizes distribution of the sound marble ranges almost between 1-50 μm with two main peaks; the first peak lies in the pore range 1-10 μm (around 3 μm) and the second one at around 50 μm . Few separate smaller peaks appear also in the micropores range.

After thermal weathering, new microcracks were developed between around 0.03 μm and 2 μm . The volume of pores around the first main peak (2-6 μm) increased significantly as new cracks were developed in this range. The other peak (at ~50 μm) was reduced due to the expansion of cracks and the shift toward larger macrocracks. This produced a uni-modal pore size distribution (main peak at around 2.4 μm) of the weathered marble that ranges from around 0.03 μm to 83 μm .

Table 7.16: Mercury intrusion porosimetry data of marble before and after thermal weathering.

Sample		MUQ	
		Before	After
Pore size distribution [%]	$r < 0.01 \mu\text{m}$	0.00	0.00
	0.01 -0.1 μm	0.00	6.06
	0.1 -1 μm	12.97	21.21
	1 -10 μm	57.32	59.36
	10 -100 μm	29.71	13.37
Avg. pore radius [μm]		2.77	2.19
Total porosity [%]		1.81	3.23
Specific surface area(SSA) [m^2/g]		0.01	0.05
Microporosity, $P_{m0.1}$ [%]		0.00	0.20
$P_{sCap.}$ (0.01 < r < 5 μm) [%]		1.01	2.26
$P_{L.Cap}$ ($r > 5 \mu\text{m}$) [%]		0.80	0.77

Generally, the proportions of micropores and small capillaries were increased after thermal weathering as a result of cracks development at grain boundaries, which is originally attributed to the anisotropic thermal expansion of the calcite crystals forming the stone.

7.1.2.2 Capillary water absorption

Owing to the increase in the proportion of small capillary pores and connected porosity, the capillary water uptake coefficient of the weathered marble sample increased distinctly. Figure (7.12) depicts the capillary curves of the stone before and after thermal weathering. It can be clearly seen that capillary water absorption is much faster and larger in the weathered marble, which indicates an improved connectivity of pores. The capillary curve after thermal weathering shows the typical trend with a higher linear uptake of water in the first part followed by only slightly increasing water absorption represented by a plateau. During the

first part of the curve, the capillary pores are filled with water until saturation or complete penetration, and in the second part the contribution of micropores to overall water absorption is very low to keep the higher initial rate of water uptake and the curve runs horizontally.

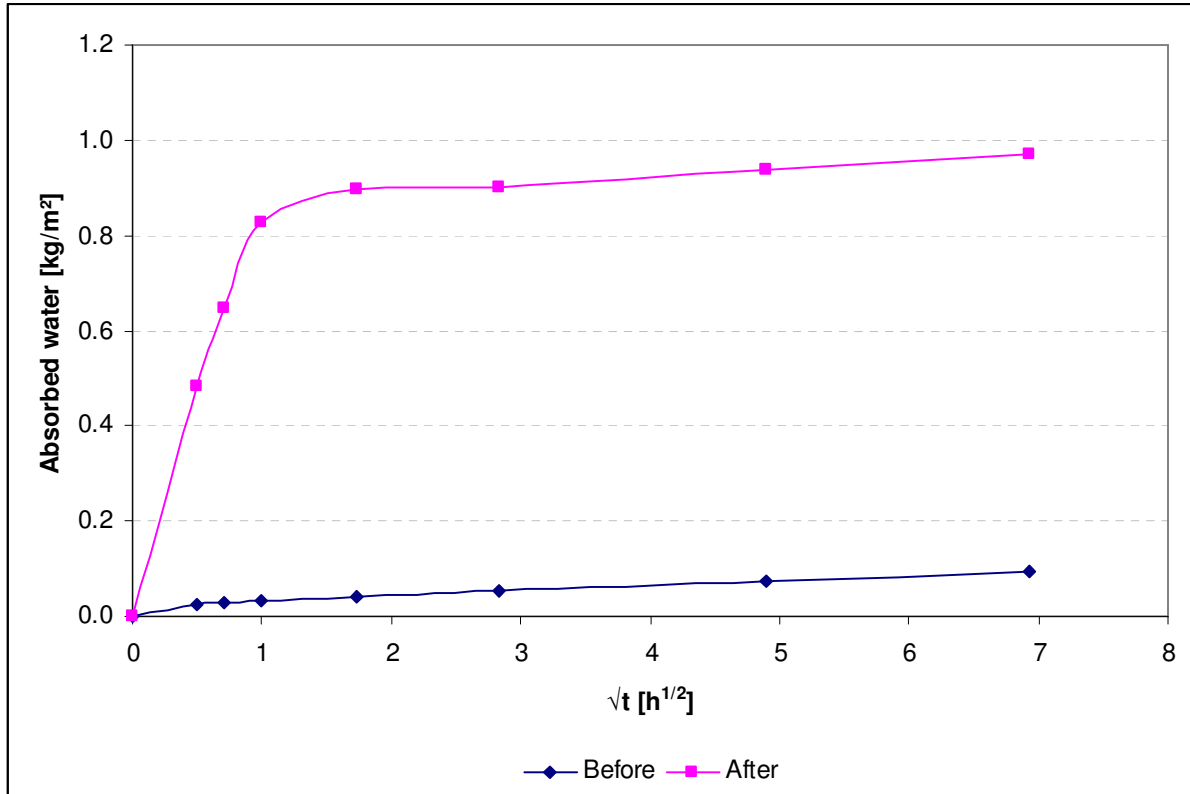


Figure 7.12: The capillary water absorption curves of the marble sample before and after weathering.

7.1.2.3 Drying curve

Figure (7.13) shows the drying curves of the marble sample before and after thermal weathering. The drying curve of the sound marble sample shows three stages of drying; the stone had dried first with almost constant drying rate (avg. $g = 7.74 \text{ g/(m}^2\cdot\text{h)}$) before a short linear drop in the drying speed occurred at around 85% of the remaining moisture, followed by a tiny, relatively constant drying speed.

The thermally-weathered marble exhibited almost the same 3-phase evolution of drying. However, the weathered stone showed a much faster drying with an average water flow rate (g) of $117.16 \text{ g/(m}^2\cdot\text{h)}$ that remained more or less constant until the moisture content dropped to 70%. Below this critical moisture content, the water evaporation rate decreased linearly. The decrease in drying speed started to slow down when the remaining moisture content dropped below 50%.

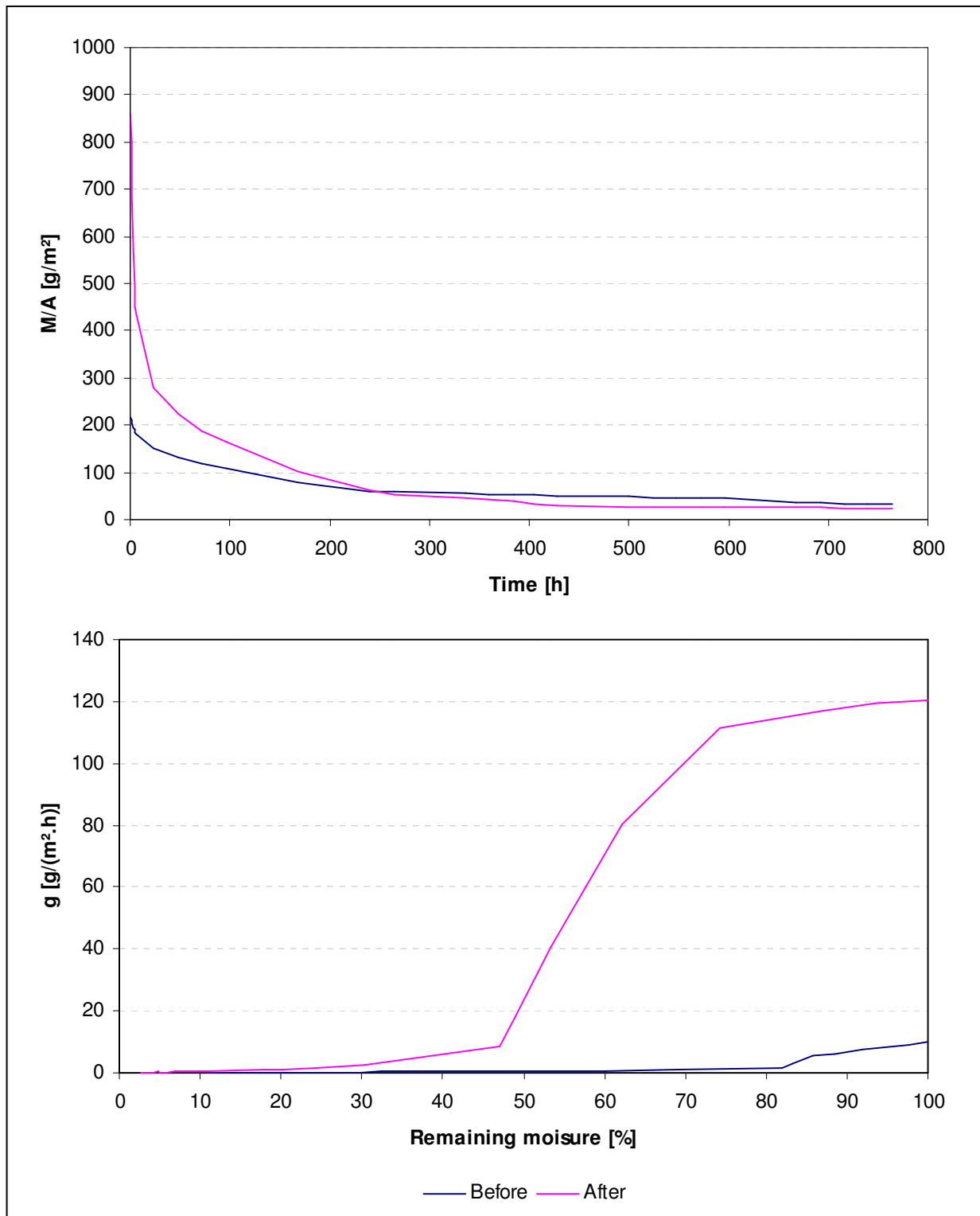


Figure 7.13: Drying curves of the marble sample before and after thermal weathering.

The thermal weathering process changed the pore structure of the marble sample and its hydric properties. The initial water content of the weathered marble is around four times higher than that of the sound stone. This is attributed to the increase of open porosity as a

result of fracturing. The critical moisture content of the stone dropped also from around 85% to 70% after weathering due to the improved connectivity of pores. This reduction led to a faster drying process of the weathered stone in the capillary phase.

Furthermore, the thermal weathering acted also to improve the permeability of the stone to water vapor diffusion, which results in a faster drying during the diffusion phase. Therefore, the drying of the weathered marble is more efficient than that of the sound stone. The evaporation rate of the sound marble was very low and approached the base line when around 65% of the moisture was still remaining in the stone. The evaporation rate of weathered marble, on the contrary, approached the base line first when the remaining moisture content dropped below 20%.

7.1.2.4 Thermal expansion

The thermal expansion coefficient of the marble sample was decreased by 46% after thermal weathering. This result is actually expected because the induced cracks provide voids where calcite grains can expand without causing further measurable displacement (Weiss et al., 2004).

7.1.2.5 Mechanical properties

The mechanical properties of the stone were greatly influence by weathering. The developed microcracks weakened grain cohesion and stone structure, causing a substantial decrease (87%) of biaxial flexural strength (β_{BFS}). Both moduli of elasticity were also reduced after weathering, especially the static modulus which was reduced by 97%. This great reduction in the static modulus of elasticity after thermal weathering is attributed to the development of large amounts of cracks, which weaken the stone structure and allow deformations at much lower stresses. The reduction in the dynamic modulus was relatively lower than in the static one because the influence of cracks is more important with measurements under static loads. This results was also observed for the limestone samples that were subject to cracking (LA and LJ1), which supports again the statement that microcracks influence the static modulus of elasticity more than the dynamic one.

7.1.2.6 Ultrasonic velocity

The velocity of longitudinal ultrasonic waves was measured in cubic specimens along three orthogonal directions using an ultrasonic transmitter vibrating at 46 kHz. The sample is characterized by anisotropy of around 7%, as calculated from the maximum and minimum ultrasonic velocity in the three directions.

The marble sample showed an average ultrasonic velocity of 4525 m/s. According to Köhler classification system (Table 5.1), the stone can be classified as fresh marble. After weathering, the ultrasonic velocity of the dried specimens was dropped steeply by 65%, due to the influence of induced cracks.

The water saturated specimens of the sound marble showed an increase of ultrasonic velocity by around 14% compared to dry specimens, which indicates already the presence of some cracks in the stone. Preexisting cracks are, however, common in fresh crystalline rocks (Siegesmund et al., 2000). This percentage was increased significantly after weathering to 40%, which again confirms the influence of cracks on ultrasonic velocity. The anisotropy of the marble sample increased after weathering by 28%, which might reflect a certain degree of directional dependence of cracking.

Ultrasonic velocity was also measured in 2x2x5 cm prismatic specimens (in one direction) using two ultrasonic frequencies, namely 46 kHz and 250 kHz. The measurements with both frequencies reported almost the same results for ultrasonic velocity; the difference in the measured velocities lies within the accuracy limit of the instrument.

The measured values of ultrasonic velocity differ slightly between the prismatic and cubic specimens. This might be attributed to the anisotropy of the marble sample as the velocity in the cubes is the average value of the velocities along three spatial directions, whereas the velocity in the prisms is measured only along one direction. The measurements on prisms reported a percentage decrease in ultrasonic velocity of 60%, which is only slightly lower than that measured on the cubes.

7.2 Properties of stones before and after consolidation

The naturally weathered limestone samples were consolidated with two silicic acid ester (SAE)-based consolidants from Remmers; KSE 300 (Funcosil 300) and KSE 300HV (Funcosil 300HV). The consolidant KSE 300HV contains an additional coupling agent and is, therefore, particularly suitable for carbonate stones. The major bulk properties of the treated stones were determined using 5 cm cubic specimens that were consolidated by capillary absorption until saturation and then by total impregnation for one hour. Drill core specimens were also used to determine certain properties of the stones in depth profile. These specimens were treated by capillary absorption for one hour. A third group of specimens comprises 2x2x5 cm prisms that were treated in a similar way to the cubic specimens (i.e. by total immersion after capillary absorption until saturation) and used to determine the dynamic modulus of elasticity. Ultrasonic velocity with two different ultrasonic frequencies (46 kHz and 250 kHz) was also measured on these prisms.

In the following sections, the various properties of stones before and after consolidation are discussed and the effectiveness of the treatments is evaluated.

7.2.1 Uptake of consolidation products

The uptake of consolidation product was calculated from the specimens' mass difference before and directly after product application. The deposited dry matter was determined after around two months of product application from the dry mass difference between treated and untreated specimens (after drying at 60 °C). The results are given in Table (7.17).

Table 7.17: Uptake of consolidation product and the amount of dry deposited material in the cubic and prismatic specimens treated by total immersion and the drill cores treated by capillary rise.

		<i>Product uptake [% w/w]</i>			<i>Deposited dry matter [% w/w]</i>		
		<i>Cubes</i>	<i>Prisms</i>	<i>Drill cores</i>	<i>Cubes</i>	<i>Prisms</i>	<i>Drill cores</i>
<i>LH</i>	KSE 300	7.5 ± 0.7	-	2.1 ± 0.5	2.4 ± 0.3	-	0.6 ± 0.2
	KSE 300HV	8.2 ± 1.1	11.9 ± 1.1	2.6 ± 0.2	2.8 ± 0.3	4.9 ± 0.4	0.7 ± 0.2
<i>LJ2</i>	KSE 300	9.3 ± 0.3	7.9	4.4 ± 0.2	2.9 ± 0.1	3.3	1.4 ± 0.0
	KSE 300HV	9.2 ± 0.6	9.3 ± 0.8	5.4 ± 0.5	3.1 ± 0.2	3.8 ± 0.4	1.8 ± 0.2
<i>LJ3</i>	KSE 300	9.6 ± 1.2	8.8 ± 3.7	4.3 ± 2.0	2.9 ± 0.4	4.0 ± 1.6	1.2 ± 0.7
	KSE 300HV	11.3 ± 2.7	12.4 ± 1.1	5.4 ± 1.7	4.0 ± 1.0	5.2 ± 0.5	1.7 ± 0.7
<i>LUQ2</i>	KSE 300	14.0 ± 1.2	14.2 ± 2.1	5.8 ± 0.1	4.2 ± 0.4	6.6 ± 1.0	1.5 ± 0.3
	KSE 300HV	14.7 ± 0.5	16.0 ± 1.0	6.9 ± 1.1	5.2 ± 0.2	6.7 ± 0.5	2.0 ± 0.2

The most porous and most weathered sample LUQ2 has the highest uptake of product and the highest dry deposited material, whereas the least porous and weathered sample LH absorbed the lowest amount of consolidation products. The uptake of consolidant is also influenced by the application method; the cubic and prismatic specimens treated by total immersion showed a greater amount of product uptake and deposited polymerized material compared to the drill core specimens treated by capillary rise.

The amount of polymerized material deposited in the pores influences the mechanical properties of the stone and its water absorption capacity (Łukaszewicz, 2004). The samples LUQ2 and LJ2 have the highest amount of dry deposited material and exhibit also the largest increase in mechanical properties. The consolidant KSE 300HV deposited a slightly higher amount of polymerized material and seem generally to perform better than KSE 300 as will be shown in the following sections.

7.2.2 Porosity properties and density

The porosity properties and density of the untreated (UT) and treated (KSE 300 and KSE 300HV) limestone samples are presented in Table (7.18).

Table 7.18: Porosity properties and density before and after consolidation.

Sample		Accessible porosity (N_t) [%]	Free porosity (N_{48}) [%]	Real density (ρ_{real}) [g/cm^3]	Bulk density (ρ_{bulk}) [g/cm^3]	Saturation coefficient (S)
LH	UT	24.03±1.29	17.26±1.83	2.71	2.06	0.72
	KSE 300	20.80±1.48	13.98±1.58	2.68	2.12	0.67
	KSE 300HV	21.58±1.10	9.44±1.03	2.68	2.10	0.44
LJ2	UT	25.76±0.72	19.79±0.52	2.71	2.01	0.77
	KSE 300	22.59±0.91	14.61±0.87	2.68	2.07	0.65
	KSE 300HV	22.61±0.46	9.20±0.38	2.68	2.07	0.41
LJ3	UT	27.23±3.43	21.94±2.97	2.68	1.95	0.80
	KSE 300	24.61±3.84	17.88±3.02	2.65	2.00	0.73
	KSE 300HV	22.65±1.93	13.85±1.27	2.65	2.05	0.61
LUQ2	UT	32.86±0.83	29.03±0.83	2.70	1.81	0.88
	KSE 300	27.51±0.59	21.53±0.55	2.65	1.92	0.78
	KSE 300HV	28.99±0.56	21.94±0.47	2.65	1.88	0.76

Figure (7.14) shows the average accessible and free porosities before and after treatment with the consolidation products KSE 300 and KSE 300HV. Both types of porosity were decreased

after treatment for all the studied samples. This decrease in porosity resulted from the deposition of the consolidants in the pores of the stones. The material silicic acid ester imparts a temporary hydrophobicity (water repellency) to the stone, which might have also contributed to the decrease in absorbed water and correspondingly calculated porosity.

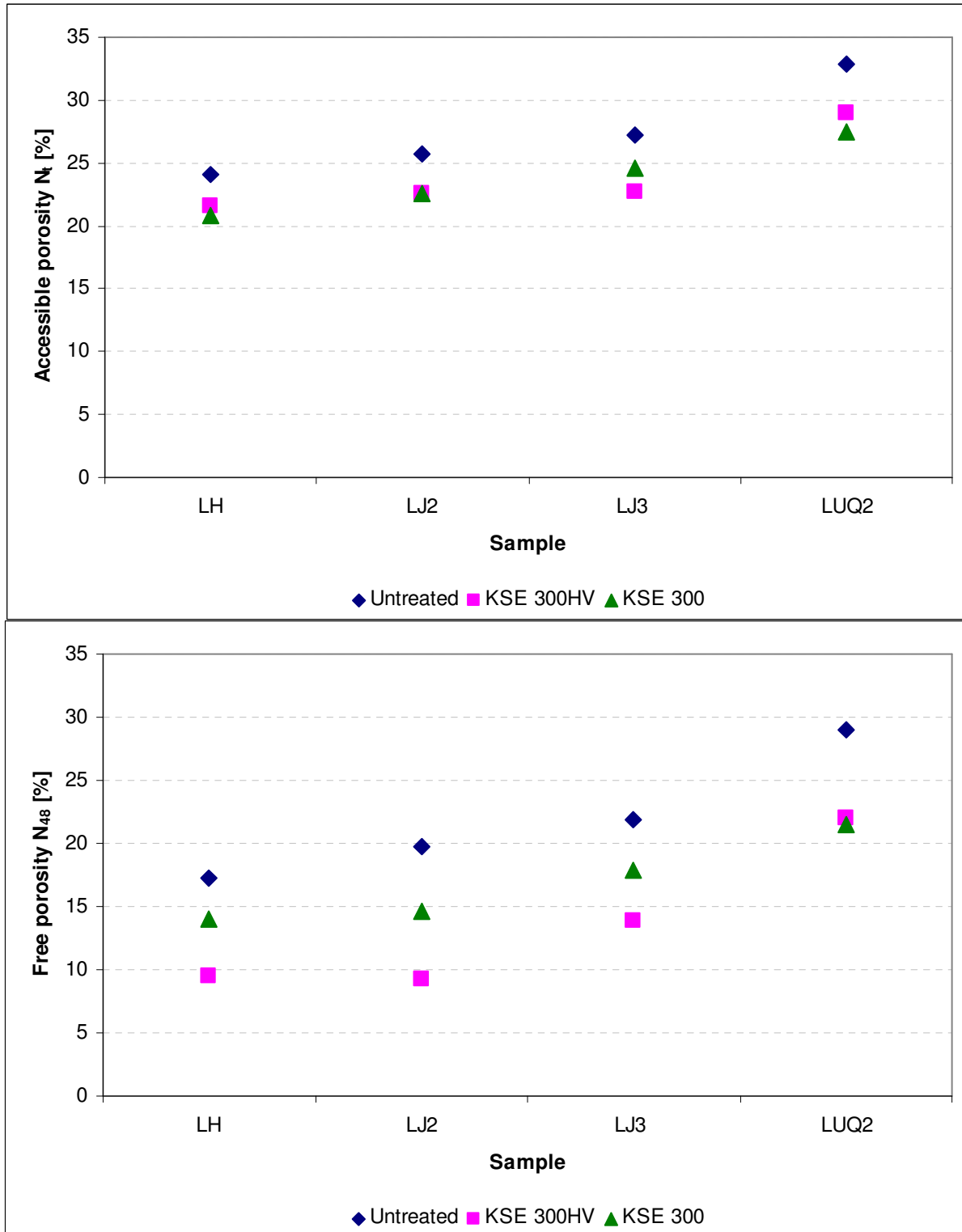


Figure 7.14: Accessible and free porosities before and after consolidation treatments.

The percentage reduction in accessible porosity (10%-17%) is almost the same for both consolidants. The free porosity exhibited a larger percentage reduction after treatment that ranges between 24% and 54% for the stones treated with the consolidant containing coupling agent KSE 300HV and between 18% and 26% for those treated with KSE 300. This difference between the two porosities might be related to the induced hydrophobic effect that reduces further the absorption of water and respectively the measured free porosity, but has no or minimum influence on the accessible porosity measured under vacuum; the hydrophobicity is not active or strongly restricted under vacuum (Meinhardt-Degen, 2005).

Contrary to porosity, the bulk density of the treated stone was increased as expected. The saturation coefficient of the treated stones was decreased particularly for those treated with KSE 300HV. This is actually related to the reported difference between the accessible and free porosity, which is higher for the stones treated with KSE 300HV.

7.2.3 Pore size distribution

Figure (7.15) shows the pore size distribution of the studied limestones before and after treatment with the consolidation products KSE 300 and KSE 300HV.

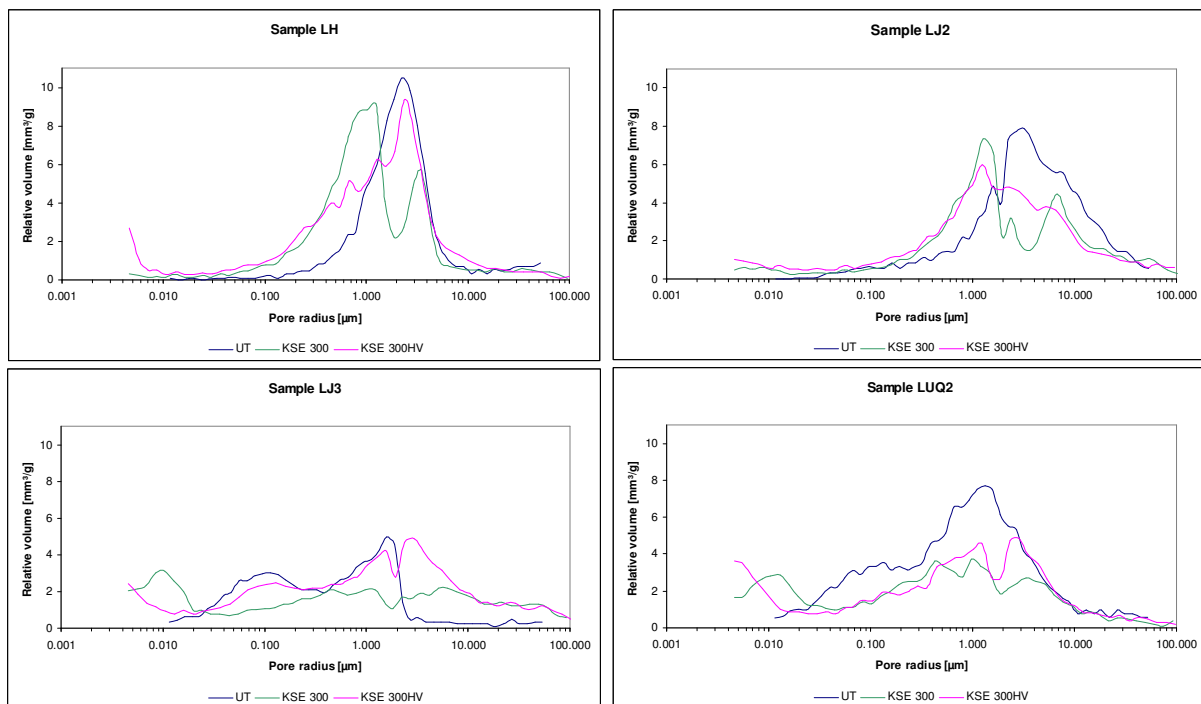


Figure 7.15: The MIP spectra of the untreated and treated samples.

The untreated Hallabat stone (LH) is characterized by a uni-modal pore size distribution with the main peak around 2 μm . The porosity is almost comprised of capillary pores, particularly small capillaries. The stone treated with KSE 300 exhibited a shift in the pores smaller than 3 μm towards smaller pores and the resulting pore size distribution is bi-modal with the main peaks around 1 μm and 3.5 μm . For the stone treated with KSE 300HV, the main peak of pores decreased slightly and a few smaller peaks appeared, producing a wider pore size distribution.

The sample LJ2 has a wide uni-modal pore size distribution with the main peak around 3 μm . The sample treated with KSE 300 exhibited a considerable reduction of the volume of pores with size around 3 μm , and the main peak was shifted towards smaller pores; the stone has nearly a bi-modal pore size distribution with two peaks around 1 μm and 7 μm . The pore size distribution of the sample treated with KSE 300HV is nearly comparable to that of the untreated sample. However, the volume of pores was generally reduced and the main peak was shifted downwards to the pore radius 1 μm .

The sample LJ3 has mainly a bi-modal distribution of pores around 2 μm and 0.1 μm . The sample treated with KSE 300 has a wide, nearly even, pore size distribution with the main groups of pores around 0.01 μm , 1 μm and 5 μm . The sample treated with KSE 300HV exhibited two families of pores that also appeared in the weathered stone, but with a smaller volume. However, this sample has a wider pore size distribution with two additional main families of pores; a relatively large peak appears around 3 μm and another smaller one around 0.005 μm .

The naturally weathered sample LUQ2 has a wide pores size distribution that ranges from 0.01–50 μm , with the main family of pores around 1 μm . After consolidation with KSE 300, the volume of pores with pore radius 0.03–5 μm was noticeably decreased and a small peak around 0.01 μm was appeared. The stone consolidated with KSE 300HV exhibited almost the same changes in its pore size distribution.

The mercury intrusion porosimetry results are also summarized in Table (7.19). For the two samples LJ2 and LUQ2, the treatments with both consolidants induced a reduction in porosity as expected. This decrease occurred in the proportion of capillary pores, particularly small

capillaries, where the consolidants seem to be mainly deposited. On the contrary, the proportion of micropores was slightly increased after treatment.

The samples LH and LJ3 exhibited unexpectedly an increase of porosity after treatment. This is most likely attributed to measurement errors and stone heterogeneity, especially for the sample LJ3. After all, a clear reduction in porosity of these samples could be proved by water absorption measurements.

Table 7.19: MIP results before and after consolidation treatments.

		Pore classes [%]					P_c [%]	SSA [m ² /g]	avg. r [μ m]	$P_{m0.1}$ [%]	$P_{m0.1-5}$ [%]	$P_{m>5}$ [%]
		<0.01 μ m	0.01- 0.1 μ m	0.1- 1 μ m	1- 10 μ m	10- 100 μ m						
LH	UT	0.63	1.25	18.81	73.37	5.93	20.16	0.42	2.24	0.38	17.88	1.90
	KSE 300	1.11	4.23	51.59	37.69	5.39	20.55	0.86	0.85	1.10	17.88	1.58
	KSE 300HV	4.95	5.65	34.92	49.83	4.65	23.21	2.72	2.30	2.46	18.67	2.08
LJ2	UT	0.00	2.73	14.15	66.77	16.35	24.22	0.27	2.75	0.66	15.08	8.47
	KSE 300	3.07	4.77	30.14	47.25	14.77	19.43	1.31	1.26	1.52	12.34	5.57
	KSE 300HV	4.36	6.86	28.04	49.13	11.61	20.88	2.10	1.27	2.34	13.87	4.67
LJ3	UT	0.74	26.08	43.26	26.45	3.48	16.51	1.52	1.57	4.43	11.31	0.77
	KSE 300	15.50	17.37	24.72	26.02	16.40	17.58	5.32	0.01	5.78	7.41	4.39
	KSE 300HV	7.40	15.00	26.90	38.14	12.56	21.45	3.93	2.34	4.81	12.32	4.33
LUQ2	UT	1.09	16.31	40.76	36.79	5.05	30.07	2.32	1.05	5.23	22.08	2.76
	KSE 300	11.88	19.30	34.93	28.24	5.65	19.58	5.17	0.97	6.11	11.28	2.20
	KSE 300HV	13.71	11.83	32.02	36.30	6.13	20.60	5.81	2.34	5.26	12.96	2.38

7.2.4 Capillary water uptake coefficient (w-value)

The naturally weathered limestone samples showed strong capacity to absorb water as indicated by their high capillary water absorption coefficients. After consolidation treatments, the absorption of water was significantly decreased for all the samples (Figures 7.16 and 7.17). For the samples treated with KSE 300, the water uptake coefficient was decreased by 81%, 65%, 70%, and 50% for LH, LJ2, LJ3, and LUQ2 respectively. A slightly larger reduction in water absorption was noticed for the samples treated with KSE 300HV (by 94%, 73%, 89%, and 87% for LH, LJ1, LJ2, and LUQ2 respectively). The reduction of water uptake coefficient can be attributed to the changes in pore size distribution and the connectivity of capillary pores (due to polymer deposition in pores), as well as to the hydrophobic effect of the consolidants (Honsinger and Sasse, 1991; Stück et al., 2008).

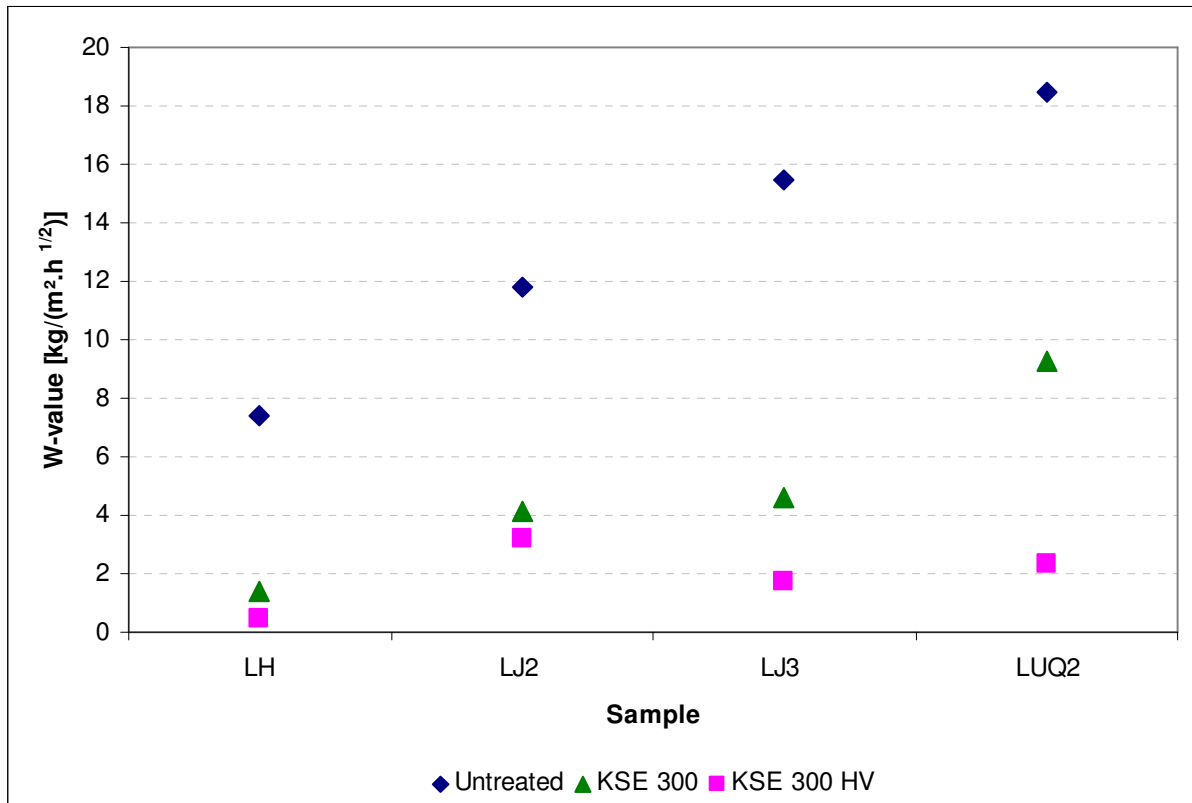


Figure 7.16: Average w-value of the stone samples before and after consolidation treatments.

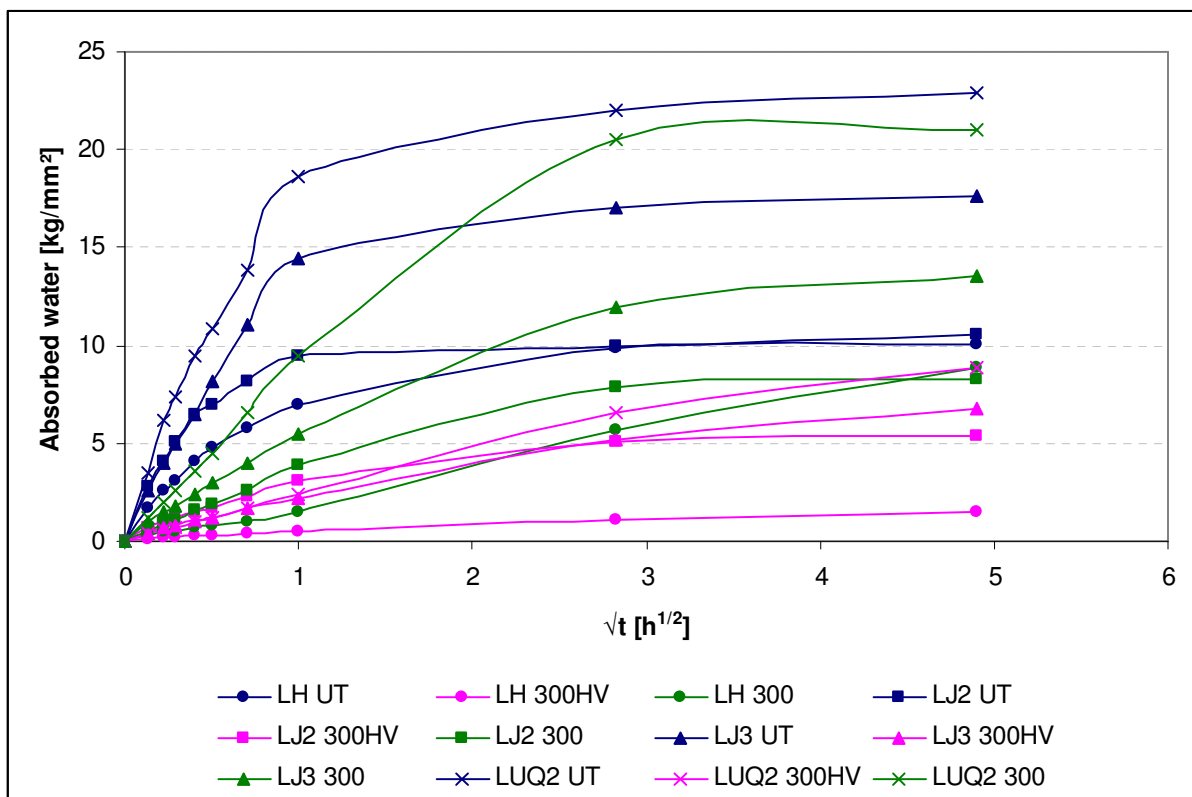


Figure 7.17: Capillary water absorption curves of the untreated and treated samples.

As for the evaluation of the effectiveness and success of consolidation treatments, the capillary water uptake coefficient of the treated stone should be equal or smaller than that of the untreated unweathered stone (see Table 4.1). This requirement is clearly fulfilled and the treatment with both consolidants seems to be successful in this regard.

In fact, the absorption of water was considerably reduced, particularly for the stone treated with KSE 300HV. This is mostly desirable, although it is not an essential requirement for a consolidant to impart hydrophobicity.

7.2.5 Water vapor diffusion resistance coefficient (μ -value)

The permeability of stone to water vapor is an important physical property that allows the escape of water vapor from inside the stone. The treated zone should not, therefore, act as a barrier against water vapor diffusion (Honsinger and Sasse, 1991). A significant decrease in water vapor permeability due to consolidation treatment can lead to trapping of water vapor inside the stone, raising thereby the risk of stone damage, particularly frost damage (Scherer and Wheeler, 2009).

The requirement for successful consolidation treatments regarding the permeability of stone to water vapor implies that the increase in water vapor diffusion resistance (μ -value) should be lower than 20% (Snethalge and Wendler, 1995; Sasse and Snethalge, 1997). This value is not based on strict scientific measurements but on general experience. Lower ratios of increase in μ -value (below 20%) are mostly located within the range of natural variation of a stone and are therefore acceptable (Snethalge, 2008).

Table (7.20) shows the water vapor diffusion resistance of the stone samples before and after consolidation with KSE 300 and KSE 300HV as well as the percentage increase associated to it. The permeability of the stone samples to water vapor was decreased after treatment as indicated by the increase in μ -value. The more weathered samples showed seemingly a greater reduction in permeability. The consolidant KSE 300 induced a lower increase in water vapor diffusion resistance compared to KSE 300HV. The increase in diffusion resistance of the stones falls within the acceptable range (< 20%) except for the sample LUQ2 treated with KSE 300HV, which showed a slightly higher increase (22%). Hence, the treatments with both

consolidants can generally be considered successful concerning their influence on water vapor permeability.

Table 7.20: Water vapor diffusion resistance of treated and untreated samples and the percentage increase after treatment.

	<i>Sample</i>	<i>LH</i>	<i>LJ2</i>	<i>LJ3</i>	<i>LUQ2</i>
μ -value	<i>UT</i>	60.12	50.57	52.78	34.95
	<i>KSE 300</i>	64.93	56.83	57.41	39.50
	<i>KSE 300HV</i>	66.63	58.09	61.42	42.52
Change [%]	<i>KSE 300</i>	8	12	9	13
	<i>KSE 300HV</i>	11	15	16	22

7.2.6 Drying curve

Figure (7.18) shows the drying curves of the naturally weathered and treated stone samples. The initial water content of all treated samples is lower than that of the untreated ones due to the reduction in free porosity brought about by consolidation treatments. The treated samples exhibit a lower drying rate compared to the weathered untreated stones (Table 7.21). This can be attributed to the decrease in the proportion of capillary pores after treatment, which could be proved by MIP measurements for all stones except for LH and LJ3 treated by KSE 300HV. The MIP data of these samples showed erroneously larger porosity values and they were most probably influenced by measuring errors and stone heterogeneity.

The treated samples, except for LH, showed also higher critical moisture content, which is attributed to the increase in the proportions of micropores after consolidation (Buj and Gisbert, 2010).

Table 7.21: Drying rate and critical moisture content before and after consolidation.

	<i>Sample</i>	<i>LH</i>	<i>LJ2</i>	<i>LJ3</i>	<i>LUQ2</i>
$g [g/(m^2 \cdot h)]$	<i>UT</i>	105 ± 6	116 ± 7	97 ± 13	132 ± 15
	<i>KSE 300HV</i>	92 ± 5	97 ± 2	88 ± 4	102 ± 7
	<i>KSE 300</i>	98 ± 2	109 ± 3	90 ± 9	101 ± 9
$\mu_c (\Psi_c)$	<i>UT</i>	62	30	47	31
	<i>KSE 300HV</i>	40	42	69	55
	<i>KSE 300</i>	56	34	63	59

These changes led to a slower drying process in the liquid phase. The permeability to water vapor was also reduced for the treated stones, leading thereby to a slower drying during the

diffusion phase as well. No significant variations in the drying behavior between the samples treated with the consolidants KSE 300 and KSE 300HV can be noticed.

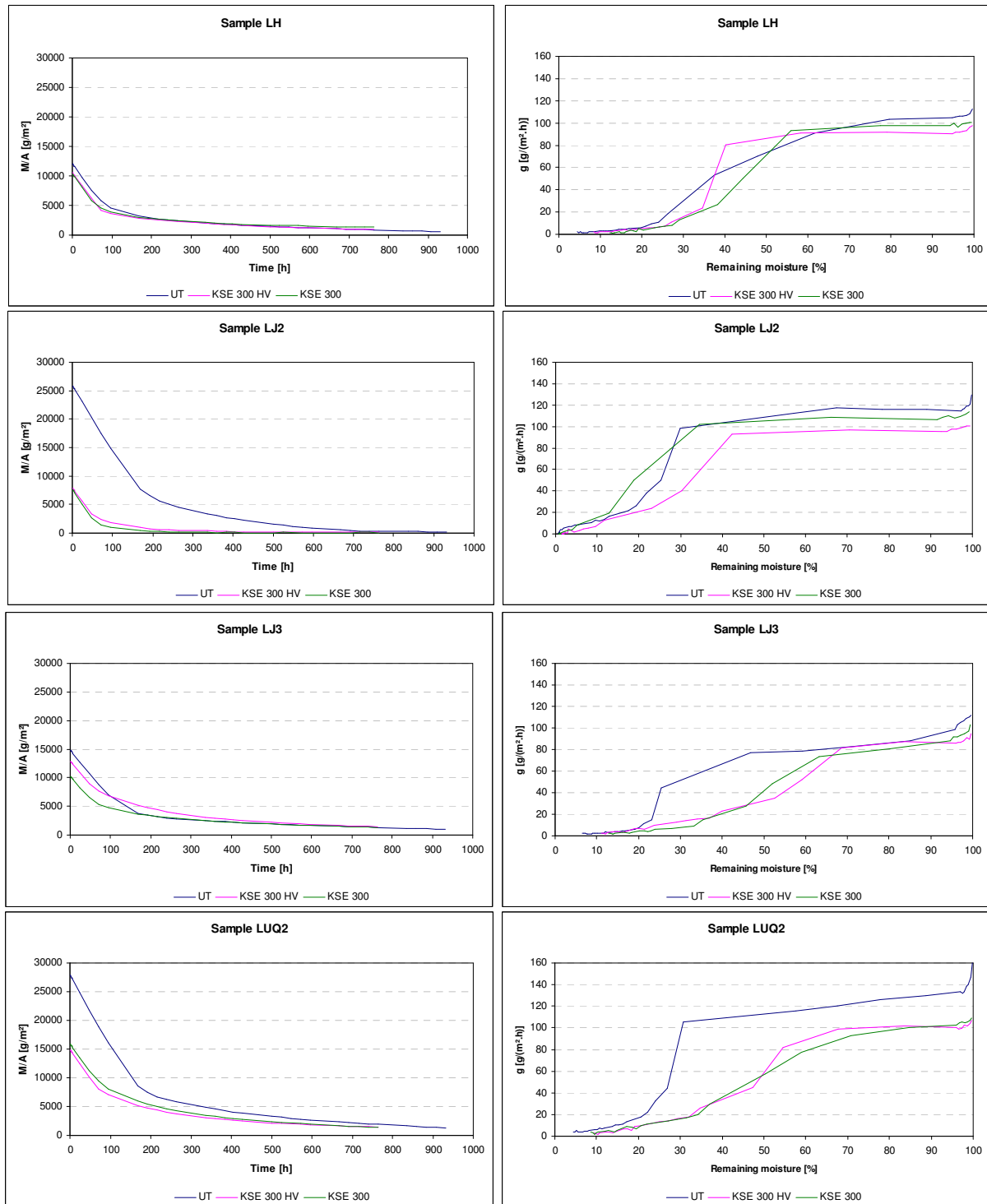


Figure 7.18: Drying curves of the weathered stones before and after consolidation with KSE 300 and KSE 300HV. Mass decrease per area (M/A) in function of time and density of vapor flow rate (g) in function of remaining moisture are displayed.

In general, the drying process of the treated samples is slightly slower than that of the untreated ones. However, the absorbed amount of water was significantly lower after

consolidation and the drying duration was not markedly increased for the treated samples. This satisfies the requirement for successful consolidation which implies no increase in the drying duration of the treated samples (Table 4.1).

7.2.7 Color changes

The changes in chromatic parameters (represented in CIEL*a*b* values) induced by consolidation treatments are given in Table (7.22). All treated samples showed a lower value of luminosity (negative ΔL^*) compared to the untreated stones for both consolidants, which indicates a tendency towards darkening. The treated samples exhibited also a slight increase in the red (a^*) (except for sample LJ2) and yellow (b^*) coordinates. The total color change (ΔE^*) of the stones lies within the acceptable range (that is $\Delta E^* \leq 5$), except for the samples LJ3 and LUQ2 treated with KSE 300HV, which showed ΔE^* values of 7.29 and 5.48 respectively. The highest degree of darkening, yellowing and total color change was induced by KSE 300HV on the sample LJ3. In general, the variations in color and visual properties of the stones after treatment can still be considered small and restricted.

Table 7.22: The variations in chromatic parameters of the treated limestone samples.

	KSE 300 HV				KSE 300			
	ΔL^*	Δa^*	Δb^*	ΔE^*	ΔL^*	Δa^*	Δb^*	ΔE^*
LH	-2.84	0.50	2.05	3.54	-0.42	0.13	1.76	1.81
LJ2	-1.40	-0.23	1.62	2.16	-0.01	-0.41	0.23	0.47
LJ3	-5.23	1.28	4.92	7.29	-2.56	0.27	2.50	3.59
LUQ2	-4.65	0.34	2.87	5.48	-2.69	0.22	2.26	3.52

7.2.8 Thermal expansion

The thermal expansion of the stones was measured in the perpendicular direction to bedding planes before and after treatment with KSE 300 and KSE 300HV (Figure 7.19). The thermal expansion coefficient increased in all consolidated samples due to the partial filling of pores with consolidant. The consolidant containing coupling agent KSE 300HV caused a greater increase in thermal dilatation compared to KSE 300; the thermal expansion coefficient of the treated samples LH, LJ2, LJ3 and LUQ2 increased respectively by 13%, 18%, 19% and 29% for KSE 300HV and by 5%, 16%, 15% and 20% for KSE 300.

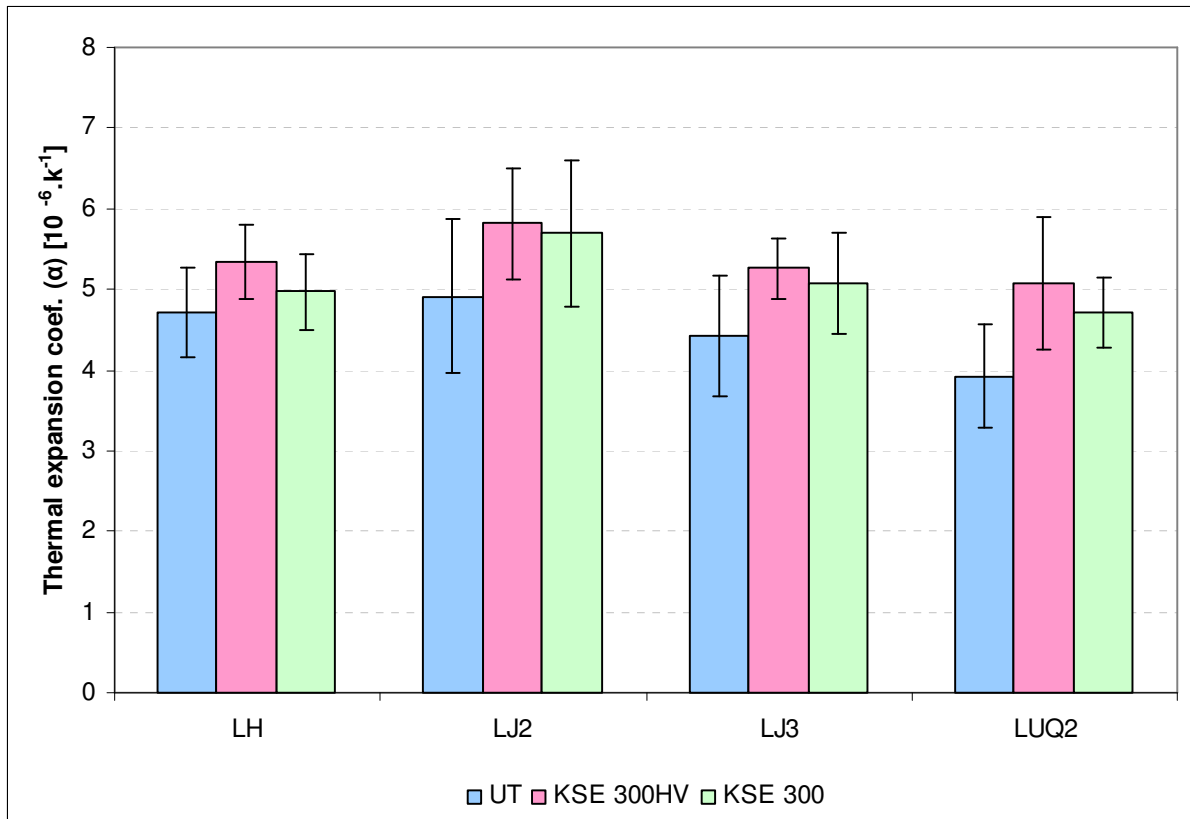


Figure 7.19: Thermal expansion coefficient of the weathered and treated samples (Temperature range 60-20°C).

7.2.9 Penetration depth as determined by water micro-drop absorption time

The penetration depth of consolidants into a stone is a critical parameter for the success of consolidation treatments. It depends on the microstructure of the stone and the properties of consolidation product such as viscosity and surface tension (Maravelaki-Kalitzaki et al., 2006). Consolidants should sufficiently penetrate and strengthen the weathered zone and increase its adhesion to the sound core of the stone. Superficial consolidation tends to fill the pores of the stone surface, which may result in the accumulation of moisture and salts behind the treated layers. Furthermore, interfacial delamination often occurs because of a marked difference in the properties of the treated and untreated stone (Clifton, 1980).

The determination of the depth of penetration of stone consolidants can be achieved by different methods (Leroux et al., 2000). In this study, measurements in depth profile of ultrasonic velocity, water micro-drop absorption time, and biaxial flexural strength as well as drilling resistance (only to a depth of 1 cm) were used to determine the penetration depth of consolidants. The results of water micro-drop absorption time are discussed below. The

measurements of other properties (ultrasonic velocity, biaxial flexural strength and drilling resistance) are discussed separately.

Water μ -drop absorption time

Owing to the expected hydrophobic effect of some consolidation materials and the filling of pores with consolidant, the absorption of water is normally decreased in treated stone. By measuring the absorption time of water micro-drops applied at regular distances (in depth profile) on treated stones, the depth of penetration of consolidants can be estimated. Figure (7.20) shows the results of this test on the studied samples.

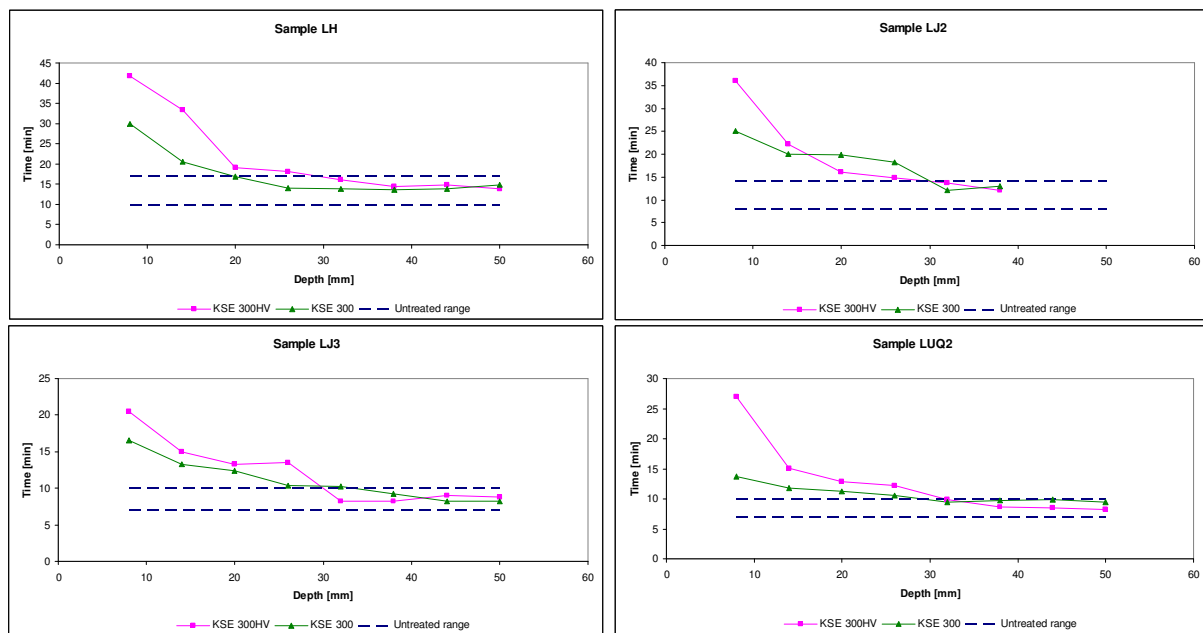


Figure 7.20: Micro-drop water absorption time of the treated sample as a measure of penetration depth.

Except for the sample LH treated with KSE 300, both consolidants penetrated all the stones up to a depth of 3 cm. Roughly speaking, the applied consolidants seem to achieve a good penetration depth; it was suggested that a good consolidant should be able to penetrate a weathered stone to a depth of at least 2.5 cm (Clifton, 1980). For a more specific evaluation of the success of treatment in this respect, the achieved penetration depth should be compared with the thickness of the weathered zone and the resulting consolidation profile should also be studied. This is done in the following sections.

7.2.10 Drilling resistance measurement

Figure (7.21) shows the drilling resistance (DR) profiles in the first 1 cm depth of the untreated and treated samples in the directions parallel and perpendicular to bedding planes. These results are the average DR curves of at least three holes measured with a 5 mm diameter drill bit under constant operative conditions of 600 rpm rotation speed and 10 mm/min penetration rate.

The drilling resistance profile of the untreated sample LH varies around a drilling force of 5.19 N (obtained by averaging the force between 2 mm and 10 mm), and it is almost comparable to the profiles of treated samples with an average force of 6.18 N and 6.28 N for KSE 300HV and KSE 300 respectively. A very slight increase in the drilling resistance can only be seen in the perpendicular direction to bedding planes and it lies actually within the resolution limit of the instrument. Therefore, it is hard to speak of any consolidation effect for this sample with this method.

The weathered sample LJ2 exhibits a very low DR of 1.47 N. The average drilling resistance of the sample was increased to 10.56 N and 6.27 N after treatment with KSE 300HV and KSE 300 respectively. The drilling resistance profiles of the consolidated samples are almost homogenous, particularly for the sample treated with KSE 300HV. A slightly higher DR can be noticed in the surface zone up to a depth of around 4 mm.

The sample LJ3 is a heterogeneous stone and some changes in the drilling profiles might thus be related to this heterogeneity rather than to consolidation treatments. The weathered untreated sample exhibits generally an average drilling resistance of around 7.76 N. The drilling resistance of the consolidated samples varies around 13.88 N and 12.03 N for KSE 300HV and KSE 300 respectively. The resulting drilling profiles are not homogenous and overlap sometimes with the drilling profile of the untreated sample, which might indicate a penetration depth lower than 1 cm. However, the heterogeneity of the stone might be responsible for this overlapping.

The weathered sample LUQ2 shows an average drilling resistance of 4.19 N along the entire 1 cm depth. The resulting drilling resistance profiles after treatment with KSE 300HV and KSE 300 are homogenous and vary around 12.35 N and 9.31 N respectively. No considerable over-

strengthening of the superficial zone was induced; only a slightly higher drilling resistance can be seen in the first 2-4 mm depth.

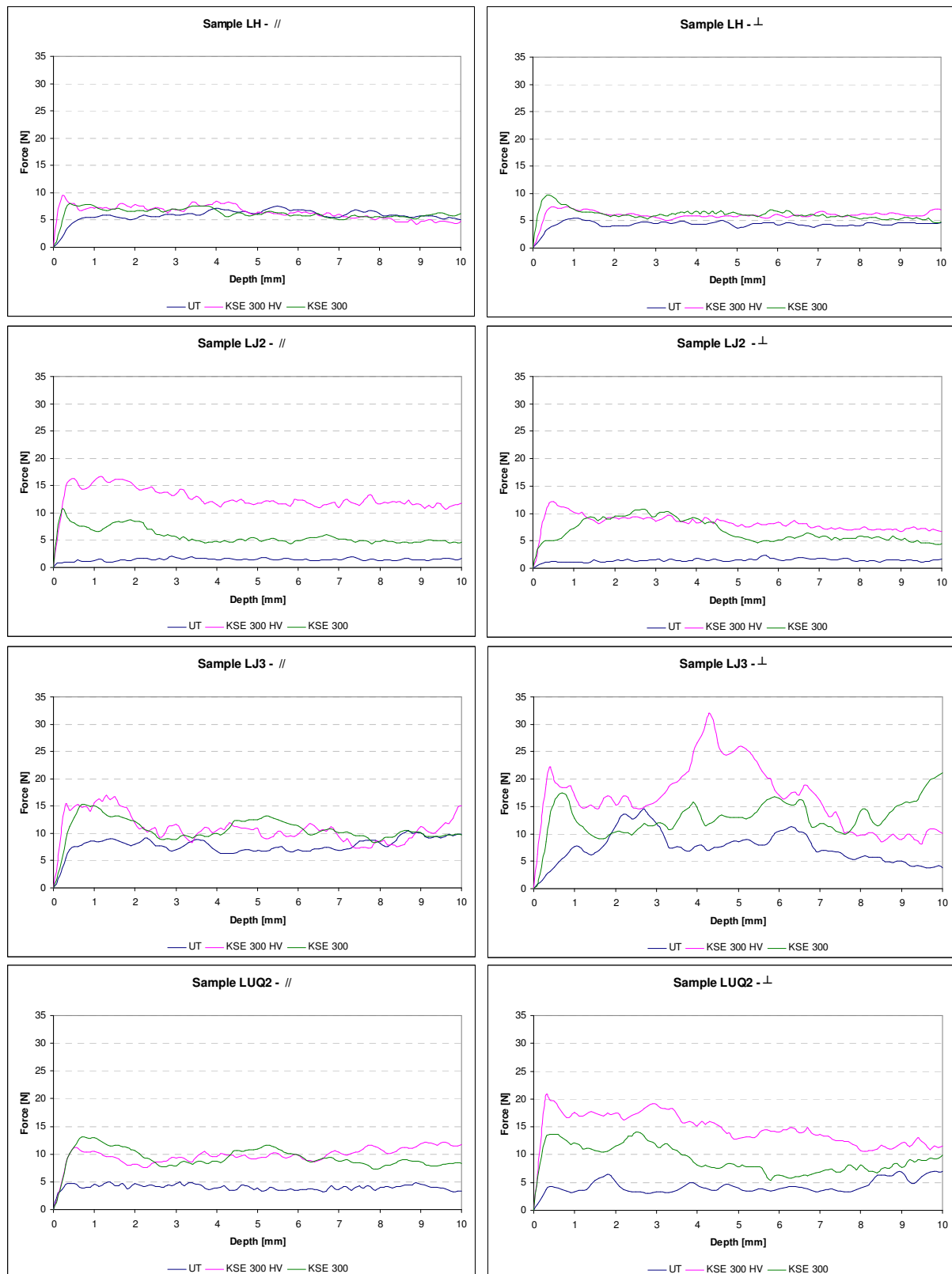


Figure 7.21: Drilling resistance profiles of the weathered and consolidated samples in the directions parallel and perpendicular to bedding.

The requirement for successful consolidation treatments regarding drilling resistance measurement implies the increase of mechanical strength in the weathered zone and the establishment of a homogenous profile. This requirement seems to be fulfilled for the samples LJ2 and LUQ2 treated with either consolidants. The sample LH exhibits no considerable consolidation effect, and the heterogeneity of the sample LJ2 makes it difficult to provide a reliable evaluation of the effectiveness of consolidation treatments. No considerable differences were noticed between the drilling resistance profiles measured in both directions; parallel and perpendicular to bedding.

The drilling resistance profiles were only examined in the first 1 cm depth. For a fully and more accurate evaluation of the consolidation treatments, the performance of the consolidants along the entire weathering depth needs to be considered.

In summary, both consolidants (KSE 300HV and KSE 300) seem to perform very well on the sample LJ2 and LUQ2 through increasing clearly the drilling resistance of the stones without causing considerable over-strengthening in the superficial zone and imparting an almost homogenous drilling profile along the whole investigated depth. The consolidant that contains coupling agent (i.e. KSE 300HV) seems to provide better results compared to KSE 300.

7.2.11 Biaxial flexural strength and moduli of elasticity

Measuring mechanical strength and elastic properties in depth profile is necessary in order to evaluate the condition of stone before and after treatment (Snethlage and Wendler, 1995). In this study, biaxial flexural strength and static modulus of elasticity were measured on 5 mm thick discs cut from drill cores of 5 cm in diameter according to Wittmann and Prim (1983). The outer 2 mm surface of the drill core samples was removed to get an even surface and several 5 mm thick discs were then cut by a diamond cutting saw with a step loss of 1 mm; that is with a net thickness of 5 mm of each cut disc (and considering the 2 mm thick lost layer of the outer surface), the first disc corresponds to a depth of 2-7 mm, the second of 8-13 mm, the third of 14-19 mm, and so on.

As explained earlier, the aim of consolidation treatment is to restore the mechanical strength of the weathered zone to the level of the unweathered stone, in order to establish a homogeneous profile of mechanical strength from the outer surface of the stone to its unweathered core. The outer zone should not be over-strengthened, and particularly the

modulus of elasticity should not disproportionately increase, as this may lead to considerable stress at the interface of treated-untreated zones (Snethlage, 2008). An over-strengthening of the outer zone can be acceptable if certain criteria (see Table 4.1) for mechanical strength and elasticity modulus can be applied (Snethlage, 2008). These require that the biaxial flexural strength and the modulus of elasticity of the treated zone are lower than 1.5-times their values in the untreated unweathered stone (i.e. $\beta_{BFS,t} \leq 1.5 \beta_{BFS,u}$ and $E_t \leq 1.5 E_u$). Furthermore, the modulus of elasticity of the treated zone should at most increase by the same factor as the strength, that is $E_t / E_u \leq \beta_{BFS,t} / \beta_{BFS,u}$. The gradient, in depth profile, of biaxial flexural strength and elasticity modulus of the treated zone should approximately be smaller than 0.2 N/mm²·mm and 1 kN/mm²·mm respectively ($\Delta\beta_{BFS,t}/\Delta x < 0.2$ N/mm²·mm, and $\Delta E/\Delta x \leq 1$ kN/mm²·mm).

Biaxial flexural strength (β_{BFS})

Figure (7.22) shows the biaxial flexural strength of the studied stones in depth profile before and after treatment with KSE 300 and KSE 300HV. The blue slashed line indicates the desired homogeneous strength profile $\beta_{BFS,t} = \beta_{BFS,u}$, and the red slashed line represents the threshold value $\beta_{BFS,t} = 1.5 \beta_{BFS,u}$ that should not be exceeded for successful treatment.

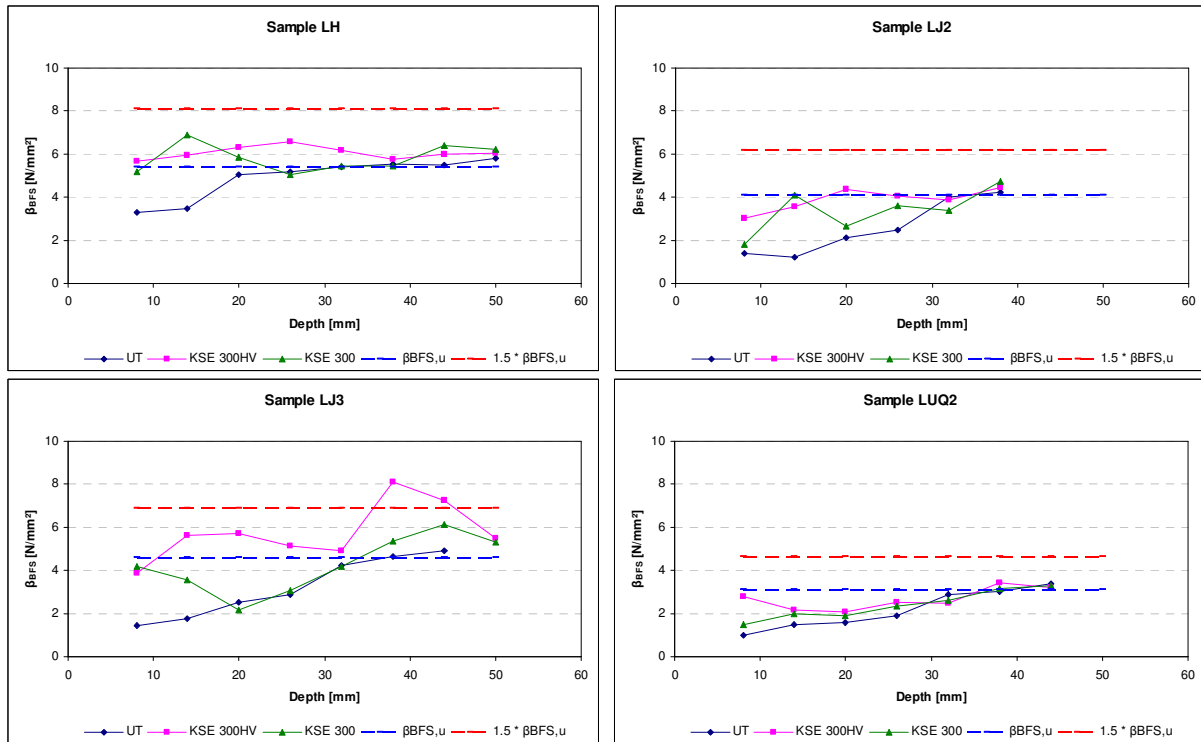


Figure 7.22: Biaxial flexural strength in depth profile of the treated and untreated samples. The strength value is plotted at the upper depth limit of the tested disc (The first disc, for example, corresponds to a depth of 2-7 mm, and the strength value is plotted at 7 mm).

For the sample LH, the depth profile of the biaxial flexural strength of the weathered untreated stone manifests a loss of mechanical strength due to weathering in the first 1.5 centimeters in depth. Both consolidants penetrated the stone beyond this depth and increased the biaxial flexural strength of the weathered zone close to the level of the unweathered stone, producing thereby an almost homogenous strength profile. No over-strengthening was noticed in the superficial zone and the increase in strength is clearly below the threshold value that should not be exceeded for successful treatment. The KSE 300HV, which contains an additional coupling agent, induced a slightly higher increase in strength than KSE 300 and led to a more homogenous strength profile.

The strength profile of the weathered sample LJ2 shows a loss of mechanical strength up to 2.5 cm. The consolidation treatment with KSE 300HV restored the biaxial flexural strength of the weathered zone and produced a homogenous strength profile. The consolidant KSE 300 induced a lower increase (the first 1 cm exhibited even almost no increase) in strength compared to KSE 300HV and the resulting strength profile is also less homogenous.

The strength depth profiles of the sample LJ3 showed several variations that are most probably related to its observed heterogeneity. This stone is criss-crossed by numerous short irregular veins and patches of compact sparry calcite. This heterogeneity makes it difficult to provide a reliable evaluation of the effects of consolidation treatments. However, the stone seems to be weathered up to an estimated depth of 2.5 cm. The consolidant KSE 300 increased the biaxial flexural strength only in the outer surface (up to a depth of 1 cm) of the stone. On the other hand, KSE 300HV brought about a clear increase in the strength of the weathered zone and produced almost homogenous profile of strength along the whole depth of weathering. At the depth between 30 mm and 45 mm, the β_{BFS} value is suddenly higher, which is more likely attributed to stone heterogeneity rather than to consolidation effect.

The sample LUQ2 exhibits the lowest biaxial flexural strength and the highest degree of weathering that extended to a depth of about 2.5-3 cm. Both consolidants penetrated the stone up to a depth of 3 cm and brought about a slight increase in mechanical strength. KSE 300HV provided better results compared to KSE 300; the resulting strength profile induced by KSE 300HV is more homogeneous and only slightly lower than the corresponding level of the unweathered stone.

The treatment with both consolidants led to an increase in the biaxial flexural strength for all the stones, without inducing considerable over-strengthening in the outer treated surface. The consolidant with coupling agent (KSE 300HV) produced more satisfactory results than KSE 300; it increased the strength of the stones more than KSE 300 and induced as well a more homogeneous strength profile.

The static modulus of elasticity (E_{stat})

The modulus of elasticity is actually considered more important for estimating the risk of over-strengthening and possible consequent damage (Snethlage and Wendler, 1995; Sasse and Snethlage, 1997). The modulus of elasticity of the treated surface zone should not considerably exceed that of the untreated sound core; otherwise, there is a risk of scaling as a result of over-strengthening (see Table 4.1). Sasse and Snethlage (1997) point out that a smooth slope of the E-modulus over the penetration depth is more important than a large increase in strength.

The depth profiles of the static modulus of elasticity (Figure 7.23) provide almost comparable results to those obtained from the corresponding strength profiles.

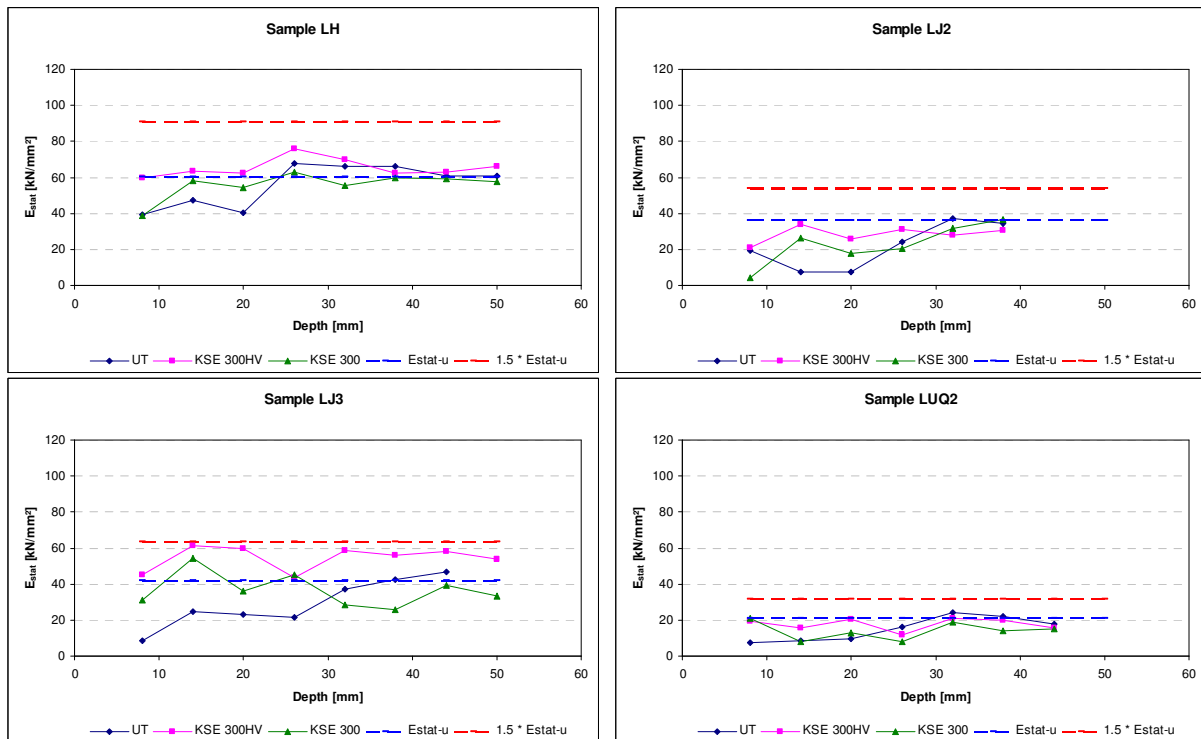


Figure 7.23: Static modulus of elasticity in depth profile of the treated and untreated samples.

Irrespective of few slight variations, the modulus of elasticity increased in the treated samples and a quite homogenous profile of elasticity modulus was almost produced, particularly in the samples treated with KSE 300HV. These results confirm again that no considerable over-strengthen took place in the samples treated by either consolidants (KSE 300 and KSE 300HV); the threshold value $1.5 E_{\text{stat}}$ (represented by the red line in the figure) was not exceeded.

The dynamic modulus of elasticity (E_{dyn})

The dynamic modulus of elasticity was measured on the prismatic specimens. The results are shown in Figure (7.24). The samples treated with KSE 300 exhibited a percentage increase in dynamic modulus by 23%, 61%, 26%, and 48% for the samples LH, LJ2, LJ3, and LUQ2 respectively. A larger increase in the dynamic modulus was induced by the consolidant KSE 300HV with 29%, 150%, 63%, and 168% for LH, LJ2, LJ3, and LUQ2 respectively.

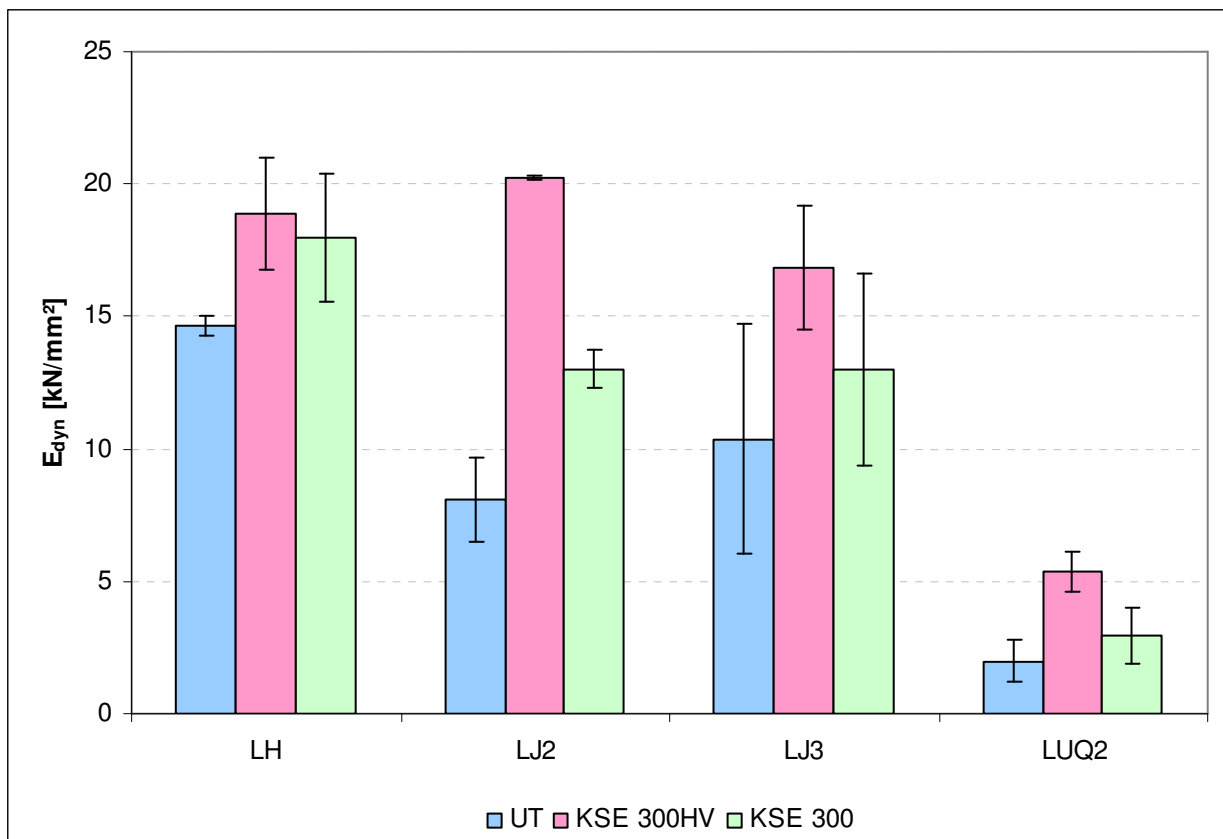


Figure 7.24: Dynamic modulus of elasticity before and after consolidation treatments.

The dynamic modulus of elasticity for all weathered and treated samples is markedly smaller than the corresponding static modulus. As explained earlier in Section (7.1.1.8), this finding disagrees with what is usually expected; microcracks in stone have greater influence on static

modulus than on dynamic one, and hence the static modulus of stone is generally assumed to be lower.

7.2.12 Ultrasonic velocity (V_p)

Ultrasonic velocity measurements were performed on different specimen forms of the studied samples before and after treatment. Ultrasonic velocity was determined in 5 cm cubes (along three orthogonal directions) and in 5x2x2 cm prismatic specimens that were treated by capillary rise until saturation and then by total immersion. The anisotropy of ultrasonic velocity was measured on the cubic specimens from the minimum and maximum velocities measured in the different directions. Ultrasonic measurements were carried out using a point-shaped ultrasonic transmitter vibrating at 46 kHz. On the prismatic specimen, however, another ultrasonic transmitter with a frequency of 250 kHz was also used.

The velocity of ultrasonic waves in depth profile was determined on drill core specimens (5 cm in diameter), treated by capillary rise for one hour, in two directions; parallel and perpendicular to bedding planes. Measurements were carried out with two different ultrasonic frequencies, 46 kHz and 350 kHz.

Ultrasonic velocity in cubic specimens (with 46 kHz)

Figure (7.25) shows the average velocity of ultrasonic longitudinal waves in the cubic specimens along three orthogonal directions before and after treatment with KSE 300 and KSE 300HV. An increase of ultrasonic velocity in the treated samples can be clearly seen. The samples treated with KSE 300 exhibited an increase of ultrasonic velocity by 6%, 9%, 11%, and 17% for LH, LJ2, LJ3, and LUQ2 respectively. The increase in ultrasonic velocity is greater for those samples treated with the consolidant KSE 300HV. The velocity here increased by 10%, 26%, 17%, and 22% for the samples LH, LJ2, LJ3, and LUQ2 respectively. The increase in ultrasonic velocity after consolidation treatment can be attributed to the filling of pores with consolidant and the enhancement of linkage between grains (Stück et al., 2008).

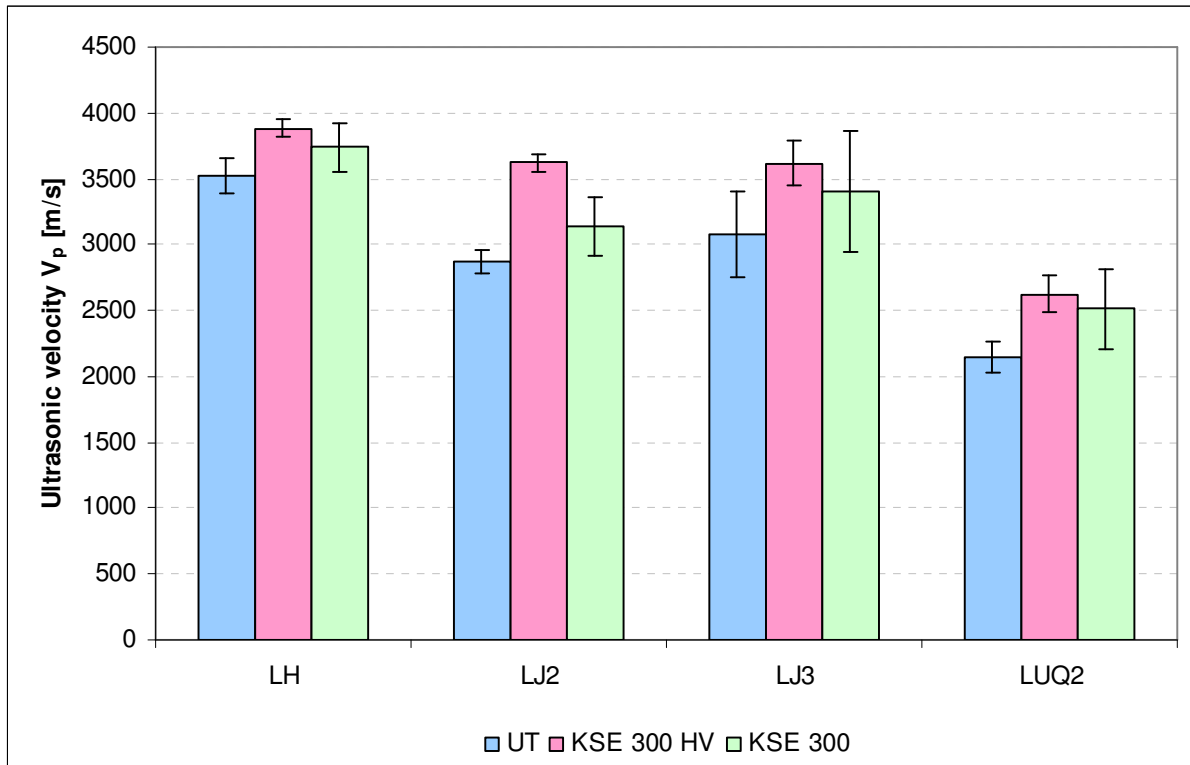


Figure 7.25: Average ultrasonic velocity of treated and untreated limestone samples measured in cubic specimens along three orthogonal directions (46 kHz ultrasonic frequency).

The samples treated with KSE 300HV exhibited a greater increase in ultrasonic velocity (360-756 m/s; 10-26%) than those treated by KSE 300 (216-364 m/s; 6-17%). This is attributed to the effect of coupling agent contained in KSE 300HV which acts to enhance the bonding with calcite grains.

The naturally weathered samples exhibit a considerable anisotropy in ultrasonic velocity, particularly LJ3 and LUQ2 with 29%, and 48% respectively. This anisotropy is attributed to the diagenetic and textural properties of the stones. The degree of anisotropy of all the samples decreased after consolidation (Table 7.23). This can be attributed to the deposition of consolidant in pore space, especially in between bedding planes along which selective weathering normally occurs. As a result, the difference between ultrasonic velocities measured in the directions parallel and perpendicular to bedding planes, and consequently the anisotropy, can be reduced.

Table 7.23: The calculated anisotropy in ultrasonic velocity before and after treatment.

<i>Sample</i>		<i>Anisotropy (A) [%]</i>
<i>LH</i>	<i>UT</i>	7
	<i>KSE 300 HV</i>	5
	<i>KSE 300</i>	4
<i>LJ2</i>	<i>UT</i>	10
	<i>KSE 300 HV</i>	6
	<i>KSE 300</i>	6
<i>LJ3</i>	<i>UT</i>	29
	<i>KSE 300 HV</i>	23
	<i>KSE 300</i>	23
<i>LUQ2</i>	<i>UT</i>	48
	<i>KSE 300 HV</i>	39
	<i>KSE 300</i>	40

Ultrasonic velocity in prismatic specimens (with 46 kHz and 250 kHz)

For the purpose of investigating the influence of used ultrasonic frequency on the accuracy of measurements, ultrasonic velocity was also measured in 2x2x5 cm prismatic specimens in the direction perpendicular to bedding with two different ultrasonic frequencies, namely 46 kHz and 250 kHz. The measured velocity with both frequencies in the treated and untreated samples, along with the percent increase in velocity after treatments, is given in Table (7.24). No significant difference between the velocities measured with both frequencies can be noticed. In fact, the velocities measured with 250 kHz are slightly higher than those measured with 46 kHz. However, the difference lies almost within the accuracy limits of the used ultrasonic instrument.

By comparing the results of velocity measurements on the prismatic specimens with those on the cubic ones, it can be seen that the measured velocities in the prismatic specimens are clearly lower, particularly for the samples LJ3 and LUQ2. This is actually attributed to the anisotropy of the samples and the fact that the velocity in the cubic specimens is the average velocity along three orthogonal directions whereas that in the prismatic specimens is only measured along the direction perpendicular to bedding.

Table 7.24: Ultrasonic pulse velocity in untreated and treated prismatic specimens measured using ultrasonic frequency of 46 kHz and 250 kHz along one direction (perpendicular to bedding planes).

<i>Sample</i>		$V_p - 46 \text{ kHz}$ [m/s]	% Increase [%]	$V_p - 250 \text{ kHz}$ [m/s]	% Increase [%]
<i>LH</i>	<i>UT</i>	3193 ± 80	-	3215 ± 67	-
	<i>KSE 300 HV</i>	3482 ± 40	9	3526 ± 47	10
	<i>KSE 300</i>	3422 ± 71	7	3416 ± 63	6
<i>LJ2</i>	<i>UT</i>	2815 ± 105	-	2964 ± 79	-
	<i>KSE 300 HV</i>	3267 ± 71	16	3458 ± 79	17
	<i>KSE 300</i>	3137 ± 74	11	3218 ± 30	9
<i>LJ3</i>	<i>UT</i>	2676 ± 115	-	2758 ± 138	-
	<i>KSE 300 HV</i>	3101 ± 94	16	3161 ± 95	15
	<i>KSE 300</i>	2897 ± 115	8	3035 ± 79	10
<i>LUQ2</i>	<i>UT</i>	1333 ± 110	-	1422 ± 86	-
	<i>KSE 300 HV</i>	1619 ± 40	21	1760 ± 56	24
	<i>KSE 300</i>	1553 ± 62	17	1670 ± 79	17

Ultrasonic velocity in depth profile (on drill cores with 46 kHz and 350 kHz)

Ultrasonic velocity in depth profile was measured on drill cores (5 cm in diameter) before and after treatment with KSE 300 and KSE 300HV. To inspect the influence of ultrasonic frequency in relation to specimen size on the accuracy of measurements, point-shaped ultrasonic transmitter vibrating at 46 kHz and 350 kHz were used. Owing to the pronounced anisotropy detected on the studied samples, measurements were performed in the directions parallel ($V_p //$) and perpendicular ($V_p \perp$) to bedding planes.

Measurement with 46 kHz

Figure (7.26) shows the velocity profiles of the limestone samples measured with ultrasonic frequency of 46 kHz before and after treatment.

The sample LH exhibited the least degree of weathering and showed a slight reduction in ultrasonic velocity by around 150-200 m/s in the first 1-1.5 cm depth. The velocity depth profiles of the weathered and treated samples are almost equivalent with only slightly higher velocity of the treated samples in the outermost surface layer. In general, the observed consolidation effect was small, but satisfactorily sufficient to produce a homogenous velocity profile.

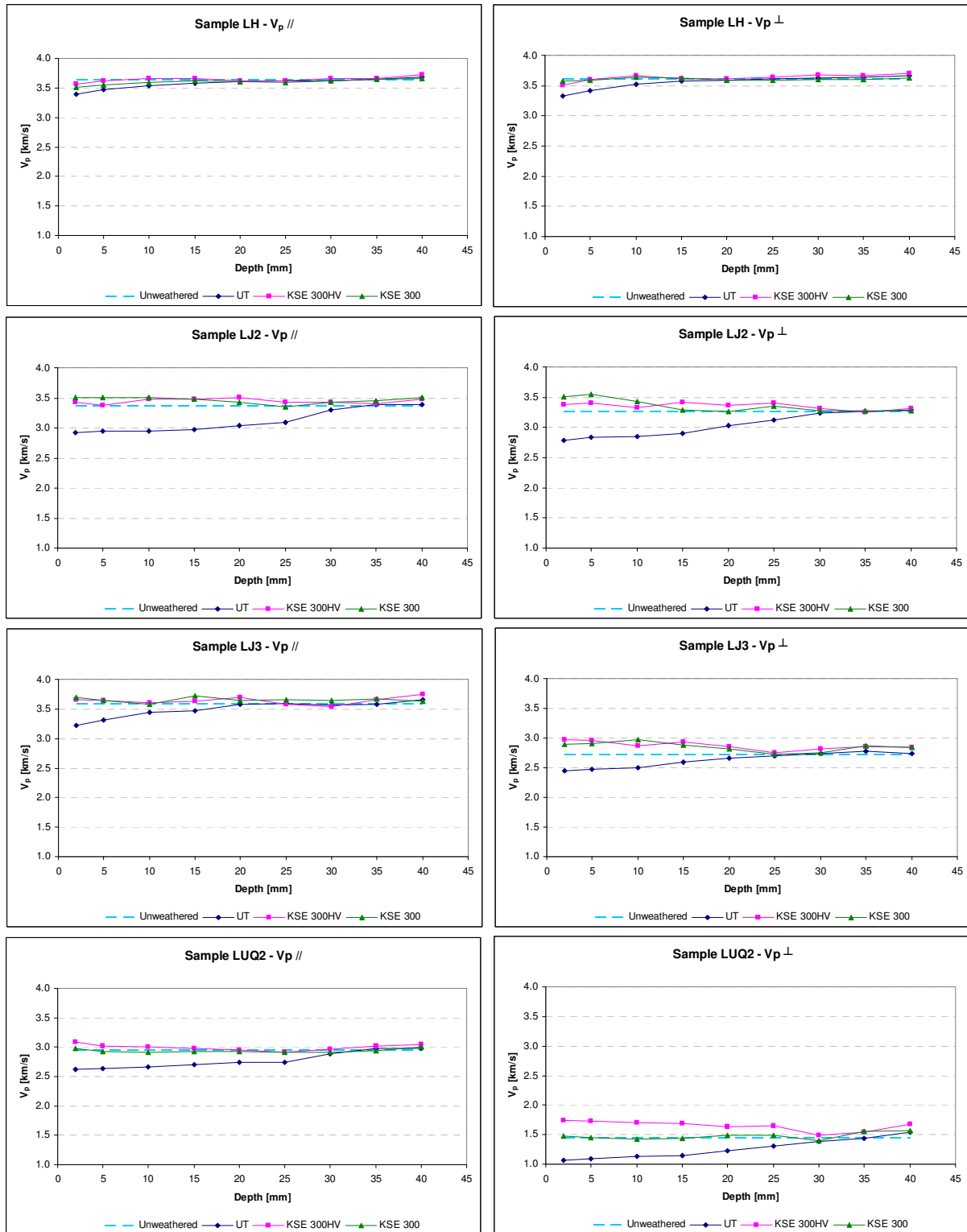


Figure 7.26: Ultrasonic pulse velocity in depth profile of the weathered and treated samples measured in two directions (parallel and perpendicular to beddings) with ultrasonic frequency of 46 kHz.

The velocity profile of the weathered sample LJ2 manifests a reduction of velocity up to 500 m/s in the first 3 centimeters. The resulting depth profiles of ultrasonic velocity after consolidation with KSE 300 and KSE 300HV fulfill clearly the requirements for successful

treatments (Table 4.1); both consolidants penetrated sufficiently into the weathered zone and produced a homogenous velocity profile almost comparable to that of the unweathered stone.

The velocity profiles of the sample LJ3 indicate an average reduction in ultrasonic velocity by around 250 m/s in the outer surface layer (~2 cm). The consolidation treatments seem to compensate for this reduction and to produce homogenous velocity profiles. This sample exhibits a noticeable anisotropy in ultrasonic velocity along and perpendicular to bedding planes.

The sample LUQ2 was subject to extensive weathering and exhibited a reduction in ultrasonic velocity up to 400 m/s to a depth of more than 3 cm. The sample is characterized by a noticeable anisotropy. Both consolidants penetrated sufficiently into the stone and restored the velocity to its value in the unweathered stone, producing a homogenous profile. The consolidant KSE 300HV induced a relatively higher increase in ultrasonic velocity, particularly in the direction perpendicular to bedding planes.

Measurement with 350 kHz

The velocity profiles of the weathered and treated samples measured using 350 kHz are shown in Figure (7.27).

For sample LH, the obtained velocity profiles are comparable to those obtained using the transmitter vibrating at 46 kHz. However, the reported velocity values with this frequency are slightly higher. The increase in velocity after treatment is small and the effect of consolidation is not that noticeable.

The velocity profiles of the sample LJ2 indicate again a weathering depth of 3 cm. Compared to the results obtained with 46 kHz, both consolidants seem to induce a slightly lower increase in ultrasonic velocity. Furthermore, the consolidant KSE 300 seems to penetrate up to a depth of around 1.5 cm only.

For the sample LJ3, the velocity profiles obtained with this frequency are almost similar to those obtained using 46 kHz. The stone is weathered to a depth of around 2.5 cm with an average loss of velocity of around 300 m/s in the weathered zone. Both consolidants,

particularly KSE 300HV, penetrated the weathered stone sufficiently and enhanced its ultrasonic velocity.

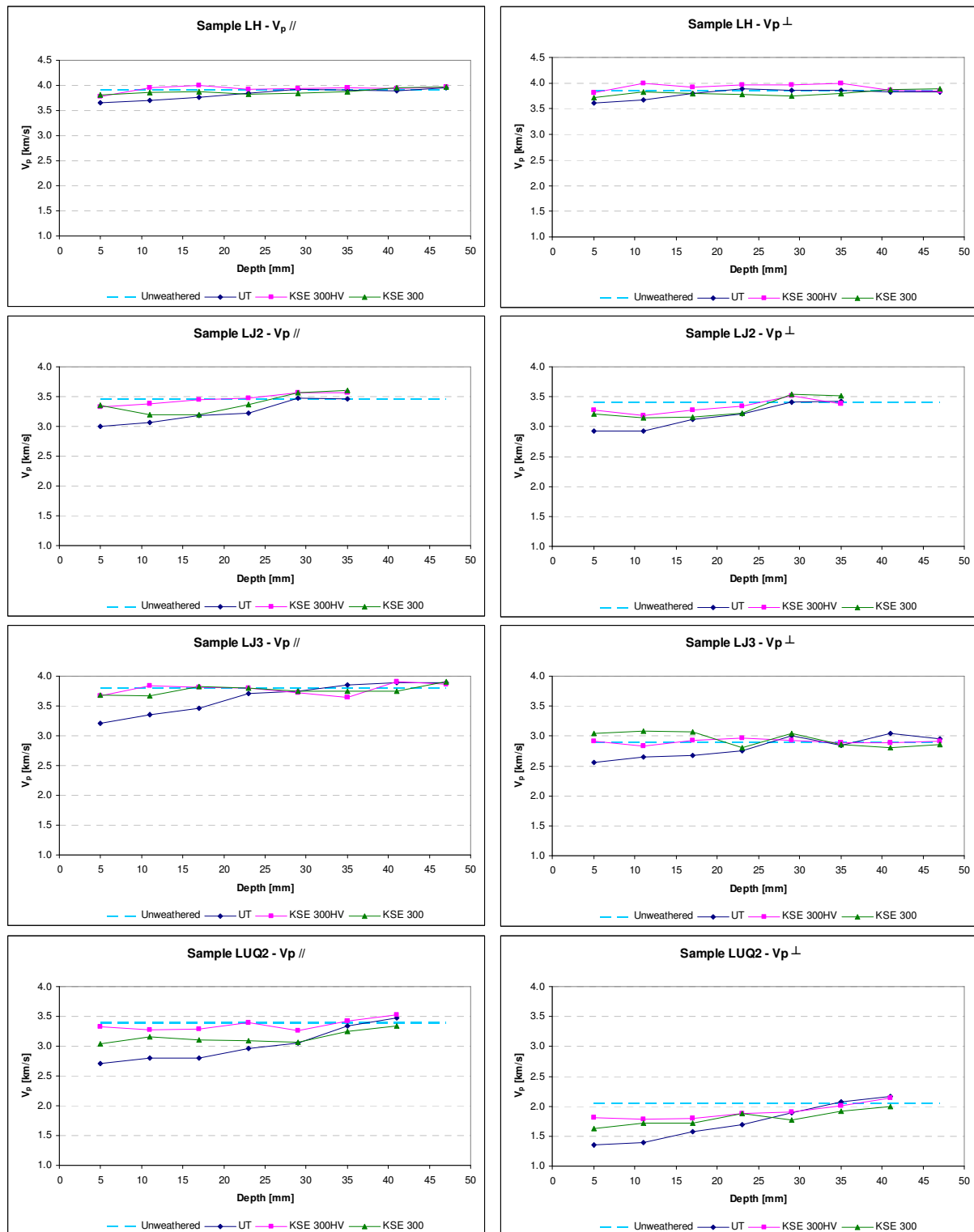


Figure 7.27: Ultrasonic pulse velocity in depth profile of the weathered and treated samples measured in two directions (parallel and perpendicular to beddings) with ultrasonic frequency of 350 kHz.

The sample LUQ2 showed comparable results for both ultrasonic frequencies. However, the ultrasonic velocities measured with 350 kHz are slightly higher than those obtained by 46 kHz. The resulting ultrasonic profiles indicate a weathering depth of 3.5 cm and a slightly deeper penetration and a better consolidation behavior of KSE 300HV compared to KSE 300.

The results obtained with both ultrasonic frequencies are comparable. The observed variations in the measured velocities with both ultrasonic frequencies are not significant to speak of a clear influence of the used ultrasonic frequency in relation to specimen size on the accuracy of measurements. However, it has to be emphasized that this does not generally mean that the used ultrasonic frequency has no influence on the accuracy of measured velocities. More specific studies with homogenous samples are needed in order to thoroughly explore the exact influence of the used ultrasonic frequency, in light of the dimensions of investigated specimens, on the accuracy of velocity measurements.

In summary, the velocity profiles of the untreated weathered samples allow the determination of the thickness of weathering zone. The depth of weathering is estimated to be around 1.5 cm, 3 cm, 2.5 cm, and 3-3.5 cm for LH, LJ2, LJ3, and LUQ2 respectively. The criterion for successful treatment requires the increase of ultrasonic velocity up to the level of unweathered stone and the establishment of a homogenous profile from the outer surface of the stone to its interior (Table 4.1). Irrespective of some small variations, this requirement was generally fulfilled for the treatments with both consolidation products. Both consolidants penetrated into the weathered zone and reached the sound core of the stone, increasing thereby the velocity of ultrasonic waves in the weathered part. The resulting velocity profiles, particularly for KSE 300HV, are almost homogenous and the consolidation treatments can be considered successful.

8 Summary and conclusions

The aim of this study was to investigate natural and consolidated archeological stone samples from north and northeast Jordan with non-destructive ultrasonic velocity validated by physico-mechanical tests. The work entailed the study of the deterioration of the stone samples upon accelerated weathering and the assessment of their durability as well as the evaluation of the effectiveness of consolidation treatments on naturally weathered samples.

The selected stone samples were characterized by physico-mechanical methods and their microstructure was studied. Consequently, the possible geological formations of the selected stone samples were determined. If compared with petrographic characteristics of stone in local quarries, this information could help to determine the most probable quarry sources of the stones. This knowledge is extremely important for the assessment of the weathering condition of the samples in reference to the corresponding fresh stone as well as for selection of restoration materials.

The study of the changes of the properties of the sound stone samples upon artificial weathering (by salt crystallization test for limestone and basalt, and thermal treatment for marble) helps to understand their weathering behavior and to evaluate their resistance to deterioration. The studied limestone samples exhibited weathering in form of granular disintegration and pitting or cracking. The damage induced in the stones after salt crystallization test was evaluated by two indicators; total dry weight loss of stone material (DWL) and change in fracture density (ΔF_D). On the one hand, the petrophysical properties of the stones seemed to be very important for determining their susceptibility to salt damage. The proportion of micropores and the water absorption capacity (or free porosity) of the stones were the most important parameters that determined the induced damage in terms of DWL. On the other hand, the mechanical and elastic properties were not directly correlated with stone damage indicated by loss of stone material. These properties were instead more related to the fracturing behavior of the stones. The degree of fracturing could be estimated by non-destructive ultrasonic velocity measurements in dry and water-saturated conditions. This is particularly important for stones with porosity in forms of crack such as marble.

Based on these results, durability estimators were developed to assess the susceptibility of stone to weathering. These estimators can be used for the selection of suitable restoration

materials as well as for the testing of stone quality and the selection of building materials in the field of architecture and civil engineering. The size of the samples used to develop these estimators was, however, small. Further research with a larger number of samples and various stone varieties would be required for confirming the results.

The effectiveness of two ethylsilicate-based consolidation products was evaluated on naturally weathered limestone samples by studying the changes in stone properties as compared to the untreated unweathered stone. Furthermore, the effect of contained coupling agents in the consolidation products for particular applications on limestone was examined. The consolidation treatments seemed to perform properly on the stones, especially for the product with coupling agent. The results from ultrasonic velocity measurements agreed satisfactorily with those from traditional physico-mechanical tests and this technique proved to be effective for evaluating the success of consolidation treatments.

This work serves as a base for future studies on the assessment of weathering condition of archaeological Jordanian stone. Classifications schemes for assessing the weathering condition of stone can be established by correlating the ultrasonic velocity values with the values of other suitable stone properties for a particular stone in fresh and various weathering conditions. Non-destructive ultrasonic velocity measurements could thus be sufficient to provide reliable evaluation of the weathering state of stone and to establish a priority list for conservation interventions.

As mentioned in this study, little work has been so far done to characterize archeological stone in Jordan. It is, therefore, recommended to conduct more research for the characterization of Jordanian archaeological stones and their historical quarries. This is a primary knowledge for any further investigation of the stones.

The present study provides additional evidence with respect to the validity of the use of non-destructive ultrasonic technique for the investigation of stone. The velocity of ultrasonic waves was able to detect the changes in stone structures induced by weathering and consolidation treatments on laboratory samples. The application of this technique for the investigation of Jordanian stone in situ would be very interesting.

In this study, the used ultrasonic frequency, in relation to specimen's size, seems to have no significant implications on the accuracy of measurements. However, this point was roughly addressed here; a thorough investigation of this issue is strongly recommended.

9 References

- Abu-Jaber, N., Al-Saad, Z., Al-Qudah, M., Smadi, N., and Al-Zoubi, A., *QuarryScapes report: Landscape, provenance and conservation of stone sources from selected archaeological sites in Jordan*, ed. N. Abu-Jaber and Z. Al-Saad, Quarry Scapes Project, (2007).
- Abu-Jaber, N., Al-Saad, Z., and Smadi, N., 'The quarriescapes of Gerasa (Jarash), Jordan', in *QuarryScapes: ancient stone quarry landscapes in the Eastern Mediterranean*, ed. N. Abu-Jaber, N., E.G. Bloxam, P. Degryse, and T. Heldal, Geological Survey of Norway, Special Publication **12** (2009) 67–75.
- Ahmad, A., Pamplona, M., and Simon, S., 'Ultrasonic testing for the investigation and characterization of stone – a non-destructive and transportable tool', *Reviews in Conservation* **10** (2009) 43-53.
- Al-Naddaf, M., *Weathering mechanisms: Technical investigation in relation to the conservation of the sandstone monuments in Petra, Jordan*, PhD dissertation, Freie Universität Berlin, Mensch & Buch Verlag, Berlin (2002).
- Al-Naddaf, M., 'The effect of salts on thermal and hydric dilatation of porous building stone', *Archaeometry* **51**(3) (2009) 495–505.
- Amoroso, G.G., and Fassina, V., *Stone decay and conservation - atmospheric pollution, cleaning, consolidation and protection*, Elsevier, Amsterdam and New York (1983).
- Angeli, A., Bigas, J.P., Benavente, D., Menéndez, B., Hébert, R., and David, C., 'Salt crystallization in pores: quantification and estimation of damage', *Environmental Geology* **52**(2) (2007) 187-195.
- Angeli, A., Benavente, D., Bigas, J.P., Menéndez, B., Hébert, R., and David, C., 'Modification of the porous network by salt crystallization in experimentally weathered sedimentary stones', *Materials and Structures* **41** (2008) 1091-1108.
- Antonova, E., Sizov, B., Simon, S., 'Evaluation of laboratory tests of consolidation products on limestone', in *Eurocare-Euromarble: Proceedings of the 8th Workshop, Rom, 15–18 October 1997*, ed. M. Monte, National Research Council CNR, ROM (1997) 49–53.
- ASTM E2167–01, *Standard guide for selection and use of stone consolidants*, ASTM International, West Conshohocken, Pennsylvania (2001).
- Bashayrih, K., *Determination of Provenance of marble and Caliche used in acinent Gadara (Um-Qais), N. Jordan*, Master thesis, Yarmouk University, Irbid, (2003).
- Benavente, D., García del Cura, M.A., Fort, R., and Ordóñez, S., 'Thermodynamic modelling of changes induced by salt pressure crystallization in porous media of stone', *Journal of Crystal Growth* **204** (1999) 168-178.

- Benavente, D., García del Cura, M.A., Bernabéu, A., and Ordóñez, S., 'Quantification of salt weathering in porous stones using an experimental continuous partial immersion method' *Engineering Geology* **59** (2001) 313-325.
- Benavente, D., García del Cura, M.A., Fort, R., and Ordóñez, S., 'Durability estimation of porous building stones from pore structure and strength', *Engineering Geology* **74** (2004) 113-127.
- Bender, F., *Geology of Jordan*, Gebrüder Borntraeger, Berlin-Stuttgart (1974).
- Blitz, J. and Simpson, G., *Ultrasonic methods of non-destructive testing*, Chapman & Hall, London (1996).
- Bouineau, A., 'L'interet des essais non destructifs utilises pour l'etude de la restauration des monuments et des sculptures', in *International Symposium on Deterioration and Protection of Stone Monuments, Paris, 5-9 June 1978*, UNESCO-RILEM, Paris (1978) Vol. III Session 7.15.
- Bourgès, A., *Holistic correlation of physical and mechanical properties of selected natural stones for assessing durability and weathering in the natural environment*, PhD dissertation, Ludwig-Maximilians-Universität München (2006).
- Bourgès, A., Hanna, S., and Simon, S., 'Stone susceptibility to frost damage: comparison of three English magnesian limestones', in *Salt Weathering on Buildings and Stone Sculptures-Proceedings from the International Conference, Copenhagen, 22-24 October 2008*, Technical University of Denmark, Copenhagen (2008a) 125-136.
- Bourgès, A., Fehr, K.T., Simon, S., and Snethlage, R., 'The role of pore shapes in elasticity properties of rocks', in *Proceedings of the 11th International Congress on Deterioration and Conservation of Stone, Torun', 15-20 September 2008*, ed. J.W. Łukaszewicz and P. Niemcewicz, Nicolaus Copernicus University Press, Torun' (2008b) Vol. I 573-580.
- Borrelli, E., 'Porosity', ARC Laboratory Handbook, volume 2/99, ICCROM, Rome (1999). [http://www.iccrom.org/pdf/ICCROM_14_ARCLabHandbook00_en.pdf] (accessed 25 July 2011).
- Building Research Establishment, 'The selection of natural building stone', *BRE Digest 269*, Building Research Establishment, HMSO, Garston, Watford (1989).
- Buj, O., and Gisbert, J., 'Influence of pore morphology on the durability of sedimentary building stones from Aragon (Spain) subjected to standard salt decay tests', *Environmental Earth Sciences* **61** (2010) 1327-1336.
- Capedri, S., Venturelli, G., and Photiades, A., 'Accessory minerals and $\delta^{18}\text{O}$ and $\delta^{13}\text{C}$ of marbles from the Mediterranean area', *Journal of Cultural Heritage* **5** (2004) 27-47.
- Capedri, S., and Venturelli, G., 'Accessory minerals as tracers in the provenancing of archaeological marbles, used in combination with isotopic and petrographic data', *Archaeometry* **46**(4) (2004) 517-536.

- Cardell, C., Rivas, T., Mosquera, M.J., Birginie, J.M., Moropoulou, A., Prieto, B., Silva, B., and Van Grieken, R., 'Patterns of damage in igneous and sedimentary rocks under conditions simulating sea-salt weathering', *Earth Surface Processes and Landforms* **28** (2003) 1-14.
- Cardu, M., Gomez, M., and Mancini, R., 'Nondestructive testing for soundness of stone architectural pieces', in *Proceedings of the European Symposium: Science, Technology and European Cultural Heritage, Bologna, Italy, 13-16 June 1989*, ed. N.S. Baer, C. Sabbioni and A.I. Sors, Butterworth-Heinemann Ltd, Brussels-Luxembourg (1991) 583-586.
- Charola, A.E., 'Salts in the deterioration of porous materials: an overview', *Journal of the American Institute for Conservation (JAIC)* **39** (2000) 327-343.
- Charola, A.E., 'Stone deterioration in historic buildings and monuments', in *Proceedings of the 10th International Congress on Deterioration and Conservation of Stone, Stockholm, 27 June - 2 July 2004*, ed. D. Kwiatkowski and R. Löfvendahl, ICOMOS, Stockholm (2004) Vol. I 3-14.
- Chatterji, S., and Christensen, P., 'A mechanism of breakdown of limestone nodules in a freeze/thaw environment', *Cement and Concrete Research* **9** (1979) 741-746.
- Chatterji, S., and Jensen, A.D., 'Efflorescence and breakdown of building materials', *Nordic Concrete Research* **8** (1989) 56-61.
- Choquette, P.W., and Pray, L.C., 'Geologic nomenclature and classification of porosity in sedimentary carbonates', *American Association of Petroleum Geologist Bulletin* **54** (1970) 207-250.
- Chiesura, G., Mecchi, A.M., and Rota Rossi Doria, P., 'La technique d'auscultation microsismique pour le diagnostic et l'evaluation des traitements sur materiaux pierreux', in *Methods of Evaluating Products for the Conservation of Porous Building Materials in Monuments, International Colloquium, Rome, 19-21 June 1995: Preprints*, ICCROM, Rome (1995) 131-145.
- Christaras, B., 'Particularities in studying the physical and mechanical properties of stones in monuments. Examples from the Mediterranean Basin', in *Proceedings of the 8th International Congress on Deterioration and Conservation of Stone, Berlin, 30 September - 4 October 1996*, ed. J. Riederer, Berlin (1996) Vol. II 819-829.
- Christaras, B., 'P-wave velocity and quality of building materials', in *Proceedings of the IAEG International Symposium on Industrial Minerals and Building Stones, Istanbul, 15-18 September 2003*, ed. E. Yuzer, H. Ergin and A. Tugrul, Istanbul (2003) 295-300.
- Clifton, J.R., *Stone consolidating materials: A status report*, National Bureau of Standards Technical Note 1118, U.S. Government Printing Office, Washington (1980). Electronic edition: <http://cool.conservation-us.org/byauth/clifton/stone/> (accessed 25 July 2011).
- Correns, C.W., and Steinborn, W., 'Experimente zur Messung und Erklärung der sogenannten Kristallisationskraft', *Zeitschrift für Kristallographie* 101 (1939) 117-33.

- Correns, C.W., 'Growth and dissolution of crystals under linear pressure', *Discussions of the Faraday Society* **5** (1949) 117-133.
- Cox, K.G., Bell, J.D., and Pankhurst, R.J., *The Interpretation of Igneous Rocks*. George Allen and Unwin, London (1979).
- Dearman, W.R., 'Weathering classification in the characterisation of rock for engineering purposes in British practice', *Engineering Geology* **9** (1974) 33-42.
- Delgado Rodrigues, J., 'Laboratory study of thermally-fissured rocks', in *Proceedings of the 4th International Congress on Deterioration and Conservation of Stone Objects, Louisville, 7-9 September 1982*, ed. K.L. Gauri and J.A. Gwinn, Kentucky (1982) 281-294.
- Delgado Rodrigues, J., 'Consolidation of decayed stones: A delicate problem with few practical solutions', in *Proceedings of the 3rd International Seminar on Historical Construction, University of Minho, Guimarães, Portugal, 7-9 November 2001*, ed. P.B. Lourenço and P. Roca, Guimarães (2001) 3-14. Internet address: http://www.civil.uminho.pt/masonry/Publications/Historical%20constructions/page%203-14_DDelgado.pdf (accessed 25 July 2011).
- Deutsch, V., 'History of NDT-instrumentation', in *Proceedings of 15th World Conference on Nondestructive Testing, Rome, 15-21 October, 2000*, <http://www.ndt.net/article/wcndt00/papers/idn378/idn378.htm> (accessed 25 July 2011).
- DGZfP, Deutsche Gesellschaft für Zerstörungsfreie Prüfung, Merkblatt B4 für Ultraschallverfahren zur zerstörungsfreien Prüfung mineralischer Baustoffe und Bauteile; DGZfP, Unterausschuss Ultraschallprüfungen, Berlin, (1999).
- DIN EN 12370, *Bestimmung des Widerstandes gegen Kristallisation von Salzen*, DIN Deutsches Institut für Normung, Berlin (1999).
- DIN EN 1925, *Bestimmung des Wasseraufnahmekoeffizienten infolge Kapillarwirkung*, DIN Deutsches Institut für Normung, Berlin (1999).
- DIN EN ISO 12571, *Hygroskopische Sorptionskurven – Bestimmungsverfahren*, DIN Deutsches Institut für Normung, Berlin (1996).
- DIN EN ISO 12572, *Bestimmung der Wasserdampfdurchlässigkeit*, DIN Deutsches Institut für Normung, Berlin (1997).
- Doehne, E., 'In situ dynamics of sodium sulfate hydration and dehydration in stone pores: observations at high magnification using the environmental scanning electron microscope', in *Proceedings of the 3rd International Symposium on the Conservation of monuments in the Mediterranean Basin, Venice, 22-25 June 1994*, ed. V. Fassina, H. Ott and F.Zezza, Soprintendenza ai Beni Artistici e Storici di Venezia, Venice (1994) 143-150.

- Doehne, E., 'Salt weathering: a selective review', in *Natural stone, weathering phenomena, conservation strategies and case studies*, ed. S. Siegesmund, T. Weiss, and A. Vollbrecht, Geological Society, London, special publication **205** (2002) 51-64.
- Doehne, E., and Price, C.A., *Stone conservation: An overview of current research*, 2nd ed., J. Paul Getty Trust, The Getty Conservation Institute, Los Angeles, California (2010).
- Dunham, R.J., 'Classification of carbonate rocks according to depositional texture', in *Classification of Carbonate Rocks-A Symposium: American Association of Petroleum Geologists Memoir 1*, ed. W.E. Ham (1962) 108-121.
- Durrast, H., Siegesmund, S., and Prasad, M., 'Die Schadenanalyse von Naturwerksteinen mittels Ultraschalldiagnostik: Möglichkeiten und Grenzen', *Zeitschrift der Deutschen Geologischen Gesellschaft* **150**(2) (1999) 359–374.
- Duttlinger, W., and Knöfel, D., 'Salzkristallisation und Salzschaadenmechanismen' in *Jahresberichte Steinerfall-Steinkonservierung, Vol. 3, 1991*, ed. R. Sneathlage, Ernst & Sohn, Berlin (1993) 197-213.
- El-Akhal, H., 'Contribution to the petrography, geochemistry, and tectonic setting of the basalt flows of the Umm-Qais plateau, north Jordan', *Geological Bulletin of Turkey* **47**(1) (2004) 1-12.
- Erfurt, W., and Krompholz R., 'Anwendung der Dehnwellenmessung für Baustoffuntersuchungen', *Beiträge zur Baustoffforschung, Wissenschaftliche Zeitschrift* **4/5** (1996) 95-101.
- Esbert, R.M., Valdeon, L., Ordaz, J., Alonso, F.J., and Grossi, C.M., 'Ultrasonic velocity and humidity in monumental stones', in *Proceedings of the European Symposium: Science, Technology and European Cultural Heritage, Bologna, Italy, 13–16 June 1989*, ed. N.S. Baer, C. Sabbioni and A.I. Sors, Butterworth-Heinemann Ltd, Brussels-Luxembourg (1991) 597–600.
- Espinosa, R.M., Franke, K., and Deckelmann, G., 'Model for the mechanical stress due to the salt crystallization in porous materials', *Construction and Building Materials* **22** (2008) 1350-1367.
- Ettl, H., and Sobott, R., 'Ultraschallmessungen an in-situ konservierten Marmorreliefs des Siegestors in Munchen', *Zeitschrift für Kunsttechnologie und Konservierung* **13**(1) (1999) 92–102.
- Everett, D.H., 'The thermodynamics of frost damage to porous solids', *Transactions of the Faraday Society* **57**(465-9) (1961) 1541-1551.
- Făcăoaru, I., 'On the use of non-destructive methods in the diagnosis and assessment of physico-mechanical residual properties of stone masonry', in *Structural Conservation of Stone Masonry, International Technical Conference, Athens, 31 October – 3 November 1989*, ICCROM, Rome (1990) 45–52.

- Făcăoaru, I., and Lugnani, C., 'Contributions to the diagnosis of stone and concrete historical structures using non-destructive techniques', in *Conservation of Stone and Other Materials, Proceedings of the International RILEM/UNESCO Congress, Paris, 29 June – 1 July 1993*, ed. M.J. Thiel, E. & F.N. Spon, London (1993) Vol. I 238–251.
- Fitzner, B., Snethlage, R., 'Einfluß der Porenradienverteilung auf das Verwitterungsverhalten ausgewählter Sandsteine', *Bautenschutz und Bausanierung* 5(3) (1982) 97-103.
- Fitzner, B., 'Porosity properties of naturally or artificially weathered sandstones', in *Proceedings of the 6th International Congress on Deterioration and Conservation of Stone, Toruń, 12-14 September 1988*, ed. J. Ciabach, Nicholas Copernicus University Press Department, Toruń (1988) 236–245.
- Fitzner, B., and Kownatzki, R., 'Bauwerkskartierung – Schadenaufnahme an Naturwerksteinen', *Der Freiberufliche Restaurator* 4 (1990) 25-40.
- Fitzner, B., and Kownatzki, R., 'Klassifizierung der Verwitterungsformen und Kartierung von Natursteinbauwerken', in *Jahresberichte Steinzerfall-Steinkonservierung, Vol. 1, 1989*, ed. R. Snethlage, Ernst & Sohn, Berlin (1991) 1-13.
- Fitzner, B., and Heinrichs, K., 'Verwitterungszustand und Materialeigenschaften der Kalksteine des Naumburger Doms' in *Jahresberichte Steinzerfall-Steinkonservierung, Vol. 2, 1990*, ed. R. Snethlage, Ernst & Sohn, Berlin (1992) 23-38.
- Fitzner, B., Heinrichs, K., and Kownatzki, R., 'Classification and mapping of weathering forms', in *Proceedings of the 7th International Congress on Deterioration and Conservation of Stone, Lisbon, 15–18 June 1992*, ed. J.D. Rodrigues, F. Henriques, F.J. Jermias, and F. Telmo, Laboratorio Nacional De Engenharia Civil, Lisbon (1992) Vol. II 957–968.
- Fitzner, B., and Basten, D., 'Gesteinsporosität – Klassifizierung, meßtechnische Erfassung und Bewertung ihrer Verwitterungsrelevanz', in *Jahresberichte Steinzerfall-Steinkonservierung, Vol. 4, 1992*, ed. R. Snethlage, Verlag Ernst & Sohn, Berlin (1994) 19-32.
- Fitzner, B., and Heinrichs, K., 'Damage diagnosis at monuments carved from bedrocks in Petra, Jordan', in *Proceedings of the 3rd International Symposium on the Conservation of Monuments in the Mediterranean Basin, Venice, 22–25 June 1994*, ed. V. Fassina, H. Ott and F. Zezza, Soprintendenza ai Beni Artistici e Storici di Venezia, Venice (1994) 663-671.
- Fitzner, B., Heinrichs, K., and Kownatzki, R., 'Weathering forms – classification and mapping (Verwitterungsformen – Klassifizierung und Kartierung)', in *Denkmalpflege und Naturwissenschaft, Natursteinkonservierung I*, ed. R. Snethlage, Verlag Ernst & Sohn, Berlin (1995) 41-88.
- Fitzner, B., 'Damage diagnosis on stone monuments - in situ investigation and laboratory studies' in *Proceedings of the International Symposium of the Conservation of the Bangudae Petroglyph, Ulsan City-Korea, 15 Juli.2002*, Stone Conservation Laboratory, Seoul National University, Seoul, Korea (2002) 29-71.

- Fitzner, B., and Heinrichs, K., 'Damage diagnosis on stone monuments - weathering forms, damage categories and damage indices', in: *Understanding and managing stone decay, Proceeding of the International Conference Stone weathering and atmospheric pollution network (SWAPNET), Prague, 7-11 May 2001*, ed. R. Prikryl and H.A. Viles, Charles University, The Karolinum Press, Pargue (2002) 11-56.
- Fitzner, B., and Heinrichs, K., 'Kartierung und Bewertung von Verwitterungsschäden an Natursteinbauwerken [Mapping and evaluation of weathering damage on stone monuments]', *Zeitschrift der Deutschen Gesellschaft für Geowissenschaften* **156**(1) (2005) 7-24.
- Flatt, R.J., 'Salt damage in porous materials: how high supersaturations are generated', *Journal of Crystal Growth* **242** (2002) 435-454.
- Folk, R.L., 'Practical petrographic classification of limestones', *American Association of Petroleum Geologists Bulletin* **43** (1959) 1-38.
- Folk, R.L., 'Spectral subdivision of limestone types', in *Classification of Carbonate Rocks-A Symposium: American Association of Petroleum Geologists Memoir 1*, ed. W.E. Ham (1962) 62-84.
- Gauri, K.L., and Bandyopadhyay, J.K., *Carbonate stone: chemical behaviour, durability and conservation*, John Wiley & Sons, New York (1999).
- Glaubitt, A., *Optimiertes Vorhersagemodell zur Ermittlung der dynamischen elastischen Konstanten von Beton mittels gesicherter Ultraschallmesstechnik*, PhD dissertation, Technische Universität Dortmund, Shaker Verlag, Aachen (2008).
- Goins, E.S., Wheeler, G.S., and Wypyski, M.T., 'Alkoxysilane film formation in quartz and calcite crystal surfaces', in *Proceedings of the 8th International Congress on Deterioration and Conservation of Stone, Berlin, 30 September – 4 October 1996*, ed. J. Riederer, Berlin (1996) Vol. III 1255-1264.
- Goudie, A., and Viles, H., 'Salt weathering hazards', J. Wiley & Sons, Chichester, (1997).
- Goudie, A., 'The salt weathering hazards in deserts', in *Geomorphological Hazards in High Mountain Areas*, ed. J. Kalvoda and C.L. Rosenfeld, Kluwer Academic Publishers, Netherlands (1998) 107-120.
- Gregg, S.J., and Sing, K.S.W., *Adsorption, surface area and porosity*, 2nd ed., Academic Press, London (1982).
- Grissom, C.A., and Weiss, N.R., 'Alkoxysilanes in the conservation of art and architecture: 1861-1981', *Art and Archeology Technical Abstract* **18** (1981) 149-200.
- Guéguen, Y., and Palciauskas, V., *Introduction to the physics of rocks*, Princeton University Press, Princeton, New Jersey (1994).

- Haake, S., Simon, S., and Favaro, M., 'The Bologna Cocktail – Evaluation of consolidation treatments in France and Italy after 20 years of natural aging', in *Proceedings of the 10th International Congress on Deterioration and Conservation of Stone, Stockholm, 27 June – 2 July 2004*, ed. D. Kwiatkowski and R. Löfvendahl, ICOMOS, Stockholm (2004) Vol.I 423-430.
- Heinrichs, K., and Fitzner, B., 'Deterioration of rock monuments in Petra/Jordan', in *Proceedings of the 9th International Congress on Deterioration and Conservation of Stone, Venice, 19–24 June 2000*, ed. V. Fassina, Elsevier, Amsterdam (2000) Vol. II 53–61.
- Heinrichs, K., 'Diagnosis of weathering damage on rock-cut monuments in Petra, Jordan', *Environmental Geology* **56**(3-4) (2008) 643-675.
- Herm, CH., Pfefferkorn, S., and Snethlage, R., 'Historische Verfahren und Handelsmarken in der Steinkonservierung 1845 bis 1940', in *Denkmalpflege und Naturwissenschaft, Natursteinkonservierung II*, ed. R. Snethlage, Fraunhofer IRB Verlag, Stuttgart (1998) 9-26.
- Hirschwald J., *Die Prüfung der natürlichen Bausteine auf ihre Wetterbeständigkeit*, Verlag von Wilhelm Ernst and Sohn, Berlin (1908).
- Hirschwald, J., *Handbuch der bautechnischen Gesteinsprüfung*, Verlag von Gebrüder Borntraeger, Berlin (1912).
- Honeyborne, D.B., and P.B. Harris, P.B., 'The structure of porous building stone and its relation to weathering behavior', in *The Structure and Properties of Porous Materials: Proceedings of the 10th Symposium of the Colston Research Society, Bristol, 24-25 March 1958*, ed. D.H. Everett and F.S. Stone, Butterworths Scientific Publications, London (1958) 343-365.
- Honsinger, D., and Sasse, H.R., 'Alteration of microstructure and moisture characteristics of stone materials due to impregnation', in *Durability of Building Materials and Components – Proceedings of the Fifth International Conference, Brighton, 7-9 November, 1990*, ed. J.M. Baker, P.J. Nixon, A.J. Majumdar and H. Davies, E. & F.N. Spon, London (1991) 213-224.
- Houck, J., and Scherer, G.W., 'Controlling stress from salt crystallization', in *Fracture and Failure of Natural Building Stones – Applications in the Restoration of Ancient Monuments*, ed. S.K. Kourkoulis, Springer, Dordrecht (2006) 299–312.
- Hudec, P.P., 'Rock weathering on the molecular level', in *Decay and Preservation of Stone, Engineering Geology Case Histories No. 11*, ed. E.M. Winkler, The Geological Society of America, Boulder (1978) 47-51.
- Hull, J.B., and John, V.B., *Non-destructive testing*, Macmillan Education, Basingstoke (1988).
- ICOMOS-ISCS, *Illustrated glossary on stone deterioration patterns*, English-French version, ICOMOS-ISCS: Monuments & Sites XV, Paris (2008).

- http://international.icomos.org/publications/monuments_and_sites/15/pdf/Monuments_and_Sites_15_ISCS_Glossary_Stone.pdf (accessed 25 July 2011).
- Jewett, J.W., and Serway, R.A., *Physics for scientists and engineers with modern physics*, 7th ed., Thomson Learning, (2008).
- Jonas, M., *Einsatzmöglichkeiten der Ultraschall-Frequenzanalyse für die zerstörungsfreie Prüfung von mineralischen Baustoffen und Bauteilen*, PhD Dissertation, Technische Universität Dortmund (1996).
- Karcz, L. and Dickman, S.R., 'Determination of fracture intensity', *Tectonophysics* **56** (1979) T1-T7.
- Karkare, M.V., and Fort, T., 'Water movement in "unsaturated" porous media due to pore size and surface tension induced capillary pressure gradients', *Langmuir* **9**(9) (1993) 2398-2403.
- Katzoff, G.Y., *Fracture of porous materials induced by crystallization of salt*, Master thesis, Massachusetts Institute of Technology (2006).
- Kessler, D.W., 'Physical and chemical tests of the commercial marbles of the United States', *Technologic Papers of the Bureau of Standards* **123**, Government Printing Office, Washington DC (1919).
- King, M.S., 'Static and dynamic elastic properties of rocks from the Canadian Shield', *International Journal of Rock Mechanics, Mining Sciences and Geomechanical Abstracts* **20** (1983) 237-241.
- Kleber, W., Bausch, H.J., Bohm, J., *Einführung in die Kristallographie*, 18th ed., Verlag Technik GmbH, Berlin (1998).
- Klopfer, H., *Das Kapillarverhalten poröser Baustoffe*, Technische Akademie Esslingen, Lehrgang Nr. 4280/79.88, (1979).
- Klopfer, H., *Bauphysikalische Aspekte-Anforderungen an Sanierungen*, Technische Akademie Esslingen, Lehrgang Nr. 4406/79.88, (1980).
- Klopfer, H., 'Feuchte', in *Lehrbuch der Bauphysik*, 6th ed., B.G. Teubner Verlag, Stuttgart (1985) 265-434.
- Klopfer, H., and Homman, M., 'Feuchte', in *Lehrbuch der Bauphysik*, 6th ed., Vieweg+Teubner Verlag, Wiesbaden (2008) 338-490.
- Knöfel, D., 'Ursachen der Natursteinverwitterung-Natursteinschäden an Bauwerken', *Bautenschutz und Bausanierung* **3**(2) (1980) 48-55, and **3**(3) (1980) 96-103.
- Kocher, M., *Quelldruckmessungen und thermische Druckmessungen an ausgewählten Sandsteinen*, PhD dissertation, Ludwig-Maximilians-Universität München (2004).

- Köhler, W., 'Untersuchungen zu Verwitterungsvorgängen an Carrara-Marmor in Potsdam Sanssouci', *Berichte zu Forschung und Praxis der Denkmalpflege in Deutschland, Steinschäden – Steinkonservierung* 2, Hannover (1991) 50–53.
- Köhler, W., 'Repeated ultrasonic measurements of selected identical marble sculptures', in *Eurocare Euromarble EU 496: Proceedings of the 9th Workshop, Munich, 8–10 October 1998*, ed. R. Snethlage, Bayerisches Landesamt für Denkmalpflege-Zentrallabor, Munich (1999) Vol. 17 127–132.
- Kracek, F.C., *International Critical Tables of Numerical Data, Physics, Chemistry and Technology*, McGraw Hill, New York (1928) Vol. III 351–385.
- Krompholz, R., Geotron-Elektronik, personal communication (March 2010).
- Künzel, H.M., 'Simultaneous heat and moisture transport in building components -One- and two-dimensional calculation using simple parameters', Fraunhofer IRB Verlag, Stuttgart (1995).
- Künzel, H., *Bauphysik und Denkmalpflege*, Fraunhofer IRB Verlag, Stuttgart (2007).
- Laurenzi Tabasso, M., and Simon, S., 'Testing methods and criteria for the selection/evaluation of products for the conservation of porous building materials', *Reviews in conservation* 7 (2006) 67–82.
- Leary, E., 'A preliminary assessment of capillarity tests as indicators of the durability of British limestones', in *The Conservation of Stone II, Preprints of the Contributions to the International Symposium, Bologna, 27–30 October 1981*, ed. R. Rossi-Manaresi, Centro per la Conservazione delle Sculture all'Aperto, Bologna (1981) 73–90.
- Leimer, H.P., 'Vorlesungsskripte zur Bauphysik: Feuchte und Feuchtetransport', 2004/05, http://www.bbs-international.com/webfm_send/496 (accessed 25 July 2011).
- Leroux, L., Vergès-Belmin, V., Costa, D., Delgado Rodrigues, J., Tiano, P., Snethlage, R., Singer, B., Massey, S., and De Witte, E., 'Measuring the penetration depth of consolidating products: Comparison of six methods', in *Proceedings of the 9th International Congress on Deterioration and Conservation of Stone, Venice, 19–24 June 2000*, ed. V. Fassina, Elsevier, Amsterdam (2000) Vol. II 361–369.
- Lewin, S., 'The susceptibility of calcareous stones to salt decay', in *Proceedings of the 1st International Symposium on the Conservation of Monuments in the Mediterranean Basin, Bari, 7–10 June 1989*, ed. F. Zezza, Grafo, Brescia (1990) 59–63.
- Lienhart, D.A., 'The mechanism of freeze-thaw deterioration of rock in the Great Lakes region', in *Rock for Erosion Control, ASTM STP 1177*, ed. C.H. McElroy and D.A. Lienhart, American Society for Testing and Materials, Philadelphia (1993) 77–87.
- Lorenz, H.G., and Ibach, H.W., 'Marmorkonservierung durch die Ibach-Voltränkung: Qualitätskontrolle und Optimierung durch mikroskopische und petrophysikalische Untersuchungen', *Zeitschrift der Deutschen Geologischen Gesellschaft* 150(2) (1999) 397–406.

- Łukaszewicz, J. 'The efficiency of the application of tetraethoxysilane in the conservation of stone monuments', in *Proceedings of the 10th International Congress on Deterioration and Conservation of Stone, Stockholm, 27 June – 2 July 2004*, ed. D. Kwiatkowski and R. Löfvendahl, ICOMOS, Stockholm (2004) Vol. I 479-486.
- Malaga-Starzec, K., Lindqvist, J.E., and Schouenborg, B., 'Experimental study on the variation in porosity of marble as a function of temperature' in *Natural stone, weathering phenomena, conservation strategies and case studies*, ed. S. Siegesmund, T. Weiss, and A. Vollbrecht, Geological Society, London, special publication **205** (2002) 81-88.
- Mamillan, M., 'Methode de classification des pierres calcaires', in *Supplément aux Annales de l'Institut Technique du Bâtiment et des Travaux Publics, Mai 1958* (1958) 270-132.
- Maravelaki-Kalaitzaki, P., Kallithrakas-Kontos, N., Korakaki, D., Agioutantis, Z., and Maurigiannakis, S., 'Evaluation of silicon-based strengthening agents on porous limestones', *Progress in Organic Coatings* **57** (2006) 140-148.
- Marini, P., Bellopede, R., and Manfredotti, L., 'About accuracy on ultrasonic measurements on stone', in *Proceedings of the 10th International Congress on Deterioration and Conservation of Stone, Stockholm, 27 June – 2 July 2004*, ed. D. Kwiatkowski and R. Lofvendahl, ICOMOS, Stockholm (2004) Vol. II 659-666.
- Matsuoka, N., 'Mechanisms of rock breakdown by frost action: an experimental approach', *Cold Regions Science and Technology* **17** (1990) 253-270.
- McDUR-Acoutherm European Project, 'Effects of the weathering on stone materials: Assessment of their mechanical durability – Draft of recommended methodologies for stone durability qualification (SDQ)', 2002, <http://www.icvbc.cnr.it/mcdur/deliver/SDQ.pdf> (accessed 25 July 2011).
- Meinhardt-Degen, J., *Geologisch-mineralogische und materialtechnische Untersuchungen zur Risikoabschätzung von Folgekonservierungen bei Sandsteinen am Beispiel von Regensburger Grünsandstein und Grünem Mainsandstein*, PhD dissertation, Ludwig-Maximilians-Universität München (2005).
- Meng, B., 'Charakterisierung der Porenstruktur im Hinblick auf die Interpretation von Feuchtetransportvorgängen . *Aachener Beiträge zur Bauforschung, Band 3*, Verlag der Augustinus Buchhandlung, Aachen (1993).
- Miglio, B.F., Richardson, D.M., Yates, T.S., and West, D., 'Assessment of the durability of porous limestones: Specification and interpretation of test data in UK practice', in *Dimension Stone Cladding: Design, Construction, Evaluation and Repair, ASTM STP 1394*, ed. K.R. Hoigard, American Society for Testing and Materials, West Conshohocken, PA (2000) 57-70.
- Mohammad, B.K., 'The salt durability of some Jordanian limestones as a function of their petrophysical properties', *The Electronic Journal of Geotechnical Engineering* **8** (2003). <http://www.ejge.com/2003/Ppr0312/Abs0312.htm> (accessed 25 July 2011).

- Montoto, M., Valdeon, L., Cotte, P., Calleja, L., Corral, N., Lopez, T., Sanchez, B., and Esbert, R.M., 'Non-destructive characterization of the state of deterioration of megaliths by ultrasonic tomography: a petrophysical interpretation', in *Proceedings of the 3rd International Symposium on the Conservation of Monuments in the Mediterranean Basin, Venice, 22–25 June 1994*, ed. V. Fassina, H. Ott and F. Zezza, Soprintendenza ai Beni Artistici e Storici di Venezia, Venice (1994) 3–9.
- Moreau, C., Simon, S., Haake, S., and Favaro, M., 'How to assess the efficiency of a stone consolidant – the example of the Bologna Cocktail', in *Proceedings of the 7th European Conference 'Sauveur' Safeguarded Cultural Heritage - Understanding and viability for the enlarged Europe, Prague, 31 May – 3 June 2006*, ed. M. Drdácý and M. Chapuis, Institute of Theoretical and Applied Mechanics ITAM, Prague (2007) Vol. I 197–205.
- Mortensen, H., 'Die ‚Salzsprengrung‘ und ihre Bedeutung für Regionalklimatische Gliederung der Wüsten', *Dr. A. Petermann's Mitteilungen aus Justus Perthes geographischer Anstalt* **79** (1933) 130-135.
- Myrin, M., and Malaga, K., 'A case study on the evaluation of consolidation treatments of Gotland sandstone by use of ultrasound pulse velocity measurements', in *Heritage, Weathering and Conservation*, ed. R. Fort, M. Alvarez de Buergo, M. Gomez-Heras and C. Vazquez-Calvo, Taylor & Francis Group, London (2006) Vol. II 749–761.
- Neisel, J.D., *Rasterelektronenmikroskopische Untersuchung der Gefügemerkmale von ungeschützten und imprägnierten Sandsteinen nach Verwitterungsbeanspruchung*, PhD dissertation, Rheinisch-Westfälische Technische Hochschule Aachen (1995).
- Nelson, S.A., 'Igneous rocks of the ocean basins', (2011), http://www.tulane.edu/~sanelson/eens212/ocean_basins.pdf (accessed 25 July 2011).
- Neugebauer, J., 'The diagenetic problem of chalk-the role of pressure solution and pore fluid', *Neues Jahrbuch für Geologie und Paläontologie Abhandlungen* **143** (1973) 223-245.
- Nicholson, D.T., and Nicholson, F.H., 'Physical deterioration of sedimentary rocks subjected to experimental freeze-thaw weathering', *Earth Surface Processes and Landforms* **25** (2000) 1295-1307.
- Nicholson, D.T., 'Pore properties as indicators of breakdown mechanisms in experimentally weathered limestones', *Earth Surface Processes and Landforms* **26** (2001) 819-838.
- Niesel, k., 'Durability of porous building stone: importance of judgement criteria related to its structure', in *The Conservation of Stone II, Preprints of the Contributions to the International Symposium, Bologna, 27–30 October 1981*, ed. R. Rossi-Manaresi, Centro per la Conservazione delle Sculture all'Aperto, Bologna (1981) 47-57.
- Norton, M., and Karczub, D., *Fundamentals of noise and vibration analysis for engineers*, 2nd ed., Cambridge University Press, Cambridge (2003).
- Ollier, C., 'Weathering', 2nd ed., Longman Inc., New York (1984).

- Ordóñez, S., Fort, R., García del Cura, M.A., 'Pore size distribution and the durability of a porous limestone', *Quarterly Journal of Engineering Geology* **30** (1997) 221-230.
- Pamplona, M., Kocher, M., Snethlage, R., and Barros, L.A., 'Drilling resistance: overview and outlook', *Zeitschrift der Deutschen Gesellschaft für Geowissenschaften* **158**(3) (2007) 665-676.
- Pamplona, M., Ahmad, A., Simon, S., Aßel, E., and Theissen, A., 'Ultrasonic pulse velocity – a tool for the condition assessment of outdoor marble sculptures', in *Proceedings of the 8th International Symposium on the Conservation of Monuments in the Mediterranean Basin, Patras, 31 May – 2 June 2010*, in press.
- Pamplona, M., Simon, S., Bauer, M., Ahmad, A., 'Marble conservation by total acrylic impregnation (IBACH Process) and induced physico-mechanical changes' in. *Jardin de Pierres, conservation de la pierre dans les parcs, jardins et cimetières, Paris, 22-24 June 2011*, 4es journées d'étude de la SFIIC, Inst. Nat. Du Patrimoine, Paris (2011) 267–276.
- Paradise, T.R., 'Sandstone weathering and aspect in Petra, Jordan', *Zeitschrift für Geomorphologie* **46**(1) (2002) 1-17.
- Pérez-Bernal, J.L., and Bello, M.A., 'Weathering effects on stone pore size distributions', in *Protection and Conservation of the Cultural Heritage of the Mediterranean Cities*, ed. Galán and Zezza, Swets & Zeitlinger, Lisse (2002) 203-208.
- Pidwirny, M., 'Weathering', *Fundamentals of Physical Geography, 2nd Edition*. (2006). <http://www.physicalgeography.net/fundamentals/10r.html> (accessed 25 July 2011).
- Powell, J., 'Stratigraphy and sedimentation of the phanerozoic rocks in central and south Jordan - Part B: Kurnub, Ajlun and Belqa Groups'. *Geological Bulletin* **11**, Geology Directorate, Natural Resources Authority of Jordan, Amman (1989).
- Powers, T.C., 'A working hypothesis for further studies of frost resistance of concrete', *Journal of the American Concrete Institute* **16**(4) (1945) 245-272.
- Punuru, A.R., Chowdhury, A.N., Kulshreshtha, N.P, and Gauri, K.L., 'Control of porosity on durability of limestone at the Great Sphinx, Egypt', *Environmental Geology and Water Science* **15**(3) (1990) 225-232.
- Recheis, A., Bidner, T., and Mirwald, P., 'Ultrasonic measurements on weathering Alpine marble: A study on field exposed samples and on the medieval marble portals of Schloss Tirol/South Tyrol-Italy', in *Proceedings of the 9th International Congress on Deterioration and Conservation of Stone, Venice, 19–24 June 2000*, ed. V. Fassina, Elsevier, Amsterdam (2000) Vol. II 139–144.
- Reinhardt, H.W [et al.], 'Echo-Verfahren in der zerstörungsfreien Zustandsuntersuchung von Betonbauteilen', *Betonkalender 2007* **96**(1), Ernst & Sohn, Berlin (2007) 481-595.
- Rentsch, W., and Krompholz, G., 'Zur Bestimmung elastischer Konstanten durch Schallgeschwindigkeitsmessungen', *Bergakademie: Zeitschrift für Bergbau, Hüttenwesen und verwandte Wissenschaften* **13**(7-8) (1961) 492-504.

- Rijniers, L.A., Huinink, H.P., Pel, L., and Kopinga, K., 'Experimental evidence of crystallization pressure inside porous media', *Physical Review Letters* **94** (2005) 075503 (4 pages).
- RILEM 25-PEM, *Recommended tests to measure the deterioration of stone and to assess the effectiveness of treatment methods*, Bordas-Dunod (1980).
- Robertson, E.C., 'Physical properties of building stone', in *Conservation of Historic Stone Buildings and Monuments*, National Academy Press, Washington D.C. (1982) 62-86.
- Rodríguez-Gordillo, J., and Sáez-Pérez, M.P., 'Effects of thermal changes on Macael marble: Experimental study', *Constructions and Building Materials* **xx** (2005) xxx-xxx.
- Rodriguez-Navarro, C., and Doehne, E., 'Salt weathering: influence of evaporation rate, supersaturation and crystallization pattern', *Earth Surface Processes and Landforms* **24** (1999) 191-209.
- Rodriguez-Navarro, C., Doehne, E., and Sebastian, E., 'How does sodium sulfate crystallize? Implications for the decay and testing of building materials', *Cement and Concrete Research* **30** (2000) 1527-1534.
- Romberg, H., 'Zementsteinporen und Betoneigenschaften', *Beton-Informationen* **18**(5) (1978) 50-55.
- Rose, D.A., 'Water movement in unsaturated porous materials', *RILEM Bulletin* **29** (1965) 119-124.
- Ross, K.D., Hart, D., and Butlin, R.N., 'Durability tests for natural building stone', in *Durability of Building Materials and Components – Proceedings of the Fifth International Conference, Brighton, 7-9 November, 1990*, ed. J.M. Baker, P.J. Nixon, A.J. Majumdar and H. Davies, E. & F.N. Spon, London (1991) 97-111.
- Rossi-Manaresi, R., and Ghezzi, 'The biocalcarene of the the Agrigento Greek Temples: Causes of alteration and effectiveness of conservation treatments', in *International Symposium on Deterioration and Protection of Stone Monuments, Paris, 5 9 June 1978*, UNESCO-RILEM, Paris (1978) Vol. III Session 7.9.
- Rossi-Manaresi, R., and Tucci, A., 'Pore structure and the disruptive or cementing effect of salt crystallization in various types of stone', *Studies in Conservation* **36** (1991) 53-58.
- Ruedrich, J., Weiss, T., and Siegesmund, S., 'Thermal behaviour of weathered and consolidated marbles', in *Natural stone, weathering phenomena, conservation strategies and case studies*, ed. S. Siegesmund, T. Weiss, and A. Vollbrecht, Geological Society, London, special publication **205** (2002) 255-271.
- Russell, S.A., *Stone preservation committee report, Appendix I*, H.M. Stationary Office, London (1927).

- Sage, J.D., 'Thermal microfracturing of marble', in *Engineering Geology of Ancient Works, Monuments and Historical Sites*, ed. P. Marions and G. Koukis, Balkema, Rotterdam (1988) 1013-1018.
- Sasse, H.R., and Snethlage, R., 'Methods for the evaluation of stone conservation treatments', in *Report of the Dahlem Workshop, Saving our Architectural Heritage – The Conservation of Historic Stone Structures, Berlin, 3-8 March 1996*, ed. N.S. Baer and R. Snethlage, John Wiley and Sons, Chichester (1997) 223-243.
- Sawdy, A., Heritage, A., and Pel, L., 'A review of salt transport in porous media, assessment methods and salt reduction treatments', in *Salt Weathering on Buildings and Stone Sculptures-Proceedings from the International Conference, Copenhagen, 22-24 October 2008*, Technical University of Denmark, Copenhagen (2008) 1-27.
- Scherer, G.W., 'Crystallization in pores', *Cement and Concrete Research* **29** (1999) 1347-1358.
- Scherer, G.W., 'Stress from crystallization of salt in pores', in *Proceedings of the 9th International Congress on Deterioration and Conservation of Stone, Venice, 19-24 June 2000*, ed. V. Fassina, Elsevier, Amsterdam (2000) Vol. I 187-194.
- Scherer, G.W., 'Stress from crystallization of salt', *Cement and Concrete Research* **34** (2004) 1613-1624.
- Scherer, G.W., and Wheeler, G.S., 'Silicate consolidants for stone', *Key Engineering Materials* **391** (2009) 1-25.
- Schild, M., Siegesmund, S., Vollbrecht, A., and Mazurek, M., 'Characterization of granite matrix porosity and pore-space geometry by *in situ* and laboratory methods', *Geophysical Journal International* **146** (2001) 111-125.
- Setzer, M.J., 'Zum Mikrogefüge des Zementsteins und dessen Einfluss auf das mechanische Verhalten des Betons', *Zement und Beton, Fachzeitschrift* **85/86** (1975) 29-33.
- Setzer, M.J., 'Micro ice lens formation and frost damage', in *Proceedings of the International RILEM Workshop on Frost damage in concrete, Minneapolis, 28-30 June 1999*, ed. D.J. Janssin, M.J. Setzer, and M.B. Snyder, RILEM Publications S.A.R.L., Cachan-Cedex (2002) 1-15.
- Shutilov, V.A., (translated by Alferrieff) *Fundamental physics of ultrasound*, Gordon and Breach Science Publishers, New York (1988).
- Siegesmund, S., Weiss, T., Vollbrecht, A., and Ullemeyer, K., 'Marble as a natural building stone: rock fabrics, physical and mechanical properties', *Zeitschrift der Deutschen Geologischen Gesellschaft* **150**(2) (1999) 237-258.
- Siegesmund, S., Ullemeyer, K., Weiss, T., and Tschegg, E.K., 'Physical weathering of marbles caused by anisotropic thermal expansion', *International Journal of Earth Science* **89** (2000) 170-182.

Siegesmund, S., Weiss, T., and Vollbrecht, A., 'Natural stone, weathering phenomena, conservation strategies and case studies: introduction', in *Natural stone, weathering phenomena, conservation strategies and case studies*, ed. S. Siegesmund, T. Weiss, and A. Vollbrecht, Geological Society, London, special publication **205** (2002) 1-7.

Simon, S., Vergès-Belmin, V., Blanc, A., and Snethlage, R., 'The marble columns in the cloister of the Primatial Church St. Trophime in Arles, France – Ultrasonic velocity measurements as a tool for anamnesis and diagnosis', in *Proceedings of the 3rd International Symposium on the Conservation of Monuments in the Mediterranean Basin, Venice, 22–25 June 1994*, ed. V. Fassina, H. Ott and F. Zezza, Soprintendenza ai Beni Artistici e Storici di Venezia, Venice (1994) 11–17.

Simon, S., 'Untersuchungen zur Verwitterung und Konservierung von Tuffeau am Pilotobjekt St. Gatien in Tours', in *Gemeinsames Erbe gemeinsam erhalten, 2. Statuskolloquium des Deutsch-Französischen Forschungsprogramms für die Erhaltung von Baudenkmalern, Bonn, 12–13 December 1996*, ed. J.-F. Filtz, Bonn (1996) 373–389.

Simon, S., and Lind, A.-M., 'Decay of limestone blocks in the block fields of Karnak Temple (Egypt): Non-destructive damage analysis and control of consolidation treatments', in *ICOM Committee for Conservation, 12th Triennial Meeting, Lyon, 29 August – 3 September 1999: Preprints*, ed. J. Bridgland, James & James, London (1999) Vol. II 743–749.

Simon, S., *Zur Verwitterung und Konservierung kristallinen Marmors*, PhD dissertation, Ludwig-Maximilians-Universität München (2001).

Simon, S., Shaer, M., and Kaiser, E., 'Conservation planning of Tomb 826 in Petra (Jordan) and accompanying investigations', in *Proceedings of the 10th International Congress on Deterioration and Conservation of Stone, Stockholm, 27 June – 2 July 2004*, ed. D. Kwiatkowski and R. Löfvendahl, ICOMOS, Stockholm (2004) Vol. II 963-970.

Simon, S., and Drdácký, M. (ed.), *European Research on Cultural Heritage. State-of-the-Art Studies, Volume 5, ARCCHIP Centre of Excellence Workshop on Problems of salts in masonry - SALTeXPert*, ITAM, Prague (2006).

Snethlage, R., and Wihr, R., 'Kolloquium über das Acrylharz-Volltränkungsverfahren der Fa. Imchemie, *Arbeitsheft 4*, Bayerisches Landesamt für Denkmalpflege, München (1979) 34p.

Snethlage, R., 'Steinkonservierung – Forschungsprogramm des Zentrallabors für Denkmalpflege 1979-1983', *Bericht für die Stiftung Volkswagenwerk, Arbeitsheft 22*, Bayerisches Landesamt für Denkmalpflege, Munich (1984).

Snethlage, R., and Wendler, E., 'Methoden der Steinkonservierung – Anforderungen und Bewertungskriterien', *Denkmalpflege und Naturwissenschaft, Natursteinkonservierung I*, ed. R. Snethlage, Verlag Ernst & Sohn GmbH, Berlin, (1995) 3-40.

Snethlage, R., Ettl, H., and Sattler, L., 'Ultraschallmessungen an PMMA-Getrankten Marmorskulpturen', *Zeitschrift der Deutschen Geologischen Gesellschaft* **150**(2) (1999) 387– 396.

- Snethlage, R., and Wendler, E., *Chemical compounds for conservation of natural stone, Vorlesungsskript*, LMU München, Fachbereich Geowissenschaften, (2000).
- Snethlage, R., *Leitfaden Steinkonservierung – Planung von Untersuchungen und Maßnahmen zur Erhaltung von Denkmälern aus Naturstein*, 3rd ed., Fraunhofer IRB Verlag, Stuttgart (2008).
- Sorge, G., and Hauptmann, P., *Ultraschall in Wissenschaft und Technik*, Verlag Harri Deutsch, Thun, Frankfurt/Main (1985).
- Sperling, C.H.B., and Cooke, R.U., ‘Laboratory simulation of rock weathering by salt crystallization and hydration processes in hot, arid environments’, *Earth Surface Processes and Landforms* 10 (1985) 541-555.
- Stark, J., and Wicht, B., *Dauerhaftigkeit von Beton: der Baustoff als Werkstoff*, Birkhäuser Verlag, Basel (2001).
- Steiger, M., ‘Crystal growth in porous materials-I: The crystallization pressure of large crystals’, *Journal of Crystal Growth* **282** (2005a) 455-469.
- Steiger, M., ‘Crystal growth in porous materials-II: Influence of crystal size on the crystallization pressure’, *Journal of Crystal Growth* **282** (2005b) 470-481.
- Steiger, M., and Asmussen, S., ‘Crystallization of sodium sulfate phases in porous materials: The phase diagram Na₂SO₄-H₂O and the generation of stress’, *Geochimica et Cosmochimica Acta* **72** (2008) 4291–4306.
- Steiger, M., Charola, A.E., and Sterflinger, K., ‘Weathering and deterioration’, in *Stone in architecture*, 4th ed., ed. S. Siegesmund und R. Snethlage, Springer, Berlin (2011) 227-316.
- Strohmeyer, D., *Gefügeabhängigkeit technischer Gesteinseigenschaften*, PhD dissertation, Georg-August-Universität zu Göttingen (2003).
- Stück, H., Forgó, L.Z., Rüdrieh, J., Siegesmund, S., Török, Á., ‘The behaviour of consolidated volcanic tuffs: weathering mechanisms under simulated laboratory conditions’, *Environmental Geology* **56** (2008) 699–713.
- Taber, S., ‘The growth of crystals under external pressure’, *American Journal of Science* **41** (1916) 532 – 556.
- Taber, S., ‘Frost heaving’, *Journal of Geology* **37** (1929) 428-461.
- Taber, S., ‘The mechanics of frost heaving’, *Journal of Geology* **38** (1930) 303-317.
- Theoulakis, P., and Moropoulou, A., ‘Microstructural and mechanical parameters determining the susceptibility of porous building stones to salt decay’, *Construction and Building Materials* **11**(1) (1997) 65-71.
- Torraca, G., *Porous building materials: materials science for architectural conservation*, 2nd ed., ICCROM, (1982).

- Tsui, N., Flatt, R.J. and Scherer, G.W., 'Crystallization damage by sodium sulfate', *Journal of Cultural Heritage* **4** (2003) 109-115.
- Tucker, M.E., and Wright, V.P., *Carbonate sedimentology*, Balkwell Science Ltd., Oxford (1990).
- Tuğrul, A., 'The effect of weathering on pore geometry and compressive strength of selected rock types from Turkey', *Engineering Geology* **75** (2004) 215-227.
- Vergès-Belmin, V., Oriol, G., Garnier, D., Bouineau, A., and Coignard, R., 'Impregnation of badly decayed Carrara marble by consolidation agents: comparison of seven treatments', in *Proceedings of the 2nd International Symposium on the Conservation of Monuments in the Mediterranean Basin, Geneva, 19–21 November 1991*, ed. D. Decrouez, J. Chamay and F. Zezza, Geneva (1991) 421-437.
- Villwock, R., *Industriegesteinskunde*, Stein-Verlag, Offenbach/Main (1966).
- Vos, B.H., 'Water absorption and drying of materials', in *The Conservation of Stone I, Proceedings of the International Symposium, Bologna, 19–21 June 1975*, ed. R. Rossi-Manaresi, Centro per la Conservazione delle Sculture all'Aperto, Bologna (1976) 679-694.
- Walsh, J.B., 'Deformation and Fracture of rock', in *Conservation of historic stone buildings and monuments*, National Academy Press, Washington D.C. (1982) 87-107.
- Water Data Banks Project, 'Overview of Middle East water resources', 1998, <http://exact-me.org/overview/p0809.pdf> (accessed 25 July 2011).
- Weiss, N.R., Slavid, I., and Wheeler, G., 'Development and assessment of a conservation treatment for calcareous stone', in *Proceedings of the 9th International Congress on Deterioration and Conservation of Stone, Venice, 19–24 June 2000*, ed. V. Fassina, Elsevier, Amsterdam (2000a) Vol. II 533-540.
- Weiss, T., Siegesmund, S., and Rasolofosaon, P.N.J., 'The relationship between deterioration, fabric, velocity and porosity constraint', in *Proceedings of the 9th International Congress on Deterioration and Conservation of Stone, Venice, 19–24 June 2000*, ed. V. Fassina, Elsevier, Amsterdam (2000b) Vol. I 215–223.
- Weiss, T., Siegesmund, S., Kirchner, D., and Sippel, J., 'Insolation weathering and hygric dilatation: two competitive factors in stone degradation', *Environmental Geology* **46** (2004) 402–413.
- Weyl, P.K., 'Pressure solution and the force of crystallization - A phenomenological theory', *Journal of Geophysical Research* **64**(11) (1959) 2001-2025.
- Wheeler, G., Méndez-Vivar, J., Goins, E.S., Fleming, S.A., and Brinker, C.J., 'Evaluation of alkoxysilane coupling agents in the consolidation of limestone', in *Proceedings of the 9th International Congress on Deterioration and Conservation of Stone, Venice, 19–24 June 2000*, ed. V. Fassina, Elsevier, Amsterdam (2000) Vol. II 541-545.

- Wheeler, G., *Alkoxysilanes and the Consolidation of Stone*, J. Paul Getty Trust, The Getty Conservation Institute, Los Angeles, California (2005).
- Willman, H. W., and Wilson, A.T., 'Salt weathering: a neglected geological erosive agent in costal and arid environments', *Nature* **205**(4976) (1965) 1097-1098.
- Willman, H. W., and Wilson, A.T., 'Salt weathering or fretting', in *Encyclopedia of geomorphology*, ed. R.W. Fairbridge, Dowden, Hutchinson & Ross, Stroudsburg, Pa (1968) 968-970.
- Winkler, E.M., and Singer, P.C., 'Crystallization pressure of salts in stone and concrete', *Bulletin of the Geological Society of America* **83**(11) (1972) 3509-3514.
- Winkler, E.M., *Stone: Properties, durability in man's environment*, 2nd ed., Springer Verlag, Vienna and New York (1975).
- Winkler, E.M., 'Stone in architecture - Properties, durability', 3rd ed., Springer-Verlag, Berlin, Heidelberg, New York (1997).
- Wittmann, F.H., Prim, P., 'Mesures de l'effet consolidant d'un produit de traitement', *Matériaux et Construction* **16**(94) (1983) 235-242.
- Wittmann, F.H., 'Porosität und Feuchtigkeitsgehalt' in *Feuchtigkeit und Dauerhaftigkeit von Beton*, WTA-Schriftenreihe Heft 3, ed. F.H. Wittmann, WTA, Baierbrunn (1992) 1-22.
- Wohletz, K.H., *MAGMA: calculates IUGS volcanic rock classification, densities, and viscosities*. Los Alamos National Laboratory computer code LA-CC 99-28, Los Alamos New Mexico (1999).
- Woo, J., 'A short History of the development of ultrasound in obstetrics and gynecology', (2002), <http://www.ob-ultrasound.net/history1.html> (accessed 25 July 2011).
- Xie, P., and Beaudoin, J.J., 'Mechanism of sulfate expansion I. Thermodynamic principle of cristallisation pressure', *Cement and Concrete Research* **22**(4) (1992) 631-640.
- Yoder, H.S., and Tilley, C.E., 'Origin of basalt magmas', *Journal of Petrology* **3** (1962) 342-532.
- Yu, S., and Oguchi, C.T., 'Role of pore size distribution in salt uptake, damage, and predicting salt susceptibility of eight types of Japanese building stones', *Engineering Geology* xxx (2009a) xxx-xxx.
- Yu, S., and Oguchi, C.T., 'Complex relationships between salt type and rock properties in a durability experiment of multiple salt-rock treatments', *Earth Surface Processes and Landforms* **34** (2009b) 2096-2110.
- Zehnder, K., and Arnold, A., 'Crystal growth in salt efflorescence', *Journal of Crystal Growth* **97** (1989) 513-521.

Zeisig, A., Siegesmund, S., Weiss, T., 'Thermal expansion and its control on the durability of marble', in *Natural stone, weathering phenomena, conservation strategies and case studies*, ed. S. Siegesmund, T. Weiss, and A. Vollbrecht, Geological Society, London, special publication **205** (2002) 65-80.

Zeza, F., 'Computerized analysis of stone decay in monuments', in *Proceedings of the 1st International Symposium on the Conservation of Monuments in the Mediterranean Basin, Bari, 7-10 June 1989*, ed. F. Zeza, Grafo, Brescia (1990) 163-184.

Curriculum Vitae

Personal information:

Name: Abdelraheem Ahmad
Date of birth: 24.01.1980
Place of birth: Malka – Irbid, Jordan
Marital status: Single

Education:

1986 - 1992 Malka Primary School
1992 - 1998 Malka Secondary School
Degree: General Secondary Certificate ,Scientific Stream
1998 - 2002 Study of Physics at Yarmouk University in Irbid, Jordan
Degree: Bachelore of Science (B.Sc)
2003 – 2005 Study of Conservation and Management of Cultural Resources
at Yarmouk University in Irbid, Jordan
Degree: Master of Arts (M.A)
Since Nov. 2006 PhD student under the supervision of Prof. Dr. Stefan Simon at
Rathgen Research Laboratory and Prof. Dr. Bernhard
Middendorf at the Faculty of Architecture and Civil Engineering
at The Technical University of Dortmund

Publications:

Ahmad, A., Pamplona, M., and Simon, S., ‘Ultrasonic testing for the investigation and characterization of stone – a non-destructive and transportable tool’, *Reviews in Conservation* **10** (2009) 43-53.

Pamplona, M., Ahmad, A., Simon, S., Aßel, E., and Theissen, A., ‘Ultrasonic pulse velocity – a tool for the condition assessment of outdoor marble sculptures’, in *Proceedings. of the 8th International Symposium on the Conservation of Monuments in the Mediterranean Basin, Patras, 31 May – 2 June 2010*, in press.

Pamplona, M., Simon, S., Bauer, M., Ahmad, A., 'Marble conservation by total acrylic impregnation (IBACH Process) and induced physico-mechanical changes' in. *Jardin de Pierres, conservation de la pierre dans les parcs, jardins et cimetières, Paris, 22-24 June 2011*, 4es journées d'étude de la SFIIC, Inst. Nat. Du Patrimoine, Paris (2011) 267–276.

